# ERODIBILITY AND SCOUR BY A VERTICAL SUBMERGED CIRCULAR TURBULENT IMPINGING JET IN COHESIVE SOILS

A Thesis Submitted to the College of

Graduate and Postdoctoral Studies

In Partial Fulfillment of the Requirements

For the Degree of Master of Science

In the Department of Civil and Geological Engineering

University of Saskatchewan

Saskatoon

By

DANIEL COSSETTE

## PERMISSION TO USE

In presenting this thesis in partial fulfilment of the requirements for a Postgraduate degree from the University of Saskatchewan, I agree that the Libraries of this University may make it freely available for inspection. I further agree that permission for copying of this thesis in any manner, in whole or in part, for scholarly purposes may be granted by the professor or professors who supervised my thesis work or, in their absence, by the Head of the Department or the Dean of the College in which my thesis work was done. It is understood that any copying or publication or use of this thesis or parts thereof for financial gain shall not be allowed without my written permission. It is also understood that due recognition shall be given to me and to the University of Saskatchewan in any scholarly use which may be made of any material in my thesis.

Requests for permission to copy or to make other use of material in this thesis in whole or part should be addressed to:

Head of the Department of Civil and Geological Engineering
University of Saskatchewan
57 Campus Drive
Saskatoon, Saskatchewan
Canada, S7N 5A9

## ABSTRACT

The erodibility of cohesive soils is commonly represented by the critical shear stress, which is the applied shear stress at the threshold for which erosion is initiated, and the erodibility coefficient, which is a measure of the rate of erosion once the critical shear stress threshold is exceeded. These erodibility parameters are typically considered properties of the soil and can be measured using a number of laboratory or field testing devices. In this study, a vertical submerged circular turbulent impinging jet was used for testing 18 natural and 10 manufactured cohesive samples. There are a number of different methods available for analyzing the test data and the first objective of this study was to compare the resulting erodibility parameters calculated using multiple methods. The second objective was to use the calculated erodibility parameters to develop a relationship that can be used for estimating the ultimate dimensions of the scour hole.

Four data analysis methods (Hanson and Cook (2004), Visual, Equilibrium, and Thomas') were used in determining the critical shear stress for the tested samples. While it is expected that the results from these four methods should provide similar results, this was not found to be the case. Differences in these calculated values was largely attributed to the disparity between theoretical estimates for the equilibrium centerline scour depths and the equilibrium scour depths observed from testing. Results were also found to be impacted by the duration of test data used in the analysis. The relative ranking of the critical shear stress values for the soils tests are reasonably consistent between analysis methods.

Two data analysis methods (Hanson and Cook (2004) and Thomas') were used in determining the erodibility coefficient for the tested samples and were also found to have a significant discrepancy in results. Each analysis method represents a theoretical model of how the scour hole depth grows with time and both are based on a form of the excess shear stress equation. This equation is generally assumed to be linear; however results from this study support the inclusion of an exponential term. This term was found to vary between 0.5 and 2.0 for Hanson and Cook's (2004) analysis method and between 0.6 and 6.1 for Thomas' method. Adopting nonlinear time development of scour equations affects how the erodibility coefficient can be compared between samples since its units are depend on the value of the excess shear stress exponent. It is recommended that use of a nondimensional form of the erodibility coefficient be

considered when using a nonlinear expression of the excess shear stress equation for data analysis.

A number of scour analysis methods from literature were highlighted in this study and Mazurek (2001) approach was chosen for use. When using the critical shear stress from Hanson and Cook's (2004) method and the equilibrium method, reasonable relationships were developed for estimating the centerline scour depth and scour hole radius at equilibrium state. As expected, data from the natural samples showed more variability than the manufacture samples.

## ACKNOWLEDGMENTS

First of all, I would like to express my gratitude to my supervisor Kerry Mazurek for all of the hard work she put into my program. I would not have been able to complete this thesis without her consistent guidance and encouragement. I would also like to acknowledge my Advisory Committee Dr. Jim Kells, Dr. Jim Bugg and Dr. Doug Milne and thank them for allowing me the opportunity to complete this work.

I would like to thank the staff and my colleagues from the University of Saskatchewan who provided assistance with my experimental program. Both Dale Pavier and Brennan Pokoyoway, technicians in the Department of Civil and Geological Engineering, were instrumental in constructing and maintaining the experimental apparatus. I would like to specifically thank Dale for the additional assistance he provided in performing a number of hydrometer tests on my soil samples as well as being my resource for any questions I had related to the hydraulics laboratory. I would also like to thank my friends and colleagues Brian Sibley, Alex Udey and Jordan Parisien for their assistance with sample collection, for providing feedback on my research and for all the happy memories created during our programs together.

I would like to acknowledge Dr. Colin Rennie of the University of Ottawa who provided the soil samples from the Ontario sample group, and Mark Lapointe, technologist in Civil Engineering at the University of Ottawa, who assisted with sample collection.

I am grateful for the financial support provided which allowed me to complete this work. Funding was provided by the Natural Sciences and Engineering Research Council of Canada (NSERC) in the form of a Discovery grant as well as by the University of Saskatchewan through graduate scholarships.

Finally, I am very thankful to my family for their support during my program and their belief in me. Most of all, my deepest appreciations are reserved for my partner, Jeness, for her love and encouragement throughout this program. I am so fortunate to have had someone as wonderful as you with me along this journey.

In loving memory of my Grandparents,
Alphonse and Christina Cossette

## TABLE OF CONTENTS

page

## LIST OF TABLES

## LIST OF FIGURES

## NOMENCLATURE

| Symbol | | Units |
|---|---|---|
| $A_o$ | cross sectional area of the jet nozzle | $mm^2$ |
| $A_T$ | cross sectional area of the testing tank | $m^2$ |
| $\overline{b_{cl\infty}}$ | average scour hole radius at half of the centerline depth at equilibrium | mm |
| $c_f$ | skin friction coefficient | - |
| $C_d$ | diffusion coefficient of a submerged circular jet | - |
| $d_o$ | diameter of jet nozzle | mm |
| $D_{50}$ | median particle diameter of the soil sample | mm |
| $\dot{E}$ | soil erosion rate | mm/s |
| $\varepsilon$ | scour depth as measured from the original sample surface | mm |
| $\varepsilon_\infty$ | scour depth at equilibrium | mm |
| $\varepsilon_{cl}$ | centerline scour depth below the sample surface | mm |
| $\varepsilon_{cl\infty}$ | centerline scour depth at equilibrium below the sample surface | mm |
| $\varepsilon_m$ | maximum scour depth below the sample surface | mm |
| $\varepsilon_{m\infty}$ | maximum scour depth at equilibrium below the sample surface | mm |
| $H$ | height from the jet nozzle to the sample surface along the jet centerline | mm |
| $H_e$ | height from the jet nozzle to the sample surface along the jet centerline at equilibrium | mm |
| $H_{e\_B}$ | height from the jet nozzle to the sample surface along the jet centerline at equilibrium determined using Hanson and Cook's (2004) method | mm |
| $H_{e\_B1}$ | height from the jet nozzle to the sample surface along the jet centerline at equilibrium determined using Hanson and Cook's (2004) method and the first 120 minutes of testing data | mm |

| | | |
|---|---|---|
| $H_{e\_B2}$ | height from the jet nozzle to the sample surface along the jet centerline at equilibrium determined using Hanson and Cook's (2004) method and the first 10 readings from the test data | mm |
| $H_{e\_B3}$ | height from the jet nozzle to the sample surface along the jet centerline at equilibrium determined using Hanson and Cook's (2004) method and the full testing data set | mm |
| $H_{e\_m}$ | height from the jet nozzle to the sample surface along the jet centerline at equilibrium measured from jet testing | mm |
| $H_i$ | initial height from sample surface to jet nozzle before testing | mm |
| $H_j$ | measured height from the nozzle to the soil surface along the jet centerline that corresponds to the $j^{th}$ reading taken during jet testing ($j \geq 1$) | mm |
| $H_p$ | height of the potential core | mm |
| $H^*$ | dimensionless height from the jet nozzle to the soil surface | - |
| $H_i^*$ | dimensionless initial height from the jet nozzle to the soil surface | - |
| $H_p^*$ | dimensionless height of the potential core | - |
| $j$ | counter which tracks the number of readings taken since test initiation | - |
| $k$ | erodibility coefficient of cohesive soil | $cm^3$/N-s |
| $k_H$ | erodibility coefficient of cohesive soil determined using Hanson and Cook's (2004) method | $cm^3$/N-s |
| $k_{H1}$ | erodibility coefficient of cohesive soil determined using Hanson and Cook's (2004) method and the first 120 minutes of testing data | $cm^3$/N-s |
| $k_{H3}$ | erodibility coefficient of cohesive soil determined using Hanson and Cook's (2004) method and the full testing data set | $cm^3$/N-s |
| $k_{H3\_E}$ | erodibility coefficient of cohesive soil determined using Hanson and Cook's (2004) method, the full testing data set, and the equilibrium | dependent on value |

| | | |
|---|---|---|
| | scour depth measured from testing | of $n$ |
| $k_T$ | erodibility coefficient of cohesive soil determined using Thomas' method | $cm^3$/N-s |
| $k_{T1}$ | erodibility coefficient of cohesive soil determined using Thomas' method and the first 120 minutes of testing data | $cm^3$/N-s |
| $k_{T3}$ | erodibility coefficient of cohesive soil determined using Thomas' method and the full testing data set | dependent on value of $n$ |
| $LL$ | liquid limit of soil sample | % |
| $\mu$ | dynamic viscosity of the eroding fluid | N-s/$m^2$ |
| $n$ | exponential term for the excess shear stress equation | - |
| $n_{HE}$ | exponential term selected as providing the best fit to between the jet test data and the time development of scour equations | - |
| $n_{T1}$ | exponential term for the excess shear stress equation determined using Thomas' method and the first 120 minutes of testing data | - |
| $n_{T3}$ | exponential term for the excess shear stress equation determined using Thomas' method and the full testing data set | - |
| $\nu$ | kinematic viscosity of the eroding fluid | $m^2$/s |
| $p_s$ | normal pressure at the stagnation point | N/$m^2$ |
| $p_w$ | normal wall pressure | N/$m^2$ |
| $PL$ | plastic limit of soil sample | % |
| $Q$ | flow rate used for jet testing | Lps |
| $Q_c$ | flow rate at which mass erosion is observed for the visual method | Lps |
| $r$ | distance from jet centerline | mm |
| $r_o$ | radius of scour hole at the surface | mm |

| | | |
|---|---|---|
| $\overline{r_o}$ | average radius of the scour hole | mm |
| $\overline{r_{o\infty}}$ | average radius of the scour hole at equilibrium | mm |
| $R$ | jet Reynolds number for jet testing | - |
| $R_{visual}$ | jet Reynolds number for the visual testing | - |
| $R^2$ | squared correlation coefficient | - |
| $\rho$ | density of the eroding fluid | $kg/m^3$ |
| $\rho_b$ | bulk density of the soil sample | $kg/m^3$ |
| $\rho_d$ | dry density of the soil sample | $kg/m^3$ |
| $S$ | average length measurement for one side of the octagonal testing tank | m |
| $t$ | elapsed time since test initiation | s |
| $t_j$ | elapsed time corresponding to the $j^{th}$ reading taken during jet testing ($j \geq 1$) | s |
| $t_m$ | measured elapsed time since test initiation | s |
| $T_R$ | test reference time | s |
| $T^*$ | dimensionless time | - |
| $T_i^*$ | dimensionless time to reach initial jet height | - |
| $T_m^*$ | dimensionless time measured from test initiation | - |
| $T_p^*$ | dimensionless time to reach potential core height | - |
| $T_{Test}^*$ | dimensionless time determined using the elapsed time from testing | - |
| $T_{Theo}^*$ | theoretical dimensionless time calculated using the measured scour depths from testing | - |
| $\tau_{avg}$ | average maximum bed shear stress between two test intervals | $N/m^2$ |
| $\tau_c$ | critical shear stress for cohesive soil | $N/m^2$ |
| $\tau_{c\_B}$ | critical shear stress determined using Hanson and Cook's (2004) | $N/m^2$ |

| | | |
|---|---|---|
| | method | |
| $\tau_{c\_B1}$ | critical shear stress determined using Hanson and Cook's (2004) method using the first 120 minutes of testing data | $N/m^2$ |
| $\tau_{c\_B2}$ | critical shear stress determined using Hanson and Cook's (2004) method using the first 10 readings from the test data | $N/m^2$ |
| $\tau_{c\_B3}$ | critical shear stress determined using Hanson and Cook's (2004) method using the full testing data set | $N/m^2$ |
| $\tau_{c\_Ec}$ | critical shear stress determined using the equilibrium method | $N/m^2$ |
| $\tau_{c\_T}$ | critical shear stress determined using Thomas's method | $N/m^2$ |
| $\tau_{c\_T1}$ | critical shear stress determined using Thomas's method using the first 120 minutes of testing data | $N/m^2$ |
| $\tau_{c\_T2}$ | critical shear stress determined using Thomas's method using the first 10 readings from the test data | $N/m^2$ |
| $\tau_{c\_T3}$ | critical shear stress determined using Thomas's method using the full testing data set | $N/m^2$ |
| $\tau_{c\_V}$ | critical shear stress determined using the visual method | $N/m^2$ |
| $\tau_e$ | effective shear stress applied to the bed | $N/m^2$ |
| $\tau_o$ | shear stress applied to the bed | |
| $\tau_{om}$ | maximum shear stress applied to the bed | $N/m^2$ |
| $U_m$ | maximum velocity of the jet at a distance x from the jet nozzle | m/s |
| $U_o$ | velocity at the jet nozzle | m/s |
| $U_{oc}$ | velocity at the jet nozzle for which mass erosion is observed, referred to as the critical nozzle velocity | m/s |
| $V_s$ | volume of the scour hole | $mm^3$ |
| $V_{s\infty}$ | volume of the scour hole at equilibrium | $mm^3$ |

| | | |
|---|---|---|
| $w_o$ | water content before sample preparation | % |
| $w_p$ | water content prior to testing (after soaking) | % |
| $w_f$ | water content after testing | % |
| $x$ | distance from the jet nozzle | mm |
| $x_p$ | length of the potential core, within which the centerline velocity is constant and equal to $U_o$ | mm |

# CHAPTER 1
# INTRODUCTION

## 1.1 BACKGROUND

Determining the erosion resistance of soils and the estimation of potential scour are essential for the design of many hydrotechnical and geotechnical projects. Estimating the erosion resistance of soils is very important for dealing with problems such as riverbed degradation, riverbank instability, headcut erosion, and levee breaching. On the local scale, excessive scouring around bridge piers and downstream of spillways and culverts can undermine the foundations of these structures and cause serviceability issues or total failure. From a design perspective, it is important to know under what conditions erosion will begin, the rate at which it will progress once initiated, and the ultimate spatial extent of scour.

The problem of erosion and scour is generally divided into two classifications: cohesive soil and non-cohesive soil. The term 'non-cohesive' refers to a soil where the particles tend to behave independently from one another and erode as individual grains. On the other hand, cohesive soils display significant inter-particle forces, typically due to the presence of a clay fraction, causing the soil to either erode particle by particle or more commonly as soil aggregates (Mazurek et al., 2001). Methods of analysis for determining erosion resistance and scour in non-cohesive soils are generally well-developed (Annandale, 2006). However, this is not true for cohesive soils.

For cohesive soils, it is common to characterize their erodibility by the critical shear stress of the soil (Annandale, 2006), $\tau_c$, which is the shear stress at which significant erosion begins, and the erodibility coefficient, $k$, which is the ratio between the rate of soil erosion and excess shear stress on a bed (Julien, 1998). These erodibility parameters are known to depend on many physical and electrochemical properties of both the soil and eroding fluid such as the soil water content, bulk density, percent clay, plasticity index and the pore and eroding water chemistry

(USBR, 2006). Additionally, for natural sediments there are also factors that are difficult to quantify such as inhomogeneity of the sample, vegetation and biological activity, which also affect the soil's erodibility (Black et al., 2002). Given the large number of factors that influence cohesive soil erodibility, it is preferable to directly test samples in order to determine the erodibility parameters rather than predicting these parameters from soil properties (USBR, 2006).

There is currently no generally accepted method for assessing the critical shear stress and the erodibility coefficient of cohesive soils. There exists a wide variety of apparatuses and testing methods. Testing has been conducted in open flumes of various sizes (Enger, 1963); (Hanson, 1990a); (Haralampides and Rodriguez, 2006); in closed flumes such as the Erosion Function Apparatus (Briaud et al., 2001); within concentric rotating cylinders (Masch et al., 1963; Lim and Khalili, 2009); using a wall jet (Mazurek et al., 2003); by drilling a hole in the sample and treating the flow as a pipe flow as in the Hole Erosion Test and Slot Erosion Tests (Wan and Fell, 2002); and by using a submerged circular turbulent impinging jet (Moore and Masch, 1962; Hollick, 1976; Hanson, 1991; Hanson and Cook, 2004; Mazurek, 2010). Of these tests, the Jet Erosion Test (JET) is commonly being used in North America for assessing cohesive soil erosion resistance (Clark and Wynn, 2007; Thoman and Niezgoda, 2008; Simon et al., 2010). The JET methodology is defined in ASTM Standard D5852 (2007) as well as in Hanson and Cook (2004). The advantage of this test is that it can be used both in-situ and in the laboratory for testing both large and small samples. However, there are still some questions about the reliability of the jet test (Annandale, 2006).

Ultimately the measurements of the erodibility of the soils are used to assess amounts of erosion and scour including that occurring around hydraulic structures. For assessing scour by flows in the form of water jets, which is the case of scour below many hydraulic structures such as weirs, drops, and culverts, methods of predicting scour in cohesive soils are not well-developed. Much of the research concerned with scour prediction using impinging jets has been conducted on noncohesive soils (Westrich and Kobus, 1973; Rajaratnam and Beltaos, 1977; Aderibigbe and Rajaratnam, 1996; Rajaratnam and Mazurek, 2003) with relatively few studies, by comparison, of scour in cohesive soils (Mazurek, 2001; Stein, 1990; Ansari, 2003). Many of

these methods look at developing relations between the dimensionless scour hole dimensions and dimensionless terms that characterize the properties of the jet and soil.

## 1.2 OBJECTIVES

The main objectives of this study are as follows:

1. To determine the effect on the critical shear stress and erodibility coefficient results that different analysis methods of the jet test data produce in both natural and manufactured cohesive soils. Four analysis methods will be used for assessing $\tau_c$: Hanson and Cook's (2004) method, the visual method, the equilibrium method, and Thomas' method (unpublished). Two analysis methods will be used for assessing $k$: Hanson and Cook's (2004) method and Thomas' method (unpublished).

2. To develop a relationship for determining the maximum centerline depth and radius of a scour hole at equilibrium state that is formed in natural and manufactured cohesive soils by a vertical submerged circular turbulent impinging jet using measured values of the soil erosion resistance.

## 1.3 SCOPE

An experimental study is to be conducted using the University of Saskatchewan Hydraulics Laboratory in order to meet these objectives. The study will be confined to jet testing of cohesive soil samples. Soil property testing will be conducted only as a means to classify the samples tested. The following will not be included as part of this study:

- Field jet testing;
- Erosion testing with devices other than the jet test;
- Investigation of relationships between soil properties other than $\tau_c$ and $k$ and sample erodibility and scour;

- Use of the measured soil erosion resistance parameters to model cohesive soil behavior in field applications.

## 1.4 CONTENT OF THESIS

This thesis is organized into 5 chapters. Chapter 2 provides a literature review on the topic of cohesive soil erosion, the mechanics and operation of a jet erosion test, the various methods in which the critical shear stress and erodibility coefficient can be determined from testing and scour prediction methods for impinging jets in cohesive soils. Chapter 3 outlines the experimental setup and methodology. Chapter 4 presents the testing results and analysis of the jet erosion test data. Last of all, Chapter 5 will give the study conclusions and recommendations for future work.

# CHAPTER 2
# LITERATURE REVIEW

This chapter presents an overview of relevant research that that is foundational to this study. Section 2.1 presents the two parameters used to describe cohesive soil erosion and gives an overview of the factors which can impact the erodibility of cohesive soils. A number of typical devices used to determine these erodibility parameters are also highlighted. Section 2.2 provides an introduction to the development and application of the jet erosion test and the analysis theory. In Section 2.3 the four methods used in this study for determining the critical shear stress of natural and manufactured cohesive soils are introduced, and in Section 2.4 two methods used for determining the erodibility coefficient are introduced. Finally, Section 2.5 presents a number of methods for assessing scour in cohesive soils.

## 2.1 COHESIVE SOIL EROSION

As previously mentioned, soils can generally be classified as either cohesive or non-cohesive largely based on the mechanics of how they erode when subject to hydrodynamic forces. When a particle's mass is large relative to its surface area, mechanical forces tend to govern its initiation of motion and transport behavior (Hoffmans, 1997). Alternatively, when a particle's surface area is large relative to its mass, electro-chemical forces between individual particles begin to have an effect. When dealing with uniform materials, grain size can generally be used to determine which of these two categories the soil will fall into: non-cohesive sediments are composed of granular materials such as sands and gravels whereas cohesive sediments are composed of remouldable material such as silts and clays. However, natural sediments rarely exist as just clays or just sands but rather a mixture of various grain sizes, along with water, organic material and sometimes gases.

As only clay particles exhibit cohesive properties, the clay fraction of a soil network is important when making a distinction between cohesive and non-cohesive behavior. The term

'mud' or 'fines' can be used to denote the combined clay and silt fraction of sediments and, depending on which soil classification system is used, the grain size for the mud and clay fraction respectively can be 60 μm and 2 μm (British Soil Classification System), 63 μm and 2 μm (Dutch Standards), or 75 μm and 5 μm (Unified Soil Classification System from ASTM D2487-11). Van Ledden et al. (2004) note the minimum clay content required for plastic behavior is about 5 – 10 % and that this fraction was also sufficient for a natural bed to exhibit cohesive properties. Transition from non-cohesive to cohesive behavior was also observed for clay contents ranging from 3 – 5% in some situations. Hanson (1991) defined noncohesive as soils with a plasticity index (PI) of no greater than 10, and erosion resistant soils as cohesive soils with a PI between 10-40 and a void ratio less than 0.7. Additionally, Mitchener and Torfs (1996) recommend using cohesive sediment transport equations when the mud fraction is greater than 15% by weight.

The topics of mechanical and hydrodynamic behavior of cohesive sediments is well covered in Partheniades (2009) and Winterwerp and van Kesteren (2004).

### 2.1.1 Excess Shear Stress and Erodibility Parameters

Erosion by water occurs along a soil/water interface when the hydrodynamic forces, due to the flowing water, are greater than the soil's ability to resist movement, resulting in detachment and transportation of soil particles. Scour can be thought of as excessive erosion on a local scale, usually caused by a concentrated water flow, and is usually described by its spatial extent (i.e., the depth or width of a scour hole). Because of this soil/water interaction, scour analysis requires an understanding of both the ability of a soil to resist scour and the erosive capacity of water (Annandale, 2006).

The erodibility of a soil can be characterized by two aspects: one, the rate at which the soil erodes when subjected to hydrodynamic forces and, two, the ease of initiation of erosion or incipient motion (Wan and Fell, 2002). The scour process begins when the erosive capacity of water barely exceeds the erosion resistance of the soil and incipient motion occurs. When the erosive capacity of water once again drops below the erosion resistance capacity of the soil, erosion stops and maximum scour extent is reached. An indication of a highly erodible soil is a

low threshold for incipient motion, that is, when scour begins for low erosive capacities of water. The erosion rate of a soil describes how quickly scour progresses or how quickly the maximum extent of scour is reached. Another indication of a highly erodible soil is fast erosion rate or a quick scour progression.

For cohesive soils the rate of erosion can be defined as a function of the excess shear stress given as:

$$\dot{E} = k(\tau_e - \tau_c)^n \qquad [2\text{-}1]$$

where $\dot{E}$ is the erosion rate of the soil, $\tau_e$ is the effective shear stress on the bed, $\tau_c$ is the critical shear stress, $k$ is the erodibility coefficient, and '$n$' is the fitted exponential term. For cases where the effective shear stress is less than $\tau_c$, no erosion occurs and the erosion rate is zero. The excess shear stress equation is often assumed linear with '$n$' equal to 1; however, Knapen et al. (2007) reported values from a number of studies in the range of 0.87 to 6.8.

Both the critical shear stress, which is an indicator of incipient motion, and the erodibility coefficient, which is an indicator of erosion rate once erosion begins, can be thought of as constant soil properties. However they can also vary with depth and time due to consolidation of soil layers and other physical, chemical or biological effects.

### 2.1.2 Factors Influencing Cohesive Soil Erosion

There have been numerous efforts to develop predictive equations relating the erodibility parameters of cohesive soils to their physical properties; most notably dry and bulk density, clay fraction, water content, vane shear strength, salinity, and plastic and elastic limits to name a few (Utley and Wynn, 2008). This approach is complicated by the large number of factors that influence soil erodibility. USBR (2006) provides a list of 28 properties used to characterize cohesive sediments which highlights the complexity of the task. Furthermore, many natural soil properties vary largely both temporally and spatially as well as with increasing depth below the soil surface. Given these considerations, predictive formulas based on soil properties tend to be empirical in nature with poor universality (Zhu et al., 2008).

Briaud et al. (2004) lists 16 factors that have been well studied and are known to affect the erosion of cohesive soils. An increase in undrained shear strength, void ratio, swell, dispersion ratio, sodium absorption ratio, and the temperature of the soil and water increase a soil's erodibility, while an increase in unit weight, plasticity index, and fines fraction decrease a soil's erodibility. Mean grain size, clay minerals, cation exchange capacity, pH, water chemical composition and water content also have an influence, although, the direction of the influence on erodibility is less obvious.

Mostafa et al. (2008) gave this subject comprehensive treatment by summarizing the efforts of a number of researchers and categorizing the factors affecting cohesive soil erodibility into four groups: the chemical and electrochemical properties of the soil, the biological properties of the soil, the chemical and physical properties of the eroding water, and the physical and mechanical properties of the soil. Research into biological effects are perhaps more qualitative than the other three categories given the expansive range of organisms that can be present and have an effect on sediment/water systems. Nevertheless, they play an important role when dealing with natural soils. Black et al., (2002) provided insight into 13 biotic processes that can stabilize or destabilize natural cohesive sediments.

### 2.1.3 Testing Devices for Cohesive Soil Erosion

Since cohesive soil erosion can be affected by almost any soil property, as well as a range of physical, biological and chemical factors, it is common to directly test cohesive soils in order to determine the critical shear stress and erodibility coefficient. Many devices and methods of analysis have been developed for this purpose. These devices typically impose a flow field along or towards a soil surface or through a soil block and then use the generated hydraulic forces along the soil-water boundary and measured soil erosion to determine these parameters.

It is common for researchers to use devices which have similar hydraulics to the problem they are studying. Open flumes have been used extensively to study natural channel processes and are often used not only for evaluating the erodibility parameters of cohesive soils, but also for studying sediment transport (Roberts et al., 2003). Sharif (2003) is a further example of a

laboratory flume being used to measure the critical shear stress of reconstituted and natural clays and muds. Gaskin et al. (2003) used a laboratory tilting flume to test undisturbed samples from the St Lawrence River up to velocities of 1.76 m/s. Large scale flumes can be cumbersome devices for field testing, however, there are in situ flume devices that can be used (Houwing and van Rijn, 1998).

Open flumes tend to have an upper limit to the velocities and therefore shear stresses that can be imposed on a bed. Closed flumes can be an appealing alternative for testing when dealing with cohesive material with low erodibility. The erosion function apparatus (EFA) developed by Briaud et al. (2001) has been used to test dense clays and weak rock and can achieve velocities of up to 6 m/s. Field samples can be collected in Shelby tubes and are tested with the surface flush to the flume floor allowing undisturbed natural samples to be conveniently tested.

Shan (2010) and the Federal Highway Administration (FHWA, 2015) present the development of a laboratory based ex situ scour test device (ESTD) which has a similar concept to the EFA. A horizontal test conduit is located between an inlet and outlet tank with a soil specimen being introduced to the flow field through the floor of the test conduit. However, in order to transform the parabolic velocity profile produced by conduit flow into a log-law profile, a belt located along the roof of the conduit is rotated in the direction of flow while testing.

Apart from flumes, another device that has been frequently used for determining cohesive soil erodibility parameters is the Hole Erosion Test (HET) presented by Wan and Fell (2002). This apparatus uses a cylindrical soil sample secured between differential head tanks with a 6 mm axial hole drilled though the center and has commonly been used on reconstituted soil samples as a test analogous to internal erosion processes in earthen dams. Luthi (2011) proposed modifications to the theory and operation of the HET and also tested natural cohesive soils.

The devices highlighted in this section are presented to give a sample of the various methods used to study cohesive soil erosion and are by no means an exhaustive list. It is not uncommon for researchers to modify a well-established test apparatus or methodology to suit the needs of their study objectives.

## 2.2 THE JET EROSION TEST

The jet erosion test device presents a number of advantages for determining the erodibility parameters of cohesive soils. First of all, the apparatus was initially developed for the purpose of field testing, so the device is relatively small and mobile and the standard testing procedure is relatively short. Field use of the device is not limited to flat surfaces but can also be conducted on inclined banks and near vertical soil faces. Nozzle velocities for the field testing apparatus are limited by the height of the constant head tank; however, very high nozzle velocities can be achieved using pumps, which allow high critical shear stress samples to be tested. Samples required for laboratory testing are small and relatively easy to collect undisturbed. Furthermore, jet erosion testing is possible not only on reconstituted samples, but also on natural soils even when imperfections such as roots and rocks are present.

### 2.2.1 Development of the Jet Erosion Test

Impinging water jets have been used to study scour and erodibility for quite some time (Moore and Masch, 1962; Hollick, 1976). Hanson (1990a and 1990b) presented a vertical jet device that could be used in situ to measure the coefficient of erodibility. A dimensionless equation for the rate of erosion was calibrated using open channel and jet testing data from three soils with the resulting model applied to a fourth soil. The analytical procedures for determining both erodibility parameters, including the critical shear stress, are outlined in Hanson and Cook (1997).

A standard test for determining soil erodibility was originally published in 1995 and reapproved in 2007 (ASTM Standard D5852, 2007) which allows a jet index value to be determined from testing and the soil to be classified as having a high, moderate or low resistance erosion. This standard also provides an estimate of the erodibility coefficient based on the jet index value. Hanson and Cook (2004) provided more comprehensive details regarding the jet apparatus, testing procedure and analysis as well as a method for determining the critical shear stress from testing.

Hanson and Hunt (2007) conducted jet tests on reconstituted soils over a range of water contents and compaction efforts. The erodibility coefficient was found to be at a minimum at the optimum water content for standard compaction. Also, values of the erodibility coefficient from the JET agreed well with values determined from field embankment erosion tests.

In an effort to further refine the device for field use, a "mini" JET apparatus was developed and compared against the original JET device by running tests on duplicate samples (Al-Madhhachi et al., 2011). Values for the erodibility coefficient compared well, however the "mini" device appeared to estimate critical shear stress values that were less than the original device. Simon et al. (2010) compared 822 tests using the original JET to 279 tests using the "mini" JET apparatus and determined that the relationship between the erodibility coefficient and critical shear stress between the two sample groups was not statistically different.

More recently, research has been conducted to understand the velocity and stress distributions in a variety of scour hole sizes using Computational Fluid Dynamics (CFD). Weidner et al. (2012) used a CFD numerical model to determine how the scour hole shape affects the applied shear stress. A variety of scour hole shapes were modelled and it was found that deviations between the maximum shear stress on a flat plate were greater when compared with narrow holes as opposed to wide holes. Mercier et al. (2013) developed a two-dimensional CFD numerical model of a circular submerged turbulent jet that is able to simulate the time development of scour. This model was validated for impingement on a flat, solid plate, the results were compared with Hanson and Cook (2004), and finally, used to study the influence of the erosion parameters on the temporal aspects of erosion and the scour hole shape.

### 2.2.2 Jet Test Applications

Given the JET's ability to be used not only for laboratory applications, but also for in situ testing, a number of field studies have been conducted on natural soils. Hanson and Simon (2001) applied the in situ test to three degrading channels and found substantial variation in critical shear stress between river bed materials in the same system and also between systems. Shugar et al. (2007) used an in situ jet to determine how hydrologic changes in an urbanized watershed would affect the susceptibility for channel erosion.

Wynn (2004) used an in situ jet testing device on stream banks to evaluate the effect of vegetation type and root-length density on erodibility. Clark and Wynn (2007) conducted 142 in situ, multi-angle, jet test runs in order to compare the resulting erodibility parameters to the Shields' diagram method and four other empirical equations. Erodibility parameters from testing were much higher than the predictive methods used, suggesting that these methods are site specific. The application of the in situ jet test in this study was not restricted to level surfaces, but in some cases conducted on channel banks with steep slopes.

Thoman and Niezgoda (2008) used an in situ jet test at 25 sites along cohesive channels and then developed a relationship between site characteristics and the critical shear stress for regional use. Karmaker and Dutta (2011) conducted 58 in situ JET along a composite river bank, using the estimated erodibility parameters to calculate the yearly bank erosion and compare with the reported range of erosion. Test durations in both of these cases were similar to the methodology presented in Hanson and Cook (2004). Khan and Kostaschuk (2011) conducted over 50 in situ JETs in two urbanized watersheds in order to study the spatial variation of erosion resistance. The authors attempted to develop a linear regression equation between the erodibility parameters and the shear strength and percent fines. Test durations ranged from 12 to 165 minutes.

Chang et al. (2011) conducted 27 jet tests at two active landslide dam locations in order to determine their susceptibility to erosion compared to the natural alluvial material and the important factors that influence the erodibility.

### 2.2.3 Comparison Studies between the Jet Test and Other Devices

Since a number of devices are currently being used for testing cohesive soil erosion, there have been several studies conducted that have tested paired soil samples on separate devices and compared the resulting soil erodibility parameters. A couple notable studies have been conducted using the HET and JET that are worth mentioning. Wahl (2010) compared the JET and HET on a set of remolded cohesive soil samples and found that while the erodibility rankings were similar for most tests, the HET produced a higher critical shear stress and erodibility coefficient for all tests. The HET was also more difficult to successfully carry out and the JET was found to be

more applicable for characterizing a wider range of soils. Marot et al. (2011) found that on average the HET critical shear stress was about 50 times higher than the JET critical shear stress for 17 tests run with both devices. An erosion resistance index was proposed based on the energy dissipation due to erosion from both devices which produced similar classifications between the HET and JET.

### 2.2.4 Theory and Operation of a Jet Erosion Test

The erodibility parameters from Equation [2-1] can be evaluated using a jet erosion test, the underlying theory of which is based on work by Beltaos and Rajaratnam (1974) and Rajaratnam (1976). These works describe the hydraulics of a vertical circular turbulent jet submerged in a body of water and impinging on a flat surface (Figure 2-1).

A submerged jet can be classified as turbulent based on the value of the jet Reynolds number defined as $R = U_o\, d_o/\nu$, where $U_o$ is the nozzle velocity, $d_o$ is the nozzle diameter and $\nu$ is the kinematic viscosity. Rajaratnam and Flint-Petersen (1989) defined a fully developed turbulent jet as having a jet Reynolds number greater than 10,000, at which point the spreading angle of the jet is constant and the laminar length along the centerline is very small as the jet becomes turbulent close to the nozzle. Under these conditions, the velocity at the nozzle can be assumed as uniformly distributed over the full nozzle diameter, with a turbulent shear layer forming around the nozzle circumference as the issuing jet interacts with the surrounding stagnant fluid. This shear layer grows in the transverse direction with increasing distance, $x$, from the nozzle (Rajaratnam, 1976). A cone of constant velocity, called the potential core, extends from the nozzle some distance, $x_p$.

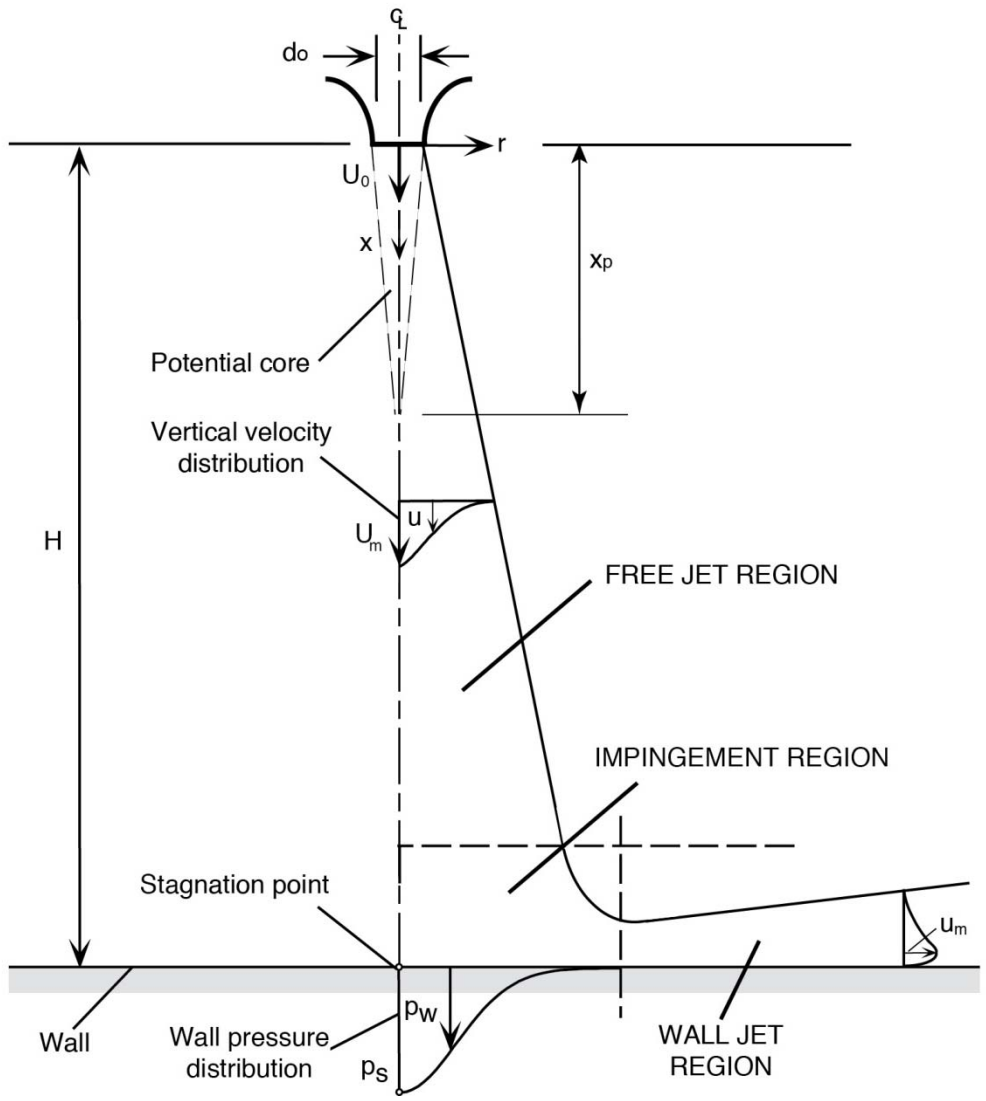


Figure 2-1. A vertical submerged circular turbulent jet impinging on a flat boundary (adapted from Rajaratnam and Mazurek, 2005).

Beyond the potential core, the shear layer envelopes the jet centerline and the centerline velocity begins to decay with increasing distance from the nozzle. At this point, the flow is considered fully developed and Beltaos and Rajaratnam (1974) give the velocity distribution along the centerline as:

$$\frac{U_m}{U_o} = C_d \left(\frac{d_o}{x}\right) \quad \text{for } x > x_p \qquad [2\text{-}2]$$

where $U_m$ is the maximum velocity at a distance, $x$, from the nozzle and $C_d$ is the diffusion coefficient. Values for $C_d$ range from 5.8 - 7.3 with a commonly accepted average of 6.3 for a fully developed turbulent jet (Beltaos and Rajaratnam, 1974). Using Equation [2-1], the length of the potential core is then determined to be $x_p = 6.3d_o$ when $U_m = U_o$ at $x = x_p$.

The threshold between the free jet region and the impingement region is about 0.86 $H$ from the nozzle. Past this threshold the presence of the wall begins to have an effect and the decay of the centerline velocity deviates from Equation [2-2] reaching a velocity of zero and a pressure of $p_s$ at the stagnation point where the centerline intersects with the wall. A pressure distribution is imposed along the boundary in the impingement region which acts to turn the vertical stream so that it flows parallel to the boundary in the wall jet region. The transition between the impinging region and wall jet region has been defined as $r/H \approx 0.22$ by Beltaos (1974).

Inside the impingement region a shear stress distribution is also imposed along the wall from zero at the stagnation point to a maximum shear stress, $\tau_{om}$, occurring at $r/H \sim 0.14$ from the centerline (Rajaratnam, 1976). The value for the maximum shear stress on the bed is then determined using the local skin friction coefficient, $c_f$, to give:

$$\tau_{om} = c_f \rho U_m^2 \qquad [2\text{-}3]$$

where $\rho$ is the fluid density. By assuming that velocity decays like a free jet in the impingement zone such that $x = H$, then Equation [2-2] can be combined with Equation [2-3] to give the maximum shear stress on the bed:

$$\tau_{om} = c_f \rho \left( C_d U_o \frac{d_o}{H} \right)^2 \quad H > x_p \qquad [2\text{-}4]$$

For a circular impinging jet the value of $c_f$ can be taken as 0.00416 based on Hanson et al.'s (1990) study of shear stresses along a smooth boundary.

If the flat, solid boundary is replaced with an erodible soil, and the jet test is run with a nozzle velocity such that the maximum shear stress on the soil surface exceeds the soil's critical shear stress, then a scour hole will begin to form. The scour hole can be defined by its centerline ($\varepsilon_{cl}$) and maximum ($\varepsilon_m$) depths as measured from the original soil surface, its average radius ( $\bar{r}$ ), and its volume ($V_s$). A definition sketch is shown in Figure 2-2 where $r$ is the radial distance from the jet axis and $\varepsilon$ is the depth measured from the original soil surface. The height from the nozzle to the original soil surface from the initial set up conditions is defined as $H_i$. As scour progresses in the sample and the depth increases, the jet velocity and therefore the maximum shear stress acting on the soil surface decreases. The applied shear stress on the surface can be designated as the critical shear stress once it has decreased to the point of no longer being able to cause scour.

One of the main assumptions implied in attributing incipient motion in the soil to the maximum applied shear stress is that the effect the wall pressure distribution has on erosion is minor.

In the standard laboratory JET test, outlined in ASTM Standard D 5852 (2007), a 13 mm nozzle is suspended 0.22 m from a sample surface which has a diameter of 0.44 m. A constant head tank feeds into the nozzle, which produces a jet that impinges on the sample surface. The recommended head on the jet is 0.91 m, though other heads may be used. A test timing sequence of 10, 20, 30, and 60 minutes is used for a total test duration of 120 minutes. A pin profile is taken after each time sequence. Other time sequences can be used at the discretion of the operator. Hanson and Cook (2004) use time intervals of 5 or 10 minutes and recommend a set of 10 to 12 readings. A point gage can be lowered through the nozzle in order to take centerline depth readings instead of using a pin profiler.

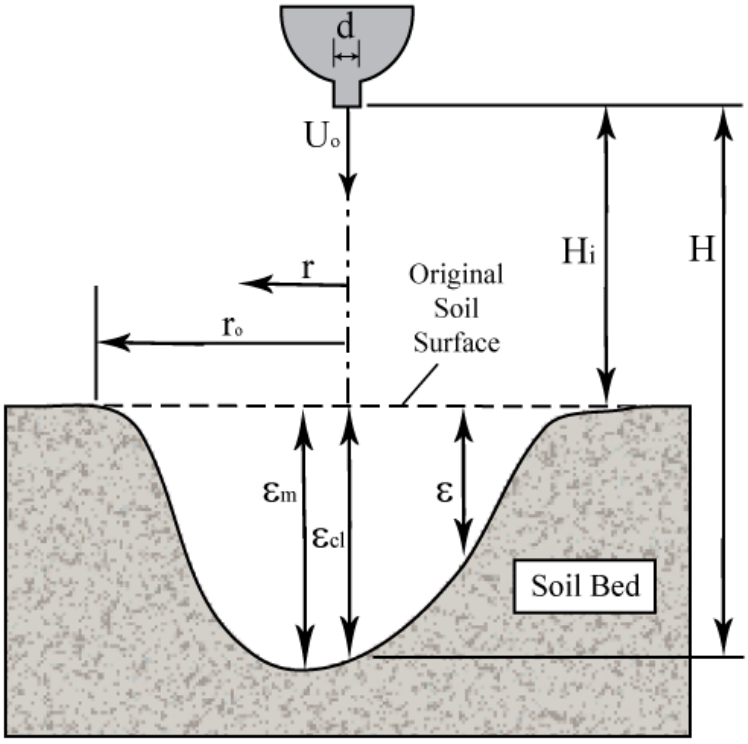


Figure 2-2. Scour hole definition sketch (adapted from Mazurek and Hossain, 2007)

## 2.3 DETERMINING CRITICAL SHEAR STRESS FROM JET TESTING

The jet test can be used to determine the critical shear stress of a soil and is typically done one of two ways. The first is by observing the point at which scour begins, estimating the maximum boundary stress at that point, and designating it as the critical shear stress. The second is by observing or estimating the ultimate state or equilibrium depth from a sample that has been subject to scour and again estimating the boundary stress at this point. This study considers four different methods for determining critical shear stress.

### 2.3.1 Hanson and Cook's (2004) Method, $\tau_{c\_B}$

Hanson and Cook (2004) presented a procedure for estimating the critical shear stress of a soil (designated $\tau_{c\_B}$ from here on) from the growth of the centerline scour depth with time, which is one of the most commonly used method for determining $\tau_c$ from a jet test. Hanson and Cook (1997) provided details on how the method was developed. This was based on Stein et al.'s (1993) theory for the time development of scour produced by obliquely impinging plane jets and

the hydraulics of a jet impinging on a flat boundary. The maximum shear stress from Equation [2-4] is applied to the soil surface assuming that the centerline jet velocity decays like a free jet in the scour hole, which is not quite the case. Along a solid boundary a vertical jet would be turned into a horizontal wall jet after impingement. In a scour hole, however, this wall jet is turned back on itself which would cause further centerline velocity decay than is predicted in Equation [2-2]. This suggests that the critical shear stress determined from Equation [2-4] may be overestimated.

Hanson and Cook (2004) assumed that there will be some scour depth that can be deemed the equilibrium scour depth, which will occur when the maximum shear stress on the bed is equal to $\tau_c$. If the maximum shear stress on the bed is equal to $\tau_c$, then scouring ends. If $H_e$ is the distance from the nozzle to the soil bed along the jet centerline at equilibrium scour, and the tests were run at a large jet impingement height ($H_i/d_o$ > 8.3) such that the potential core is not impinging on the soil surface, then one would find:

$$\tau_{c\_B} = c_f \rho C_d^2 U_o^2 \left(\frac{d_o}{H_{e\_B}}\right)^2 \quad [2\text{-}5]$$

However, in the standard JET, the tests are not run until equilibrium is reached. Instead, the equilibrium height is determined from the curve fitting approach developed by Blaisdell et al. (1981) and herein designated as $H_{e\_B}$. This work proposed a hyperbolic logarithmic equation for the relationship between the centerline scour depth and time given as:

$$(f - f_o)^2 - x^2 = A^2 \quad [2\text{-}6]$$

where:

$$f = log\left(\frac{H}{d_o}\right) - log\left(\frac{U_o t}{d_o}\right) \quad [2\text{-}7]$$

$$f_o = log\left(\frac{H_{e\_B}}{d_o}\right) \quad [2\text{-}8]$$

$$x = log\left(\frac{U_o t}{d_o}\right) \quad [2\text{-}9]$$

and $H$, $d_o$, $U_o$ and time, $t$, are measured values used to calculate $x$ and $f$. The constant, $f_o$, can then be evaluated iteratively by determining the value, $A$, for every scour measurement and then minimizing its standard deviation in order to find the best fit. The corresponding depth, $H_{e\_B}$, is then designated as the ultimate state and is an estimate of the scour hole depth at infinite time. Mazurek (2010) ran nine jet tests on a single type of manufactured clay and found that the critical shear stress determined from Blaisdell et al.'s (1981) method could vary by up to 45% of the average value.

### 2.3.2 Visual Method, $\tau_{c\_V}$

A vertical submerged circular turbulent impinging jet has also been used for determining the critical shear stress based on visual observation (designated $\tau_{c\_V}$ from here on) of mass erosion on a sample surface (Dunn, 1959). Using Beltaos and Rajaratnam's (1974) theory, which is similar to Hanson and Cook's (2004) method, Equation [2-4] for the maximum shear stress on the boundary can be modified to:

$$\tau_{c\_V} = c_f \rho C_d^2 U_{oc}^2 \left(\frac{d_o}{H_i}\right)^2 \qquad [2\text{-}10]$$

where $U_{oc}$ is jet velocity at the nozzle for which mass erosion is observed on the surface of the sample. This critical velocity can be determined from the un-scoured sample before the jet test is run. The jet is positioned above the sample and flow rate is increased incrementally from near zero to a value where mass erosion is observed from the sample surface. The nozzle velocity of the jet at which mass erosion first occurs is designated as the critical velocity. This approach is dependent on the operator's judgment for determining when mass erosion occurs; however, the hydraulic conditions more closely follow the assumptions made in Equation [2-4], which is that the jet is impinging on a flat, rigid boundary instead of a scour hole.

### 2.3.3 Equilibrium Method, $\tau_{c\_Ec}$

Following Hanson and Cook (2004), studies by Mazurek and Gheisi (2009) and Mazurek (2010) also assumed that if the scour hole had reached its equilibrium size, the shear stress on the scour hole must be equal to the critical shear stress of the soil. However, as an alternative to using Blaisdell et al.'s (1981) ultimate scour depth at infinite time, the jet test is run until a plot of the scour depth with time reaches a horizontal asymptote and the sample appears to stop scouring. Once this equilibrium state is reached the centerline scour depth relative to the original bed level, $\varepsilon_{cl\infty}$, can be measured and the critical shear stress can be written as:

$$\tau_{c\_Ec} = c_f \rho C_d^2 U_o^2 \left(\frac{d_o}{H_i + \varepsilon_{cl\infty}}\right)^2 \qquad [2\text{-}11]$$

The critical shear stress determined from this method is designated $\tau_{c\_Ec}$ from here on. The measured equilibrium height between the jet nozzle and the sample surface at the centerline can be expressed as $H_{e\_m} = H_i + \varepsilon_{cl\infty}$. One of the main challenges with this method is that it is subject to the operator's judgment in determining if a sample has reached equilibrium state. Since equilibrium state is reached asymptotically the scour hole may take a long time to stop eroding and, theoretically, the ultimate scour state may never be reached due to the random nature of turbulent flow. Blaisdell et al. (1981) found that scour continued in some samples even after 14 months. Since it is possible that a sample deemed to reach equilibrium state using a graphical approach could be terminated prior to actually reaching its ultimate state, this method is likely biased towards overestimating the critical shear stress. Mazurek (2010) tested manufactured clay samples to equilibrium and found that Blaisdell et al.'s (1981) method produced values of critical shear stress which were approximately half of what the equilibrium method predicted.

### 2.3.4 Thomas' Method, $\tau_{c\_T}$

A graphical method for determining the critical shear stress for cohesive soils using the data produced from a jet-type test was suggested by Robert Thomas (Personal Communication, 2010). In this method the critical shear stress is determined by plotting the average shear stress against the erosion rate collected from testing and extrapolating to an erosion rate of zero.

At every time interval for the jet test, the average maximum bed shear stress ($\tau_{avg}$) can be calculated as:

$$\tau_{avg} = c_f \rho C_d^2 U_o^2 d_o^2 \frac{\left(\frac{1}{H_{j-1}} - \frac{1}{H_j}\right)}{\left(H_j - H_{j-1}\right)} \quad [2\text{-}12]$$

where $H_j$ is the measured height from the nozzle to the soil surface along the jet centerline that corresponds to the $j^{th}$ reading taken during jet testing ($j \geq 1$) and where $H_0$ represents the initial setup conditions before testing began (ie. $H_i$). The corresponding erosion rate was taken as the change in height with time:

$$\dot{E} = \frac{\left(H_j - H_{j-1}\right)}{\left(t_j - t_{j-1}\right)} \quad [2\text{-}13]$$

where $t_j$ is the elapsed time corresponding to the $j^{th}$ reading taken during jet testing ($j \geq 1$).

If the erosion rate is plotted against the average maximum bed shear stress the critical shear stress can be determined by extrapolating a best fit line to an erosion rate of zero as seen below in Figure 2-3. The critical shear stress determined in this manner is designated as $\tau_{c\_T}$ from here on.

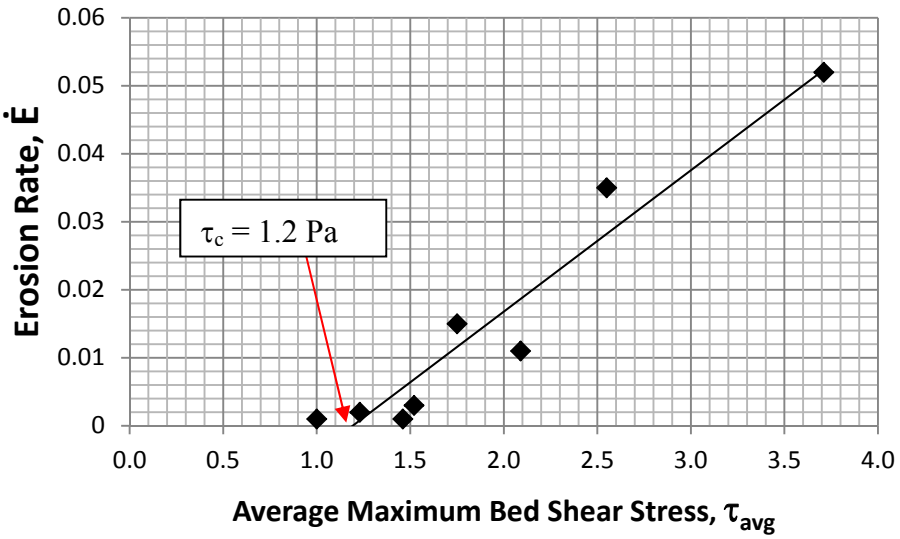


Figure 2-3. Graphical analysis for determining critical shear stress

## 2.4 DETERMINING THE ERODIBILITY COEFFICIENT FROM JET TESTING

Once a soil's critical shear stress is determined from the jet test, the erodibility coefficient can then be resolved. Hanson and Cook (1997) wrote the excess shear stress equation as:

$$\frac{dH}{dt} = k(\tau_e - \tau_c)^n \qquad [2\text{-}14]$$

where the erosion rate is defined as the change in height between the nozzle and bed with time. This model applies only to the case where the effective shear stress is greater than the critical shear stress as erosion rates cannot be negative.

### 2.4.1 Hanson and Cook's (2004) Method, $k_H$

Hanson and Cook's (2004) method to determine the erodibility coefficient, $k$, finds a solution to the differential Equation [2-14] with exponent, $a$, equal to one, and closely follows Stein et al. (1993) in order to develop an equation between the dimensionless height of scour and dimensionless time given as:

$$\frac{t_m}{T_r} = \left[0.5 \ln\left(\frac{1+H^*}{1-H^*}\right) - H^* - 0.5 \ln\left(\frac{1+H_i^*}{1-H_i^*}\right) + H_i^*\right] \quad [2\text{-}15]$$

$$T_r = \frac{H_e}{k\tau_c} \quad [2\text{-}16]$$

$$H^* = \frac{H}{H_e} \quad [2\text{-}17]$$

$$H_i^* = \frac{H_i}{H_e} \quad [2\text{-}18]$$

where $t_m$ is the measured time from testing since scour began, $H$ is the depth of scour from the nozzle to the bed at any time of scour, and $H_i$ is the initial height from the nozzle to the original bed. Using the value of $\tau_c$ and $H_e$ from Blaisdell et al.'s (1981) method, a solution can be found for the erodibility coefficient, referred to as $k_H$ for this method, by minimizing an error function between the measured data and Equation [2-15].

Hanson and Cook (1997) also considered an approach where both the critical shear stress and the erodibility coefficient are solved simultaneously in Equation [2-15] using a curve fitting routine; however, it was found to produce multiple answers depending on the initial parameters selected. It should be noted that Mazurek (2010) tested samples to equilibrium state and found that the erodibility coefficient calculated in this manner strongly depended on the test duration and that values of $k$ decreased as more data points were added into the analysis. The difference between using 8 hours of data or 116 hours of data resulted in an order of magnitude change in the erodibility coefficient.

### 2.4.2 Thomas' Method, $k_T$

Thomas's method for determining the erodibility coefficient is again a graphical solution which estimates $k$ and $n$ from Equation [2-14] by fitting a power curve to the experimental data. The erodibility coefficient for this method is referred to as $k_T$ from here on. By using the critical shear stress determined from the jet test and calculating the average maximum shear stress on the

bottom of the scour hole using Equation [2-12], the excess shear stress can be expressed as ($\tau_{avg} - \tau_{c\_T}$), as seen in Figure 2-4.

Although the excess shear stress equation is often assumed to be linear, this is not always the case. Research has shown that the exponential term can vary between 1.0 and 6.8 (Knapen et al., 2007). This method allows the exponential term to be solved for in addition to $k$ instead of assuming it to be unity as in Hanson and Cook (2004).

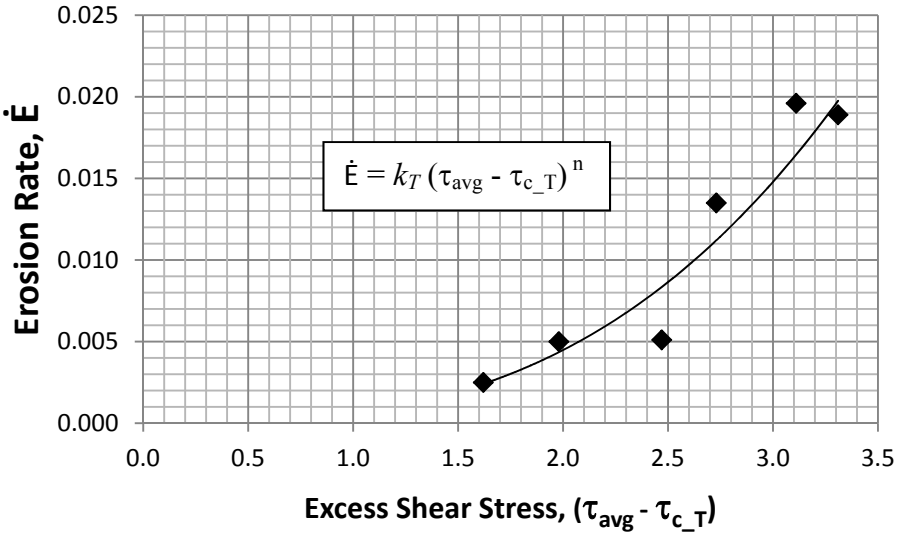


Figure 2-4. Graphical solution for the erodibility coefficient and exponential term from the excess shear stress equation

## 2.5 SCOUR ASSESSMENT IN COHESIVE SOIL

Information regarding the anticipated spatial extents of a scour hole is not provided by just determining the threshold for initiation of soil erosion and the rate of erosion. Only a few researchers have studied the problem of scour in cohesive soils using jets. The jets used for this research have used a number of nozzle shapes and sizes, jet orientations and tail water levels. Abt (1980) studied scour at a culvert outlet in one type of soil. Hedges (1990) studied the scour problem of ship thrusters in narrow channels using an inclined jet. Stein (1990) used inclined plane impinging jets to further understand the mechanics of headcut migration. Given the large

number of factors influencing scour, it is a common approach to use dimensional analysis for defining the significant terms followed by experimentation in order to develop empirical solutions.

### 2.5.1 Moore and Masch (1962)

Moore and Masch (1962) use a submerged vertical circular jet impinging on a horizontal soil sample surface to study scour both natural and remolded cohesive soils. In the tests, 127 mm diameter and 102 mm high cylindrical samples were used. Tests were run for fully turbulent jet conditions and large impingement heights with nozzle velocities in the range of 0.63 to 8.4 m/s. Total test durations were at least 60 minutes with measurements taken every 10 minutes. At each interval the sample was weighed, which allowed the scour hole volume to be determined by measuring the soil density. The average scour hole depth was determined by taking the cube root of the scour volume.

Moore and Masch (1962) suggested that the average scour depth, $\overline{\varepsilon}$, could be expressed as:

$$\bar{\varepsilon} = f_1\{U_o, d, H_i, \rho, \mu, \sigma_s, t\} \qquad [2\text{-}19]$$

where $\mu$ is the dynamic viscosity of the fluid, $\sigma_s$ is the resistance property of the soil with dimensions of a stress, and $t$ is the test duration. Using dimensional analysis it was found that:

$$\frac{\bar{\varepsilon}}{H_i} = f_2\left\{\frac{t\mu}{\rho d^2}, \frac{\rho U_o d}{\mu}, \frac{H_i}{d}, \frac{\sigma_s \rho d^2}{\mu^2}\right\} \qquad [2\text{-}20]$$

where the dimensionless average scour hole depth is a function of four dimensionless terms: time factor, velocity factor, jet height factor and soil erodibility factor.

### 2.5.2 Hanson (1990B)

Hanson (1990b) developed an in-situ submerged vertical circular turbulent jet device for evaluating erodibility and scour in cohesive soils. Four soils were tested for which the erodibility

coefficients had already previously been determined using an open channel test (Hanson 1990a). The jet tests were run at a constant height and diameter ($H_i/d$ = 16.9) and scour hole profiles were measured at 10, 30, 60, and 100 minute intervals for a total test duration of 200 min with an 1000 minute interval was added to the end of the test for more scour resistant soils.

An analysis similar to that of Moore and Masch (1962) was followed for developing the dimensionless parameters used to describe scour. The main difference is that the soil resistance parameter, $\sigma_s$, is replaced with the erodibility coefficient, $K$, in the soil erodibility factor. The relation is given as:

$$\frac{\sqrt[3]{\xi}}{H_i} = f_1\left\{\frac{t\mu}{\rho d^2}, \frac{\rho U_o d}{\mu}, \frac{H_i}{d}, \frac{\mu K}{d}\right\} \qquad [2.21]$$

where $\xi$ is the volume of material removed by scour. As $H_i/d$ is held constant, and $K$ was determined by large scale open channel testing (Hanson, 1990a) an empirical relationship between the three remaining factors and the dimensionless average scour hole depth was developed based on three of the tested soils:

$$\frac{\sqrt[3]{\xi}}{H_i} = 0.0436\left(\frac{\rho U_o d}{\mu}\right)^{0.67}\left(\frac{t\mu}{\rho d^2}\right)^{0.67}\left(\frac{\mu K}{d}\right)^{0.138} \qquad [2.22]$$

The results for the fourth soil were used as a check on the newly developed equation and it was found that the observed and predicted average scour hole depths for this soil had a significant agreement. By rearranging Equation [2.22] to solve for $K$, this approach was recommended for use at other sites for determining the erodibility coefficient, presumably under the assumption that the erodibility coefficient was the only term dependent on the soil characteristics. This method assumes a linear relationship between the erosion rate and the excess shear stress. Although Hanson (1990b) uses this method for determining the erodibility coefficient of soils, if $K$ were determined by an alternate method, then it seems logical that Equation [2.22] could be used for estimating the average scour depth for a given test duration.

### 2.5.3 Mazurek (2001)

Mazurek (2001) studied jet scour in a single manufactured pottery clay using an impinging jet. The submerged vertical circular turbulent impinging jet was run at either 4 or 8 mm nozzle diameters with nozzle velocities ranging from 4.97 to 25.9 m/s. Jet Reynolds numbers were kept in the range of 26000 to 98500 and test temperatures varied from 3.5 to 23.6ºC. Samples were tested at large impingement heights only ranging from values for $H_i/d$ of 8.1 to 29.0. Samples were 244 mm long, 175 mm wide and 85 mm high. Eroding water conductivity and pH were monitored for each test.

The maximum scour depth, centerline scour depth and scour hole volume were measured at 2 min, 5 min, 15 min, 30 min, 1h, 2h, 4h, 8h, 24h, 48h, 72h and 96h from the beginning of the test. Measurements were then taken at 24h intervals until equilibrium conditions were reached (volume and depth constant for 24h). Volume measurements were taken by filling the empty scour hole with water from a graduated cylinder and depth measurements were taken by touching a small wooden rod to the scoured surface and measuring the distance to the watermark. At the end of the test two cross sectional profiles were taken as well as two vane shear strength tests. Water contents were taken before testing, after soaking (if necessary) and after testing.

Since Beltaos and Rajaratnam (1974) found that the jet characteristics in the impinging region for a large impingement height depend on the momentum flux of the jet ($M_o = \pi / 4\rho U_o^2 d^2$), it was suggested that:

$$\varepsilon_{m\infty} = f_1\{M_o, \rho, H_i, \mu, \tau_c\} \qquad [2.23]$$

where $\varepsilon_{m\infty}$ is the maximum scour depth at equilibrium state and the critical shear stress term was used to define the soil erodibility. Dimensional analysis of the functional relationship gave:

$$\frac{\varepsilon_{m\infty}}{H_i} = f_2\left\{\frac{\rho U_o^2}{\tau_c}\left(\frac{d}{H_i}\right)^2, \frac{U_o d}{\nu}\right\} \qquad [2.24]$$

where $\nu$ is the kinematic viscosity of the eroding fluid. It is known that the bed shear stress does not depend strongly on the Reynolds number in the impingement region (Beltaos and Rajaratnam, 1974) and so the second term in Equation [2.24] was neglected. Furthermore the first term of Equation [2.24] can be rewritten as a ratio of the maximum shear stress on the bed to the critical shear stress such that:

$$\frac{\varepsilon_{m\infty}}{H_i} = f_3\left\{\frac{\tau_{om} - \tau_c}{\tau_c}\right\} \quad [2.25]$$

Similar equations can be written for the centerline scour depth at equilibrium, average radius at equilibrium and the scour hole volume at equilibrium. Since Mazurek (2001) only uses manufactured pottery clays for testing, the empirical equations developed may not apply to natural samples that may contain fissures, layering, or are inhomogeneous. Furthermore, the equations for scour prediction are limited to jets with Reynolds number greater than 10,000 and large impingement heights. This approach is useful for predicting the scour hole size at ultimate state, however, given the absence of a time dependent factor, it cannot be used for estimating scour hole geometry during development.

### 2.5.4 Ansari et al. (2003)

Ansari et al. (2003) used a submerged, circular, vertical jet to study scour in non-cohesive and cohesive sediments. Samples were prepared by mixing a base material (medium sand) in various proportions with clay. Clay contents ranged from 10 to 60% in 10% increments. Tests were run using a nozzle diameter of 12.5 mm and a nozzle velocity of 1.7 or 2.0 m/s corresponding to jet heights 0.15 and 0.20 m respectively. Similar tests were run on the non-cohesive material. It is not explicitly stated how the test samples were determined to reach equilibrium.

Ansari et al. (2003) describes the temporal variation of the maximum scour depth in the cohesive soils as:

$$\frac{d_{sc}}{d_{smc}} = \left[sin\left(\frac{\pi t}{2T_c}\right)\right]^{m_c} \quad [2.26]$$

where $d_{sc}$ is the maximum scour depth at time $t$, $m_c$ is an exponential term, $T_c$ is the time required to reach equilibrium depth and $d_{smc}$ is the equilibrium depth at time $T_c$. The maximum scour depth at equilibrium is proposed to be a function of the maximum depth at equilibrium in noncohesive soils for the same flow conditions ($d_{sms}$), and a number of cohesive soil properties. The functional relationship is given as:

$$\frac{d_{smc}}{d_{sms}} = f\left(\frac{W}{W_*}, \frac{C_*}{\phi_*}, \frac{\gamma_d}{\gamma_\omega}\right) \quad [2.27]$$

where $C_*$ is the weighted cohesion and $\phi_*$ is the weighted internal friction given as:

$$C_* = \frac{P_c C_u}{(\gamma_s - \gamma_\omega) d_a} \quad [2.28]$$

$$\phi_* = \frac{P_c tan\ \phi_c + (1 - P_c) tan \phi_s}{tan\ \phi_s} \quad [2.29]$$

and $W$ is the antecedent moisture content, $W_*$ is the moisture content at saturation, $P_c$ is the percent clay, $d_a$ is the arithmetic mean size of cohesive sediment, $C_u$ is the cohesion, $\phi_c$ is the angle of internal friction of the sand, $\phi_s$ is the angle of internal friction of the clay, $\gamma_d$ is the dry density, $\gamma_\omega$ is the specific weight of water, and $\gamma_s$ is the specific weight of sediment. These soil properties as a group essentially define the erodibility of the cohesive soil rather than using an individual term such as the critical shear stress. The ultimate scour depth for noncohesive soil in Equation [2.27] is a function of four hydraulic test parameters (jet height, nozzle diameter, average velocity of the jet, mass density of the fluid) and two soil properties (mean particle diameter, mass density of the soil) as defined in Ansari et al. (2003).

It was found that the following equation fit the nonplastic soils (samples where the clay content was 20% or less) data with a maximum error of ± 20%:

$$\frac{d_{smc}}{d_{sms}} = 0.38\left(\frac{C_*}{\varphi_*}\right)^{0.3}\left(\frac{W}{W_*}\right)^{0.11}\left(\frac{\gamma_d}{\gamma_\omega}\right)^{2.0} \quad [2.30]$$

On the other hand, the maximum scour depth in samples with 30% to 60% clay content and which had values for the plasticity index ranging from 4 to 13 could be represented with the following relationship:

$$\frac{d_{smc}}{d_{sms}} \cong 1.5 \pm 0.3 \quad [2.31]$$

Similar empirical equations can be written for the scour hole volume at equilibrium. Since these equations were developed for predicting scour using mixed sands and clays, they likely are not applicable to natural soils and would only be valid for the range of data used in this study. Furthermore, application of this method is burdened by the need to conduct equivalent tests in noncohesive soil in order to determine the maximum scour dimensions in a cohesive soil.

### 2.5.5 Mercier et al. (2013, 2014)

More recently, 2D numerical models of circular impinging turbulent jets have been used to study the scour process in cohesive soils. Mercier et al. (2013) evaluated the impact of several turbulence models on the developed CFD model and compared the results to the case of a flat nonerodable plate for validation. It was found that the critical shear stress of the soil largely governed the shape and size of the scour hole and that when $\tau_c$ decreased both the zone affected by scour and the maximum scour depth increased. The erodibility coefficient had very little effect on the final shape and size of the scour hole, but initially governed the kinetics of the process. As scouring progressed, the time required to reach equilibrium state was also dependent on the critical shear stress.

Mercier et al. (2014) compared the CDF numerical results to experimental results from three cohesive soil samples tested in accordance with Hanson and Cook (2004). The erodibility parameters obtained from Hanson and Cook's (2004) method were used in the numerical model

which was found to predict the evolution of centerline depth within reasonable accuracy. The error in the final centerline scour depth between the numerical and experimental study was less than 25%.

# CHAPTER 3
# EXPERIMENTAL STUDY

This chapter presents a summary of the experimental program undertaken to evaluate scour produced by a submerged circular vertical turbulent impinging jet in natural and manufactured cohesive soils. All jet testing was conducted in the Hydraulics Laboratory in the College of Engineering at the University of Saskatchewan, Saskatoon, Canada.

The experimental jet apparatus used in this study is presented in Section 3.2. Included in Section 3.3 is a description of the three cohesive sample groups that were tested along with details on how and where they were collected. The general experimental methodology is given in Section 3.4. Section 3.5 summarizes the range of hydraulic conditions under which the samples were tested.

## 3.1 EXPERIMENTAL APPARATUS

The experimental apparatus consisted of a jet hung vertically over the center of a 1.2 m high and 1.1 m wide octagonal, Plexiglas tank. A table within the water tank was used to support the soil samples underneath the jet apparatus during testing such that the sample surface was at a distance $H$ from the nozzle. The jet apparatus was suspended from a steel frame on hinges so that it could be swung away from the centreline. In order to keep the jet in a vertical position during testing, an elastic cord held the hanging jet tight against an angle iron rod which was fixed across the top of the water tank. The hinges, elastic cord, and angle iron support allowed the jet to be pulled aside for measurements and then returned to the exact same position to resume testing. The apparatus was also suspended from a steel cable attached to a hand winch, allowing the jet to be raised out of, or lowered into, the tank. When the winch was fully lowered, the jet nozzle was positioned below the top edge of the octagonal tank keeping the nozzle submerged while the tank was full of water. Figure 3-1, Figure 3-2, and Figure 3-3 show the jet apparatus, plenum and water supply with their key components labeled.

In order to create the circular turbulent jet, City of Saskatoon tap water was pumped from the laboratory reservoir, to a 1.2 m by 1.2 m by 0.65 m constant head tank, which had an overflow line back to the laboratory reservoir. An LB 304 ½ horsepower centrifugal pump manufactured by Goulds Water Technology was used with a 38 mm diameter suction and discharge waterline to draw water from the constant head tank, through a magnetic flow meter and to the top of the jet plenum. The flow meter was a FMG-3000 Series Magmeter manufactured by OMEGA. The flow rate was controlled using a gate valve on the pump suction line. The jet plenum was 0.95 m long and contained 2 sets of flow straighteners along with an 8 mm circular nozzle at its end which were designed to attenuate turbulence and create a nearly uniform velocity at the outflow. The flow meter was used for setting or monitoring flow rates during testing; however, all discharges were also measured volumetrically.

During jet operation the water tank containing the test sample was kept full. The incoming discharge from the jet nozzle spilled over the top edge of the water tank, collected in a catch basin, and circulated back into the laboratory reservoir. In order to access the sample surface to collect measurements during testing, a drain line with a gate valve could be used to draw down the water level in the water tank, while a supply line could be used to fill the tank back up with tap water.

A square frame housing an optoNCDT 1700-750 Laser Triangulation Displacement Sensor manufactured by Micro-Epsilon (Figure 3-4) was constructed around the tank for the purpose of creating digital profiles of the sample scour holes. This sensor had a measuring range between 200 mm to 950 mm from the light source and a static resolution of 12.5 μm. The laser sensor was suspended from a motorized beam, which spanned the length of the frame and allowed the sensor to be positioned anywhere in the horizontal plane above the water tank. Both the positioning motor and laser sensor were controlled by a computer that could be used to set the extents and resolution of a grid pattern and then automatically collect depth measurements at each node. Amin and Mazurek (2016) provide a schematic of the experimental setup.

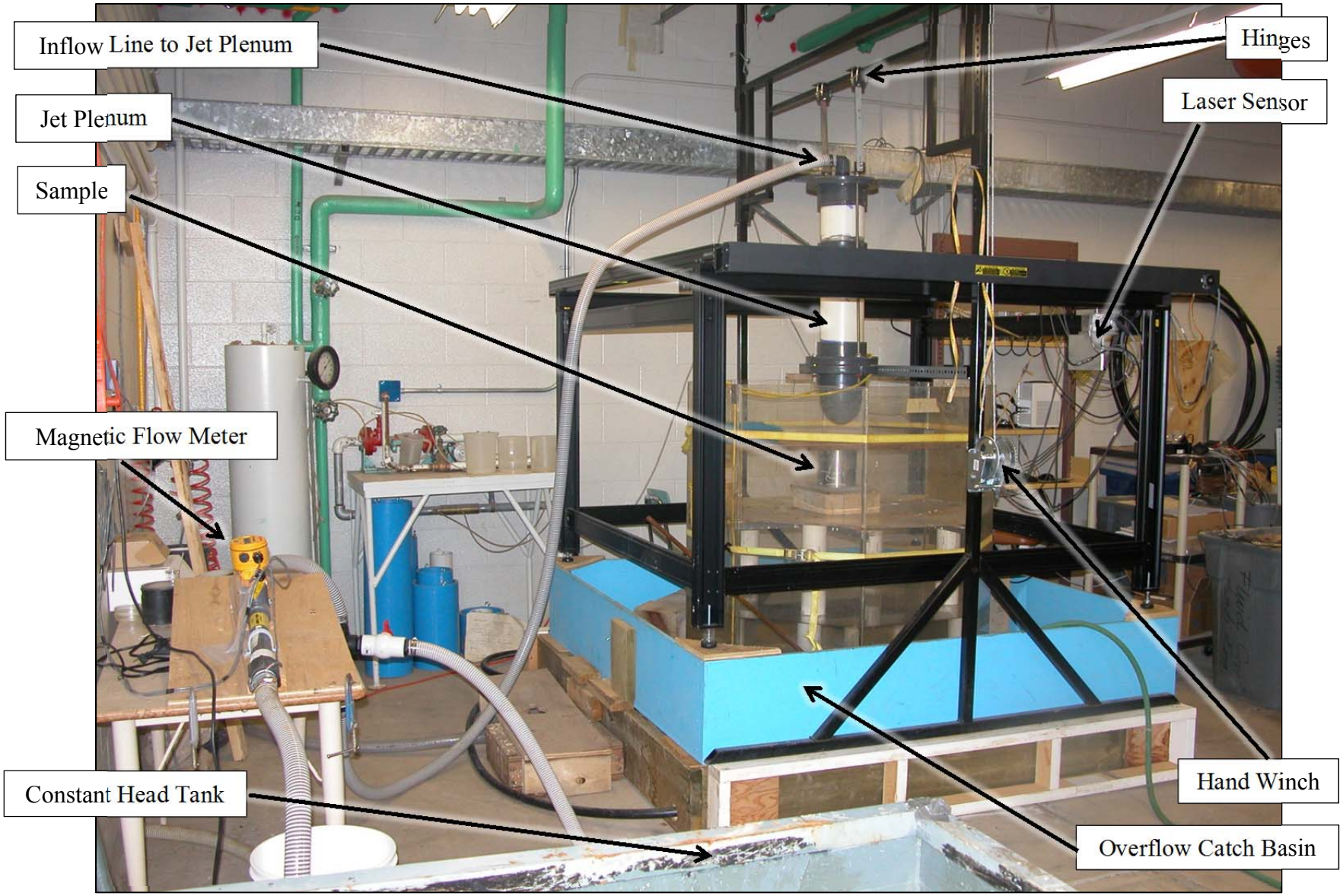


Figure 3-1. Jet apparatus

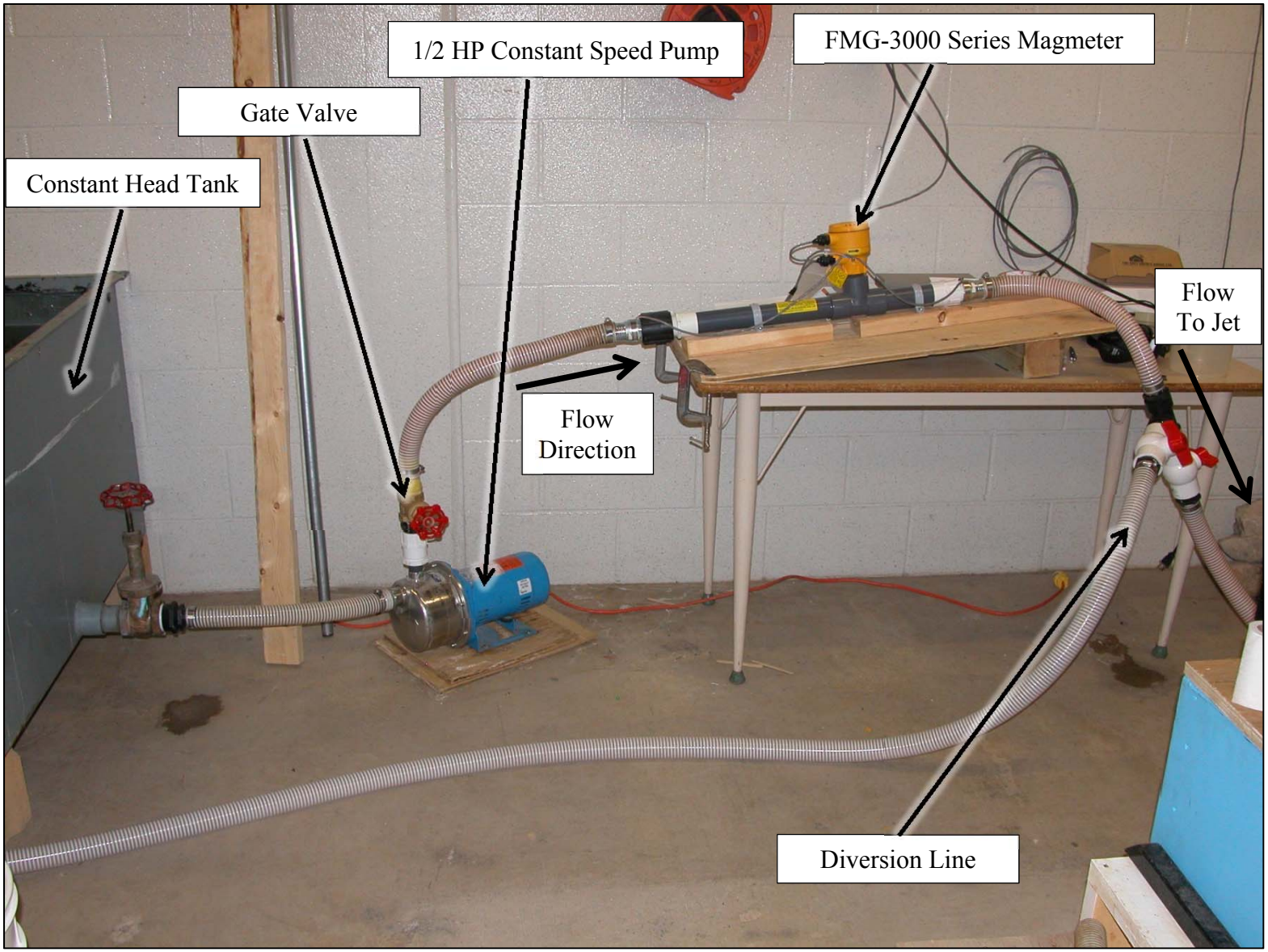


Figure 3-2. Water supply to jet apparatus

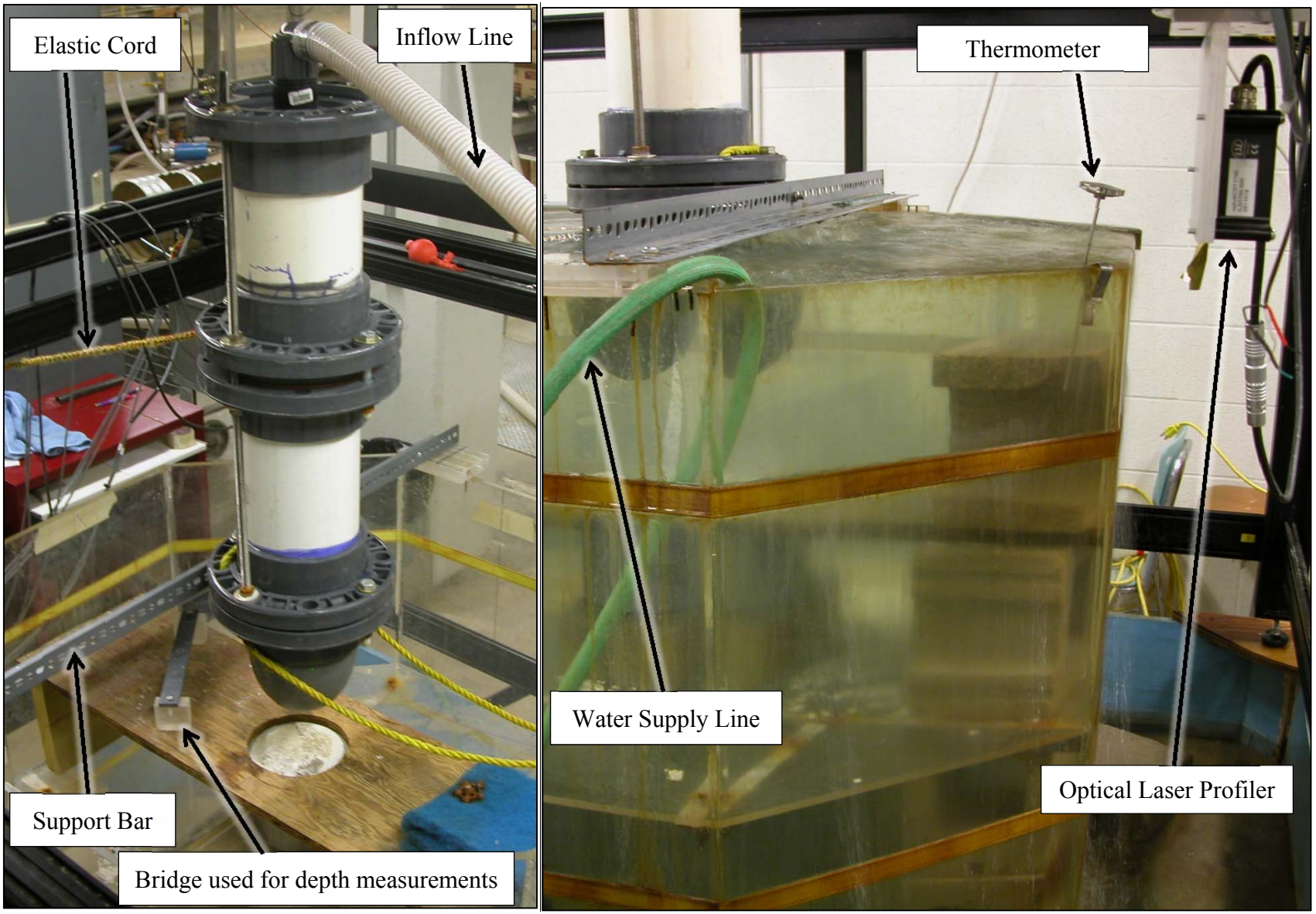


Figure 3-3. Jet plenum (left) and jet during testing (right)

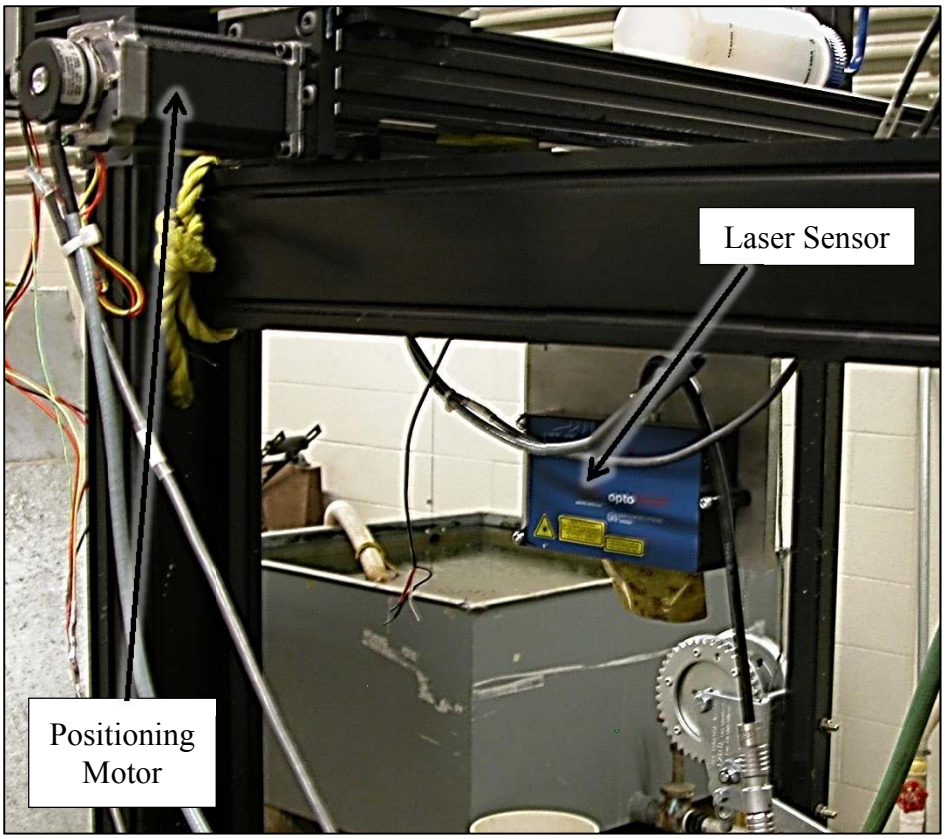


Figure 3-4. The positioning motor and laser sensor used for measuring scour depth

## 3.2 SOIL SAMPLES AND THEIR PROPERTIES

Three sets of soil samples were tested using the impinging jet: 14 samples collected in duplicate from the banks of 7 Ontario rivers, 4 samples collected in duplicate from 2 field locations outside of Saskatoon, SK, and 10 manufactured pottery clay samples tested in duplicate or triplicate. The first two sets, called the Ontario and Saskatoon samples, were natural, undisturbed, cohesive soils/sediments typically with the majority of the sample consisting of silt and clay sized particles. The third sample set consisted of uniform, pottery clays manufactured by Plainsman Clay Ltd.

The sample properties were classified using a number of soil tests. The bulk ($\rho_b$) and dry densities ($\rho_d$) were taken by the direct measurement method outlined in ASTM standard D7263-09 (2009). The soil grain size distribution and median particle diameter ($D_{50}$) was obtained from

a mechanical sieve and hydrometer analysis according to ASTM standard D421-85 (2007) and D422-63 (2007). Grain sizes were defined based on the ASTM standard D2487-11 (2011) Unified Soil Classification System (USCS), where medium sands are classified as being in the range of 2.0 to 0.425 mm, fine sands are 0.425 to 0.075 mm, silts are 0.075 to 5 μm, and clays are less than 5 μm. The liquid and plastic limits (LL and PL respectively) were determined following ASTM standard D4318-10 (2010). Figure 3-5 shows the plasticity chart along with the USCS classifications for samples in all three groups.

The water content of the soil samples were determined before ($w_o$) and after soaking ($w_p$) and after jet testing ($w_f$), following the methodology outlined in ASTM standard D2216-10 (2010). The soil samples were soaked before testing in order to saturate the samples and keep the water content consistent while being submerged during testing. Table 3-1 gives a summary of the soil properties for the samples in this study. It can be seen that the water content generally changed very little over the course of testing and most samples were saturated when testing began.

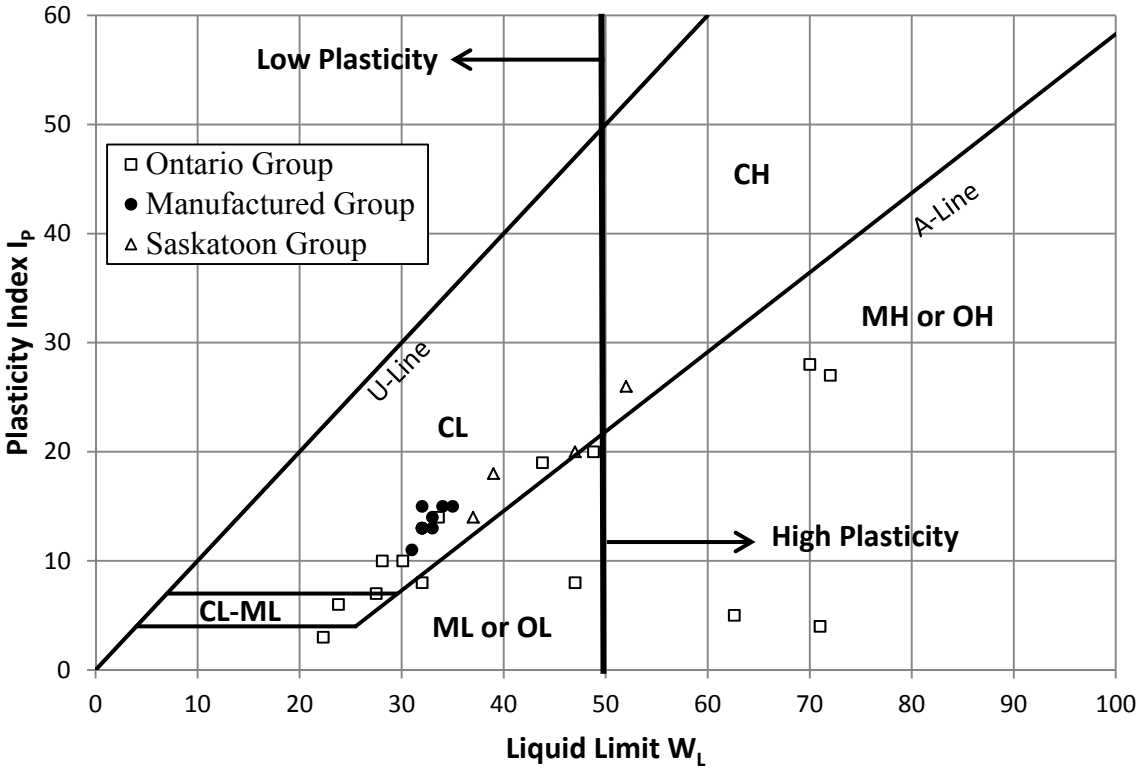


Figure 3-5. USGS plasticity chart and soil classifications for all three sample groups

Table 3-1. Soil properties of the clay samples

| Sample Origin | Group | Sample ID | > 2 mm (%) | Medium Sand (%) | Fine Sand (%) | Silt (%) | Clay (%) | PL (%) | LL (%) | PI (%) | USCS | $\rho_B$ (kg/m$^3$) | $\rho_d$ (kg/m$^3$) | $w_o$ (%) | $w_p$ (%) | $w_f$ (%) | $D_{50}$ (μm) |
|---|---|---|---|---|---|---|---|---|---|---|---|---|---|---|---|---|---|
| South Nation 1/2 | ONTARIO | SN(1) | 0 | 16 | 32 | 49 | 3 | 38 | 47 | 8 | ML | 1571 | 1036 | 49 | - | 51 | 73 |
| South Nation 2/2 | | SN(2) | 27 | 10 | 28 | 30 | 5 | 24 | 32 | 8 | ML | 1534 | 1114 | 27 | - | 36 | 164 |
| Wilton Creek 1/2 | | WC(1) | 0 | 0 | 21 | 65 | 13 | 18 | 28 | 10 | CL | 1881 | 1488 | 16 | - | 28 | 58 |
| Wilton Creek 2/2 | | WC(2) | 2 | 2 | 41 | 50 | 5 | 18 | 24 | 6 | CL-ML | 1961 | 1500 | 16 | - | 30 | 69 |
| Little Cataraqui 1/2 | | LC(1) | 1 | 12 | 3 | 70 | 15 | 29 | 49 | 20 | ML | 2180 | 1204 | 22 | - | 40 | 53 |
| Little Cataraqui 2/2 | | LC(2) | 1 | 8 | 10 | 64 | 17 | 25 | 44 | 19 | CL | 1882 | 1413 | 22 | - | 32 | 48 |
| SawMill Creek 1/2 | | SC(1) | 0 | 7 | 39 | 40 | 14 | 20 | 34 | 14 | CL | 1822 | 1443 | 31 | - | 26 | 71 |
| SawMill Creek 2/2 | | SC(2) | 1 | 6 | 43 | 37 | 13 | 20 | 30 | 10 | CL | 1858 | 1481 | 25 | - | 25 | 74 |
| SawMill Creek 2/2 repeat | | SC(2)R | (same as row above) | | | | | | | | | | | | | | - |
| Bear Brook 1/2 | | BB(1) | 0 | 0 | 29 | 58 | 13 | 20 | 28 | 7 | CL | 1899 | 1557 | 16 | - | 21 | 58 |
| Bear Brook 2/2 | | BB(2) | 0 | 1 | 37 | 56 | 6 | 19 | 22 | 3 | CL-ML | 1601 | 1241 | 3 | - | 27 | 64 |
| Bear Brook 2/2 repeat | | BB(2)R | (same as row above) | | | | | | | | | | | | | | - |
| Jock River 1/2 | | JR(1) | 0 | 4 | 33 | 61 | 2 | 57 | 63 | 5 | OH | 1250 | 480 | 136 | - | 136 | 57 |
| Jock River 1/2 repeat | | JR(1)R | (same as row above) | | | | | | | | | | | 132 | 212 | 196 | - |
| Jock River 2/2 | | JR(2) | 0 | 5 | 29 | 64 | 2 | 67 | 71 | 4 | OH | 1098 | 430 | 107 | 149 | 158 | 55 |
| Raisin River 1/2 | | RR(1) | 0 | 10 | 20 | 57 | 13 | 42 | 70 | 28 | OH | 2363 | 1319 | 69 | 90 | 117 | 56 |
| Raisin River 2/2 | | RR(2) | 0 | 8 | 25 | 53 | 14 | 45 | 72 | 27 | OH | 1155 | 626 | 67 | 131 | 91 | 58 |
| M-390-1 | MANUFACTURED CLAY | M-390(1) | 0 | 0 | 6 | 48 | 46 | 19 | 32 | 13 | CL | 2029 | 1606 | 24 | - | 28 | 5 |
| M-390-2 | | M-390(2) | 0 | 0 | 5 | 47 | 48 | 19 | 32 | 13 | CL | 2011 | 1601 | 25 | 29 | 31 | 5 |
| P-300-1 | | P-300(1) | 0 | 0 | 1 | 45 | 54 | 20 | 31 | 11 | CL | 1979 | 1551 | 27 | 29 | 31 | 4 |
| P-300-2 | | P-300(2) | 0 | 0 | 0 | 44 | 56 | 19 | 32 | 13 | CL | 1963 | 1564 | 25 | 29 | 42 | 3 |
| P-300-3 | | P-300(3) | 0 | 0 | 1 | 45 | 54 | 20 | 35 | 15 | CL | 1969 | 1565 | 26 | 33 | 34 | 4 |
| M-332-1 | | M-332(1) | 0 | 0 | 17 | 44 | 39 | 17 | 32 | 15 | CL | 2051 | 1654 | 23 | 29 | 34 | 7 |
| M-370-1 | | M-370(1) | 0 | 0 | 1 | 43 | 56 | 20 | 33 | 13 | CL | 1973 | 1570 | 25 | 36 | 35 | 4 |
| M-370-2 | | M-370(2) | 0 | 0 | 1 | 44 | 55 | 19 | 34 | 15 | CL | 2059 | 1663 | 23 | 27 | 34 | 3 |
| BSC-1 | | BSC(1) | 0 | 0 | 7 | 43 | 50 | 19 | 32 | 13 | CL | 1983 | 1576 | 25 | 31 | 30 | 4 |
| BSC-2 | | BSC(2) | 0 | 0 | 6 | 45 | 49 | 19 | 33 | 14 | CL | 1958 | 1549 | 25 | 37 | 29 | 4 |
| ECPSD-1 | SASK. | ECP(1) | 0 | 0 | 12 | 66 | 22 | 23 | 37 | 14 | CL | 1052 | 852 | 26 | 57 | 68 | 27 |
| LWSD-1 | | LW(1) | 0 | 0 | 9 | 52 | 39 | 27 | 47 | 20 | CL | 2392 | 1960 | 22 | 36 | 37 | 7 |
| ECPSD-2 | | ECP(2) | 0 | 0 | 11 | 70 | 19 | 21 | 39 | 18 | CL | 1353 | 1161 | 18 | 48 | 45 | 26 |
| LWSD-2 | | LW(2) | 0 | 0 | 3 | 53 | 44 | 26 | 52 | 26 | CH | 1729 | 1397 | 22 | 55 | 47 | 8 |

### 3.2.1 Ontario Sample Group

The Ontario samples consisted of duplicate riverbank samples from seven different rivers and streams in Ontario as seen in Figure 3-6: South Nation (SN), Wilton Creek (WC), Little Cataraqui (LC), Sawmill Creek (SC), Bear Brook (BB), Jock River (JR), and Raisin River (RR). These 14 samples were supplied by Dr. Colin Rennie of the University of Ottawa. They were collected in 150 mm diameter by 150 mm high thin-walled, stainless steel, cylindrical containers by driving the tube into the soil and then excavating the tube by hand. All samples were sealed with plastic-wrap for transportation to the hydraulics laboratory and then tested in the same containers.

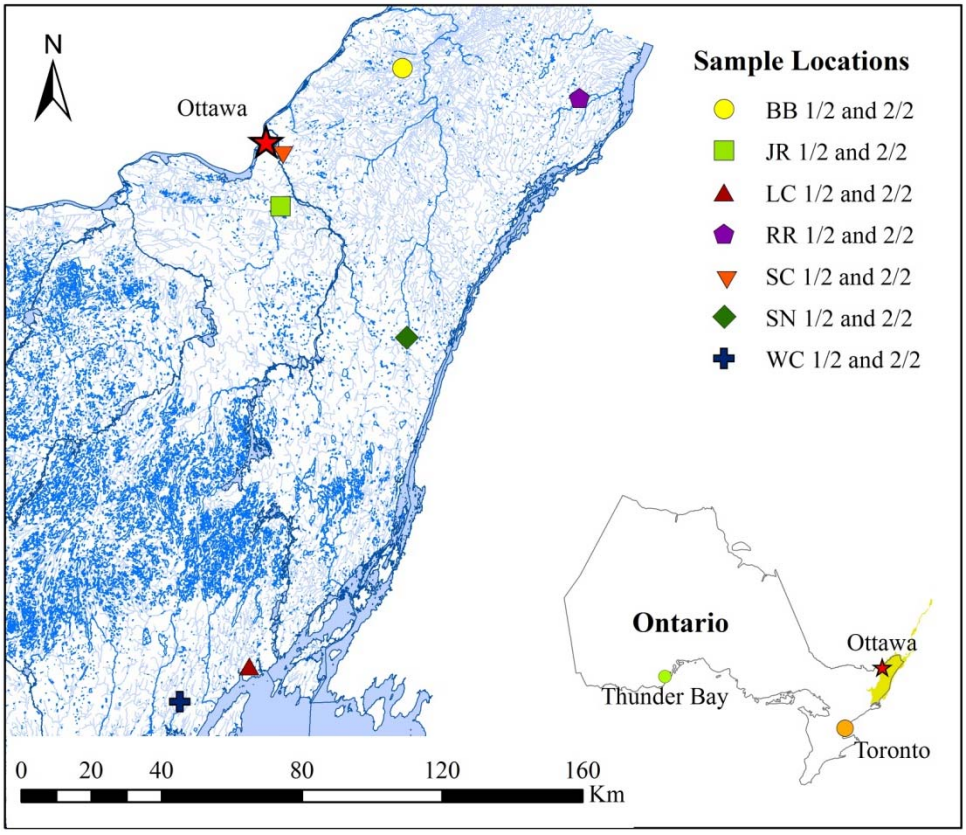


Figure 3-6. Sample collection locations for the Ontario Group

The Ontario samples can be described as clays and silts with clay content ranging from 2% to 17% and silt content ranging from 30% to 70%. Most samples were loosely compacted with bulk densities ranging from 1.25 to 2.36 g/cm$^3$. All samples displayed cohesive behaviour during testing, such as mass erosion and the formation of well-defined scour holes. Roots and vegetation

were present in most samples ranging in diameter from 1 to 15 mm and in volume from single roots to a network of roots permeating the whole sample.

### 3.2.2 Saskatoon Sample Group

In order to supplement the Ontario samples, four additional natural samples were collected from Saskatoon, Saskatchewan to be used for testing. These samples were taken from undeveloped fields in the Lakewood subdivision (LW) and the East College Park subdivision (ECP). Undisturbed block samples were collected and then transported to the hydraulics laboratory to be stored until ready for testing. Sample collection was performed similar to the procedure used by Mostafa et al. (2008) and photos of the process are given in Figure 3-7. First, the ground surface was cleared of vegetation and about 100 mm of topsoil was removed. A rough block of soil was formed using spades and hand tools by digging a trench around a rectangular perimeter. This block was then carefully trimmed until it was about 200 mm deep and had a surface area of about 300 by 350 mm. At this point a wooden box was fitted over the block and the base was cut away using a larger knife and cutting wire. The sample boxes were wrapped in plastic and stored until ready for testing. Before testing, one of the cylindrical sample containers was driven into the block sample filling it with soil. The cylindrical sample was then prepared as outlined in Section 3.4. The LW 1/2, LW 2/2, and ECP 1/2 samples were all tested in a larger container measuring 200 mm diameter by 250 mm high in order to allow more space in the sample for a scour hole to form. Surplus soil from the block sample was used for soil classification testing.

Using the USCS classification system, the Saskatoon samples can be described as lean or fat clays, with clay content ranging from 21% to 43%, silt content ranging from 48% to 68%, and bulk density ranging from 1.05 to 2.39 g/cm$^3$. There was little to no vegetation present in these samples.

(a)

(b)

(c)

(d)

Figure 3-7. (a) Hole dug by hand with a rectangular block of soil formed in the center; (b) wooden sample box fit over the soil block; (c) base of soil block cut away showing sample ready for transport to the lab; (d) cylindrical sample container after being driven into the soil in preparation for jet testing

### 3.2.3 Manufactured Clay Sample Group

The third set of clay samples tested were pottery clays manufactured by Plainsman Clays Ltd. of Medicine Hat, Alberta, Canada. The types that were tested had designations of M-390, M-370, M-332, P-300 and Buff Stone Clay (BSC) with 10 samples tested in total. Each different clay type was produced in batches with each batch being relatively homogeneous. Duplicate samples of each different clay type tested were from the same batch with the exception of the BSC samples. The clay blocks were sealed in plastic wrap and once ready for testing a 150 mm

diameter by 150 mm high thin-walled, stainless steel, cylindrical container was driven into the clay blocks. Surplus clay from the block sample was used for soil classification testing.

Using the USCS classification system, all of these samples are described as lean clays with clay content ranging from 47 % to 55% and silt content ranging from 36 % to 45 %. Most samples were densely compacted with bulk densities ranging from 1.96 to 2.36 g/cm$^3$.

## 3.3 TESTING PROCEDURE

The testing procedure for a single sample took place in five stages: sample preparation, visual determination of critical flow rate, jet testing, jet test conclusion, and soil properties testing. The procedure varied slightly depending on the type of sample being tested and the container being used to house the sample.

### 3.3.1 Sample Preparation

The three sample groups were tested in one of two cylindrical containers. The first was a thin-walled stainless steel cylinder with a diameter of 150 mm and a height of 150 mm, which was used for the Ontario group and the Manufactured Clay group. Most of the samples from the Saskatoon group were tested using a larger cylinder with an internal diameter of 200 mm and a height of 250 mm.

Before testing, soil samples were extruded about 10 mm from the cylindrical container using a hydraulic ram. The remaining space in the bottom of the container was packed with medium grade silica sand, covered with a circular plastic cap, and sealed shut. Care was taken to vibrate the sand into place in order to achieve high compaction and minimize potential sample movement in the container during testing. The extruded surface was then cut flush with the container edge using a thin wire or knife. The sample was then submerged in water and gently agitated to remove any loose surface particles, before being left to soak between 24 to 48 hours in order to ensure complete saturation of the soil. The water content was measured both before and after soaking.

After soaking, the sample was placed in the drained octagonal tank. A wooden table with a 160 mm diameter circular hole in the center was used to hold the sample in place below the jet and provide a platform for taking depth measurements. The jet plenum was lowered into the tank using the hand winch and positioned vertically above the sample surface. A ruler was used to locate the centre point of the sample, which was then centered under the jet by lining up this point with a plumb bob hung vertically from the nozzle opening. The impingement height from the nozzle to the sample surface, $H_i$, was measured using an inside diameter, mechanical caliper and a digital caliper.

### 3.3.2 Visual Determination of Critical Flow Rate

Before jet testing was started, the flow rate which initiated observable mass erosion was determined. Mass erosion was defined as the erosion of chunks of soil rather than individual particles. The water supply line was used to fill the tank, submerging both the sample and the jet nozzle. The first ½ hp pump was primed and started, supplying water from the laboratory reservoir to the constant head tank, after which the second ½ hp pump was primed and started, supplying water from the constant head tank to the jet plenum.

When the pumps were running, the gate value on the jet inflow line was initially closed. Once the constant head tank stabilized, the gate valve was opened until the magnetic flow meter produced a discharge of about 1 L/min. The sample was observed for signs of soil aggregates being removed from the surface for a period of about 5 minutes. The act of incrementally increasing the flow rate by about l L/min and observing the surface was repeated until mass erosion was observed. For the natural samples this typically occurred as a few aggregates, or clumps of soil, being ejected from near the centerline during the observation period. For the manufactured clays this typically presented as a small, axisymmetric scour hole with radial scars from the centerline pointing towards the edge of the container.

Once it was determined that mass erosion was observed, a deflector plate was inserted between the jet nozzle and the sample surface allowing the jet to be pulled aside and secured to the tank wall. The water temperature in the tank was recorded and the tank was drained to get access to the sample surface. Photos were taken of the manufactured clay samples at this point

since the surface effects were clearly visible against the smoothly cut surface. As most of the natural samples had lower critical discharges, the flow rate was confirmed volumetrically by inserting a 2 to 5 L container under the nozzle and using a stop watch to determine the time it took to fill. This approach was not able to be used for the higher discharges associated with the manufactured clays due to significant splash back. Instead a measuring tape was attached to the side of the tank and the duration of time required for the surface to rise 100 mm was measured with a stop watch. The plan view surface area of the tank was measured and used to calculate the volumetric discharge. The flow rate verified by volumetric measurement was recorded as the critical flow rate, $Q_c$, which could be used to calculate the maximum critical velocity, $U_{oc}$.

Often the selected visual critical discharge would be confirmed by increasing the flow rate once again to observe if a small scour hole began to form. This technique was useful in confirming that the mass erosion observed was not greatly affected by sample preparation (i.e. due to the removal of particles loosened by surface cutting). It could also be used for defining an upper limit to the calculated critical shear stress which was helpful in assessing how sensitive the value was to the increment by which the flow rate was increased.

### 3.3.3 Jet Testing

Next, to initiate more substantial scouring in the sample, the flow rate was increased to about 40 - 60% of the critical flow rate. To begin testing, the tank was filled and the jet was moved into place above the sample using the deflector plate. Once the jet was impinging on the sample surface, a preset timer was started in order to track elapsed time. For the natural soil samples, target times for depth measurements were set at 5 min, 10 min, 20 min, 30 min, 60 min, 2 h, 4 h, and 8 h from the beginning of testing. After this, measurements were taken at about 24 – 48 hour intervals until the scour hole was deemed to reach equilibrium. For the manufactured clay samples the testing sequence was modified to include more readings early on and target times for depth measurements were set at 5 min, 10 min, 15 min, 20 min, 30 min, 40 min, 60 min, 1.5 h, 2.5 h, 4.5 h, and 8.5 h from the beginning of testing. After this, measurements were taken at about 24 – 48 hour intervals until the scour hole was deemed to reach equilibrium.

To take a depth measurement the timer was paused, the jet moved aside, and the tank drained to obtain access to the sample surface. Every time the water jet was moved across the sample surface, the deflector plate was held in place beneath the nozzle in order to avoid disturbing the sample. The water temperature and flow rate from the magnetic flow meter were recorded before emptying the tank. Depth measurements were then taken by lightly touching a small wooden rod to the sample surface and measuring it, using a digital caliper, against a plastic bridge of known height above the original sample surface (Figure 3-8). One measurement was taken at the center of the sample, $\varepsilon_{cl}$, and another at the location of the maximum depth, $\varepsilon_m$. Care was taken not to disturb the soil surface while taking depth readings. Photos were taken of the sample surface; after which, the tank was then refilled, the jet re-centered using the deflector plate, and the timer started. Given the long test durations, water was recirculated from the laboratory reservoir in order to avoid large consumption of water. This reservoir was periodically refreshed between tests.

The depth measurement methodology is similar to the pin profiling used in ASTM Standard D 5852 (2007), but modified to allow use with this specific test apparatus and allow measurements to be taken at any location on the sample surface. It was not possible to use the laser profiler for depth readings during testing as this would have required shutting off the jet and lifting it out of the tank, significantly increasing the duration of testing. There would also be the possibility of introducing errors when reestablishing the flow rate and jet position.

For the purpose of the work herein, equilibrium was determined graphically when a plot of the scour hole centerline depth versus time appeared to approach an asymptotic state and there was no noticeable increase in the scour hole width or depth. This approach was similar to the graphical approach detailed in Amin and Mazurek (2016).

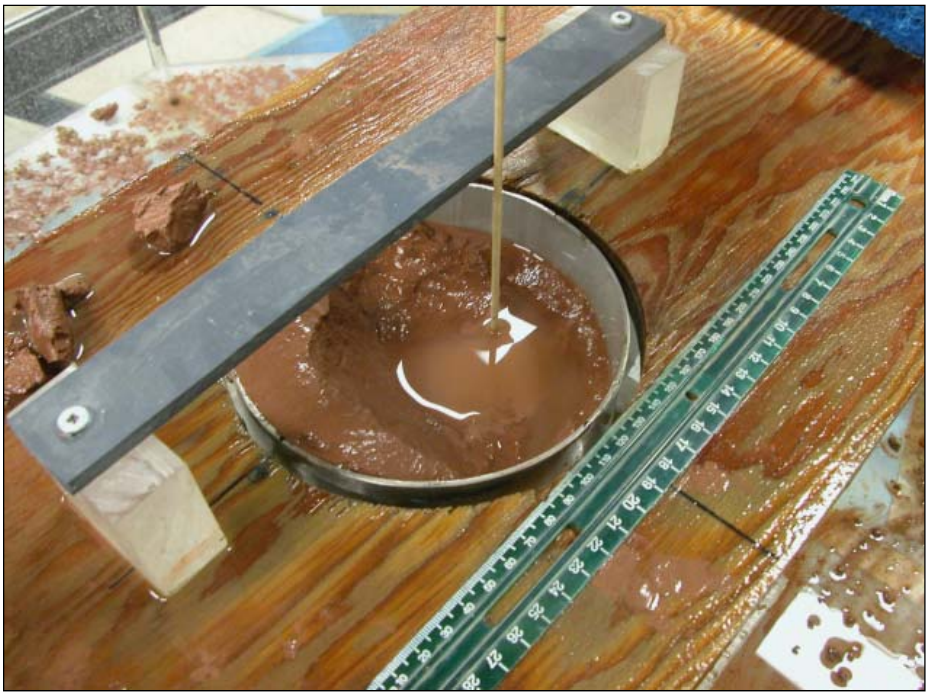

Figure 3-8. Depth measurements technique used during testing

### 3.3.4 Jet Testing Conclusion

Once the sample was deemed to be at equilibrium state, the magnetic flow meter reading was checked with a volumetric measurement before stopping the test. The flow through the system was then shut off, the jet was lifted out of the tank, and the tank was drained. The laser sensor was moved into place above the sample and two perpendicular profiles were taken of the scoured surface. These profiles crossed at the center of the sample and were used to determine the equilibrium centreline depth. Vegetation present in the scour hole was trimmed before profiling.

In addition to the two cross sections, the laser controller was set to take depth readings on a 2 mm by 2 mm grid for the full extent of a number of the sample surfaces. These point files could be used to recreate a digital surface of the scour hole and calculate the volume of soil sample removed. Scour volumes were checked in some of the less permeable samples by filling the scour hole with water using a graduated cylinder and determining the scour volume by the volume of water required to fill the hole.

### 3.3.5 Soil Property Testing

After the jet testing was complete and the sample surfaces were profiled, the soil classification tests outlined in Section 3.2 were performed. The bulk density and water content tests were performed on the sample material remaining after jet testing. The grain size distribution tests and Atterberg limits were performed in the College of Engineering Geotechnical Laboratory at the University of Saskatchewan. For the Ontario sample group these tests were conducted on the material remaining in the sample containers after jet testing. For the manufactured clays and Saskatoon sample groups, the grain size and Atterberg limits testing were performed on material remaining from the original bulk sample.

### 3.3.6 Modifications to the Jet Testing Apparatus and Procedure

While the jet test procedure for this study was largely based off of Hanson and Cook (2004) and ASTM Standard D5852-00 (2007), there were a few modifications to the apparatus setup and procedure. Both Hanson and Cook (2004) and ASTM Standard D5852-00 (2007) made use of a portable jet test apparatus, with nozzle diameters of 6.4 mm and 13 mm respectively, which allows soils to be tested in situ rather than through sample collection. In both cases the soil surface area available for testing was 0.44 m in diameter. The apparatus can also be mounted on a frame for use in a laboratory setting; in which case, cylindrical samples are collected and tested in a mold 0.18 m deep. The device presented in the ASTM Standard has a fixed initial impingement height of 0.22 m, while the device presented in Hanson and Cook (2004) can be adjusted between 40 and 220 mm.

The apparatus used in this study gives enhanced control over the hydraulic test parameters since the jet nozzle can be adjusted to any height above the sample surface. Furthermore, the smaller sample surfaces used in this study provide less room for the scour hole to grow. However, the sample size was selected based on collection and shipping considerations.

The main difference regarding testing procedure between this study and standard testing is the timing sequence used for depth measurements. ASTM Standard D5852-00 (2007) recommends only taking four depth measurements with a timing sequence of 10 min, 30 min, 60 min, and 120

min from the beginning of testing, and mentions that other timing sequences are at the user's discretion. The purpose of this standard is to quickly assess an erosion performance index for the soil in order to evaluate high, moderate, or low resistance to erosion. The focus is not to calculate the erodibility coefficient or critical shear stress; although a method for determining $k$ is provided by assuming a negligible critical tractive stress.

Hanson and Cook (2004) recommended testing for a similar duration, but added in more point gauge readings during testing, with depths measured every 5 to 10 minutes until a set of 10 to 12 data points are collected. This procedure allows tests to be run in 2 hours or less and uses this data to extrapolate a theoretical equilibrium depth without necessarily having to run the test until equilibrium state is reached.

The procedure used in this study builds on the test procedure from ASTM Standard D5852-00 (2007) and Hanson and Cook (2004) in two ways. First, it allows more depth measurements to be collected early in testing when erosion rates are highest. Second, later in testing, readings are collected less frequently until the sample can be graphically determined to have reached equilibrium state.

### 3.4 JET TEST OVERVIEW AND HYDRAULIC CONDITIONS

The hydraulic parameters from each of the 31 jet tests are presented in Table 3-2. Columns two and three give conditions for the visual determination of the critical shear stress, where $Q_c$ is the discharge for which mass erosion was observed (ranging from 0.9 L/minute to 32.3 L/minute), and $R_{visual}$ is the associated jet Reynolds number defined as $U_{oc}\, d_o/\nu$ (ranging from 1,668 to 89,048). Thirteen out of twenty natural samples had jet Reynolds numbers less than 10,000 for the visual testing, which is the threshold where the growth of the jet no longer depends on the Reynolds number (Rajaratnam and Flint-Petersen, 1989). All of the manufactured samples had fully turbulent conditions for the visual tests.

Table 3-2. Summary of jet testing and hydraulic parameters

| Group | Sample ID | $Q_c$ (Lpm) | $R_{visual}$ | Q (Lpm) | $U_o$ (m/s) | $H_i$ (mm) | $\rho$ (kg/m$^3$) | $\nu$ (m$^2$/s) | R | $H_i$/d | Scour Equilibrium Achieved? | Number of Depth Readings | Test Duration (hrs) |
|---|---|---|---|---|---|---|---|---|---|---|---|---|---|
| ONTARIO | SN(1) | 3.3 | 5945 | 7.5 | 2.5 | 66.0 | 1000.0 | 1.47E-06 | 13485 | 8.3 | yes | 13 | 68 |
| | SN(2) | 2.3 | 4143 | 6.3 | 2.1 | 60.0 | 1000.0 | 1.47E-06 | 11304 | 7.5 | yes | 18 | 45 |
| | WC(1) | 2.3 | 4364 | 5.4 | 1.8 | 60.0 | 999.9 | 1.45E-06 | 9823 | 7.5 | yes | 16 | 103 |
| | WC(2) | 1.2 | 2084 | 3.8 | 1.3 | 60.0 | 1000.0 | 1.47E-06 | 6860 | 7.5 | yes | 12 | 71 |
| | LC(1) | 2.5 | 4737 | 5.8 | 1.9 | 60.0 | 999.9 | 1.43E-06 | 10717 | 7.5 | yes | 21 | 162 |
| | LC(2) | 0.9 | 1668 | 3.2 | 1.1 | 60.0 | 999.9 | 1.41E-06 | 6023 | 7.5 | yes | 18 | 116 |
| | SC(1) | 9.1 | 16429 | 17.3 | 5.7 | 63.5 | 1000.0 | 1.47E-06 | 31144 | 7.9 | | 9 | 18 |
| | SC(2) | 3.6 | 7367 | 7.6 | 2.5 | 59.0 | 999.9 | 1.39E-06 | 14534 | 7.4 | yes | 15 | 92 |
| | SC(2)R | 10.1 | 20437 | 11.7 | 3.9 | 60.0 | 999.9 | 1.41E-06 | 22028 | 7.5 | yes | 19 | 137 |
| | BB(1) | 3.6 | 7856 | 4.6 | 1.5 | 60.0 | 999.5 | 1.22E-06 | 10089 | 7.5 | yes | 21 | 165 |
| | BB(2) | 2.5 | 5322 | 4.6 | 1.5 | 60.0 | 999.5 | 1.24E-06 | 9822 | 7.5 | | 12 | 66 |
| | BB(2)R | - | - | 4.8 | 1.6 | 67.1 | 999.5 | 1.24E-06 | 10259 | 8.4 | yes | 16 | 116 |
| | JR(1) | 3.5 | 8829 | 6.4 | 2.1 | 66.3 | 998.8 | 1.08E-06 | 15567 | 8.3 | yes | 11 | 42 |
| | JR(1)R | 4.3 | 10875 | 11.1 | 3.7 | 86.9 | 998.8 | 1.08E-06 | 27300 | 10.9 | yes | 34 | 420 |
| | JR(2) | 4.3 | 10867 | 10.1 | 3.4 | 84.8 | 999.2 | 1.15E-06 | 23200 | 10.6 | yes | 32 | 391 |
| | RR(1) | 8.3 | 23000 | 17.7 | 5.9 | 91.3 | 997.9 | 9.57E-07 | 49160 | 11.4 | yes | 35 | 622 |
| | RR(2) | 4.6 | 12251 | 14.1 | 4.7 | 98.3 | 998.2 | 1.00E-06 | 37299 | 12.3 | yes | 18 | 236 |
| MANUFACTURED CLAY | M-390(1) | 26.9 | 72802 | 44.5 | 14.8 | 80.54 | 998.3 | 1.02E-06 | 116106 | 10.1 | | 10 | 3 |
| | M-390(2) | 27.4 | 77656 | 37.7 | 12.5 | 101.3 | 997.7 | 9.46E-07 | 105635 | 12.7 | yes | 14 | 236 |
| | P-300(1) | 22.1 | 60456 | 32.4 | 10.7 | 78.8 | 998.0 | 9.69E-07 | 88733 | 9.9 | yes | 19 | 111 |
| | P-300(2) | 22.7 | 65077 | 31.7 | 10.5 | 110.1 | 997.5 | 9.24E-07 | 91074 | 13.8 | yes | 15 | 241 |
| | P-300(3) | 30.3 | 89048 | 43.0 | 14.3 | 123.3 | 997.6 | 9.35E-07 | 121959 | 15.4 | yes | 16 | 551 |
| | M-332(1) | 32.3 | 80111 | 42.0 | 13.7 | 98.0 | 998.7 | 1.07E-06 | 104330 | 12.3 | yes | 25 | 759 |
| | M-370(1) | 22.7 | 63589 | 35.2 | 11.7 | 98.1 | 997.9 | 9.57E-07 | 97489 | 12.3 | yes | 15 | 245 |
| | M-370(2) | 23.8 | 66822 | 31.3 | 10.4 | 89.9 | 997.7 | 9.46E-07 | 87878 | 11.2 | yes | 13 | 274 |
| | BSC(1) | 24.7 | 74875 | 34.8 | 11.5 | 87.6 | 997.6 | 9.35E-07 | 98709 | 11.0 | yes | 20 | 671 |
| | BSC(2) | 17.6 | 49908 | 26.5 | 8.8 | 88.0 | 997.4 | 9.14E-07 | 76856 | 11.0 | yes | 18 | 317 |
| SASK. | ECP(1) | 3.2 | 8963 | 14.0 | 4.7 | 109.0 | 997.7 | 9.46E-07 | 39280 | 13.6 | | 11 | 9 |
| | LW(1) | 4.2 | 14393 | 11.7 | 3.9 | 100.5 | 997.3 | 9.04E-07 | 34303 | 12.6 | yes | 14 | 141 |
| | ECP(2) | 2.9 | 8595 | 6.2 | 2.1 | 92.0 | 997.2 | 8.93E-07 | 18418 | 11.5 | yes | 15 | 160 |
| | LW(2) | 2.0 | 5852 | 7.9 | 2.6 | 104.0 | 997.3 | 9.04E-07 | 23280 | 13.0 | | 11 | 9 |

The discharge used for jet testing, $Q$, is given in column five. The jet nozzle velocities associated with these flow rates ranged from 1.1 to 14.8 m/s, which produced jet Reynolds numbers in the range of 6,023 to 121,959. All but four jet tests, WC(1), WC(2), LC(2), and BB(2), were run with a Reynolds number greater than 10,000.

Jet Reynolds numbers which are below 10,000 can begin to effect the value of the diffusion coefficient, $C_{d,}$ or whether or not the jet is fully turbulent. For low Reynolds numbers, the jet issuing from the nozzle is laminar for a certain length; however, Rajaratnam and Flint-Petersen (1989) found that for $R > 3000$ the jet becomes turbulent very close to the nozzle. Likewise, for $R > 9{,}000$ the growth of the jet half width is approximately constant with distance from the nozzle and works out to give a diffusion coefficient of about 6.3. For $R < 9{,}000$ the diffusion coefficient decreases with decreasing jet Reynolds number; however, the jet growth is not very sensitive to the nozzle velocity. As an example, Rajaratnam and Flint-Petersen (1989) reported a growth rate which works out to give a diffusion coefficient of about 5.0 for $R = 2{,}000$. There is considerable scatter in the data used to develop a relationship between the jet growth rate and $R$.

The initial impingement height from the nozzle to the sample surface ranged from 59.0 to 110.1 mm, which gave a range for $H_i/d$ of 7.4 to 13.8. Beltaos and Rajaratnam (1974) defined a large impingement height as $H/d > 8.3$, which is the approximate height required for the jet to be fully developed as it enters the impingement zone. Ten tests were run with initial conditions just inside the transitional range of $5.5 \leq H_i/d \leq 8.3$, with SC(2) having the lowest ratio with its initial height being 7.4 mm short of meeting the $H_i/d = 8.3$ threshold. All samples, with the exception of SC(2), entered the large impingement height range within the first 5 to 10 minutes of testing as the impingement height increased with increasing scour depths. None of the tests were run at a small impingement height, defined by Beltaos and Rajaratnam (1974) as $H/d < 5.5$, with the potential core impinging on the bed.

Overall, 26 of the 31 jet tests were determined to have reached equilibrium state and test durations for all samples ranged from 3 hours for M-390(1), to 759 hours for M-332(1). The flow meter was only used to track flow rates during testing when volumetric measurements could not

be taken and when setting flow rates for the visual analysis. All discharges used in calculations are volumetrically verified flows.

# CHAPTER 4
# RESULTS AND ANALYSIS

This chapter presents the results of the experimental program outlined in Chapter 3 as well as the data analysis and discussion of these results. The test results are presented in Section 4.1 including a description of the samples and how they eroded. Section 4.2 presents the critical shear stress values determined using visual analysis, equilibrium analysis, Hanson and Cook's (2004) method, and Thomas' method. Details are given on how these methods were applied and interpreted, as well as a comparison of results between methods and a discussion on the variability of results between duplicate and triplicate samples. In Section 4.3 the time development of scour results are discussed along with the process of determining the erodibility coefficient using both Hanson and Cook (2004)'s and Thomas' method for both a linear and non-linear excess shear stress equation. Values are compared between methods. An example of the spreadsheet for the critical shear stress and erodibility coefficient analysis is given in Appendix B. Section 4.4 discusses a method of using the critical shear stress of the soil to estimate the scour hole dimensions at equilibrium state.

## 4.1 JET TEST RESULTS

Appendix A gives the experimental observations for each test, including photos of the samples before and after each test, along with the test parameters and the maximum and centerline scour depth measurements throughout the test. The characteristics of erosion observed during testing are also included because they are helpful in understanding the time development of scour results. A description of each sample is given in the following sections, which include the physical characteristics of the soil, vegetation present, how the scour progressed with time, how the test was terminated, and the shape and size of the equilibrium scour hole.

It was also important to note which samples had the scour hole fully contained within the soil, since the exposure of large areas of the testing container wall may affect the jet hydraulics in the

scour hole. Moreover, the equilibrium state measurement of the scour hole radius in samples that scoured to the container wall will likely be an underestimation to what would have been measured had the sample been larger in diameter.

### 4.1.1 Ontario Sample Group Descriptions and Test Observations

The first sample tested from the Ontario Sample group was SN(1), South Nation. This was a brown to dark brown soil classified as sandy silt with medium size roots (up to 3 mm thick) present throughout the entire sample. The sample was relatively homogenous in depth. During testing, the soil eroded as medium to fine clumpy aggregates and produced a small, axisymmetric scour hole that was fully contained within the soil sample. It never reached the edge of the sample container, which means the scour hole did not extend through the sample edge.

SN(2), South Nation, was dark greyish brown, sandy silt with similar medium sized, woody roots present throughout the sample. It had a 30 – 40 mm diameter rock located near the surface that was too large to be dislodged by the water jet during testing. This rock was offset from the jet centerline and did not directly impede the growth of the centerline depth. This sample eroded as medium clumpy aggregates and the scour hole at equilibrium state was irregular, poorly defined, and completely contained within the sample. A photo of SN(2) is provided in Figure 4-1 (d).

WC(1), Wilton Creek, was a predominantly grey soil with brownish orange speckling throughout and is classified as a lean clay with sand. The brown speckling appeared to be silty sandy pockets embedded in the clay matrix. Roots, 2 – 3 mm thick, were present in the sample in a medium to low density. The sample eroded as plate like aggregates with some of the sandy material depositing around the container edge. The scour hole at equilibrium was deep and narrow, similar in form to that produced by a strongly deflected jet, and had a slight oblong shape. The hole was completely contained within the soil sample.

WC(2), Wilton Creek, was a greyish brown soil classified as a sandy silty clay with large 4 – 5 mm diameter roots located under the surface, but not completely dispersed throughout the sample. These roots were located near the container edge and did not appear to directly impede

the growth of the centerline depth. During testing there were heavy deposits of fine soil around the edge of the sample. The scour hole at equilibrium was deep and bowl-shaped. The edge of the scour hole at the sample surface scoured far enough to reach the wall of the testing container. A photo of WC(2) is provided in Figure 4-1 (f).

LC(1), Little Cataraqui, was a grey colored soil classified as silt with sand and had little to no vegetation present. During testing the sample eroded as small aggregates with sandy silty material depositing around the sample edge. The scour hole at equilibrium state was deep and bowl-shaped and extended to the edge of the sample, exposing a significant area of interior wall of the stainless steel sample container. Medium sand particles and spherical cohesive aggregates lined the bottom of the scour hole after testing, as they were too large to be ejected from the scour hole.

LC(2), Little Cataraqui, was a greyish light brown soil classified as lean clay with sand and had little to no vegetation. During testing the sample eroded as small aggregates with sandy silty material depositing around the edge of the sample. The scour hole at equilibrium was moderately deep, axisymmetric, and contained completely within the sample material. Medium sand particles and spherical cohesive aggregates lined the bottom of the scour hole after testing as they were too large to be ejected from the scour hole.

SC(1), Sawmill Creek, was a greyish light brown soil that was classified as a sandy, lean clay. Layering was observed in this soil with a network of fine to medium roots forming a high density mat just beneath the sample surface, but absent in the rest of the sample. Very quickly after testing began, a deep and narrow scour hole formed which was offset from the jet centerline. After 18 hours of testing, the scour hole reached the bottom of the sample container and the test was terminated without reaching equilibrium. A photo of SC(1) is provided in Figure 4-1 (e).

SC(2), Sawmill Creek, was a brownish grey soil classified as a sandy, lean clay. There was a network of fine to medium roots forming a high density mat just beneath the sample surface, similar to the SC(1) sample. The scour hole at equilibrium state was relatively wide, shallow, and

completely contained within the soil surface. Since there was plenty of soil left in the container the sample was extruded, re-cut, and re-tested at a higher flow rate with the designation SC(2)R.

Scour in SC(2)R initially progressed slowly until the bottom of the hole had advanced past the network of fine roots under the surface. At this point the soil appeared lighter grey with some gravel present (10 – 30 mm diameter pieces), but less sand. The scour hole at equilibrium was offset from the centerline with one side of the hole reaching the container's edge and a large portion of the surface still flush with the top of the container. Only one set of soil classification tests were run on the SC(2) and SC(2)R samples.

BB(1), Bear Brook, was a brown soil classified as a silty clay with sand and appeared uniform in depth. Medium and fine diameter roots were present throughout the whole sample with a medium density. During testing the sample eroded as fine aggregates and particles, which deposited on and around the sample surface. Initially a small, axisymmetric, bowl shaped scour hole formed. As the test progressed, one side of the sample began to erode more rapidly and advanced to the sample edge. The scour hole at equilibrium state was deep, irregular, and completely contained within the soil sample.

BB(2), Bear Brook, was a brown soil classified as a sandy silt, which was relatively uniform in depth. Fine roots were present in the sample with a low density, with a few exceptions. There was a 5 mm, woody root near the surface which caused some small, local disturbance to the surface while extruding and cutting. This root was located near the edge and was not deemed to affect the visual analysis under the jet centerline. The soil eroded as fine aggregates and particles and initially scour was bowl shaped and relatively axisymmetric. As scour progressed, a 20 mm diameter root was exposed about 30 mm under the jet centerline which ran the length of the entire sample. This root restricted the growth of the centerline depth and instead the scour hole expanded laterally. Testing was terminated before a convincing equilibrium was reached. The root was then removed and the sample was extruded, re-cut, and re-tested with the designation BB(2)R. A photo of BB(2) is provided in Figure 4-1 (a).

BB(2)R eroded as medium sized aggregates and some fine roots were present with low density. The scour hole at equilibrium state was wide, shallow, and axisymmetric. The surface of the scour hole reached the sample's edge.

JR(1), Jock River, was a dark brown, almost black, soil with a muddy texture that was classified as a sandy, organic silt. There was a high density network of fine to coarse roots permeating the whole sample, which gave a porous and spongy feel to the soil. The sample took a relatively longer duration to reach equilibrium and the final scour hole was shallow, poorly defined, and completely contained within the soil sample. Since there was plenty of soil left in the container, the sample was extruded, re-cut, and re-tested at a higher flow rate with the designation JR(1)R.

JR(1)R had a lumpy, irregular surface with a couple shells embedded in the sample. During testing the soil eroded primarily as lumpy aggregates, and a small diameter, irregular scour hole formed, which slowly increased in depth. The root network restricted lateral growth. Part way through testing, the water jet 'tunneled' from the bottom of the scour hole horizontally to the side of the container and then back vertically along the smooth container edge to exit the hole. This caused half of the sample surface to lift and detach from the soil underneath; however, the thick network of roots kept this section from being removed altogether. An increase in the rate of growth of the centerline depth occurred at this point, indicating that the sample lifting likely relieved the hydraulic pressure within the scour hole and allowed shear velocities to increase. The sample was deemed to reach equilibrium state after 420 hours, with the final scour hole narrow at the surface, irregular, and with holes around the container edge where the jet came back to the surface. A photo of JR(1)R is provided in Figure 4-1 (b).


(a) BB(2)

(b) JR(1)R

(c) RR(2)

(d) SN(2)

(e) SC(1)

(f) WC(2)

Figure 4-1. Photos from selected samples in the Ontario Group: (a) the second Bear Brook sample at the end of testing with a large root exposed; (b) repeat test for the first Jock River sample when the surface lifted; (c) the second Raisin River sample near the end of testing; (d) the second South Nation sample with a large rock exposed near the surface; (e) the first Sawmill Creek sample near the beginning of testing and (f) the second Wilton Creek sample near the beginning of testing

JR(2), Jock River, was a dark brown, almost black, soil with a muddy texture that was classified as a sandy, organic silt. There was a high density network of fine to coarse roots permeating the whole sample, which gave a porous and spongy feel to the soil. The surface was lumpy, irregular, and had shells embedded in it. During testing the soil eroded primarily as lumpy aggregates and a small diameter scour hole formed. Not long after the test started, one side of the scour hole gave way allowing the jet an outlet from the scour hole to flow radially along the surface and towards the container's edge. At equilibrium state the majority of the scour hole was contained within the soil sample.

RR(1), Raisin River, was a dark brownish grey soil classified as a sandy, organic silt. There was a medium density network of fine to coarse roots permeating the entire sample; however, it was not quite as dense as the Jock River samples. During testing the soil eroded primarily as lumpy aggregates and the scour hole quickly became asymmetrical and migrated to one side of the container. The jet test was run for 622 hours in order to confirm equilibrium state, which was the longest test duration from the Ontario group, and the final scour hole was relatively deep, narrow, and irregular.

RR(2), Raisin River, was a dark brownish grey soil classified as a sandy, organic silt. There was a medium to low density network of fine and medium roots permeating the whole sample. During testing the soil eroded primarily as lumpy aggregates and formed a wide, bowl shaped scour hole. At equilibrium state the scour hole was fairly axisymmetric, slightly off centered, and mostly contained within the soil sample. A photo of RR(2) is provided in Figure 4-1 (c).

### 4.1.2 Manufactured Clay Sample Group Descriptions and Test Observations

M390(1) was a brown soil classified as a lean clay. During testing the sample initially formed an axisymmetric, concave scour hole until there was sudden mass failure 10 minutes into testing which caused removal of chunks multiple centimeters in diameter. After this point, scour continued gradually until the jet nozzle blew out of the testing apparatus due to the high operating discharge. The test was terminated at this point before the sample convincingly reached equilibrium state. A photo of M390(1) is provided in Figure 4-2 (c).

M390(2) was a brown soil classified as a lean clay. Shortly after testing began, a large mass of soil was eroded along the containers edge. This caused the scour hole to initially be irregular and offset from the jet centerline. As testing progressed, scour continued gradually with the maximum depth shifting back towards the centerline and the occasional ejection of larger clumps. At equilibrium state the scour hole was wide and bowl shaped and just reached the sample edge.

P300(1) was a white soil classified as a lean clay. For the duration of testing, scour progressed gradually with no large mass failures in the sample taking place. Initially the scour hole was offset from the centerline and slowly migrated back towards the centerline as testing progressed. At equilibrium state, the scour hole had a bowl shape that was deep and wide, with the hole completely contained within the soil sample. A photo of P300(1) is provided in Figure 4-2 (e).

P300(2) was a white soil classified as a lean clay. At first scour progressed fairly gradually with some large chunks being removed. Two hours into testing, a large portion of the sample broke free with a large amount of mass erosion occurring suddenly, after which erosion continued gradually. At equilibrium state the scour hole was wide and bowl shaped. The top edge of the scour hole barely reached the side of the testing container, with a small portion of the stainless steel container wall exposed.

P300(3) was a white soil classified as a lean clay. During testing, scour occurred in two locations. A depression formed under the centerline which slowly increased with depth. Also, scour began around the sample edge and advanced towards the center of the sample. Once these two converged in the center a large amount of mass erosion took place with soil removed in large chunks. After this point, scour progressed gradually, and at equilibrium state the scour hole was wide, deep, and irregular and exposed the container wall around the majority of the sample.


(a) BS(1)

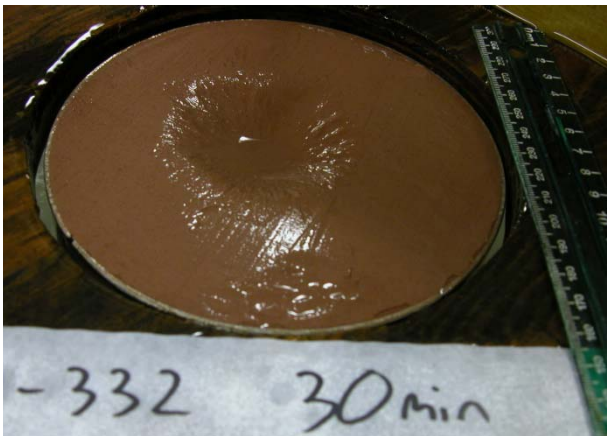


(b) M332(1)


(c) M390(1)

(d) M370(2)


(e) P300(1)


(f) M332(1)

Figure 4-2. Photos from selected samples in the Manufactured Clay Group: (a) the first Buff Stone Clay sample midway through testing; (b) M332 30 minutes into testing; (c) the first M390 sample midway through testing; (d) the second M370 sample near the end of testing; (e) the first P300 sample near the end of testing and (f) M332 sample near the end of testing

M332(1) was a brown soil classified as a lean clay with sand. Initially the jet formed a smooth, concave, axisymmetric hole that gradually grew in width and depth. Once the edge of the hole reached the container, mass erosion began along the stainless steel wall causing the sample to lose its bowl shape. At equilibrium state the scour hole was flat and irregular with a think band of the stainless steel container exposed around the sample perimeter. A photo of M332(1) is provided in Figure 4-2 (b) and (f).

M370(1) was a white soil classified as a lean clay. Early in the test, half of the sample surface eroded very quickly, with removal of large chunks causing the maximum depth to be located near the sample edge. Erosion continued gradually after this until about 72 hours, where there was another mass surface failure which removed the remaining half of the sample surface. At equilibrium state the scour hole was flat and irregular with a think band of the stainless steel sample container exposed around the sample perimeter.

M370(2) was a white soil classified as a lean clay. Early during testing a crack appeared underneath the sample surface along one side of the container. This crack slowly propagated towards the centerline causing erosion of large soil chunks as it went. Once it reached the center the scour hole appeared bowl shaped with an irregular surface. Later in the test a second mass failure occurred along the container edge exposing a large area of the stainless steel container wall. At equilibrium state, the scour hole was deep and wide with an asymmetrical, irregular shape. A photo of M370(2) is provided in Figure 4-2 (d).

BS(1), buff stone clay, was a light grey soil classified as a lean clay. In the early stages of testing, a well-defined concave scour hole formed and grew in width and depth until the scour hole reached the sample edge. At this point mass failure of the sample occurred at its edge, which exposed a large circumference of the stainless steel sample container. At equilibrium state the scour hole was located deep in the testing container and had a shallow concave shape. A photo of BS(1) is provided in Figure 4-2 (a).

BS(2), buff stone clay, was a light grey soil classified as a lean clay. In the early stages of testing, a relatively deep scour hole formed which was offset from the jet centerline. As testing

progressed, the hole grew in depth and width as it shifted towards the center of the sample. At equilibrium state the scour hole was fairly axisymmetric, bowl shaped, and mostly contained within the soil sample.

### 4.1.3 Saskatoon Sample Group Descriptions and Test Observations

ECP(1), East College Park, was a brown soil classified as a lean clay. A low density network of fine roots was present in the sample. The soil eroded primarily as small aggregates and formed a bowl shaped, symmetrical scour hole early in testing. As testing progressed the hole became deep and narrow, and at about 2.5 hours, scoured to one side of the container. The scour hole increased in depth along the inside wall of the container until it reached the bottom of the sample and blew out the complete soil sample. The test was terminated before scour in the sample reached equilibrium state. A photo of ECP(1) is provided in Figure 4-3Figure 4-2 (c) and (d).

ECP(2), East College Park, was a brown soil classified as a lean clay and had three or four thick woody roots present in the center of the sample. The soil primarily eroded as medium to large clumpy and angular aggregates, with a wide and shallow scour hole forming quickly in the sample. The hole progressed to the edge of the sample, exposing the stainless steel wall of the sample container almost all the way around the edge. At equilibrium state the scour hole was relatively flat, irregular and poorly defined. A photo of ECP(2) is provided in Figure 4-3Figure 4-2 (b).

LW(1), Lakewood, was a darker brown soil classified as a lean clay with very little vegetation present. The soil texture was like a stiff mud and the LW samples had the highest clay and silt fractions of all the natural samples. The sample initially eroded as very wide and flat, plate-like particles, which appeared to be torn from the irregular, blocky scour hole. Early in testing these particles covered the majority of the sample surface. At equilibrium state the scour hole was wide, shallow, and poorly defined.

LW(2), Lakewood, was a darker brown soil classified as a fat clay and contained very little vegetation. Early during testing, a deep, bowl shaped, axisymmetric scour hole formed with a high ridge of fine aggregates depositing around the edge. The deflected jet created a murky cloud

of suspended material above the surface while testing. As testing progressed, the hole grew to reach the sides of the container and finally scoured through the bottom of the sample. The test was terminated before scour reached equilibrium state. A photo of LW(2) is provided in Figure 4-3 (a).

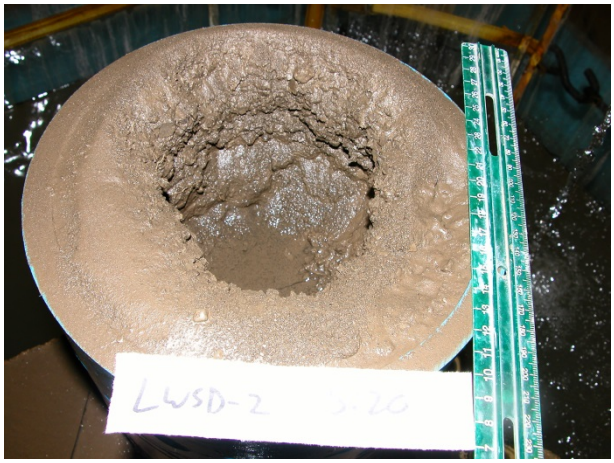


(a) LW(2)


(b) ECP(2)


(c) ECP(1)


(d) ECP(1)

Figure 4-3. Photos from selected samples in the Saskatoon Group: (a) the second Lakewood sample midway through testing; (b) the second East College Park sample near the beginning of testing; (c) the second East College Park sample near the beginning of testing and (d) the second East College Park sample near the end of testing just before the soil blew out of the testing container

### 4.1.4 Time Development of Scour

In Figure 4-4 the growth of the scour hole centerline for all three sample groups are shown for the full duration of testing. Samples are grouped according to their test duration in order to help illustrate equilibrium conditions at the end of testing. Samples SC(1), ECP(1), and LW(2) (Frame a) and sample M390(1) (Frame c) were run for shorter durations than the rest of the samples and, for reasons discussed in Sections 4.1.1 - 4.1.3, did not reach equilibrium state.

For samples that were designated as having reached equilibrium state (as defined in Section 3.3.4), the change between depth readings near the end of testing tended to be less than one mm in a 24 hour period. Most of these samples have three to five data points that are nearly horizontal at the end of testing; however, a handful of samples still appear to have a slight upward trend.

JR(1)R and JR(2) did not appear to reach a very convincing equilibrium state in the time development plots for the centerline depth. However, for both samples the maximum depth near the end of testing was slightly offset from the centerline. The time development of the maximum depths did appear to reach an asymptotic value near the end of testing and the increase in centerline depth was attributed to the location of the maximum depth shifting towards the centerline. What is not shown in Figure 4-4 is that the centerline and maximum depths converged near the end of testing, and for that reason these samples were deemed to reach equilibrium. This rationale is illustrated more clearly from the scour depth plots shown in Appendix A.

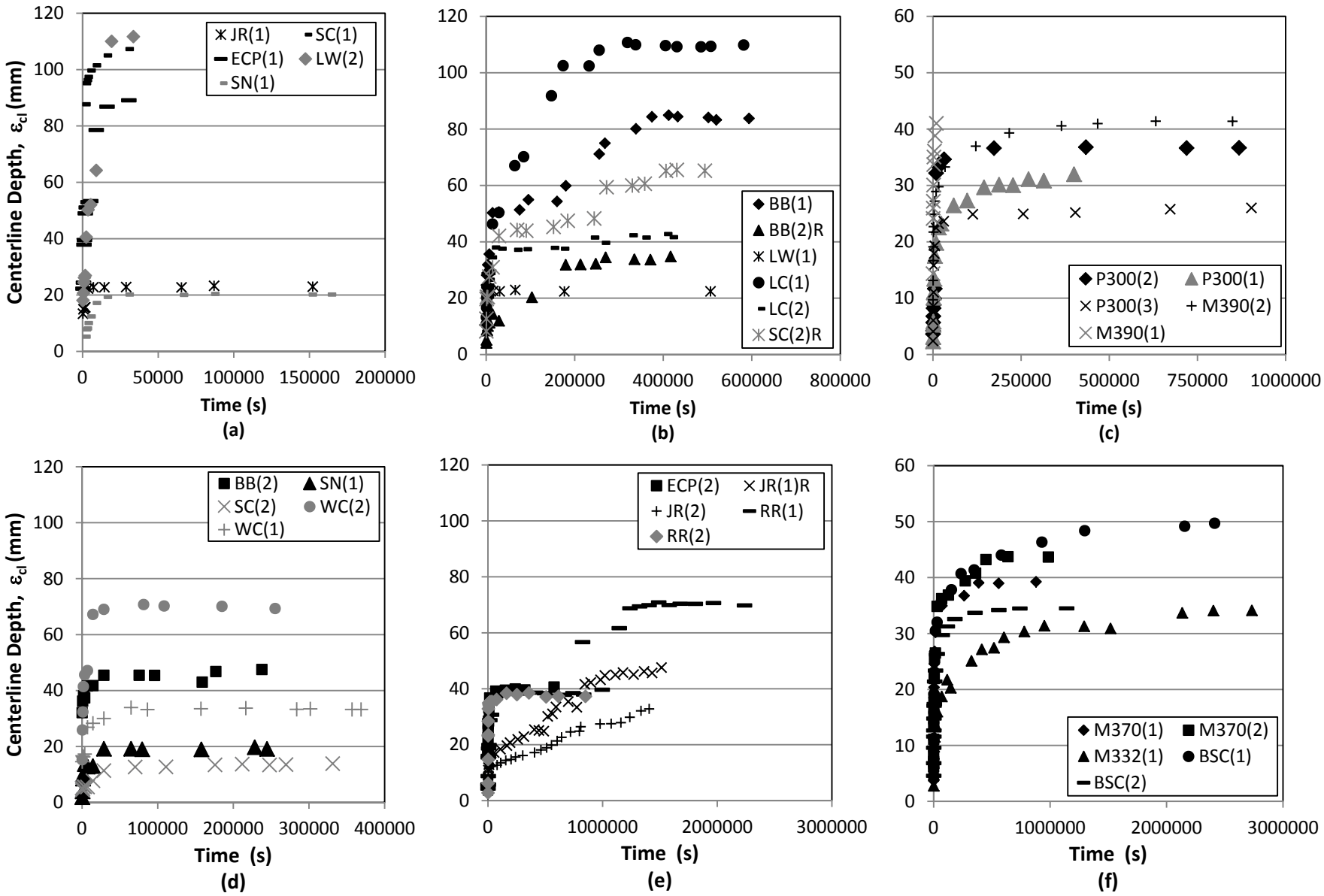


Figure 4-4. Centerline depth scour progression for the tested natural samples (Frames a, b, d, and e) and manufactured clays (Frames c and f)

P-300(1) and BSC(1) also appear to have an upward trend when looking at the last three data points. The last three centerline depth readings for P-300(1) went from 31.12 mm to 30.87 mm to 32.00 mm over a 36 hour period. The sample surface was beginning to show slight discoloration indicating very little surface disturbance for long periods. It was observed that very small dimples were beginning to form on the surface where measurements were being taken, indicating that local erosion was likely occurring from the measuring stick touching the surface during readings. The last three maximum depth readings for BSC(1) went from 49.06 mm to 49.38 mm to 49.71 mm over a 13 day period, with the centerline depth increasing about 1.3 mm. Any observed changes to the sample surface over this period were confined locally to the soil directly below the nozzle. Based on these observations, P-300(1) and BSC(1) were deemed to have reached a reasonable equilibrium state and data analysis was conducted based on the final readings.

## 4.2 CRITICAL SHEAR STRESS ANALYSIS AND RESULTS

The critical shear stress for each soil sample tested was determined using the four methods presented in Section 2.3. A spreadsheet tool was developed, which was used for recording and analyzing the test data, and the calculated critical shear stress values are presented in Table 4-1.

The critical shear stress determined using visual analysis is designated $\tau_{c\_V}$, $\tau_{c\_Ec}$ is the critical shear stress from the measured centerline depth at equilibrium state, $\tau_{c\_B1}$ is the critical shear stress based on Blaisdell et al.'s (1981) estimated equilibrium depth used in Hanson and Cook's (2004) analysis, and $\tau_{c\_T1}$ is the critical shear stress based on Thomas' method. The maximum shear stress at the beginning of jet testing, $\tau_{om}$, ranged from 93.2 Pa to 223.9 Pa for the manufactured clays and 3.3 Pa to 86.1 Pa for the natural samples. Critical shear stresses from all four methods ranged from 0.1 Pa to 32.7 Pa for the natural samples and 13.5 - 173.5 Pa for the manufactured samples. A number of challenges were encountered in calculating these values and these are discussed below.

Table 4-1. Critical shear stress results

| Sample ID | $\tau_{om}$ (Pa) | $\tau_{c\_V}$ (Pa) | $\tau_{c\_Ec}$ (Pa) | $\tau_{c\_B1}$ (Pa) | $\tau_{c\_T1}$ (Pa) |
|---|---|---|---|---|---|
| SN(1) | 14.9 | 2.9 | 8.8 | 2.8 | 9.5 |
| SN(2) | 12.7 | 1.7 | 7.1 | 2.4 | 8.6 |
| WC(1) | 9.3 | 1.7 | 3.8 | 2.0 | 5.4 |
| WC(2) | 4.7 | 0.4 | 1.0 | 0.1 | 1.4 |
| LC(1) | 10.7 | 2.0 | 1.3 | 0.8 | 5.6 |
| LC(2) | 3.3 | 0.3 | 1.1 | 0.5 | 1.5 |
| SC(1) | 86.1 | 23.2 | - | 6.9 | 13.1 |
| SC(2) | 19.3 | 4.0 | 12.6 | 14.6 | 15.8 |
| SC(2)R | 44.0 | 32.7 | 10.1 | 3.3 | 22.2 |
| BB(1) | 6.9 | 4.2 | 1.2 | 0.9 | 3.1 |
| BB(2) | 6.8 | 2.0 | - | 1.3 | 2.5 |
| BB(2)R | 5.9 | - | 2.6 | 2.1 | 4.4 |
| JR(1) | 10.6 | 3.2 | 5.8 | 2.4 | 6.5 |
| JR(1)R | 19.0 | 2.9 | 7.9 | 8.7 | 15.4 |
| JR(2) | 16.6 | 3.1 | 8.6 | 6.0 | 13.2 |
| RR(1) | 43.8 | 9.6 | 13.9 | 7.4 | 27.3 |
| RR(2) | 23.9 | 2.6 | 12.4 | 0.7 | 7.5 |
| M-390(1) | 353.6 | 129.3 | - | 20.5 | 170.7 |
| M-390(2) | 160.4 | 99.3 | 80.8 | 23.5 | 103.8 |
| P-300(1) | 196.3 | 69.1 | 99.2 | 24.2 | 116.2 |
| P-300(2) | 96.3 | 71.4 | 54.1 | 41.0 | 80.7 |
| P-300(3) | 140.9 | 71.0 | 96.1 | 26.4 | 91.9 |
| M-332(1) | 213.2 | 125.7 | 117.2 | 80.7 | 173.5 |
| M-370(1) | 151.0 | 52.4 | 77.0 | 14.5 | 90.6 |
| M-370(2) | 141.2 | 69.8 | 63.9 | 19.3 | 94.2 |
| BSC(1) | 181.0 | 90.9 | 74.0 | 18.7 | 114.2 |
| BSC(2) | 93.2 | 46.3 | 49.7 | 18.9 | 66.1 |
| ECP(1) | 19.2 | 1.0 | - | 0.9 | 8.7 |
| LW(1) | 15.7 | 2.1 | 10.4 | 9.2 | 10.5 |
| ECP(2) | 5.3 | 1.2 | 2.5 | 1.2 | 3.2 |
| LW(2) | 6.7 | 0.4 | - | 0.3 | 3.3 |

### 4.2.1 Analysis and Results for Hanson and Cook's (2004) Method, $\tau_{c\_B}$

In order to determine the critical shear stress according to the procedure presented in Hanson and Cook (2004), the equilibrium scour depth is first estimated using the curve fitting approach developed by Blaisdell et al. (1981) and outlined in Section 2.3.1. A spreadsheet routine was developed based on Equation [2-6] where values of $f$ and $x$ were calculated from the measurements taken at each scour reading (Figure 4-5). An initial value for the constant $f_o$ was selected and used to calculate the value of $A^2$ for every reading. The Excel solver function was then used to iteratively determine the value of $f_o$ by minimizing the standard deviation calculated using all values of $A^2$. The estimate for the scour depth at ultimate state, $H_{e\_B}$, was then calculated from Equation [2-8] and then used in Equation [2-5] to calculate the critical shear stress. An example of the analysis spreadsheet is given in Appendix B.

During the initial stages of data analysis, it was found that the value of $H_e$ for a sample strongly depended on the number of data points used for curve fitting. Since the test duration was determined by the time it took each sample to reach equilibrium, no two samples had the same number of data points. In order to ensure consistency when comparing the results from different samples, an effort was made to standardize the number of data points used for calculating $H_e$ and $\tau_c$.

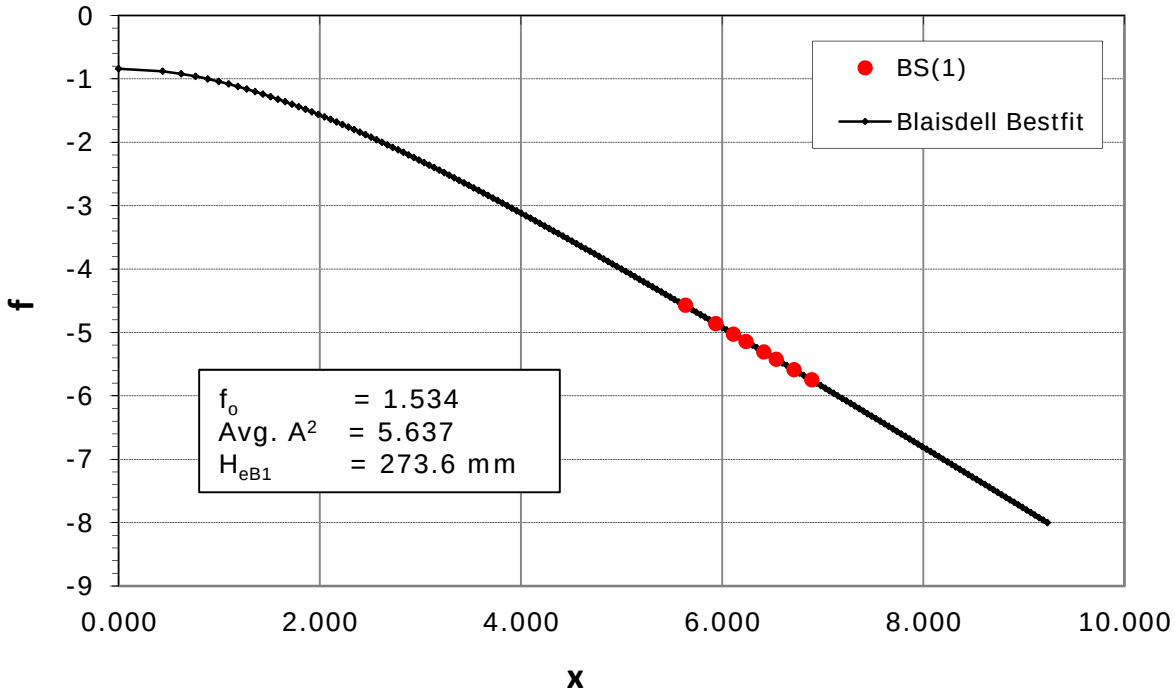


Figure 4-5. Equilibrium height for the first Buff Stone sample determined using Blaisdell et al.'s (1981) approach as outlined in Hanson and Cook (2004).

Hanson and Cook (2004) recommend that depth measurements be taken at 5 to 10 minute intervals for a set of 10 to 12 readings which gives a typical maximum test duration of 120 minutes. Although this study used two different testing sequences, one for the natural samples and one for the manufactured samples, the data sets used for analysis were based on Hanson and Cook's (2004) recommendations. The first data set for calculating $H_e$, and subsequently $\tau_c$, used all measurements up to and including the first 120 minutes of testing (designated $H_{e\_B1}$, and $\tau_{c\_B1}$), the second data set included the first 10 readings from the testing sequence (designated $H_{e\_B2}$ and $\tau_{c\_B2}$) and the third data set included all measurements taken for the full duration of testing (designated $H_{e\_B3}$ and $\tau_{c\_B3}$).

Figure 4-6 and show how the number of points included for analysis impacts the value of $H_{e\_B}$ calculated for BS(1). Using all data points from the first 120 minutes of testing (8 points) gives a value for $H_{e\_B1}$ of 274 mm and using the first 10 data points from testing gives a value for $H_{e\_B2}$ of 300 mm. Using all of the depth readings collected during testing (20 points) gives a value for $H_{e\_B3}$ of 261 mm. Although the equilibrium scour depth varied by 39 mm depending on how many data points were used, Blaisdell et al.'s (1981) method still produced values over 123 mm above what was measured as equilibrium depth for BS(1). Figure 4-7 shows a similar progression for a natural sample, LC(1), where the addition of subsequent data points early on can have a large impact on the value of $H_{e\_B}$. Using the first 120 minutes of testing (6 points) produces a value of $H_{e\_B1}$ that is about 1.3 times the magnitude of the measured depth, whereas using all of the available data produces a value about 7 times the measured depth.

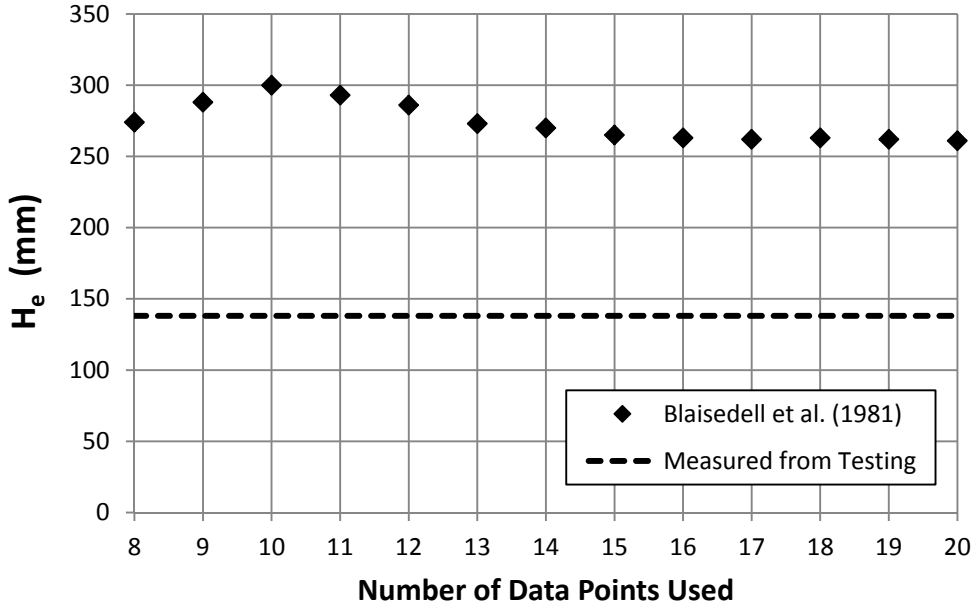


Figure 4-6. Comparison of theoretical and measured equilibrium height for BS(1) and influence of test duration on the results

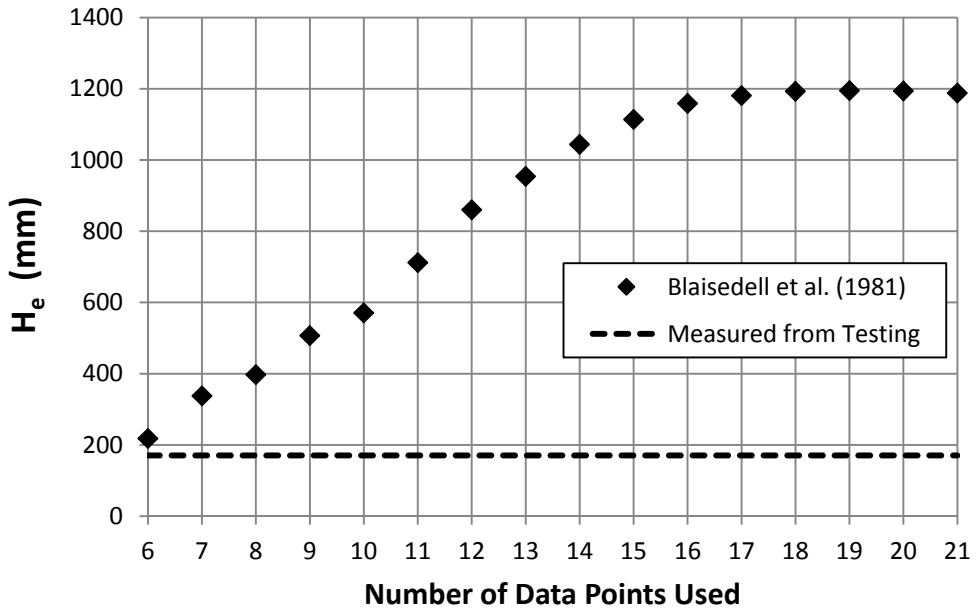


Figure 4-7. Comparison of theoretical and measured equilibrium height for LC(1) and influence of test duration on the results

Furthermore, it can be seen that as more points are added in to the analysis, the value of $H_{e\_B}$ seems to stabilize. This is due to the dampening effect that a larger data set has on the addition of one individual measurement when calculating the best fit. Additionally, most mass failures that occurred in the samples were observed near the beginning of testing when shear stresses and pressures on the surface were relatively high. These sudden changes in depth can have a noticeable impact on the results of $H_{e\_B}$ when using smaller data sets for analysis.

Table 4-2 presents the measured equilibrium depth along with Blaisdell et al.'s (1981) estimated equilibrium depth for the three data sets, with the later method providing larger estimates of the equilibrium depth for almost every sample. Simon et al. (2010) noted a similar observation regarding Blaisdell et al.'s (1981) model when applied to longer test durations. Since the applied shear stress on the soil surface is inversely related to the height from the jet nozzle, an overestimation of the equilibrium depth would produce a smaller value for $\tau_{\_c}$.

Table 4-2. Measured and theoretical equilibrium depths from nozzle to scour hole centerline for each sample

| Sample ID | $H_{e\ m}$ (mm) | $H_{e\ B1}$ (mm) | $H_{e\ B2}$ (mm) | $H_{e\ B3}$ (mm) | $H_{e\_B1}/H_{e\_m}$ | $H_{e\_B2}/H_{e\_m}$ | $H_{e\_B3}/H_{e\_m}$ |
|---|---|---|---|---|---|---|---|
| SN(1) | 86 | 152 | 138 | 128 | 1.78 | 1.61 | 1.50 |
| SN(2) | 80 | 137 | 133 | 124 | 1.71 | 1.65 | 1.54 |
| WC(1) | 94 | 128 | 163 | 149 | 1.36 | 1.73 | 1.58 |
| WC(2) | 131 | 437 | 415 | 344 | 3.34 | 3.18 | 2.63 |
| LC(1) | 171 | 220 | 578 | 1205 | 1.29 | 3.38 | 7.06 |
| LC(2) | 103 | 160 | 151 | 145 | 1.56 | 1.47 | 1.41 |
| SC(1) | - | 225 | - | 260 | - | - | - |
| SC(2) | 73 | 68 | 94 | 98 | 0.93 | 1.29 | 1.34 |
| SC(2)R | 126 | 220 | 284 | 357 | 1.76 | 2.27 | 2.84 |
| BB(1) | 145 | 167 | 247 | 396 | 1.15 | 1.70 | 2.73 |
| BB(2) | - | 137 | 133 | 136 | - | - | - |
| BB(2)R | 102 | 112 | 151 | 196 | 1.10 | 1.48 | 1.92 |
| JR(1) | 90 | 140 | 117 | 114 | 1.56 | 1.31 | 1.27 |
| JR(1)R | 135 | 129 | 131 | 229 | 0.96 | 0.98 | 1.70 |
| JR(2) | 117 | 140 | 138 | 162 | 1.20 | 1.18 | 1.38 |
| RR(1) | 162 | 222 | 258 | 350 | 1.37 | 1.59 | 2.16 |
| RR(2) | 137 | 558 | 364 | 197 | 4.08 | 2.66 | 1.44 |
| M-390(1) | - | 329 | 315 | - | - | - | - |
| M-390(2) | 143 | 264 | 242 | 219 | 1.85 | 1.70 | 1.53 |
| P-300(1) | 111 | 224 | 244 | 213 | 2.02 | 2.20 | 1.92 |
| P-300(2) | 147 | 169 | 319 | 255 | 1.15 | 2.17 | 1.74 |
| P-300(3) | 149 | 285 | 275 | 236 | 1.91 | 1.84 | 1.58 |
| M-332(1) | 132 | 159 | 157 | 204 | 1.21 | 1.19 | 1.55 |
| M-370(1) | 137 | 316 | 312 | 236 | 2.30 | 2.27 | 1.72 |
| M-370(2) | 133 | 243 | 257 | 270 | 1.82 | 1.93 | 2.03 |
| BSC(1) | 138 | 274 | 300 | 261 | 1.99 | 2.18 | 1.89 |
| BSC(2) | 128 | 207 | 216 | 206 | 1.62 | 1.69 | 1.61 |
| ECP(1) | - | 511 | 762 | 750 | - | - | - |
| LW(1) | 123.4 | 131.4 | 128.3 | 124.7 | 1.06 | 1.04 | 1.01 |
| ECP(2) | 132.6 | 192.1 | 212.5 | 186.0 | 1.45 | 1.60 | 1.40 |
| LW(2) | - | 516.3 | 1096.3 | 1329.8 | - | - | - |
| | | | | Average | 1.673 | 1.818 | 1.942 |

On average over the 31 tests that were run, the more data points from jet testing that were used, the larger the discrepancy between the measured and estimated equilibrium depth. Since most jet erosion tests conducted by other practitioners wound not likely be run to equilibrium state, and since $H_{e\_BI}$ gave the closest results on average when compared with the measured equilibrium scour depths, it was determined that the first 120 minutes of testing data would be the default data set for further analysis. This typically resulted in 6 to 8 data points being included in the analysis. It was also found that this data set also gave the best fit to Hanson and Cook's (2004) time development of scour equation when calculating $k$ which is discussed at greater length in Section 4.3. Values for $\tau_{c\_BI}$ are presented for each of the 31 jet tests in Table 4-1.

### 4.2.2 Analysis and Results for the Visual Method, $\tau_{c\_V}$

Data analysis for the visual method is relatively simple and followed the theory presented in Section 2.3.2. The critical flow rate recorded from testing was divided by the nozzle area to determine the critical nozzle velocity, $U_{oc}$, for which mass erosion occurred. This value was used as an input to Equation [2-10], along with the diameter, $d_o$, the water density, $\rho$, and the initial height between the nozzle and the sample surface, $H_i$, to calculate the critical shear stress. A value of 6.3 was used for the diffusion coefficient, $C_d$, and a value of 0.00416 was used for the friction coefficient, $c_f$. Of the four methods presented, the jet hydraulics for the visual test are the closest to resembling the assumptions under which the analysis theory was developed, which is impingement on a flat, smooth, surface rather than impingement in a scour hole. However, there is an expected degree of variability in the results since they rely in part on the operator's judgment to determine the point of incipient motion for mass erosion. The values of $\tau_{c\_V}$ for each of the 31 tests are presented in Table 4-1 and an example of the analysis spreadsheet is given in Appendix B.

The Manufactured Clay Group was an ideal sample set for testing the visual critical shear stress. The uniform consistency of the clay and lack of vegetation helped to minimize surface disturbances when cutting and preparing the sample for testing. The smooth, flat surface provided conditions very similar to that for which the analysis theory was developed and it is expected that the choice of the friction coefficient is a good fit for this group. Furthermore, the smooth surface made it easy to observe and document any surface disturbances that occurred during testing. The high erosion resistance of this group meant that higher nozzle velocities were required to initiate erosion, which produced jet Reynolds numbers well above the turbulent jet threshold of 10,000 for which the theory was developed.

The main challenge for this method was determining at which point mass erosion could be said to occur in the sample. Mazurek (2001) differentiates between flake erosion and mass erosion in similar manufactured samples with designation M390 and found the critical shear stress for flake erosion to be 16 Pa whereas the critical shear stress for mass erosion was estimated as 48 Pa.

In this study, flake erosion typically presented as the removal of small flat particles with a depth of about 1 mm and is likely attributed to the alignment of surface particles during cutting. For mass erosion, chunks of clay were typically ripped or torn from the sample surface. In order to determine the critical shear stress for mass erosion determine in this study, the operator had to make a distinction between flake erosion and mass erosion. Often this presented as long radial gashes 2-4 mm deep that were torn out of the sample surface pointing away from the jet centerline along with the formation of very shallow scour holes. Examples of mass erosion for which the critical shear stress was calculated can be seen on two samples in Figure 4-8.

(a) BS(2) (b) P370(1)

Figure 4-8. Photos from selected samples in the Manufactured Clay Group - (a) the second Buff Stone Clay sample showing the surface condition from which the visual critical shear stress was determined; (b) the first P370 sample showing the surface conditions from which the visual critical shears stress was determined.

Assessment of the visual critical shear stress for the natural samples was more reliant on the operator's judgment. Due to the rough, natural surface of the samples, it was not always obvious that particles had been removed just by looking at the sample surface after visual testing was completed. For this reason, the threshold at which erosion occurred was only able to be documented by the operator's notes and not with photos. When the visual test was first started it was not unusual for a small cloud of fine particles to appear over the sample centerline as the loose particles disturbed by sample preparation were washed away. Once this cloud dissipated the sample centerline was watched closely to detect signs of mass erosion.

The presence of vegetation added additional complications to assessing the visual critical shear stress. It was more difficult to minimize surface disturbances during sample preparation when cutting the surface if vegetation was close to the surface. In some samples with heavy vegetation, such as Raisin River and Jock River, there were instances where a clump of soil was physically detached from the rest of the soil matrix during testing but still bound to the surface by thin roots.

There are a couple ways in which the application of this method for the natural samples deviated from the assumptions made in the theory. The lower critical flow rates needed to cause erosion in the samples were often not large enough to produce a jet Reynolds number greater than 10,000. This means that the actual diffusion coefficients of the jets would likely be less than the value of 6.3 used; however, the subsequent overestimation of the critical shear stress resulting from this unaccounted reduction in $C_d$ is expected to be negligible in most cases.

Overall, the way in which the test procedure is run likely results in the calculated values being an overestimation of the actual critical shear stress. Consider testing at 'discharge 1' where no mass erosion is detected while observing the sample surface for 5 minutes. The flow rate is then increased to 'discharge 2' and mass erosion is observed on the sample surface underneath the jet. This second discharge becomes the designated critical flow rate and is used to calculate the value of $\tau_{c\_V}$, however, the real value of $\tau_{c\_V}$ is somewhere between discharge 1 and 2.

### 4.2.3 Analysis and Results for the Equilibrium Method, $\tau_{c\_Ec}$

Analysis of the sample data according to the equilibrium method followed the theory presented in Section 2.3.3. Once a sample was deemed to reach equilibrium state as per Section 3.3.3, the critical shear stress was calculated using the measured centerline depth and Equation [2-11]. The diameter, $d_o$, the water density, $\rho$, and the initial height between the nozzle and the sample surface, $H_i$, were determined from the apparatus setup and test data. A value of 6.3 was used for the diffusion coefficient, $C_d$, and a value of 0.00416 was used for the friction coefficient, $c_f$. The values of $\tau_{c\_Ec}$ for each of the 31 tests are presented in Table 4-1 and an example of the analysis spreadsheet is given in Appendix B.

The equilibrium method assumes that the centerline velocity decays as a free jet in the scour hole and can be used to calculate the maximum shear stress on the soil surface once the scour depth has reached an asymptotic state. This assumption ignores the effect of the wall pressure distribution in the impingement zone as well as additional velocity decay caused by the return flow in the scour hole. The impact of the width and depth of a scour hole on the maximum applied shear stress has been studied by Weidner et al. (2012) using a numerical model. It was found that wider scour holes caused less velocity dissipation than narrow holes. Due to this unaccounted velocity decay, it is expected that the equilibrium method would tend to overestimate values of $\tau_c$, and this overestimation would be less pronounced in wider, shallower holes. Mazurek and Gheisi (2009) have also studied the impacts of scour hole geometry on velocity decay and have proposed a modified diffusion coefficient based on the scour hole aspect ratio.

The centerline depths for JR(1)R and JR(2) did not appear to reach a very convincing asymptotic state when plotting the scour depth vs time. Asymptotic state was more apparent with the maximum depth measurements, and since the rate of erosion near the end of testing was very small, they were deemed to have reached equilibrium. Therefore, values of $\tau_{c\_Ec}$ were calculated for JR(1)R and JR(2) which had test durations of 420 hours and 391 hours respectively.

### 4.2.4 Analysis and Results for Thomas' Method, $\tau_{c\_T}$

Analysis of the sample data according to Thomas' method followed the theory presented in Section 2.3.4. Using the time and depth data from testing, the average shear stress and erosion rate were calculated using Equations [2-12] and [2-13] and plotted. A linear trend line was fit to the data and used to calculate the average shear stress corresponding to an erosion rate of zero. An example of the analysis spreadsheet is given in Appendix B.

The critical shear stress values determined using Thomas' method were also found to vary based on the number of data points used in the analysis. For the sake of consistency, the same three data sets from testing that were used for Hanson and Cook's (2004) analysis were also used for this analysis. The first data set for calculating $\tau_c$ used all measurements up to and including the first 120 minutes of testing (designated $\tau_{c\_T1}$), the second data set included the first 10 reading from the testing sequence (designated $\tau_{c\_T2}$) and the third data set included all measurements taken for the full duration of testing (designated $\tau_{c\_T3}$). The squared correlation coefficient, $R^2$, was used to assess the goodness of fit.

For the first 120 minutes of testing, a linear trend line tended to produce a reasonable fit to the data for almost all of the manufactured samples and over half of the natural samples. The erosion rate versus the average shear stress data for the natural samples tended to have a lot more scatter than the manufactured samples, in a couple cases making the applicability of a linear fit questionable. Mass failure and rapid scour progression early in testing typically contributed to the data variability at the higher average shear stresses in cases where the analysis produced a poor fit. Figure 4-9 shows the application of this method for a manufactured clay sample while Figure 4-10 shows a natural sample with more variability.

As the test progressed, longer time intervals were needed to see the same scour progression in the sample, causing the data to approach the zero erosion condition asymptotically. Linear trend lines tended to produce a poor fit to the data for the full test duration as shown by example in Figure 4-9 (b). Fitting nonlinear trend lines either caused the average shear stress intercept to be highly sensitive to the test duration, and number of data points included, or caused the intercept to occur at the origin and therefore a critical shear stress of zero. Due to these issues, nonlinear equations were not considered for use with this method.

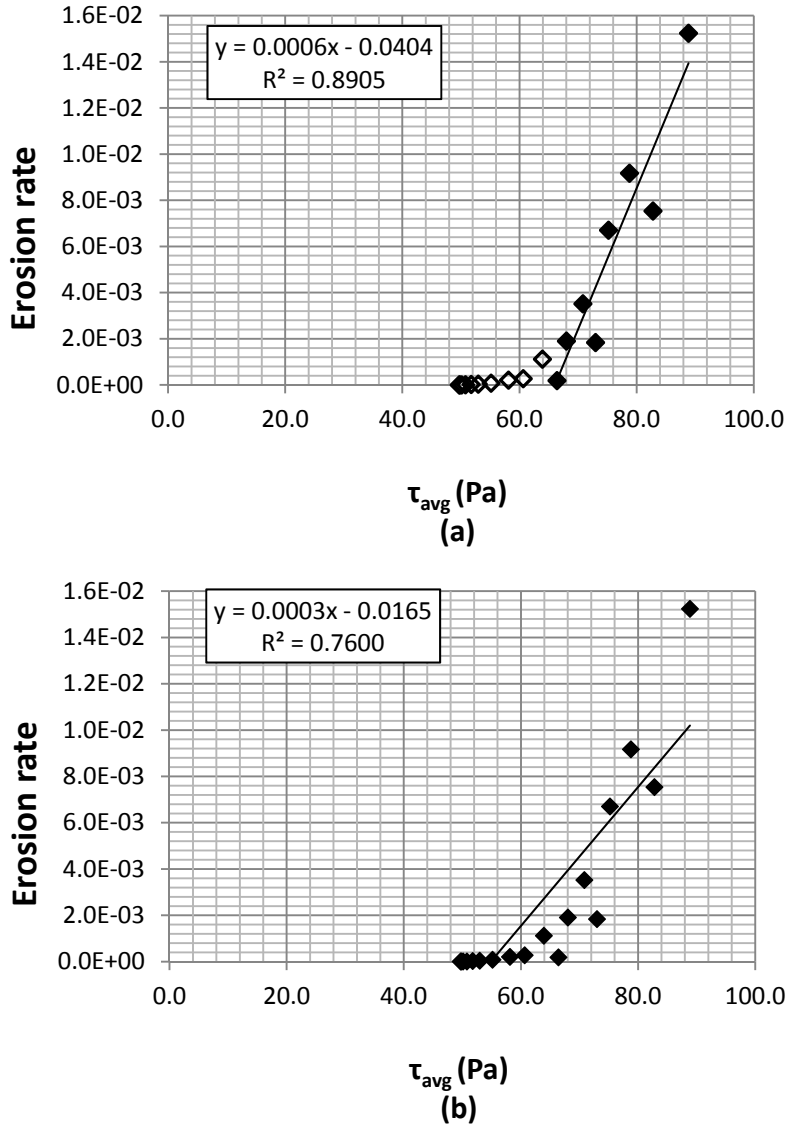


Figure 4-9. Erosion rate vs. average shear stress for BS(2) using the first 120 minutes of testing (a) and the full duration of testing (b). Only the solid black data points were fit with the trend line.

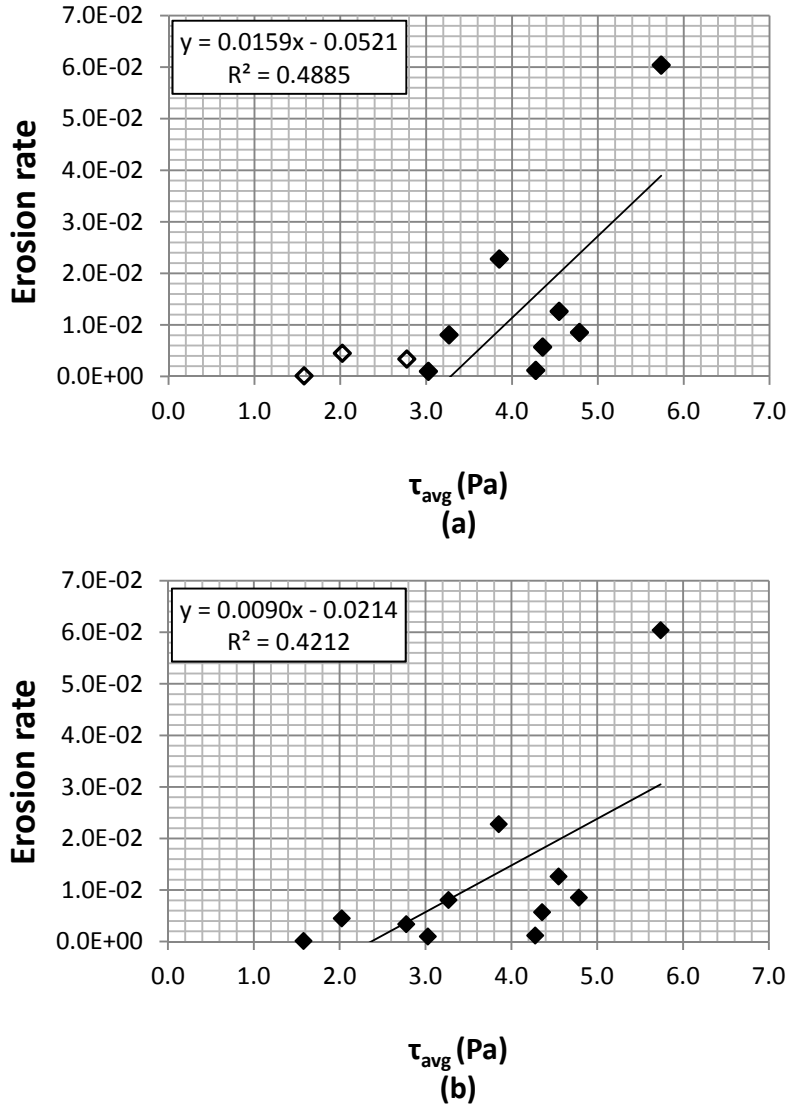


Figure 4-10. Erosion rate vs. average shear stress for LW(2) using the first 120 minutes of testing (a) and the full duration of testing (b). Only the solid black data points were fit with the trend line.

The asymptotic behavior of the plot in Figure 4-9 also shows that in most cases the first 120 minutes of data will estimate a value for $\tau_{c\_TI}$ which is higher than the measured equilibrium critical shear stress. As more data points are added into the analysis, the value of $\tau_{c\_T}$ will approach the value of $\tau_{c\_Ec}$. For this reason, using the full test duration for Thomas' analysis method was not considered a useful approach for determining the critical shear stress. The values of $\tau_{c\_TI}$ for each of the 31 tests are presented in Table 4-1.

Results shown in Figure 4-9 and Figure 4-10 illustrate a break in slope between the erosion rate data from early in testing and near the end of testing. This was typical for most samples, which might suggest that the change in erosion rate constants represent different modes of erosion. USBR (2006, pp. 4-15) differentiates between mass erosion and surface erosion and assigns both thresholds a critical shear stress value and erosion rate constant. A similar concept might be at work here, especially since it was less likely to observe mass erosion later in testing. As an example, during the first 120 minutes of testing, BS(2) was largely experiencing continuous mass erosion and mass failure. As testing progressed, mass erosion became more intermittent with removal of small aggregates becoming more prominent.

While the change in centerline depth with time provides a reasonable approximation of the erosion rate, it should ideally be expressed as the change in volume or mass with time. One of the main instances where the change in depth may not be a good approximation of the erosion rate is when mass failure occurs along the edge of the scour hole away from the centerline such that its removal is not captured by the centerline readings. These types of mass failures typically occurred maybe once or sometimes twice during testing and usually early on in the test sequence when applied shear stresses were high. It is expected that these events will have a minor impact on the data analysis due to their infrequent nature. Plots for the scour development are provided in for the 31 tests in Appendix A and readings associated with mass failure can usually be identified at specific times where the centerline and maximum depths suddenly depart or converge.

### 4.2.5 Comparison of the Critical Shear Stress Methods

In order to visualize the critical shear stress results, the values published in Table 4-1 are presented in graphical form in Figure 4-11 for the natural samples and Figure 4-12 for the manufactured samples. With a couple exceptions, Hanson and Cook's (2004) method tended to produce the lowest estimate of $\tau_c$ for a given sample while Thomas' method tended to produce the highest estimate.

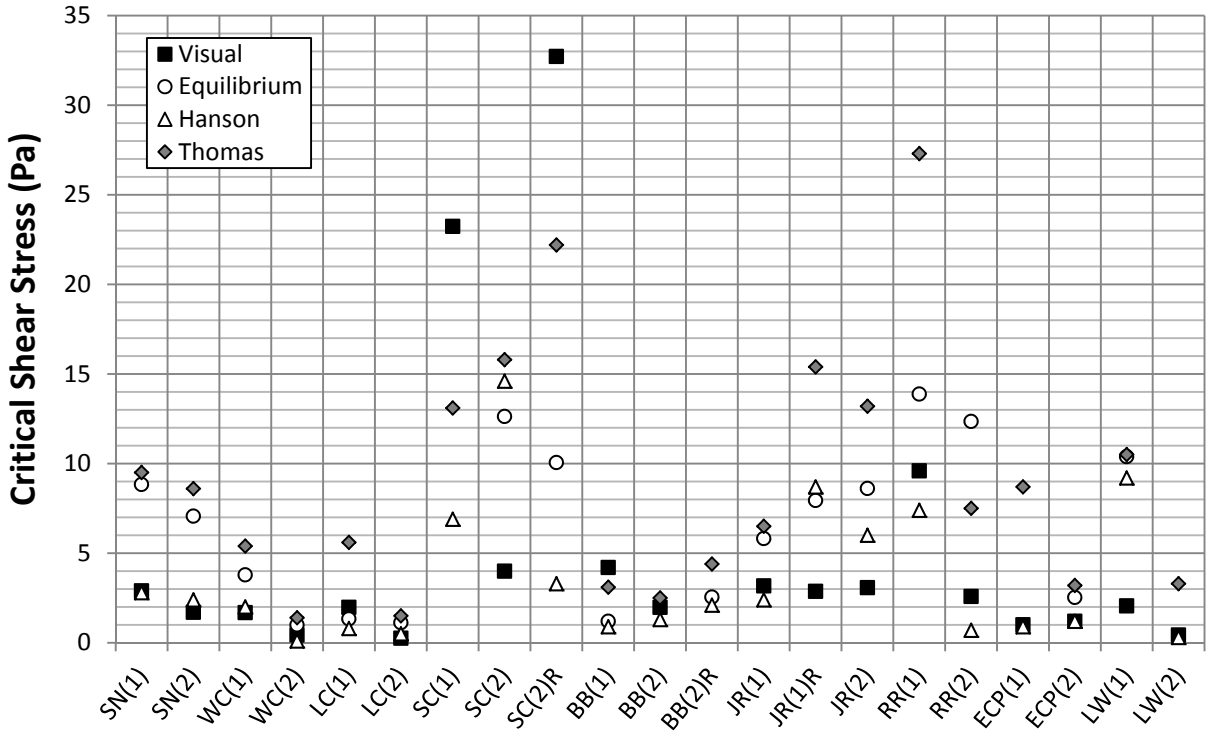


Figure 4-11. Ontario and Saskatoon Group critical shear stress values for all four analysis methods

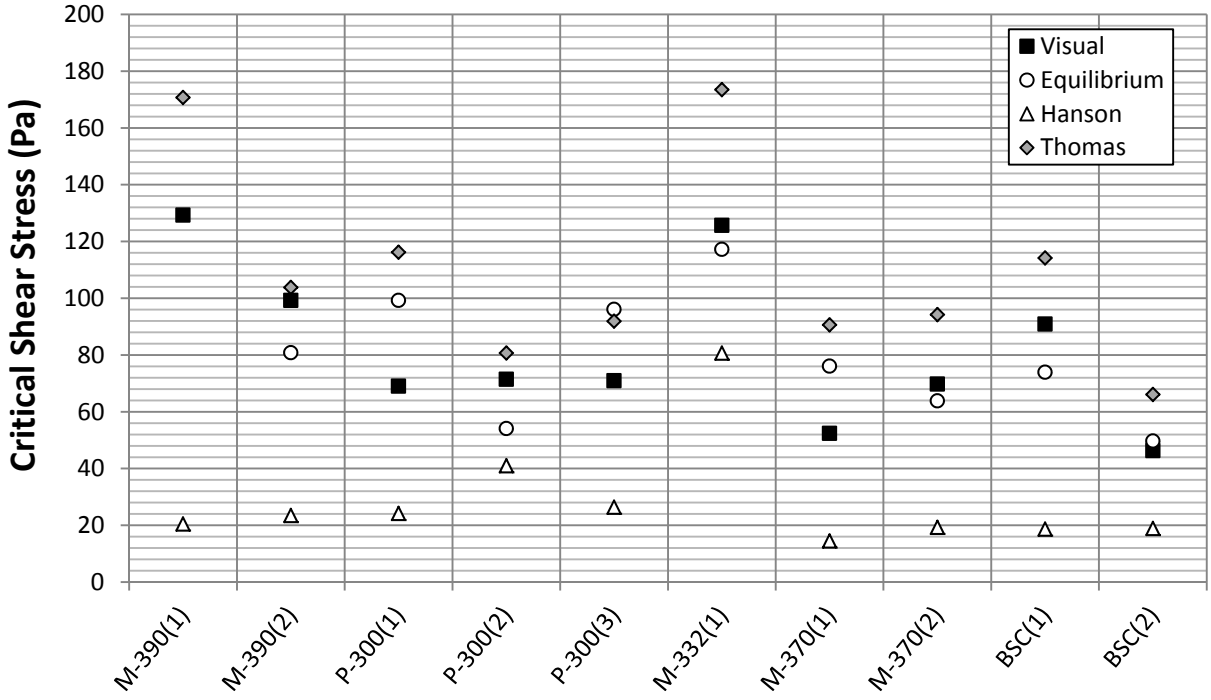


Figure 4-12. Manufactured Clay Group critical shear stress values for all four analysis methods

For the natural samples it can be seen that SC, JR and RR have noticeably more variation between the four methods than the other samples. It is likely that the presence of vegetation had some effect on the wider range of results as these three samples had the highest density root networks of any that were tested. The expectation that all four methods will converge to a single critical shear stress value in part depends on the degree of vertical uniformity in the sample since the visual method evaluates $\tau_{\_c}$ near the surface, Hanson and Cook (2004) and Thomas' method evaluate $\tau_{\_c}$ throughout the sample scour depth, and the equilibrium method evaluates $\tau_{\_c}$ at the final scour hole depth. If the soil shows significate layering or changes in composition over the full scour depth, these methods may be producing an incipient motion threshold for different materials. Alternatively, the presence of vegetation can create non uniform samples if it is not distributed evenly throughout the whole soil column with consistent root size and network density.

The ranking of the four methods was fairly consistent across all of the manufactured samples as was the range of values from the four methods. It should be noted that Hanson and Cook's (2004) method consistently produces values that are lower than the rest. This could possibly be the result of the high erosion rates that were generally observed near the beginning of testing due to mass failure and the analysis approach of extrapolating equilibrium conditions based on these initial measurements. Extrapolating this high initial rate to infinite time would expectedly result in large predictions for equilibrium depths and therefore smaller values of $\tau_c$.

The visual and equilibrium approach for determining the critical shear stress can both be considered direct methods since $\tau_c$ is calculated using a single set of either initial or final test conditions. These methods allow the operator to observe the sample at incipient motion without having to extrapolate to a theoretical time or stress. They also produce results that are independent of factors such as timing sequence, scour progression in non-uniform soils and mass failure during the early stages of testing. For these reasons both $\tau_{c\_V}$ and $\tau_{c\_Ec}$ are considered useful bench marks for comparing against $\tau_{c\_B1}$ and $\tau_{c\_T1}$.

Figure 4-13 compares the critical shear stress from Hanson and Cook's (2004) method and equilibrium method. As Blaisdell et al.'s (1981) curve fitting method provides an estimate of the equilibrium scour depth at "infinite time", it is reasonable to expect these values to be larger than the measured equilibrium scour depth, $H_{em}$, estimates. This was found to be the case for all but a few samples and since critical shear stress is inversely related to $H$, it is found that values of $\tau_{c\_B1}$ are generally less than $\tau_{c\_Ec}$.

The two samples which had measured depths slightly larger than Blaisdell et al.'s (1981) were SC(2) and JR(1)R. The scour depth with time plots for these samples shows that both tests began with a fairly linear erosion rate, but once they scoured to a certain depth, erosion accelerated producing a noticeable discontinuity in the slope of the erosion rate. Values of $\tau_{c\_B1}$ and $\tau_{c\_B3}$ were also significantly different for these samples since they use early test data and full test data respectively. With this in mind, it can be a bit misleading comparing these two samples in Figure 4-13 since $\tau_{c\_Ec}$ is calculated based on end of test conditions when scour is at its maximum extent and $\tau_{c\_B1}$ is calculated using early scour readings which represents the erosion properties of the top soil layer.

Figure 4-14 compares the values of $\tau_c$ calculated for the visual and equilibrium methods. There is noticeable scatter when comparing all three sample groups but the data appears to fit an identity line reasonably well. When comparing just the two natural sample groups, the values of $\tau_{c\_Ec}$ are almost twice as large on average compared to $\tau_{c\_V}$. The sample SC(2)R had noticeable layering with the surface being reinforced with a high density network of vegetation and deeper soil appearing more erodible. This likely explains why the value of the visual critical shear stress is much higher than the equilibrium method and for that reason SC(2)R was not included when calculating the best fit.

The weakly deflected jets observed at the end of testing for the manufactured clay samples ($r/\varepsilon > 1.5$) likely produced hydraulic conditions similar to a flat plat, causing the $\tau_{c\_Ec}$ values in this sample group not to be as noticeably overestimated as compared to the natural samples.

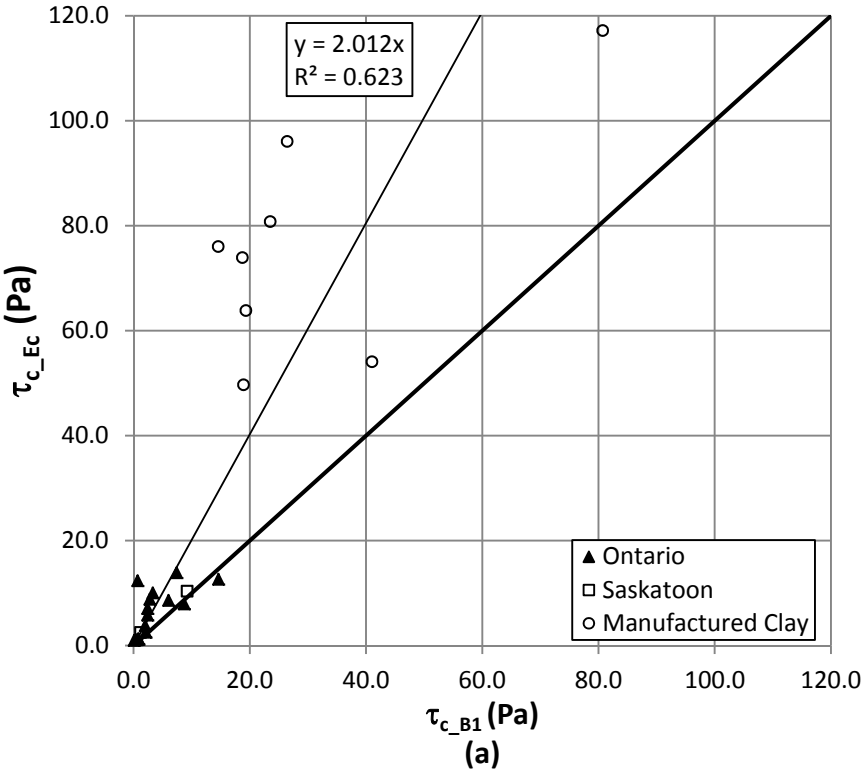


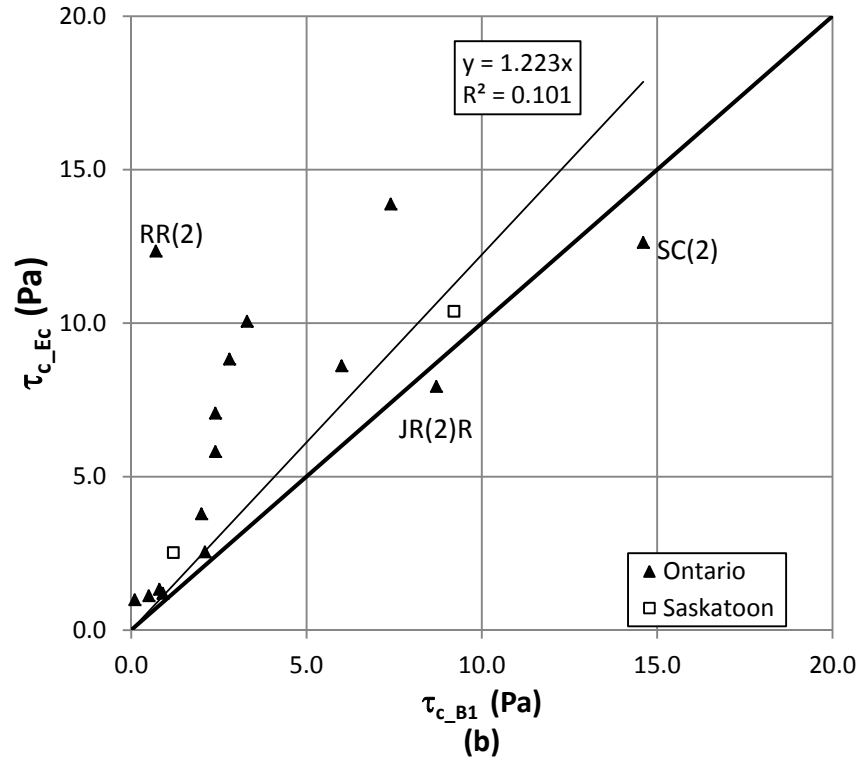


Figure 4-13. Comparison of the Blaisdell et al. (1981) and equilibrium methods for calculating critical shear stress for all samples (a) and the natural samples (b)

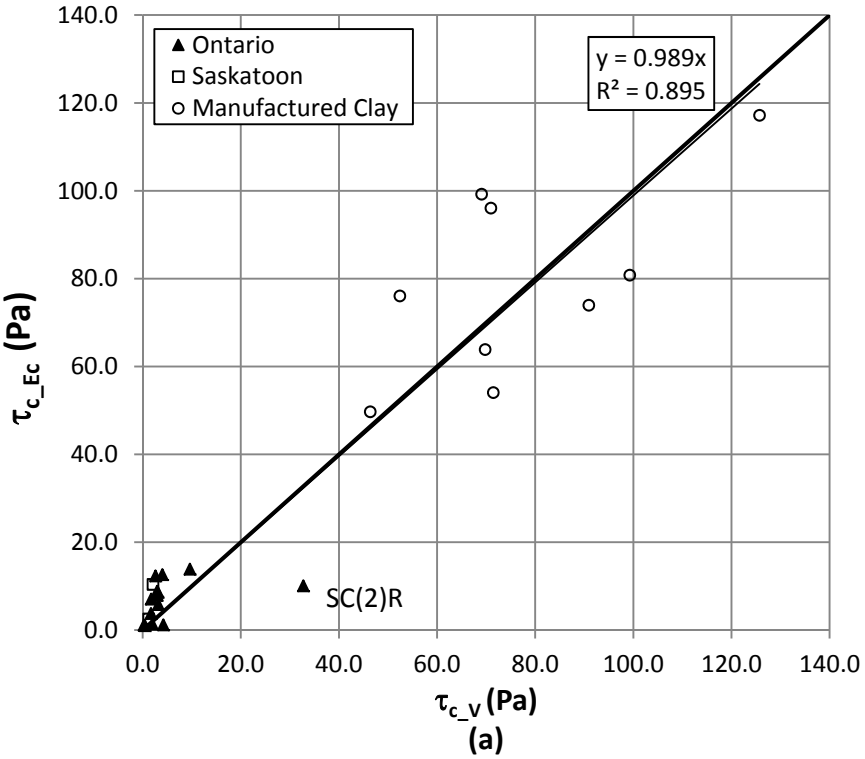


Figure 4-14. Comparison of the visual and equilibrium methods for calculating critical shear stress for all samples (a) and the natural samples (b)

Figure 4-15 compares the results from the equilibrium method and Thomas' method. Jet test data used in analysis of P-300(3) and RR(2) both had considerable scatter when plotting the erosion rate against the average shear stress, which helps explains why the best fit trend line in these two cases estimated values of $\tau_{c\_Tl}$ which are larger than $\tau_{c\_Ec}$. Other than these two samples, Thomas' method consistently produces smaller values for the critical shear stress.

The determination as to which of these methods produces a critical shear stress value closest to the actual value for the sample is not necessarily straightforward. Being able to observe a tested sample at or near its ultimate scour state lends confidence to the equilibrium method's determination of the critical shear stress and for this reason it was taken as the best representation of the actual critical shear stress value for the samples. However, it should be noted that the smooth boundary assumption for the friction coefficient will likely cause bias towards underestimating $\tau_c$ and the neglect of additional centerline velocity decay due to confined flows in the scour hole would cause a bias towards overestimating $\tau_c$.

Of all the methods, test conditions for the visual method are closest to the assumptions made in the analysis theory. While results from this method compare favorably with the equilibrium method for the manufactured sample group, their disagreement for the natural samples suggests a sensitivity to surface preparation and conditions as well as operator judgment.

Equilibrium scour depths determined using Hanson and Cook (2004) departed significantly from test observations, which is taken as an indication that the resulting critical shear stress is an underestimation of the actual value. The manufactured samples had a larger discrepancy between Hanson and Cook's (2004) results and observed results, which is likely caused in part by the large initial increases in depth caused by mass failure in the samples.

In general, Thomas' method tends to overestimate the critical shear stress when compared with the equilibrium values. Critical shear stress values converge to the equilibrium value as more data points are added into the analysis.

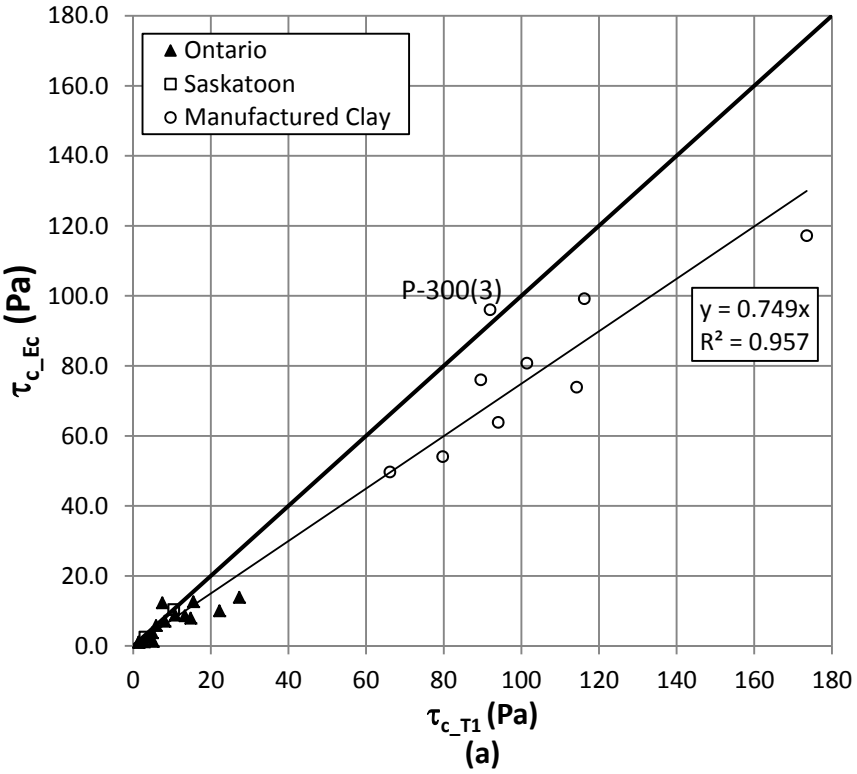


Figure 4-15. Comparison of Thomas' and equilibrium methods for calculating critical shear stress for all samples (a) and the natural samples (b)

### 4.2.6 Sample Ranking and Variation between Duplicate Tests

In order to determine how the ranking of critical shear stress values compared between analysis methods, values for each duplicate and triplicate sample was averaged and presented in Table 4-3. The average value from all four methods is given for each sample in column 6 which was used to rank samples from highest to lowest critical shear stress. All of the manufactured clays ranked in the top 5 with M-332 having the highest average $\tau_c$. Of the natural samples, the Little Cataraqui samples had the lowest average critical shear stress. Even though the $\tau_c$ values for a specific sample can vary significantly depending on the method of analysis, it is found that the sample rankings are fairly consistent when compared between methods.

Table 4-3. Averaged critical shear stress from duplicate samples and relative ranking

| Sample ID | Average $\tau_{c\_V}$ (Pa) | Rank | Average $\tau_{c\_Ec}$ (Pa) | Rank | Average $\tau_{c\_B1}$ (Pa) | Rank | Average $\tau_{c\_T1}$ (Pa) | Rank | Average from all methods (Pa) | Rank |
|---|---|---|---|---|---|---|---|---|---|---|
| M-332 | 125.7 | 1 | 117.2 | 1 | 80.7 | 1 | 173.5 | 1 | 124.3 | 1 |
| M-390 | 114.3 | 2 | 80.8 | 3 | 22.0 | 3 | 137.3 | 2 | 88.6 | 2 |
| P-300 | 70.5 | 3 | 83.1 | 2 | 30.5 | 2 | 96.3 | 3 | 70.1 | 3 |
| M-370 | 61.1 | 5 | 70.4 | 4 | 16.9 | 5 | 92.4 | 4 | 60.2 | 4 |
| BS | 68.6 | 4 | 61.8 | 5 | 18.8 | 4 | 90.2 | 5 | 59.8 | 5 |
| SC | 20.0 | 6 | 11.3 | 7 | 8.3 | 6 | 17.0 | 7 | 14.2 | 6 |
| RR | 6.1 | 7 | 13.1 | 6 | 4.1 | 9 | 17.4 | 6 | 10.2 | 7 |
| JR | 3.0 | 9 | 7.5 | 10 | 5.7 | 7 | 11.7 | 8 | 7.0 | 8 |
| LW | 1.2 | 11 | 10.4 | 8 | 4.8 | 8 | 6.9 | 10 | 5.8 | 9 |
| SN | 2.3 | 10 | 8.0 | 9 | 2.6 | 10 | 9.1 | 9 | 5.5 | 10 |
| ECP | 1.1 | 13 | 2.5 | 11 | 1.1 | 12 | 6.0 | 11 | 2.7 | 11 |
| BB | 3.1 | 8 | 1.9 | 13 | 1.4 | 11 | 3.3 | 14 | 2.4 | 12 |
| WC | 1.1 | 14 | 2.4 | 12 | 1.1 | 12 | 3.4 | 13 | 2.0 | 13 |
| LC | 1.1 | 12 | 1.2 | 14 | 0.7 | 14 | 3.6 | 12 | 1.6 | 14 |

The variability in the critical shear stress results between duplicate and triplicate samples was represented by the percent difference. For each of the four methods, the percent difference was calculated as the difference between the maximum and minimum critical shear stress values divided by the average critical shear stress for the paired or triplicate sample. These results are presented in Table 4-4 and Figure 4-16.

Table 4-4. Percent difference between duplicate and triplicate samples

| Sample ID | Percent Difference in $\tau_{c\_V}$ | Percent Difference in $\tau_{c\_Ec}$ | Percent Difference in $\tau_{c\_B1}$ | Percent Difference in $\tau_{c\_T1}$ |
|---|---|---|---|---|
| SN | 52% | 22% | 15% | 10% |
| WC | 118% | 117% | 181% | 118% |
| LC | 155% | 17% | 46% | 115% |
| SC | 144% | 23% | 137% | 53% |
| BB | 72% | 72% | 84% | 57% |
| JR | 10% | 37% | 111% | 76% |
| RR | 115% | 12% | 165% | 114% |
| ECP | 18% | | 29% | 92% |
| LW | 131% | | 187% | 104% |
| M-390 | 26% | | 14% | 4% |
| P-300 | 3% | 54% | 55% | 37% |
| M-370 | 28% | 17% | 28% | 4% |
| BSC | 65% | 39% | 1% | 53% |
| Maximum | 155% | 117% | 187% | 118% |
| Minimum | 3% | 12% | 1% | 4% |
| Average | 72% | 41% | 81% | 64% |

On average, Blaisdell et al.'s (1981) method for determining the critical shear stress produces the most variation when applied to duplicate samples. This fits with results from Section 4.2.2 which show the calculated value using data from the beginning of testing can be sensitive to the addition of a single measurement. The second highest variation on average is observed for the visual method which is also reasonable to expect given the dependence that the results have on surface preparation, the discharge intervals when increasing flows and the operator's judgment of incipient motion. The critical shear stress determined from running tests until equilibrium state is reaches has the least amount of variation of the four methods considered.

As expected, some of the highest variation is seen in the natural sample sets rather than the manufactured clays. It is interesting to note that the variation ranking of the four methods changes slightly for the manufactured clay sample group. The relative reduction in variation for the visual method can be explained by the more consistent surface conditions achieved for sample preparation. Additionally the relative increase in variation seen for the equilibrium method could potentially be explained by the occurrences of bulk sample failures early in testing which can initially define the shape of the scour hole.

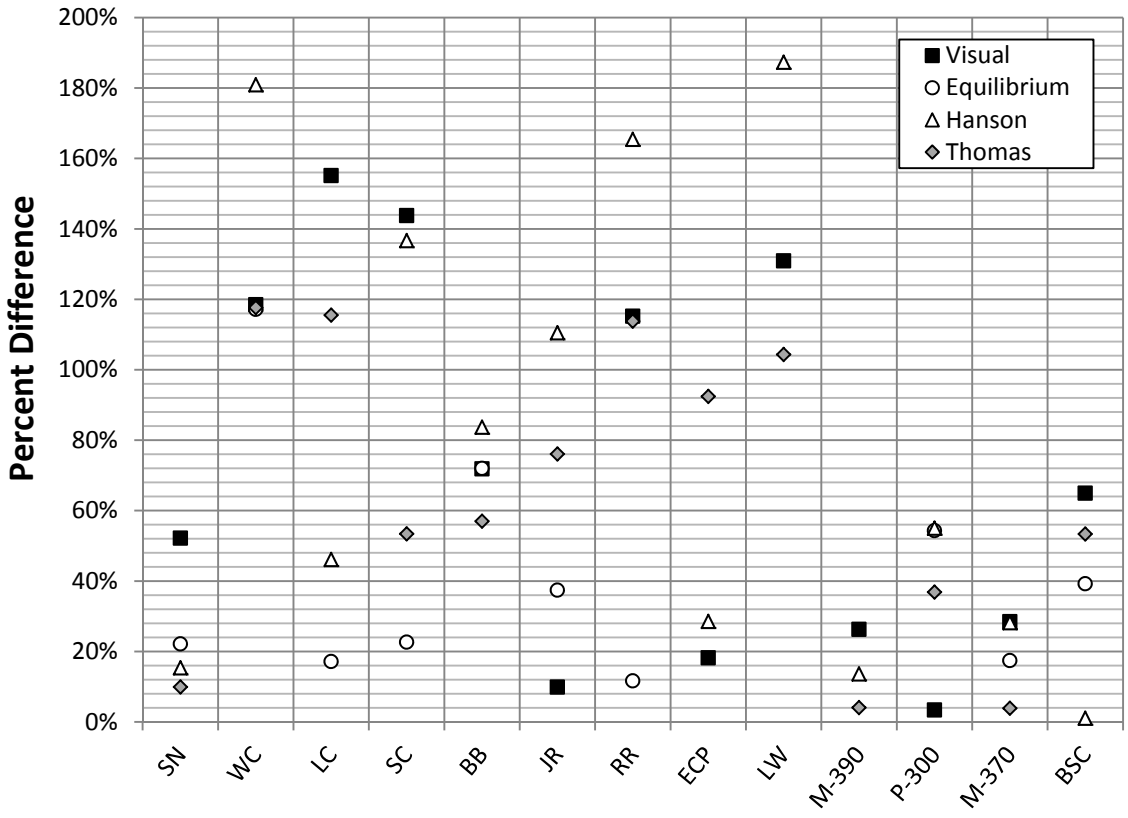


Figure 4-16. Percent difference between duplicate samples for all four methods

Luthi (2011) also ran HET on the duplicate samples from the Ontario group. Five out of fourteen samples tested successfully and in some cases produced critical shear stress values that were one or two orders of magnitude larger than the values presented in this section.

## 4.3 TIME DEVELOPMENT OF SCOUR AND ERODIBILITY COEFFICIENT ANALYSIS AND RESULTS

Other than providing the threshold for incipient motion, the critical shear stress is also a strong factor in determining equilibrium scour dimensions. The second soil parameter from the excess shear stress equation, the erodibility coefficient, largely describes the temporal aspect of scour such as how quickly the soil will erode and length of time required to reach equilibrium state. Two methods are considered for calculating the value of $k$ for the samples in this study.

Both methods used in this study solve the two erodibility parameters independently in sequence, however, it should be noted that there are iterative analysis methods that solve both parameters simultaneously (Simon et al., 2010; Hanson and Cook, 1997). The benefit of using the critical shear stress as an input for the erodibility coefficient analysis is that any of the four $\tau_c$ methods can be used in calculating *k*. Furthermore, if the excess shear stress equation is not assumed linear, then the exponent *n* is introduced as a third parameter, further complicating a simultaneous analysis method. Iterative solutions used in other studies typically define an upper and lower limit for each parameter in order to increase the analysis stability, while constraining the possible outcomes.

### 4.3.1 Analysis and Results for Hanson and Cook's (2004) Method, $k_H$

The method that Hanson and Cook (2004) use for calculating the erodibility coefficient is outlined in detail in Hanson and Cook (1997) A set of equations is produced to describe the time development of scour in cohesive soils subject to jet testing using a linear excess shear stress equation and the hydraulics of an impinging jet on a flat surface. This work is largely based off of Stein et al.'s (1993) work which shows the development of scour rate equations for jet scour downstream of a headcut using the general nonlinear form of the excess shear stress Equation [[2-14].

An analysis spreadsheet was developed following a similar procedure in order to determine *k*. The theoretical relationship between the dimensionless time, $T^* = t/T_R$, and the dimensionless height, $H^* = H/H_e$, are given as:

$$T^* = H^*\left(\frac{H_p^{*2}}{1\text{-}H_p^{*2}}\right) \qquad \text{for } H^* \leq H_p^* \qquad [4\text{-}1]$$

$$T^* - T_p^* = 0.5ln\left(\frac{1+H^*}{1-H^*}\right) - H^*\Big|_{H_p^*}^{H^*} \qquad \text{for } H^* > H_p^* \qquad [4\text{-}2]$$

where *H* is the height between the nozzle and sample surface, $H_e$ is the equilibrium height, $H_p^* = H_p/H_e$, *t* is time, and the reference time is given as:

$$T_r = \frac{H_e}{k\,\tau_c} \quad [4\text{-}3]$$

The height of the potential core, $H_p = C_d\, d_o$, with a diffusion coefficient of $C_d = 6.3$ was used for this analysis. The theoretical dimensionless time, $T^*_{Theo}$, was determined for each reading by using the measured scoured heights from testing in Equation [4-2]. The dimensionless time $T_p^*$ was determined by using $H^* = H_p^*$ in Equation [4-1].

The dimensionless time from testing, $T^*_{Test}$, was then determined using the measured time, $t_m$, which corresponded to $H$, and the following relationship:

$$T^* = T_m^* + T_i^* \quad [4\text{-}4]$$

where $T_m^* = t_m / T_R$ and $T_i^*$ was determined using $H^* = H_i^*$ in Equation [4-2]. Values of $H_e$ and $\tau_c$ determined from Section 4.2 were used in calculating $T_R$, along with an initial value of $k$.

The mean absolute relative error (MARE) between the dimensionless time measured from testing, $T^*_{Test}$, and the theoretical dimensionless time calculated from $H$, $T^*_{Theo}$, is given as:

$$MARE = \frac{1}{N}\sum_{1}^{N}\left|\frac{T^*_{Test} - T^*_{Theo}}{T^*_{Test}}\right| \quad [4\text{-}5]$$

The value of $k$ was determined iteratively by minimizing the MARE to fit the testing data to the theoretical curve.

#### 4.3.1.1 Linear Time Development of Scour

Initially, $\tau_{c\_B1}$ and $H_{e\_B1}$ from the first 120 minutes of testing were used to calculate the reference time from Equation [4-3]. In general, the $H^*$ versus $T^*$ data from testing appeared linear and fit the theoretical curve from Equation [4-2] relatively well as shown in Figure 4-17 (a). Table 4-5 provides the erodibility coefficients, $k_{H1}$, for each sample, which are shown to range from 0.031 to 16.195 $cm^3$/N-s. MARE values between the test data and theoretical curves

range from 0.029 to 0.550. As more data points were added in to the analysis, the data began to noticeable depart from the theoretical curve and as a result it was generally observed that the calculated erodibility coefficient values decreased. A similar dependence between the erodibility coefficient and the duration of testing was found by Mazurek (2010).

Using all the scour measurements from testing showed that the range of $H^*$ values from the data were different than the theoretical curve (ie. all values of $H^* < 1.0$). This occurred when the value of $H_{e\_B}$, which was used for normalizing the data, was significantly different that the largest depth value in the data set measured from testing, $H_{e\_m}$. This departure from the theoretical curve can be seen in Figure 4-17 (b) and was observed in all of the time development of scour plots when the full test duration was used.

In order remedy this difference in scale between the theoretical and measured values of $H^*$, values of $H_{e\_m}$ and $\tau_{c\_Ec}$ were instead used for calculating the reference time from Equation [4-3]. The BS(2) data analyzed in this manner can be seen in Figure 4-17 (c) and the erodibility coefficients associated with this modification are designated $k_{H3\_E}$. Daly et al. (2013) dealt with this discrepancy in scale from Hanson and Cook's (2004) method in a similar manner. Alternatively, Walder (2016) used the initial impingement height, $H_i$, as the reference length for normalization in order to avoid this problem altogether.

Values for $k_{H3\_E}$ for each sample are provided in Table 4-5, along with the MARE score, with values ranging from 0.000 to 15.573 $cm^3$/N-s and 0.146 to 0.742 respectively.

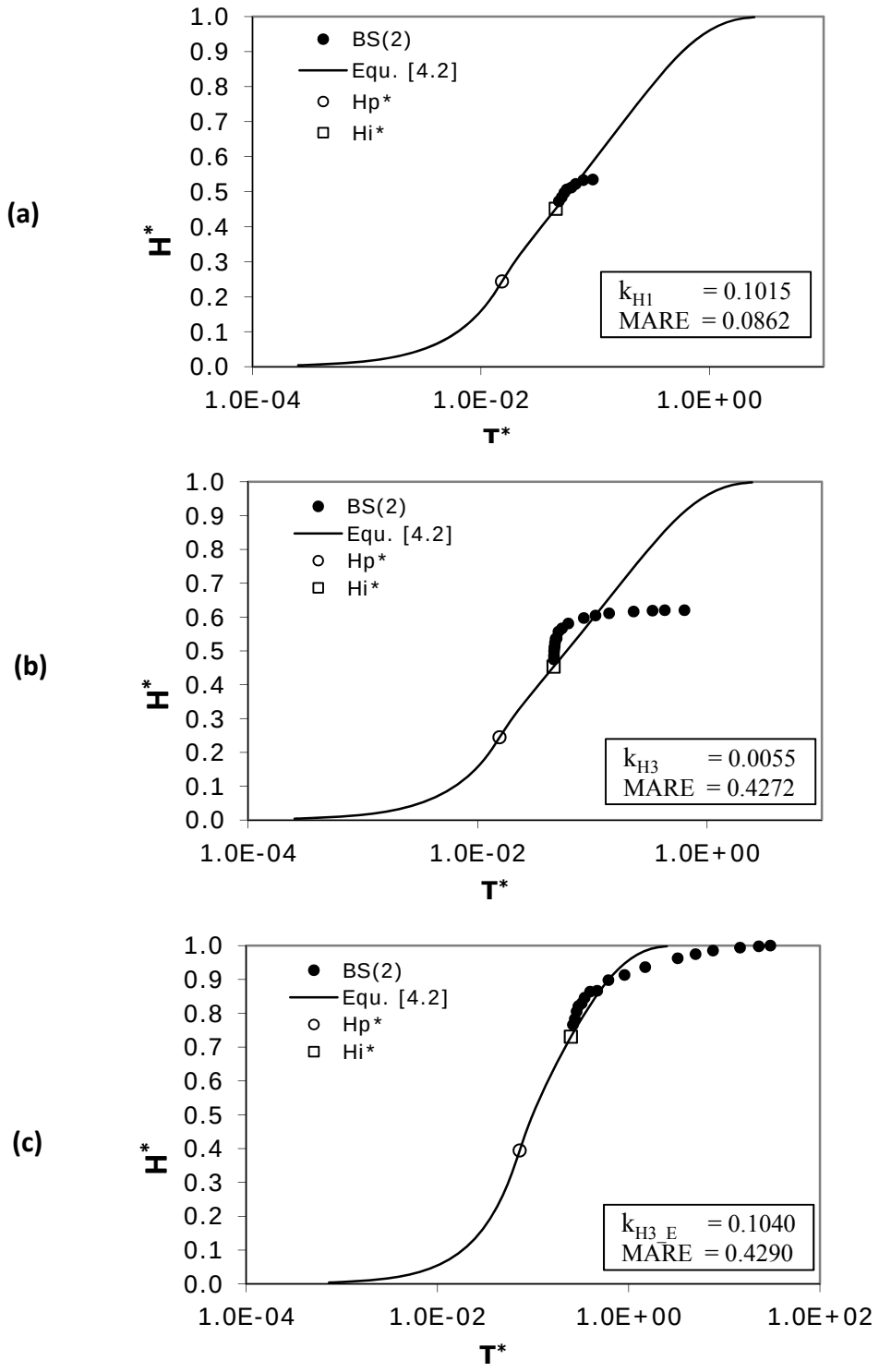


Figure 4-17. Time development of scour for BS(2) using $H_{e\_B1}$ and $\tau_{c\_B1}$ for the first 120 minutes of testing (a), the full duration of testing (b) and using $H_{e\_m}$ and $\tau_{c\_Ec}$ for the full duration of testing (c)

Table 4-5. Results for the linear excess shear stress equation using Hanson and Cook's (2004) method

| Sample ID | $k_{H1}$ ($cm^3$/N-s) | MARE | $k_{H3\ E}$ ($cm^3$/N-s) | MARE |
|---|---|---|---|---|
| SN(1) | 0.406 | 0.079 | 0.033 | 0.272 |
| SN(2) | 0.434 | 0.089 | 0.039 | 0.280 |
| WC(1) | 0.970 | 0.231 | 0.054 | 0.505 |
| WC(2) | 9.458 | 0.209 | 9.693 | 0.548 |
| LC(1) | 1.572 | 0.165 | 0.194 | 0.374 |
| LC(2) | 8.686 | 0.294 | 0.175 | 0.669 |
| SC(1) | 9.002 | 0.553 | 7.929 | 0.691 |
| SC(2) | 0.570 | 0.167 | 0.008 | 0.146 |
| SC(2)R | 0.398 | 0.182 | 0.012 | 0.393 |
| BB(1) | 6.640 | 0.322 | 0.115 | 0.530 |
| BB(2) | 16.195 | 0.484 | 7.775 | 0.742 |
| BB(2)R | 0.957 | 0.108 | 0.044 | 0.172 |
| JR(1) | 1.441 | 0.209 | 0.818 | 0.497 |
| JR(1)R | 0.532 | 0.108 | 0.005 | 0.165 |
| JR(2) | 0.367 | 0.060 | 0.004 | 0.156 |
| RR(1) | 0.151 | 0.047 | 0.003 | 0.323 |
| RR(2) | 0.680 | 0.093 | 0.810 | 0.533 |
| M-390(1) | 0.064 | 0.214 | - | - |
| M-390(2) | 0.090 | 0.149 | 0.076 | 0.524 |
| P-300(1) | 0.031 | 0.029 | 0.002 | 0.298 |
| P-300(2) | 0.077 | 0.066 | 0.038 | 0.319 |
| P-300(3) | 0.060 | 0.037 | 0.049 | 0.405 |
| M-332(1) | 0.036 | 0.071 | 0.000 | 0.293 |
| M-370(1) | 0.069 | 0.057 | 0.049 | 0.400 |
| M-370(2) | 0.069 | 0.071 | 0.032 | 0.457 |
| BSC(1) | 0.050 | 0.065 | 0.025 | 0.511 |
| BSC(2) | 0.102 | 0.086 | 0.006 | 0.427 |
| ECP(1) | 2.320 | 0.201 | 1.773 | 0.330 |
| LW(1) | 6.239 | 0.399 | 15.573 | 0.653 |
| ECP(2) | 4.908 | 0.214 | 4.333 | 0.520 |
| LW(2) | 3.846 | 0.140 | 2.861 | 0.217 |

#### 4.3.1.2 Development of Non-Linear Equations

Even though normalizing the scour height readings with the measured equilibrium height produced a better fit, there were still many samples that did not appear to have the same shape as the linear time development of scour equation given in [4-2].

In an effort to find a theoretical time development of scour equation that best fit the measured data, it was considered that perhaps the assumption of a linear excess shear stress equation did not hold true for some samples. Knapen et al. (2007) reported exponent values from a number of studies in the range of 0.87 to 6.8 and FHWA (2015) reported values from 1.2 to 2.0 while constraining values inside this range. Stein et al. (1993) presented time development of scour equations downstream of a head cut using $n$ values equal to 1, 1.5, and 2.0 and used them for analyzing experimental data collected from two noncohesive and one cohesive soil. This theory was essentially adapted for use with an impinging jet by Hanson and Cook (1997) assuming a linear excess shear stress equation ($n$ = 1.0). To test the assumption of a linear shear stress equation, similar time development of scour equations were adapted for discrete values of $n$ equal to 0.5, 1.5 and 2.0 starting from the integral form of the nonlinear excess shear stress equation given by Hanson and Cook (1997):

$$\int_0^{T^*} dT^* = \int_0^{H^*} \left(\frac{H_p^{*2}}{1-H_p^{*2}}\right)^n dH^* \qquad \text{for } H^* \leq H_p^* \qquad [4\text{-}6]$$

$$\int_{T_p^*}^{T^*} dT^* = \int_{H_p^*}^{H^*} \left(\frac{H^{*2}}{1-H^{*2}}\right)^n dH^* \qquad \text{for } H^* > H_p^* \qquad [4\text{-}7]$$

For a value of $n$ = 0.5 Equations [4-6] and [4-7] become:

$$T^* = H^* \left(\frac{H_p^{*2}}{1-H_p^{*2}}\right)^{0.5} \qquad \text{for } H^* \leq H_p^* \qquad [4\text{-}8]$$

$$T^* - T_p^* = \frac{-H^*}{\sqrt{-H^{*2}/(H^{*2}-1)}}\Bigg|_{H_p^*}^{H^*} \qquad \text{for } H^* > H_p^* \qquad [4\text{-}9]$$

For a value of $n$ = 1.5 Equations [4-6] and [4-7] become:

$$T^* = H^* \left( \frac{H_p^{*2}}{1\text{-}H_p^{*2}} \right)^{1.5} \qquad \text{for } H^* \leq H_p^* \qquad [4\text{-}10]$$

$$T^* - T_p^* = \left( \frac{2}{H^*} - H^* \right) \times \sqrt{\frac{-H^{*2}}{H^{*2} - 1}} \Bigg|_{H_p^*}^{H^*} \qquad \text{for } H^* > H_p^* \qquad [4\text{-}11]$$

For a value of $n$ = 2.0 Equations [4-6] and [4-7] become:

$$T^* = H^* \left( \frac{H_p^{*2}}{1\text{-}H_p^{*2}} \right)^{2} \qquad \text{for } H^* \leq H_p^* \qquad [4\text{-}12]$$

$$T^* - T_p^* = \left( \frac{H^*}{2 - 2H^{*2}} \right) + H^* + \frac{3}{4} ln \left( \frac{1 - H^*}{1 + H^*} \right) \Bigg|_{H_p^*}^{H^*} \qquad \text{for } H^* > H_p^* \qquad [4\text{-}13]$$

For these six equations the reference time used for normalization is:

$$T_r = \frac{H_e}{k\, \tau_c^n} \qquad [4\text{-}14]$$

These non-linear equations were added in to the analysis spreadsheet and the same procedure outlined in Section 4.3.1 was used to fit the test data.

#### 4.3.1.3 Comparison of Linear and Non-Linear Results

Scour data for each sample were fit to the equations presented in Section 4.3.1 and 4.3.1.2 with the respective erodibility coefficients and MAREs given in Table 4-6. An example analysis plot is provided in Figure 4-18 which shows the fit achieved between the four theoretical sets of equations and the BSC(2) manufactured sample. Initially, the lowest MARE produced by the four sets of equations was taken as an indication of which time development of scour exponent best described the test data for a given sample. However, since the time development of scour equations approach $H^*$ = 1.0 asymptotically, it was not uncommon for the last data points to have

a relatively large residual error in $T^*$. These residuals tended to be more pronounced for the larger exponents, since a higher value meant a more gradual approach to $H^* = 1.0$. This caused the goodness of fit score to be bias towards selecting the curve developed for $n = 0.5$ even when this curve produced a poor visual fit (see Figure 4-19).

Table 4-6. Results from linear and non-linear time development of scour equations based on Hanson and Cook (1997)

| Sample ID | n = 1 | | n = 0.5 | | n = 1.5 | | n = 2.0 | | Selected $n_{HE}$ |
|---|---|---|---|---|---|---|---|---|---|
| | $k_{H3\_E}$ ($cm^3$/N-s) | MARE | $k_{H3\_E}$ * | MARE | $k_{H3\_E}$ † | MARE | $k_{H3\_E}$ ‡ | MARE | |
| SN(1) | 0.546 | 0.301 | 0.233 | 0.214 | 0.758 | 0.315 | 0.506 | 0.416 | 1.0 |
| SN(2) | 1.129 | 0.169 | 1.060 | 0.191 | 1.255 | 0.203 | 1.816 | 0.548 | 1.5 |
| WC(1) | 1.992 | 0.308 | 2.607 | 0.246 | 1.659 | 0.338 | 1.430 | 0.348 | 2.0 |
| WC(2) | 10.486 | 0.237 | 10.945 | 0.316 | 14.992 | 0.261 | 64.759 | 0.636 | 1.0 |
| LC(1) | 0.653 | 0.237 | 0.536 | 0.259 | 0.742 | 0.376 | 1.801 | 0.744 | 1.0 |
| LC(2) | 9.241 | 0.669 | 0.283 | 0.540 | 10.828 | 0.651 | 18.963 | 0.543 | 2.0 |
| SC(1) | - | - | - | - | - | - | - | - | - |
| SC(2) | 0.056 | 0.192 | 0.050 | 0.137 | 0.074 | 0.212 | 0.084 | 0.333 | 1.5 |
| SC(2)R | 0.057 | 0.434 | 0.083 | 0.320 | 0.053 | 0.525 | 0.133 | 0.860 | 1.5 |
| BB(1) | 1.790 | 0.608 | 0.271 | 0.461 | 2.750 | 0.601 | 5.598 | 0.804 | 0.5 |
| BB(2) | - | 0.731 | - | 0.654 | - | 0.730 | - | 0.669 | 2.0 |
| BB(2)R | 0.194 | 0.206 | 0.156 | 0.136 | 0.398 | 0.346 | 1.112 | 0.620 | 1.0 |
| JR(1) | 5.371 | 0.397 | 2.936 | 0.354 | 6.752 | 0.392 | 13.026 | 0.544 | 1.5 |
| JR(1)R | 0.016 | 0.222 | 0.025 | 0.116 | 0.016 | 0.422 | 0.020 | 0.558 | 0.5 |
| JR(2) | 0.010 | 0.206 | 0.018 | 0.111 | 0.007 | 0.391 | 0.045 | 0.648 | 0.5 |
| RR(1) | 0.015 | 0.426 | 0.022 | 0.258 | 0.014 | 0.523 | 0.011 | 0.609 | 1.5 |
| RR(2) | 2.044 | 0.386 | 3.367 | 0.374 | 1.174 | 0.417 | 0.608 | 0.522 | 1.5 |
| M-390(1) | - | - | - | - | - | - | - | - | 2.0 |
| M-390(2) | 0.208 | 0.472 | 0.039 | 0.435 | 0.032 | 0.459 | 0.005 | 0.352 | 2.0 |
| P-300(1) | 0.013 | 0.365 | 0.038 | 0.245 | 0.005 | 0.312 | 0.001 | 0.164 | 2.0 |
| P-300(2) | 0.156 | 0.194 | 0.551 | 0.144 | 0.045 | 0.278 | 0.025 | 0.607 | 1.5 |
| P-300(3) | 0.167 | 0.347 | 0.027 | 0.327 | 0.035 | 0.335 | 0.010 | 0.335 | 2.0 |
| M-332(1) | 0.001 | 0.303 | 0.007 | 0.218 | 0.0003 | 0.398 | 0.0002 | 0.506 | 2.0 |
| M-370(1) | 0.128 | 0.339 | 0.031 | 0.357 | 0.020 | 0.266 | 0.004 | 0.327 | 2.0 |
| M-370(2) | 0.090 | 0.386 | 0.098 | 0.342 | 0.014 | 0.343 | 0.002 | 0.285 | 2.0 |
| BSC(1) | 0.067 | 0.485 | 0.020 | 0.390 | 0.009 | 0.463 | 0.001 | 0.371 | 2.0 |
| BSC(2) | 0.104 | 0.429 | 0.071 | 0.326 | 0.027 | 0.359 | 0.007 | 0.262 | 2.0 |
| ECP(1) | - | - | - | - | - | - | - | - | - |
| LW(1) | 22.497 | 0.542 | 8.010 | 0.424 | 33.236 | 0.482 | 41.856 | 0.429 | 2.0 |
| ECP(2) | 9.001 | 0.482 | 6.697 | 0.439 | 8.842 | 0.452 | 7.736 | 0.313 | 2.0 |
| LW(2) | - | - | - | - | - | - | - | - | - |

* units of ($cm^3$/N-s) ($N^{0.5}$/m)

† units of ($cm^3$/N-s) ($m/N^{0.5}$)

‡ units of ($cm^3$/N-s) ($m^2$/N)

For this reason, the best fit curve was decided by visual inspection with the MARE only being considered when two curves appeared to produce similarly adequate fits. The exponent that was selected as giving the best fit to the time development of scour equation is given in Table 4-6 as $n_{HE}$. The associated erodibility coefficient and MARE are can be found in the column corresponding to the selected exponent. For example, it was found that an exponent of 1.0 produced a time development of scour equation that best fit the test data for SN(1) with an erodibility coefficient of 0.546 $cm^3$/N-s and a MARE of 0.301. This was despite the fact that the time development of scour equation with $n = 0.5$ produced a smaller MARE.

In general, the larger exponent values of $n = 2.0$ produced the best fit for the manufactured clay samples while the natural samples had quite a bit more variability in the exponents that provided the best time development of scour fit. For the natural samples it was found that $n = 0.5$ produced the best fit for 3 samples, $n = 1.0$ produced the best fit for 4 samples, $n = 1.5$ produced the best fit for 6 samples, and $n = 2.0$ produced the best fit for 5 samples. Since the dimensions of the erodibility coefficient determined using the non-linear time development of scour equations depend on the value of $n$, the erodibility coefficients cannot be meaningfully compared in their current form.

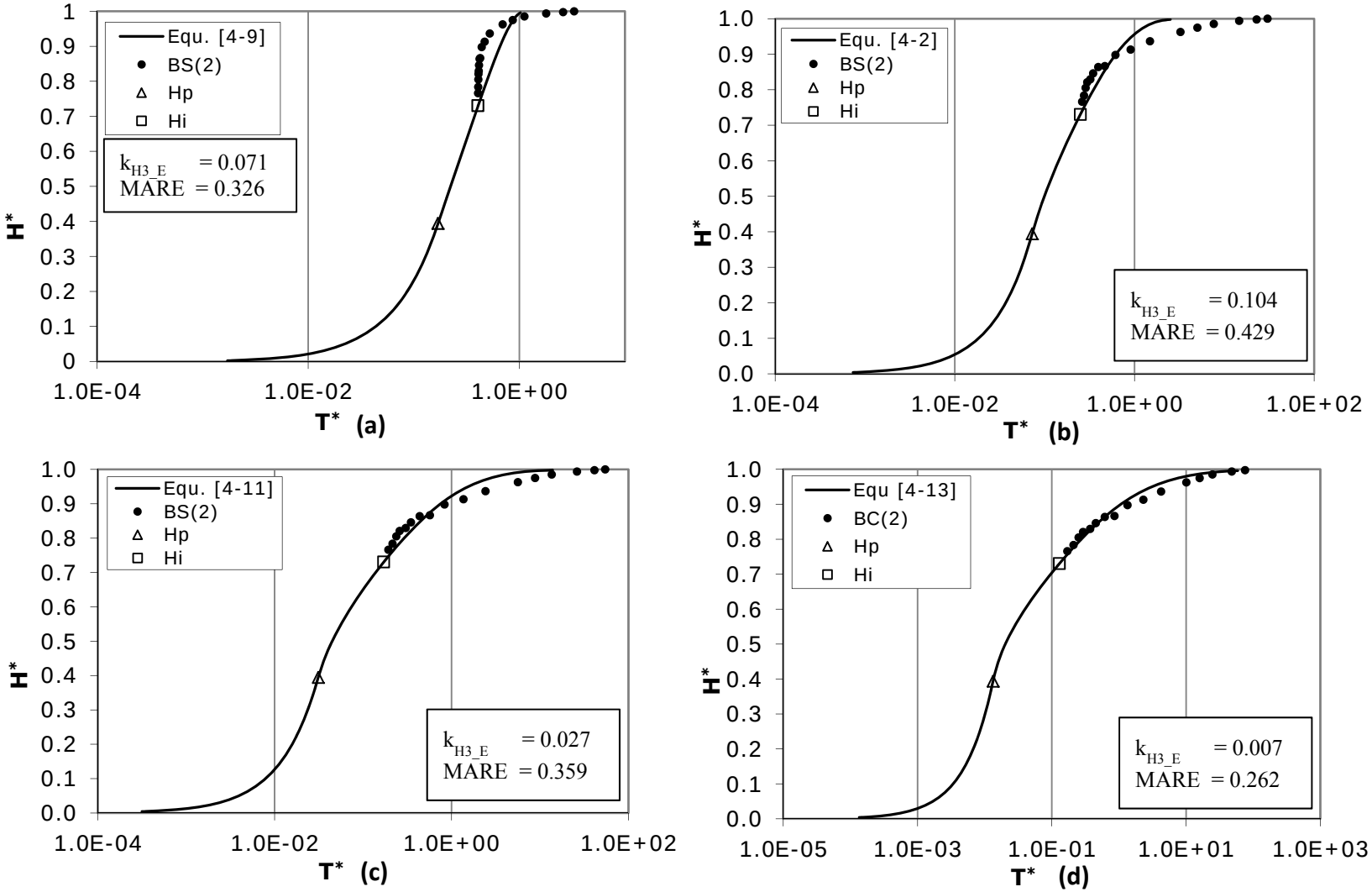


Figure 4-18. Time development of scour for BSC(2) for n = 0.5 (a), n = 1.0 (b), n = 1.5 (c), and n = 2.0 (d)

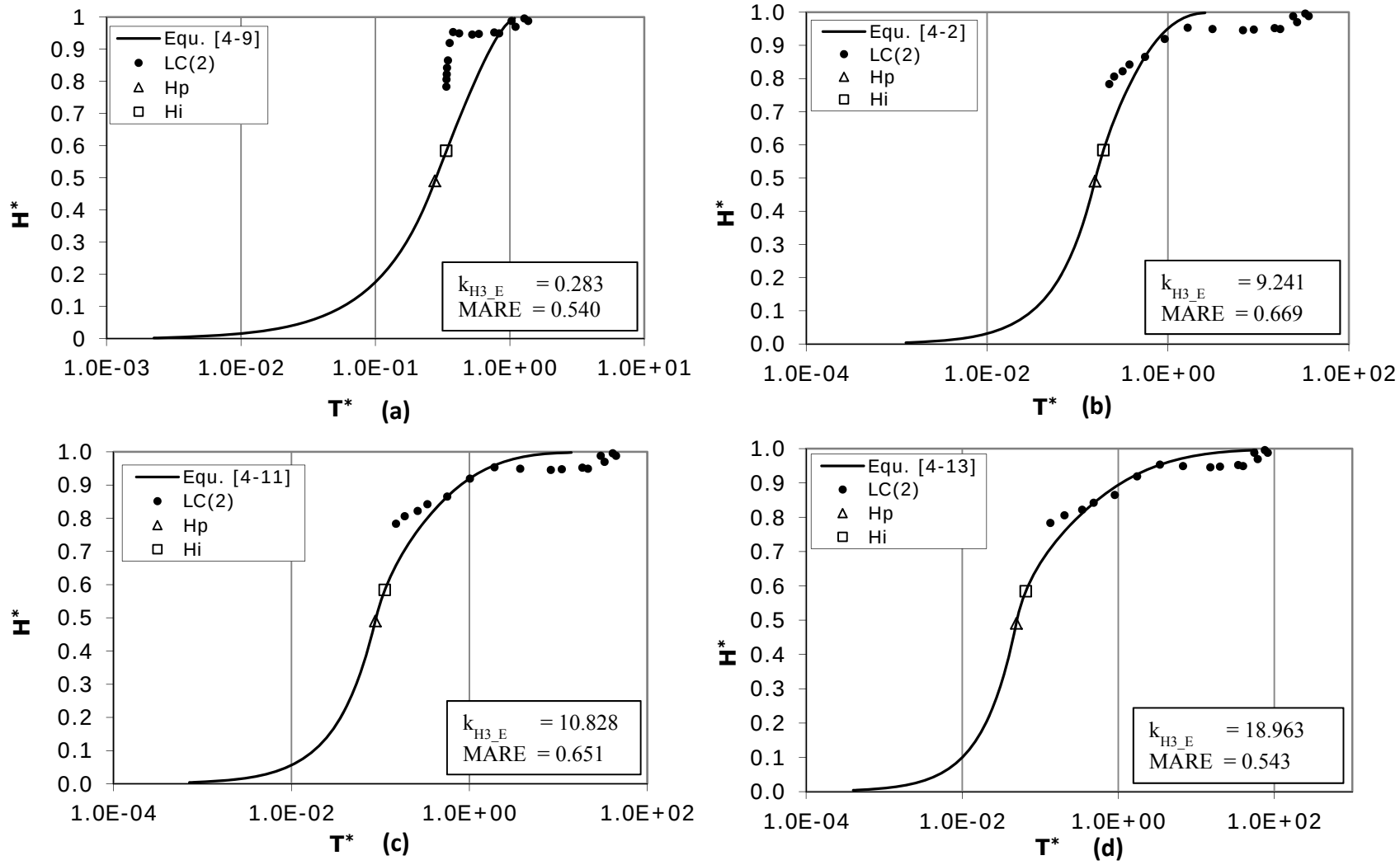


Figure 4-19. Time development of scour for LC(2) for n = 0.5 (a), n = 1.0 (b), n = 1.5 (c), and n = 2.0 (d)

### 4.3.2 Analysis and Results for Thomas' Method, $k_T$

Analysis of the sample data according to Thomas' method followed the theory presented in Section 2.4.2. Equation [2-1] was modified to produce a power function in the form of $k_T (\tau_{avg} - \tau_{c\_T})^n$ that was used to calculate the theoretical erosion rate at for each depth reading. $\tau_{avg}$ from Equation [2-12] was used to represent the effective stress on the bed while the critical shear stress was taken the smaller value of either $\tau_{c\_T}$ or $\tau_{avg}$ from the last test reading. This selection was required in order to keep the excess shear stress near the end of testing non-negative, and the difference between these critical shear stress values was usually negligible. In some cases, usually near the end of a jet test, a depth reading was taken that was smaller than a preceding reading. These readings were ignored for the purpose of this analysis method in order to avoid negative erosion rates.

The Residual Sum of Squares (RSS) between the theoretical power equation and the erosion rate determined from testing using Equation [2-13], was minimized using the solver function in excel to iteratively optimize values of $k_T$ and $n$. These values were initialized as 0.1 and 1.0 respectively before the optimization process was run. An example of the analysis spreadsheet is given in Appendix C.

Figure 4-20 shows an example output for this analysis method using the BS(2) sample. Similar to the analysis of $\tau_{c\_T}$, the relationship between the erosion rate and excess shear stress for the first 120 minutes of testing tended to be linear in almost all samples tested. Increasing the duration of test data used in the analysis generally caused the resulting value of $n$ to increase as the sample approached the equilibrium depth asymptotically. Since the value of the exponent was found to be sensitive to the test duration, it became important for the operator to make a distinction as to when the sample achieved equilibrium state and exclude further readings from the analysis. Running a test indefinitely would cause a continuous increase in the value of $n$.

(a)

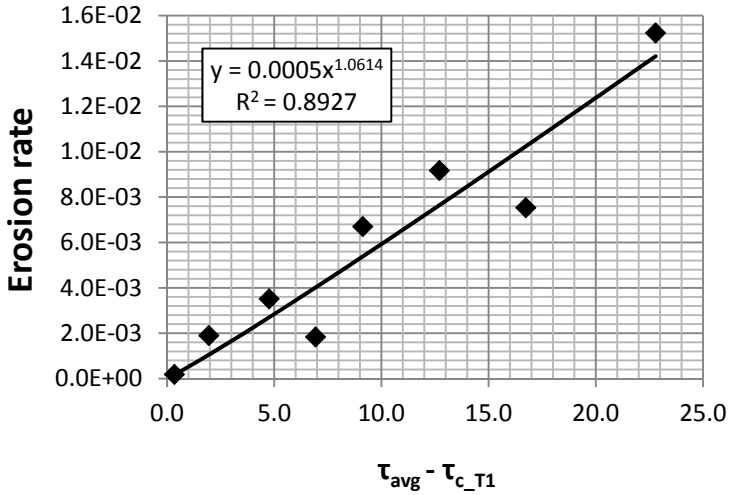


(b)

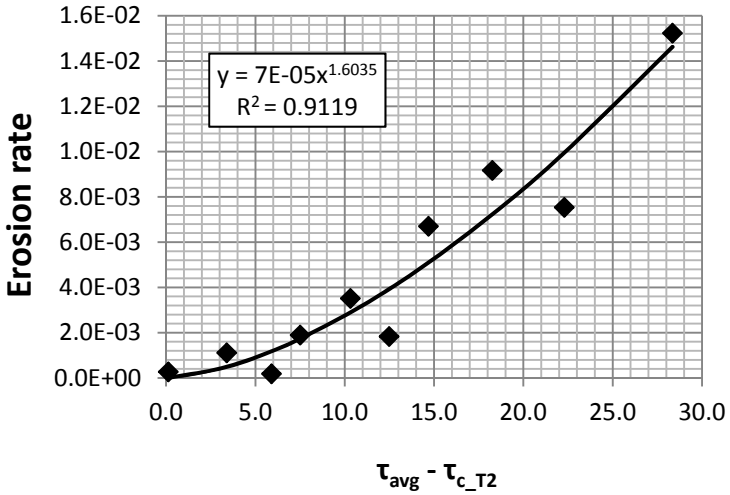


(c)

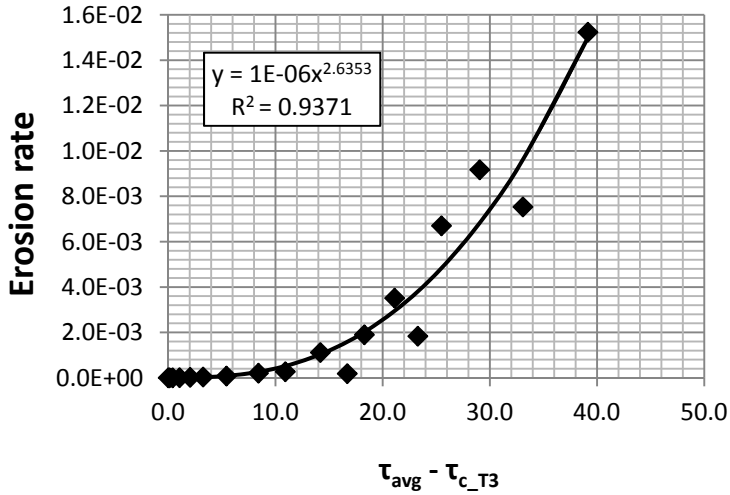


Figure 4-20. Thomas' Method for BS(2) using the first 120 minutes of testing and a linear fit (a), using the first 10 data points (b), and using the full test duration with a power fit (c)

The excess shear stress parameters determined using Thomas' method for the first 120 minutes of testing ($k_{T1}$ and $n_{T1}$) and for the full duration of testing ($k_{T3}$ and $n_{T3}$) are presented in Table 4-7. When using the full duration of testing data, exponent values ranged from 0.6 to 6.1. Only two samples produced exponents that were less than 1.0 and very rarely was a linear excess shear stress equation selected as a best fit to all the data. Values for the coefficient of determination, $R^2$, are provided to give an indication of goodness of fit.

Table 4-7. Results for the excess shear stress equation using Thomas' Method

| Sample ID | $k_{T1}$ ($cm^3$/N-s) | $n_{T1}$ | $R^2$ | $k_{T3}$* | $n_{T3}$ | $R^2$ |
|---|---|---|---|---|---|---|
| SN(1) | 2.290 | 1.00 | 0.431 | 0.905 | 1.25 | 0.786 |
| SN(2) | 4.768 | 1.00 | 0.757 | 0.163 | 3.06 | 0.931 |
| WC(1) | 20.531 | 1.00 | 0.852 | 0.250 | 5.80 | 0.997 |
| WC(2) | 22.812 | 1.00 | 0.929 | 14.030 | 1.32 | 0.930 |
| LC(1) | 8.442 | 1.00 | 0.822 | 0.001 | 5.12 | 0.989 |
| LC(2) | 69.500 | 1.00 | 0.921 | 26.942 | 3.24 | 0.999 |
| SC(1) | 12.667 | 1.00 | 0.999 | 0.773 | 1.82 | 0.996 |
| SC(2) | 8.321 | 1.00 | 0.924 | 0.001 | 6.10 | 0.991 |
| SC(2)R | 1.654 | 1.00 | 0.953 | 0.004 | 2.62 | 0.958 |
| BB(1) | 33.915 | 1.00 | 0.952 | 0.160 | 4.50 | 0.998 |
| BB(2) | 56.703 | 1.00 | 0.992 | 15.995 | 2.29 | 1.000 |
| BB(2)R | 10.399 | 1.00 | 0.799 | 0.026 | 5.71 | 0.909 |
| JR(1) | 15.720 | 1.00 | 0.796 | 1.215 | 3.25 | 0.989 |
| JR(1)R | 7.009 | 1.00 | 0.822 | 0.000 | 4.94 | 0.809 |
| JR(2) | 2.392 | 1.00 | 0.509 | 0.002 | 4.09 | 0.682 |
| RR(1) | 0.498 | 1.00 | 0.133 | 0.001 | 3.39 | 0.453 |
| RR(2) | 1.141 | 1.00 | 0.147 | 4.376 | 0.60 | 0.433 |
| M-390(1) | 0.375 | 1.00 | 0.896 | 0.051 | 1.38 | 0.901 |
| M-390(2) | 0.668 | 1.00 | 0.921 | 0.002 | 2.35 | 0.975 |
| P-300(1) | 0.083 | 1.00 | 0.317 | 0.004 | 1.61 | 0.690 |
| P-300(2) | 0.692 | 1.00 | 0.663 | 0.000 | 2.99 | 0.472 |
| P-300(3) | 0.177 | 1.00 | 0.490 | 0.238 | 0.95 | 0.813 |
| M-332(1) | 0.260 | 1.00 | 0.946 | 0.000 | 5.00 | 0.563 |
| M-370(1) | 0.219 | 1.00 | 0.864 | 0.018 | 1.55 | 0.936 |
| M-370(2) | 0.347 | 1.00 | 0.494 | 0.001 | 2.20 | 0.703 |
| BSC(1) | 0.219 | 1.00 | 0.893 | 0.004 | 1.75 | 0.944 |
| BSC(2) | 0.611 | 1.00 | 0.891 | 0.001 | 2.64 | 0.937 |
| ECP(1) | 8.667 | 1.00 | 0.682 | 0.014 | 3.33 | 0.748 |
| LW(1) | 26.147 | 1.00 | 1.000 | 20.342 | 1.23 | 0.999 |
| ECP(2) | 39.773 | 1.00 | 0.744 | 1.812 | 4.97 | 0.955 |
| LW(2) | 15.872 | 1.00 | 0.489 | 0.032 | 5.28 | 0.838 |

* units are dependent on the value of $n_{T3}$ and will be different for every sample

One of the challenges with using a nonlinear excess shear stress equation with unconstrained, non-integer values of $n$ is that the erodibility coefficient becomes an empirical curve fitting parameter rather than a soil property with physical dimensions. Comparison of the erodibility coefficient between samples becomes meaningless when the excess shear stress exponent differs. Walder (2016) provides a method for nondimensionalizing the erodibility coefficient which allows the results from a nonlinear time development of scour analysis to be compared; however, this method was not applied to the current study.

### 4.3.3 Comparison of Erodibility Coefficient Methods

Both Hanson and Cook's (2004) and Thomas' analysis of the first 120 minutes of testing appear to fit reasonably well with the assumption of a linear erosion rate. The resulting erodibility coefficients from these methods are compared in Figure 4-21, and it can be seen that values from Thomas' method are about 4 to 6 times larger on average than Hanson and Cook's (2004).

Part of this discrepancy is due to the use of Blaisdell et al.'s (1981) equilibrium depth in Hanson and Cook's (2004) analysis, where the value of the erodibility coefficient is dependent on the critical shear stress and equilibrium depth. It was found that as the difference between the measured and estimated equilibrium depths increased, the value of $k$ decreased. In Thomas' method the critical shear stress does not affect the slope of the excess shear stress equation and therefore does not impact the erodibility coefficient.

Erodibility coefficients determined using a nonlinear time development of scour equation for Hanson and Cook's (2004) method or the full duration of test data for Thomas' method were not directly compared and discussed due to the discrepancy in units.

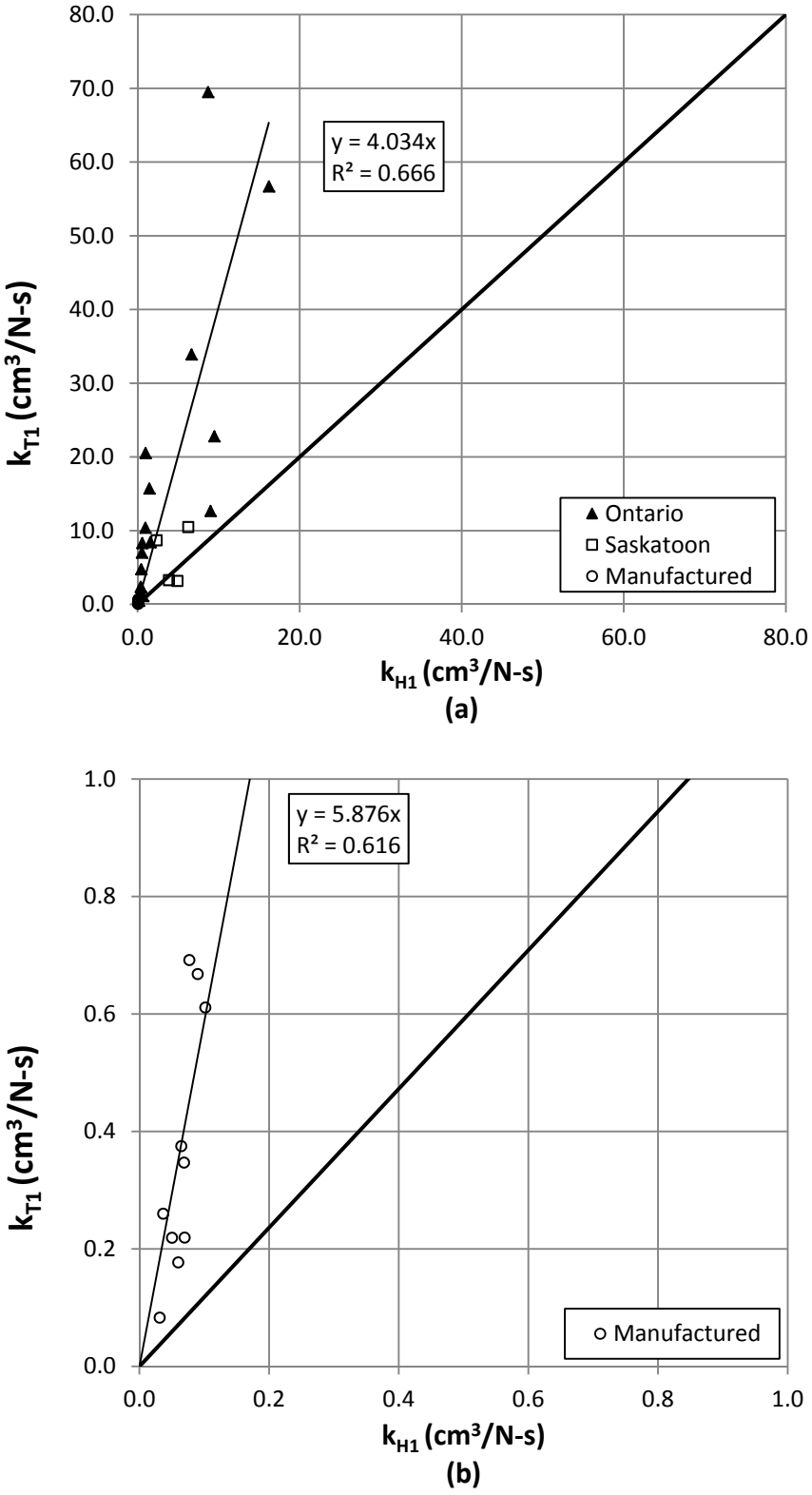


Figure 4-21. Comparison between the erodibility coefficients determined from Hanson and Cook's (2004) Method and Thomas' Method for all samples (a) and the manufactured samples (b)

For the full duration of testing both methods appear to favor non-linear excess shear stress equations as the best fit to the data. It is difficult to compare the best fit excess shear stress equations from Hanson and Cook (2004) and Thomas' method since the units of $k$ depend on the value of $n$. However, fitting all the data to both analysis methods suggests that most samples tested are best described by a non-linear excess shear stress equation. Values for the exponents are shown for both methods in Figure 4-22.

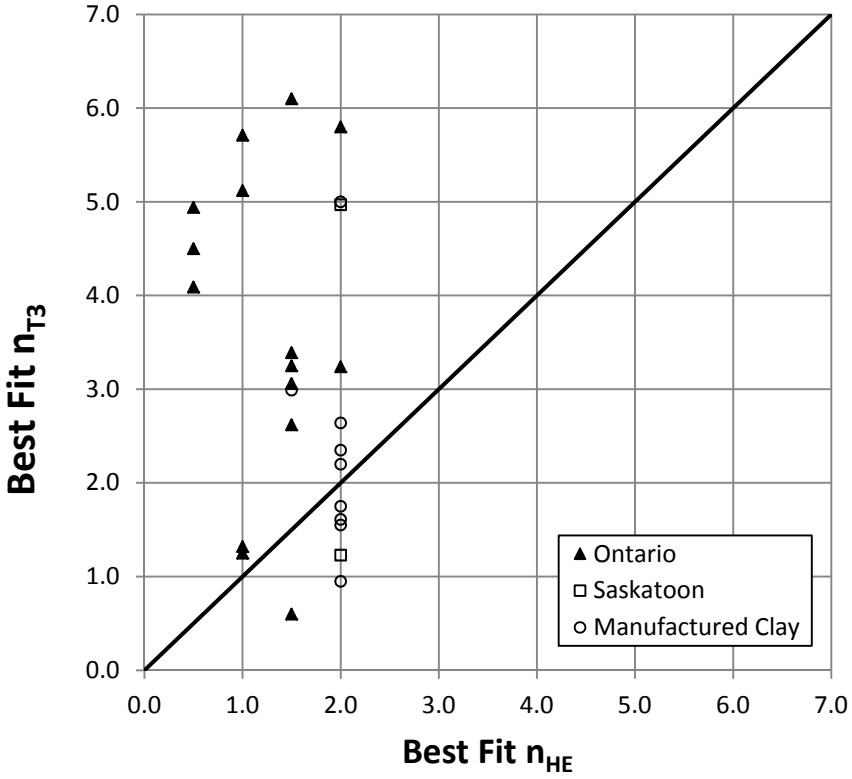


Figure 4-22. Best fit values of $n$ from Hanson and Cook's (2004) Method and Thomas' Method

The benefit of Thomas' method is that it is not limited to discrete solutions of the time development of scour equations. It is interesting to note that the exponent values from Thomas' method falls within a similar range as Knapen et al. (2007).

## 4.4 SCOUR HOLE GEOMETRY ANALYSIS

The equilibrium centerline depth ($\varepsilon_{cl\infty}$), maximum depth ($\varepsilon_{m\infty}$), average scour hole radius at half of the centerline depth ($\overline{b_{cl\infty}}$), and average radius of the scour hole at the surface ($\overline{r_{o\infty}}$) are provided in Table 4-8 for the samples that were deemed to reach equilibrium state.

Table 4-8. Scour hole dimensions at equilibrium state

| Sample ID | $\varepsilon_{cl\infty}$ | $\varepsilon_{m\infty}$ | $\overline{b_{cl\infty}}$ | $\overline{r_{o\infty}}$ | $\overline{r_{o\infty}}/\varepsilon_{cl\infty}$ |
|---|---|---|---|---|---|
| | (mm) | (mm) | (mm) | (mm) | |
| SN(1) | 19.8 | 23.3 | 14.2 | 30.0 | 1.5 |
| SN(2) | 20.4 | 26.0 | 32.5 | 45.0 | 2.2 |
| WC(1) | 34.0 | 34.9 | 33.0 | 43.5 | 1.3 |
| WC(2) | 70.7 | 70.7 | 51.3 | 75.5 | 1.1 |
| LC(1) | 110.7 | 110.7 | 54.3 | 69.0 | 0.6 |
| LC(2) | 42.7 | 42.7 | 46.0 | 65.0 | 1.5 |
| SC(1) | - | - | - | - | - |
| SC(2) | 13.9 | 13.9 | 24.3 | 30.5 | 2.2 |
| SC(2)R | 65.5 | 65.5 | 33.3 | 48.5 | 0.7 |
| BB(1) | 85.0 | 85.0 | 27.8 | 36.5 | 0.4 |
| BB(2) | - | - | - | - | - |
| BB(2)R | 34.8 | 34.8 | 45.3 | 52.5 | 1.5 |
| JR(1) | 23.3 | 23.3 | 31.0 | 35.3 | 1.5 |
| JR(1)R | 47.6 | 47.8 | 17.0 | 27.0 | 0.6 |
| JR(2) | 32.8 | 37.0 | 18.0 | 34.5 | 1.1 |
| RR(1) | 70.8 | 70.8 | 28.5 | 31.3 | 0.4 |
| RR(2) | 38.5 | 39.7 | 41.8 | 57.5 | 1.5 |
| M-390(1) | - | - | - | - | - |
| M-390(2) | 41.4 | 42.5 | 48.8 | 75.0 | 1.8 |
| P-300(1) | 32.0 | 34.6 | - | - | - |
| P-300(2) | 36.8 | 45.3 | 48.3 | 73.5 | 2.0 |
| P-300(3) | 26.0 | 40.1 | 58.5 | 69.5 | 2.7 |
| M-332(1) | 34.2 | 36.1 | 58.8 | 69.5 | 2.0 |
| M-370(1) | 39.3 | 48.9 | 61.5 | 75.0 | 1.9 |
| M-370(2) | 43.7 | 44.9 | 50.3 | 72.0 | 1.6 |
| BSC(1) | 49.7 | 49.7 | 51.8 | 75.0 | 1.5 |
| BSC(2) | 34.5 | 34.5 | 29.8 | 55.5 | 1.6 |
| ECP(1) | - | - | - | - | - |
| LW(1) | 22.9 | 30.7 | - | 73.0 | 3.2 |
| ECP(2) | 40.6 | 51.4 | 66.0 | 72.5 | 1.8 |
| LW(2) | - | - | - | - | - |

The radius to depth ratio provides an indication of the scour hole shape with lower values representing a narrow, deep scour hole, characteristic of a strongly deflected jet, and higher values representing a wide, shallow scour hole, characteristic of a weakly deflected jet. Values range from 0.4 for BB(1) and RR(1) to 3.2 for LW(1). It was found that the presence of root networks can affect the scour hole shape as it develops. Dense root networks near the surface can inhibit lateral erosion and the growth of the scour hole diameter, even if the soil around it is highly erodible, and create conditions for a strongly deflected jet.

Of all the scour assessment methods highlighted in Section 2.5, the approach presented by Mazurek (2001) was used for analyzing the natural and manufactured samples tested in this study. Mazurek (2001) shows the critical shear stress to be a reasonable indicator of scour in manufactured clay soils, indicating that it may also be a reasonable indicator of scour in natural samples. Results from Mercier et al. (2013) also suggest the shape of scour hole is related to the critical shear stress and note that higher values of $\tau_c$ tend to produce weakly deflected jets and lower values of $\tau_c$ tend to produce a strongly deflected jet.

Based on the theory presented in Section 2.5.3, relationships between the equilibrium centerline depth and the dimensionless excess shear stress were developed using selected critical shear stress values from this study:

$$\frac{\varepsilon_{cl\infty}}{H_i} = 0.32 \left\{ \frac{\tau_{om} - \tau_{c\_B1}}{\tau_{c\_B1}} \right\}^{0.29} \quad [4\text{-}15]$$

$$\frac{\varepsilon_{cl\infty}}{H_i} = 0.25 \left\{ \frac{\tau_{om} - \tau_{c\_B2}}{\tau_{c\_B2}} \right\}^{0.38} \quad [4\text{-}16]$$

$$\frac{\varepsilon_{cl\infty}}{H_i} = 0.48 \left\{ \frac{\tau_{om} - \tau_{c\_V}}{\tau_{c\_V}} \right\}^{0.01} \quad [4\text{-}17]$$

with correlation coefficients, $R^2$, of 0.3208, 0.6041, and 0.0002 respectively. The plots used for developing Equations [4-15], [4-16], and [4-17] are provided in Figure 4-23, Figure 4-24, and Figure 4-25 respectively.

In all cases there is noticeably more scatter in the natural data sets than the manufactured samples, which is to be expected. Furthermore, in the plots where $\tau_{c\_B}$ was as the indicator for soil erodibility there appeared to be better agreement in the lower ranges of dimensionless excess shear stresses, with most of the noticeable departure between the data and proposed relationship occurring at the higher ranges. Interestingly enough using $\tau_{c\_B2}$, which includes the first 10 data points from testing in the analysis, produced a better agreement in the proposed relationship than $\tau_{c\_B1}$, which only uses the first 120 minutes of jet test data.

The visual critical shear stress was found to have a very poor correlation with the equilibrium centerline depth. A relationship was not developed using $\tau_{c\_Ec}$ since both the dimensionless centerline depth and excess shear stress are not independent parameters.

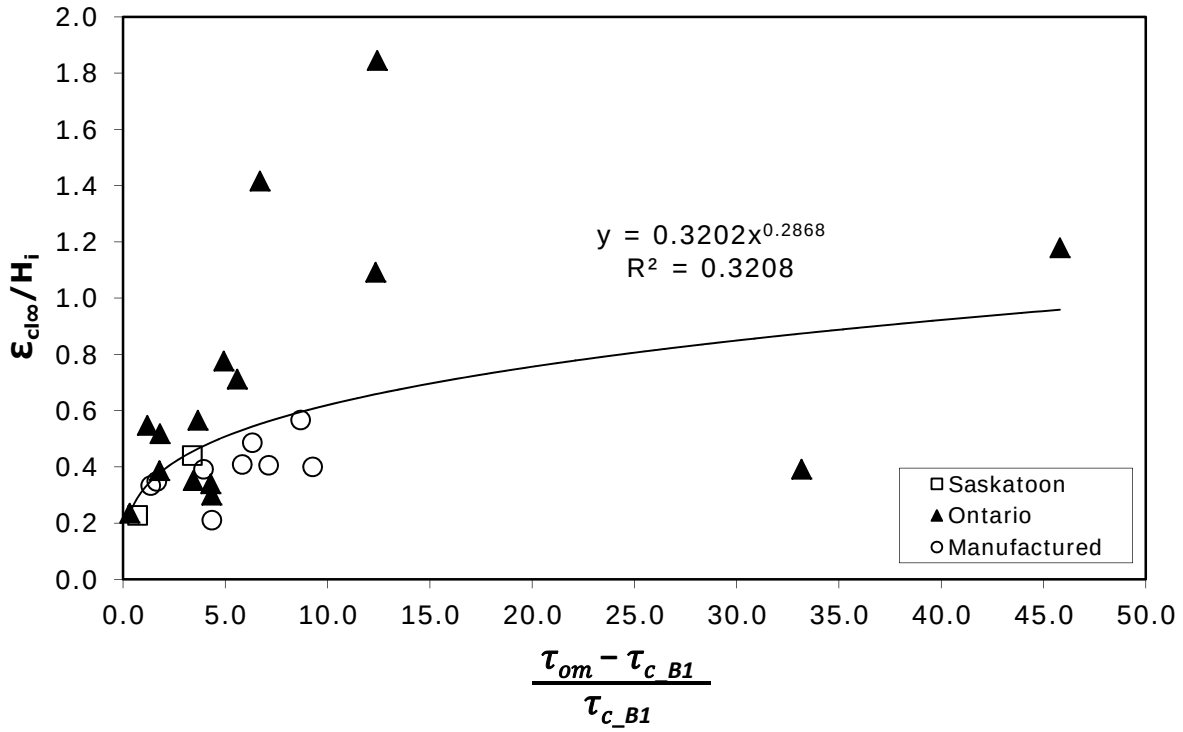


Figure 4-23. Scour analysis for the equilibrium centerline depth using Hanson and Cook's (2004) Method with the first 120 minutes of test data

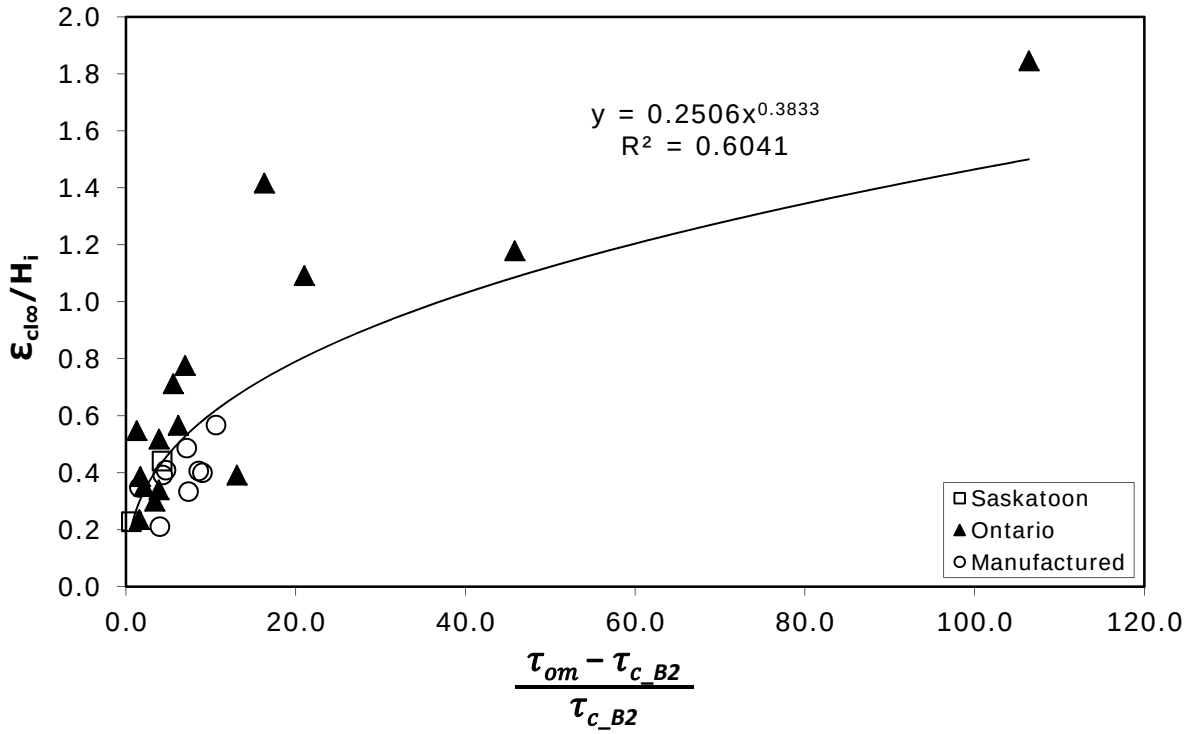


Figure 4-24. Scour analysis for the equilibrium centerline depth using Hanson and Cook's (2004) Method with the first 10 readings from the test data

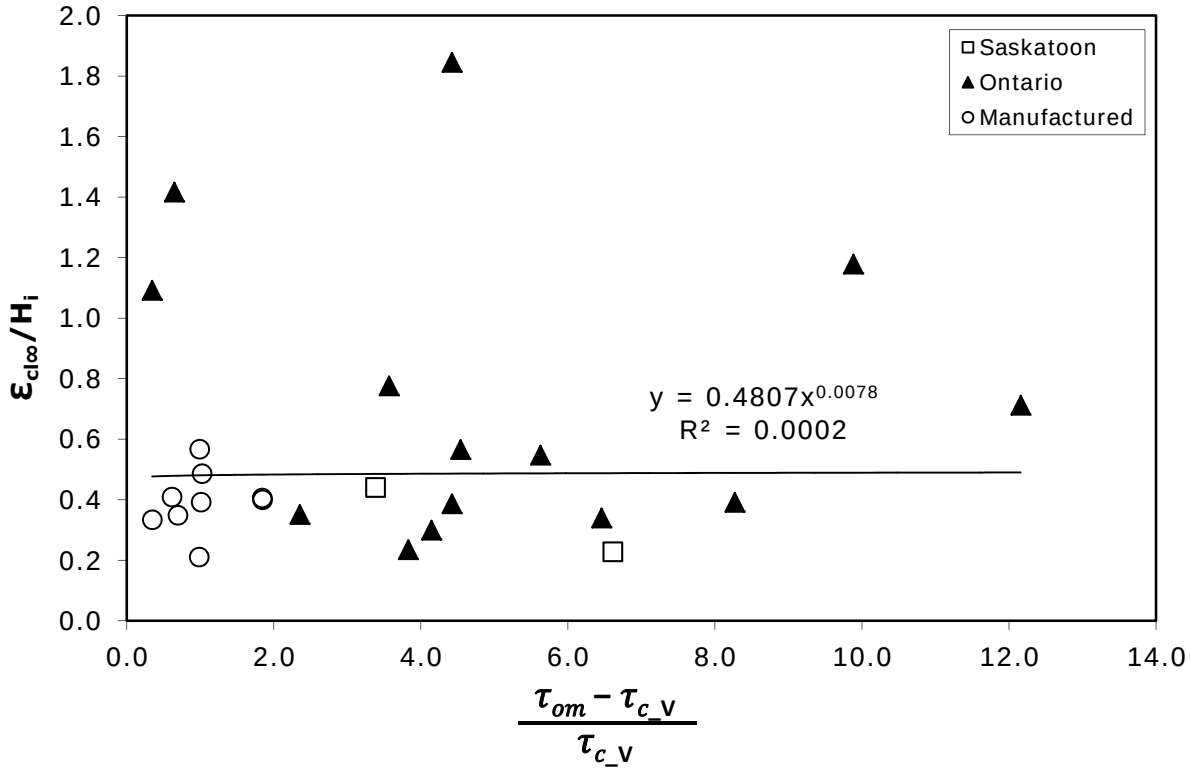


Figure 4-25. Scour analysis for the equilibrium centerline depth using the visual method

The relationships between the dimensionless scour hole radius at equilibrium and the dimensionless excess shear stress using selected critical values were found to be:

$$\frac{\overline{r_{o\infty}}}{H_i} = 0.62 \left\{ \frac{\tau_{om} - \tau_{c\_Ec}}{\tau_{c\_Ec}} \right\}^{0.21} \quad [4\text{-}18]$$

$$\frac{\overline{r_{o\infty}}}{H_i} = 0.50 \left\{ \frac{\tau_{om} - \tau_{c\_B2}}{\tau_{c\_B2}} \right\}^{0.17} \quad [4\text{-}19]$$

with $R^2$ values of 0.1802 and 0.4240, respectively. The plots used for developing Equations [4-18] and [4-19] are provided in Figure 4-26 and Figure 4-27 respectively.

Since $\tau_{c\_Ec}$ is independent of the average scour hole radius at equilibrium, a relationship was developed between these two parameters. Again, using $\tau_{c\_B2}$ as the indicator of soil erodibility produced a relationship with a better correlation coefficient than using $\tau_{c\_B1}$ (not shown), perhaps suggesting that using longer scour datasets in calculating the critical shear stress improves the ability to predict scour hole geometry at equilibrium. This is not surprising since the longer a test is run, the closer a sample becomes to reaching equilibrium state.

When $\tau_{c\_V}$ was used to calculate the dimensionless excess shear stress it was found to have a very poor correlation with the average scour hole radius at equilibrium and so analysis results are not presented here. Results from this study appear to indicate that the critical shear stress determined by visual analysis is not a very good indicator of scour hole geometry

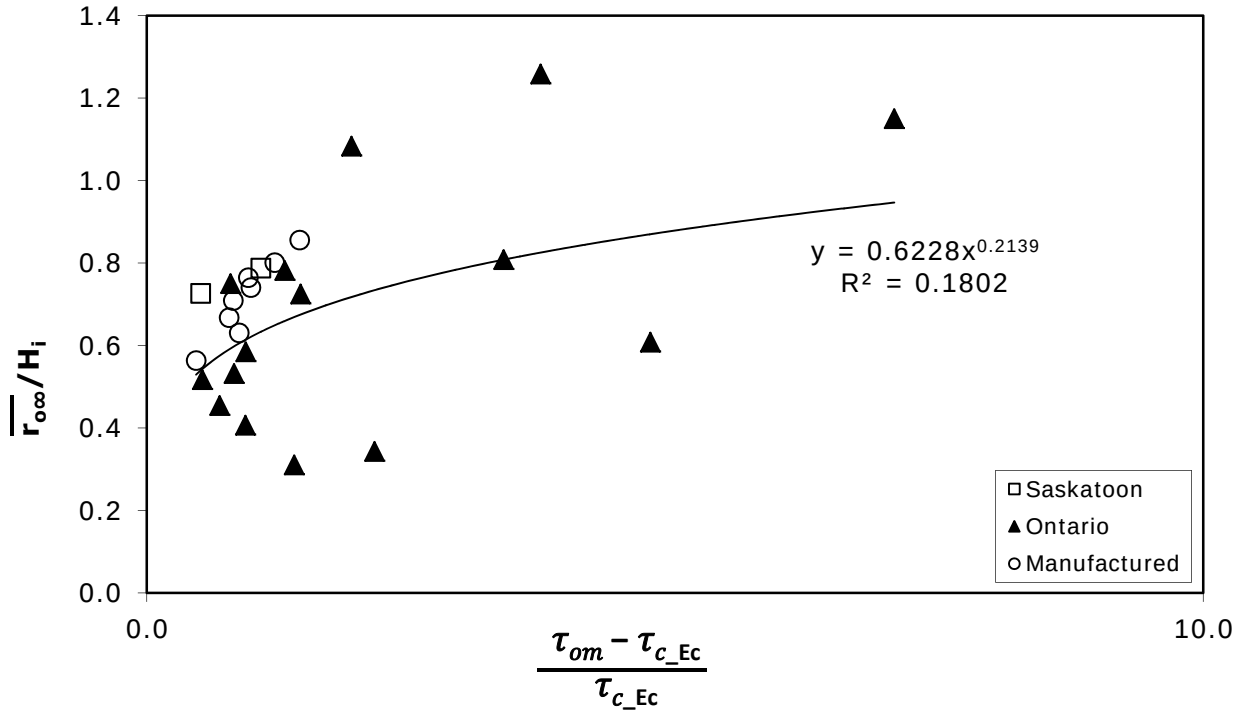


Figure 4-26. Scour analysis for the equilibrium radius using the equilibrium method

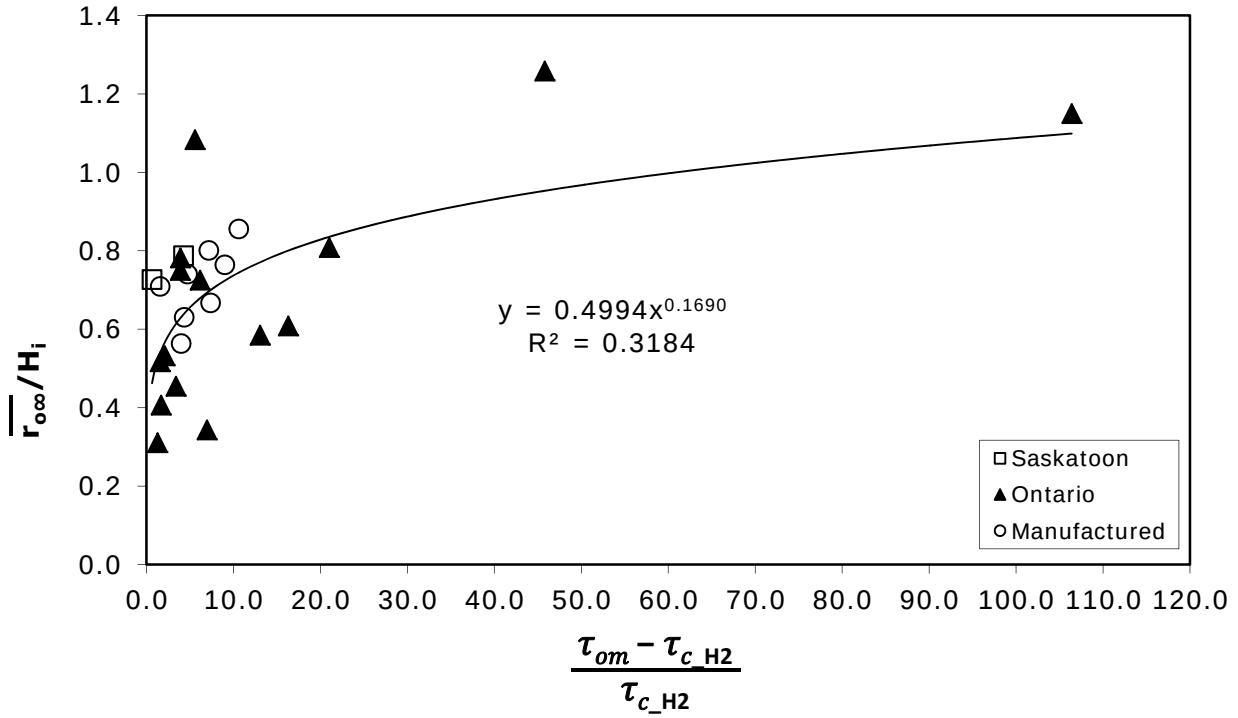


Figure 4-27. Scour analysis for the equilibrium radius using Hanson and Cook's (2004) method with the first 10 readings from the test data

## 4.5 EXPERIMENTAL ERROR

Errors in both the measured and derived quantities used in this study were estimated following Topping (1972). Unless otherwise stated, this section presents the maximum errors which represent the worst case for each quantity.

The FMG-3000 Series Magmeter used in this study has a manufacturer's specified accuracy of ±1.0%. The manufacturers specifications for the flow meter also gives a performance flow range from a minimum of 0.05 m/s to a maximum of 10 m/s. Using the 38 mm diameter discharge line to calculate the range of acceptable flow rates that can be measured with this meter gives a minimum of 3.4 Lpm and a maximum of 680 Lpm. A number flow rates used in the visual analysis testing were below this range making it necessary to determine these measurements volumetrically.

For low flow rates, the discharge was determined volumetrically using a pan and graduated cylinder as outlined in Section 3.3.2. The 2000 mL graduated cylinder used for collection could be read to ±100 ml giving a maximum error of ±5.00%. The shortest collection duration was 13.25 seconds, with a precision of ±0.01 seconds, giving a maximum error of ±0.08%. Combining the error in the time and volume measurements gives a maximum error in the flow rate of ±5.08% for this method.

For high flow rates the discharge was determined volumetrically using the cross sectional area of the test tank and the rate of change in water level as outlined in Section 3.3.2. The sides of the octagonal tank were on average 0.450 m, with a precision of ±0.001 m, giving a maximum error of ±0.22% and a maximum error in the tank cross sectional area of ±0.44%. The rate of change in the water surface was measured over a 100 mm height with a precision of ±1 mm, giving a maximum error of ±1.00% and an overall error in the collected volume of ±1.44%. The shortest collection time was 196.97 seconds with a precision of ±0.01 seconds giving a maximum error of ±0.01%. Combining the error in the time and volume measurements gives a maximum error in the flow rate of ±1.45% for this method.

Jet testing was conducted with the octagonal tank full of water and the jet plenum fully lowered so that the nozzle was submerged by approximately 10 - 20 cm. The flow rate was measured volumetrically with the plenum in the same position but with the nozzle unsubmerged so that a collection pan could be inserted to collect the discharge. In order to determine the effect that the unsubmerged conditions have when determining the flow rate, paired volumetric readings were collected with the plenum fully lowered and then with the nozzle at the same elevation as the top of the tank for a number of flow rates. Comparison of these two data sets showed that using an unsubmerged jet to collect volumetric flow rates caused a negligible difference in the readings.

The initial impingement height varied over the full range of jet tests and was a combination of two measurements: the height from the nozzle to a fixed reference point (the plastic 'bridge') determined using a caliper and digital micrometer, and the height from the fixed reference point to the soil surface determined using the 'bridge and dowel' technique outlined in Section 3.3.3. The digital micrometer had a precision of ±0.01 mm. In order to determine the accuracy of the 'bridge and dowel' technique, multiple height measurements were taken on an object of known height. The precision was determined to be ±0.39 mm using the worst case readings. Combining the precision of the micrometer and 'bridge and dowel' method gives a measurement error of 0.40 mm which, when applied to the smallest $H_i$ value of 59.0 mm from the SC(2) testing, gave a maximum error of ±0.68%. The maximum error in the nozzle diameter was estimated at ±1.25%. Errors for the flow rate and jet parameters are summarized in Table 4-9.

Based on the errors in the measured quantities, the maximum errors in the derived quantities are provided in Table 4-10. For quantities that are determined using curve fitting methods, the error is represented using goodness of fit measures which are provided in their respective analysis sections. The error associated with the maximum applied shear stress is twice the error in $d_o/H_i$ in addition to twice the error in the nozzle velocity for a total of ±19.0%. The maximum error in critical shear stress was associated with the equilibrium method at ±19.8% with the excess shear stress having a maximum error of ±21.0%.

Table 4-9. Maximum errors in flow rate and jet parameters

| Quantity | Maximum Error | Notes |
|---|---|---|
| **Magnetic Flow Meter** | | |
| $Q$ (Lpm) | 1.00% | Maximum error in the Magmeter flow rate based on manufacturer's specifications sheet. |
| **Measured Flow using Graduated Cylinder** | | |
| $t$ (s) | 0.08% | Time measurement for volumetric flow rate. RR(1) had highest flow rate, and therefore the shorted collection time, of all the tests verified using the pan and graduated cylinder. |
| Vol. (L) | 1.28% | Volume of water collected with the 1L graduated cylinder (used for WC(2)). |
| Vol. (L) | 5.00% | Volume of water collected with the 2L graduated cylinder (used for ECP(1)). |
| $Q$ (Lpm) | 5.08% | Maximum error in volumetric flow rate based on the 2L cylinder. |
| **Measured Flow using Water Level in Tank** | | |
| $t$ (s) | 0.01% | Time measurement for volumetric flow rate. P-300(3) had highest flow rate, and therefore the shortest collection time, of all the tests verified using the tank's volume. |
| $S$ (m) | 0.22% | Average length measurement for one side of the octagonal tank. |
| $A_T$ ($m^2$) | 0.44% | Cross sectional area of the tank. |
| Water Depth (cm) | 1.00% | Change in water depth as recorded by a tape on the side of the tank. |
| Vol. (L) | 1.44% | Volume of water collected in the tank. |
| $Q$ (Lpm) | 1.45% | Maximum error in volumetric flow rate based on the water tank. |
| **Jet Parameters** | | |
| $d_o$ (mm) | 1.25% | |
| $H_i$ (mm) | 0.68% | The accuracy was determined to be +/- 0.4 mm based on multiple measurements of a fixed height. The smallest height used was from SC(2). |
| $A_o$ ($mm^2$) | 2.50% | |
| $U_o$ (m/s) | 7.58% | Maximum error in velocity based on the error in the measured flow using the graduated cylinder. |

The minimum equilibrium centerline depth from all the samples tested was from SC(2) at 13.9 mm with a precision of ±0.4 mm resulting in a maximum error of ±2.88%. The traverse system controlling the position of the LASER used a Stepper Motor and Encoder manufactured by National Instruments Incorporated. The manufacturer's specifications give an angular accuracy of ±3.0% for each revolution of the drive shaft, and each full rotation resulted in 2 mm of linear displacement along the shaft. The minimum displacement of the LASER when measuring the scour hole profiles was 2 mm, therefore the maximum error in $\overline{r_{o\infty}}$ was about ±3.0% or ±0.06 mm. The error in $\varepsilon_{cl\infty} / H_i$ and $\overline{r_{o\infty}} / H_i$ becomes 3.56% and 3.68% respectively by adding the maximum error associated with the initial impingement height.

Table 4-10. Maximum errors in derived quantities

| Quantity | Maximum Error | Notes |
|---|---|---|
| **Critical Shear Stress Analysis** | | |
| $d_o / H_i$ | 1.93% | |
| $\tau_o$ (Pa) | 19.0% | |
| $\tau_{c\_v}$ (Pa) | 19.0% | |
| $H_{em}$ (mm) | 1.10% | The maximum error is taken as 2 times 0.40 mm since this quantity is based on adding the height from the nozzle to the "bridge" and the height from the "bridge" to the soil surface. The smallest measured equilibrium height was from SC(2). |
| $d_o / H_{em}$ | 2.35% | |
| $\tau_{c\_Ec}$ (Pa) | 19.8% | |
| $x$ | 8.83% | |
| $f$ | 10.8% | |
| $A^2$ | 39.2% | The value for the semi-transverse and semi-conjugate axis of the hyperbola. |
| $f_o$ | - | Since this parameter is determined by curve fitting, it's error is represented by the standard deviation in $A^2$ |
| $H_{eB}$ (mm) | - | Since this parameter is determined by curve fitting, it's error is represented by the standard deviation in $A^2$ |
| $\tau_{c\_B}$ (Pa) | - | Since this parameter is determined by curve fitting, it's error is represented by the standard deviation in $A^2$ |
| $\tau_{avg}$ (Pa) | 21.0% | |
| $\tau_{c\_T}$ (Pa) | - | Since this parameter is determined by linear regression, it's error is represented by $R^2$ |
| **Erodibility Coefficient Analysis** | | |
| $t$ (s) | 0.00% | The shortest scour interval time of 5 minutes. |
| $\dot{E}$ (mm/s) | 1.36% | |
| $(\tau_o - \tau_{avg})$ | 21.0% | |
| $k_T$ | - | Since this parameter is determined by linear regression, it's error is represented by $R^2$ |
| $k_H$ | - | Since this parameter is determined by curve fitting, it's error is represented by the MARE. |
| **Scour Analysis** | | |
| $(\tau_o - \tau_c)/\tau_c$ | 39.7% | The equilibrium method critical shear stress was used since it has the largest maximum error. |
| $\varepsilon_{cl\infty}$ | 2.88% | From sample SC(2). |
| $\overline{r_{o\infty}}$ | 3.0% | Based on manufacturer's specifications. |
| $\varepsilon_{cl\infty} / H_i$ | 3.56% | |
| $\overline{r_{o\infty}} / H_i$ | 3.68% | |

.

# CHAPTER 5
# CONCLUSION

This chapter presents a summary of the findings from this study as well as recommendations for further research.

## 5.1 SUMMARY OF KEY FINDINGS

The following are key findings from this study related to the jet test methodology and applicability for laboratory use with natural soil samples:

- In this study, the jet erosion test was found to be reasonably effective at testing natural soil samples in a laboratory setting, even when these samples contain vegetation such as extensive networks of roots or other imperfections. Even in cases where thick woody roots or large rocks were uncovered, impacting the growth of the scour hole and causing the tests to be prematurely terminated, samples were still able to be recut and retested successfully.

The following are key findings from this study related to the critical shear stress analysis and results:

- Caution should be taken when analyzing natural samples which have defined layering that may cause soil properties to vary with depth. The four methods used in this study for data analysis provide critical shear stress values based on different locations in the soil column. The visual method assesses $\tau_c$ at the surface, Thomas' and Hanson and Cook's (2004) method provides a bulk sample determined using the full scour depth from testing, and the equilibrium method is essentially a measure of $\tau_c$ for the material near the bottom of the ultimate state scour hole. When comparing these methods it is important to note that the actual critical shear stress of the soil may change with depth.

- For this study, the equilibrium method critical shear stress values were taken as being closest to the actual $\tau_c$ of the samples since they represent a physical observation of the sample at or near ultimate state. From a practical point of view however, this method has the disadvantage of requiring long test durations and is likely limited to laboratory application. The jet hydraulics for this method, do not take into account the dissipation of maximum centerline velocity due to the reverse flow in the scour hole. This method can successfully be applied to natural samples providing there are no prominent imperfections in the soil, such as thick root or large rocks, that obstruct the scour hole growth.

- The critical shear stress determined using the visual method compared well the critical shear stress determined from the equilibrium method for the manufactured clay samples. In the natural samples however, the visual method was almost half the equilibrium value on average. This reduction may be due to surface disturbances during sample preparation that would cause the appearance of mass erosion at lower applied shear stresses. The visual method is theoretically one of the preferred analysis methods since it is quick to run and the test hydraulics are the closest match to the assumptions made in the analysis theory. However, the method's dependence on operator skill and judgment as well as its sensitivity to surface preparation and conditions creates additional uncertainty in the results.

- Blaisdell et al. (1981) consistently overestimated the equilibrium scour depth when compared with the equilibrium scour depth measured from testing, causing Hanson and Cook's (2004) method to produce lower values of $\tau_c$ that the equilibrium method.

- As seen with the results from Hanson and Cook's (2004) analysis, the length of the jet test data set used in the analysis can largely impact the calculated erodibility parameters. For this reason test durations should be similar when comparing results between 2 or more tests;

- Since data plots of the average shear stress against erosion rate approached an erosion rate of zero asymptotically, using a linear extrapolation to determine the critical shear stress in Thomas' method consistently produced values that were lower than the equilibrium method. As more test data was added into the analysis, the value of $\tau_{c\_T}$ was found to converge to the value of $\tau_{c\_Ec}$.

- Depending on the application for which the critical shear stress is being determined, it may be prudent to use an analysis method that gives a low estimate, high estimate, or an envelope of values. For example, if the critical shear stress of a soil is being investigated for the design hydraulic structures, it may be appropriate to use Hanson and Cook's (2004) method as it represents a low, and therefore conservative, estimate of erodibility.

The following are key findings from this study related to the erodibility coefficient analysis results and the time development of scour:

- The Hanson and Cook (2004) time development of scour equations used to determine a soil's erodibility coefficient tended to produce a reasonable fit to the jet test data for test durations up to 120 minutes. For longer durations, the test data significantly departed from the theoretical equations mainly due to the disparity that was found to occur between Blaisdell et al.'s (1981) predicted equilibrium scour depth and the equilibrium depth measured from testing.

- Values calculated for the erodibility coefficient using Hanson and Cook's (2004) method were found to be sensitive to the duration of test data used in the analysis. In general, adding in more jet test data to the analysis caused the value of $k$ to decrease.

- Normalizing the jet test data using the measured equilibrium scour depth allowed a better comparison to be made between the time development of scour equations and the test data. In some cases it was found that the assumption of a linear excess shear

stress equation where $n$ is equal to 1 was inadequate, so nonlinear time development of scour equations were produced for exponent values of 0.5, 1.5 and 2.0. In general, the time development of scour equations with an exponent of 2.0 fit the manufactured samples best, while there were samples from the natural soils group that fit well with each of the exponents. This finding brings into question the validity of assuming a linear excess shears stress equation for all analysis of jet testing data.

- When only using the first 120 minutes of data for both Thomas' and Hanson and Cook's (2004) analysis methods, it was determined that the assumption of a linear excess shear stress equation produced a reasonable fit for the samples tested in this study. The suitability of this assumption for other soils will depend in part on the duration of testing which is required to achieve equilibrium scour conditions in the sample. Once a plot of the centerline scour depth with time begins to reach an asymptotic value, if the test is continued and additional data points are included in the analysis, it is likely that the assumption of a linear excess shear stress equation will be questionable. When using the full jet test data sets for analysis, both methods used in this study found that the majority of samples favored a nonlinear excess shear stress equation.

- When comparing the values of Thomas' and Hanson and Cook's (2004) erodibility coefficient calculated using only the first 120 minutes of jet test data, it was found that overall $k_{T1}$ was approximately four to six times larger than $k_{H1.}$ It is not obvious which of this methods produced the most realistic estimates of the erodibility coefficient.

The following are key findings from this study related to the scour hole analysis and results:

- Using Mazurek's (2001) scour analysis approach, the dimensionless excess shear stress was shown to be a reasonable indicator of dimensionless centerline depth and average scour hole radius at equilibrium state for the three soil sample groups tested in this study when using $\tau_{c\_B}$ and $\tau_{c\_Ec}$ as indicators of soil erodibility. That being said, using scour data from natural soil samples appeared to produced lower correlation

coefficients than what would have been expected if the relationships were developed only using manufactured clay samples.

- When using Hanson and Cook's (2004) critical shear stress as the soil erodibility indicator, it was found that using the critical shear stress value calculated from longer jet test datasets produced a better agreement for the developed relationships.

- For this study, it was determined that $\tau_{c\_V}$ was not useful as an indicator of soil erodibility when developing a relationship to predict scour hole geometry at equilibrium state.

## 5.2 RECOMMENDATIONS FOR FUTURE RESEARCH

The following are key recommendations for future jet testing and research:

- Shear stresses on the sample surface are highest at the beginning of testing which is when mass failure of the soil is likely to occur. It is possible that wall pressure or normal stresses may play a role in this type of soil failure, since mass failure can influence the initial shape of the scour hole and, in some cases, the critical shear stress analysis results were found to be sensitive to the first couple scour measurements, it is recommended that test flow rates be chosen that do not impose large excess shear stresses on the sample. This can be done by targeting applied stresses that are close to the anticipated shear stress of the sample being tested. The visual critical shear stress analysis may be useful for determining the anticipated critical shear stress of the sample.

- Since this study shows a noticeable discrepancy between the measured equilibrium scour depths and Hanson and Cook's (2004) theoretical depth, it is recommended that an alternative reference height, (ie. $H_i$) be considered for the time development of scour analysis. This way the uncertainty in $H_e$ is not carried forward in the analysis.

- For both Thomas' and Hanson and Cook's (2004) method of analysis, the erodibility coefficient units are dependent on the value of the excess shear stress exponent, *n*. In the physical sense, the units of *k* for the linear excess shear stress can be understood as a volumetric rate of soil erosion per unit of force. While the units of *k* for the nonlinear expressions of Hanson and Cook's (2004) time development of scour equations are able to be calculated for the discrete values of n, their physical meaning is less obvious. Furthermore, in Thomas' analysis method, *k* becomes more curve fitting parameter rather than a physically apparent property of the soil. For these reasons, it may be useful to normalize the erodibility coefficient in order to avoid conflicting units when comparing results between multiple samples. This would especially be useful when analyzing data using a nonlinear expression of the excess shear stress equation. One approach for nondimensionalizing the erodibility coefficient is provided in Walder (2015).

- It is likely that scour in the manufactured clay samples can be influenced by the size of the container. In cases where the stainless steel container was exposed by scour it can act as a fixed boundary, confining the jet and likely contributing to velocity decay that may have not otherwise occurred. Even when the container wasn't exposed, it still has a confining effect on the clay samples which may cause internal stresses and induce mass failures, especially when exposed to the high velocities and pressures that were necessary to initiate erosion. The size or need for a sample container should be considered when conducting laboratory based jet erosion tests.

- Variability in results for the four critical shear stress methods was only briefly touched on in this study. It may be beneficial to run a large number of jet erosion tests on a single manufactured sample to better understand the expected uncertainty associated with each analysis method.

- One of the main assumptions present in most of the critical shear stress analysis methods is that the maximum velocity in the scour hole decays as if it were impinging on a flat solid boundary. It would be useful to explore the validity of this assumption further. One option might be to create fixed boundary molds of scour holes for a variety of radius to depth ratios and directly measure velocity profiles in the scour hole and/or applied shear stress along the scour hole surface.

## LIST OF REFERENCES


Abt, S. R. (1980). *Scour at Culvert Outlets in Cohesive Bed Material*. Ph.D. Thesis, Colorado State University, Fort Collins, Colorado.

Aderibigibe, O.O., and Rajaratnam, N. (1996). Erosion of Loose Beds by Submerged Circular Impinging Jets Vertical Turbulent Jets. *J. Hydraul. Res.*, 34(1): 19-33.

Al-Madhhachi, A., Hanson, G., Fox, G., Tyagi, A., and Bulut, R. (2011). Measuring Erodibility of Cohesive Soils Using Laboratory Jet Erosion Tests. *Proc. World Environ. and Water Resource Congress 2011*, Palm Springs, California, USA, 22-26 May 2011. ASCE, 2350-2359.

Amin, M. R., and Mazurek, K. A. (2016). Assessment of Equilibrium Scour by a Submerged Circular Turbulent Impinging Jet in Cohesive Soils. *Proc. 6th International Symposium on Hydraulic Structures*, Portland, Oregon, USA, 27-30 June 2016. IAHR and USSD.

Annandale, G. W. (2006). *Scour Technology: Mechanics and Engineering Practice*. McGraw Hill, New York, USA.

Ansari. S. A., Kothyari, U.C., and Ranga Raju, K.G. (2003). Influence of Cohesion on Scour Under Submerged Circular Vertical Jets. *J. Hydraul. Eng.*, 129(12): 1014-1019.

ASTM Standard D421-85 (2007). Standard Practice for Dry Preparation of Soil Samples for Particle-Size Analysis and Determination of Soil Constants. *ASTM International*, West Conshohocken, Pennsylvania, USA.

ASTM Standard D422-63 (2007). Standard Test Method for Particle-Size Analysis of Soils. *ASTM International*, West Conshohocken, Pennsylvania, USA.

ASTM Standard D2216-10 (2010). Standard Test Methods for Laboratory Determination of Water (Moisture) Content of Soil and Rock by Mass. *ASTM International*, West Conshohocken, Pennsylvania, USA.

ASTM Standard D2487-11 (2011). Standard Practice for Classification of Soils for Engineering Purposes (Unified Soil Classification System). *ASTM International*, West Conshohocken, Pennsylvania, USA.

ASTM Standard D4318-10 (2010). Standard Test Methods for Liquid Limit, Plastic Limit, and Plasticity Index of Soils. *ASTM International*, West Conshohocken, Pennsylvania, USA.

ASTM Standard D5852-00 (2007). Standard Test Method for Erodibility Determination of Soil in the Field or in the Laboratory by the Jet Index Method. *ASTM International*, West Conshohocken, Pennsylvania, USA.

ASTM Standard D7263-09 (2009). Standard Test Methods for Laboratory Determination of Density (Unit Weight) of Soil Specimens. *ASTM International*, West Conshohocken, Pennsylvania, USA.

Beltaos, S., and Rajaratnam, N. (1974). Impinging Circular Turbulent Jets. *J. Hydraulics Division* 100 (HY10): 1313-1328.

Beltaos, S. (1974). *Turbulent Impinging Jets*. Ph.D. Thesis, Univ. of Alberta, Edmonton, Alberta, Canada.

Black, K. S., Tolhurst, T. J., Paterson, D. M., Hagerthey, S. E. (2002). Working with Natural Cohesive Sediments. *J. Hydraul. Eng.*, 128(1): 2-8.

Blaisdell, F. W., Anderson, C. L., and Hebaus, G. G. (1981). Ultimate Dimensions of Local Scour. *J. Hydraulics Division,* 107(HY3): 327-337.

Briaud, J. L., Chen, H. C., Li, Y., Nurtjahyo, P., and Wang, J. (2004). Pier and Contraction Scour in Cohesive Soils. *National Cooperative Highway Research Program Report 516*, Transportation Research Board, National Research Council, Washington, D.C.

Briaud, J. L., Ting, F. C. K., Chen, H. C., Cao, Y., Han, S. W., and Kwak, K. W. (2001). Erosion function apparatus for scour rate predictions. *J. Geotech. Geoenviron. Eng.,* 127(2): 105–113.

Change, D. S., Zhang, L. M., Xu, Y., and Huang, R. Q. (2011). Field Testing of Erodibility of Two Landslide Dams Triggered by the 12 May Wenchuan Earthquake. *Landslides*, 8(3): 321-332.

Clark, L. A., and Wynn, T. M. (2007). Methods for Determining Streambank Critical Shear Stress and Erodibility: Implications for Erosion Rate Predictions. *Trans. Of the ASABE*, 50 (1): 95-106.

Daly, E. R, Fox, G. A., Al-Madhhachi, A. T., and Miller R. B. (2013). A Scour Depth Approach for Deriving Erodibility Parameters from Jet Erosion Tests. *Trans. of ASABE*, 56(6): 1343-1351.

Dunn, I. S. (1959). Tractive resistance of cohesive channels. *J. Soil Mech. and Found. Div.*, 85(3): 1–24.

Enger, P. F. (1963). Canal Erosion and Tractive Force Study- Analysis of Data from a Boundary Shear Flume. Report No. Hyd-532, United States Department of the Interior Bureau of Reclimation, Denver, Colorado.

Shan, H., Shen, J., Kilgore, R., and Kerenyi, K. (2015). Scour in Cohesive Soils. *Report No. FHWA-HRT-15-033*, Federal Highway Administration, McLean, Virginia.

Gaskin, S. J., Pieterse, J., Al Shafie, A., and Lepage S. (2003). Erosion of Undisturbed Clay Sample from the Banks of the St. Lawrence River. *Can. J. Civ. Eng.*, 30(3): 585-595.

Hanson, G. J. (1990a). Surface Erodibility of Earthen Channels at High Stresses Part I - Open Channel Testing. *Trans. of ASAE,* 33(1): 127-131.

Hanson, G. J. (1990b). Surface Erodibility of Earthen Channels at High Stresses Part II – Developing an *In Situ* Testing Device. *Trans. of ASAE*, 33(1): 132-137.

Hanson, G. J. (1991). Development of a Jet Index to Characterize Erosion Resistance of Soils in Earthen Spillways. *Trans. of ASAE*, 34(5): 2015-2020.

Hanson, G. J., and Cook, K. R. (1997). Development of Excess Shear Stress Parameters for Circular Jet Testing. *Proc., ASAE Annual International Meeting: Paper 972227*, Minneapolis, Minnesota, 10-14 August 1997. ASAE, 1-21.

Hanson, G. J., and Cook, K. R. (2004). Apparatus, Test Procedures, and Analytical Methods to Measure Soil Erodibility In-Situ. *Trans. ASAE*, 20(4): 455-462.

Hanson, G. J., and Hunt, S. L. (2007). Lessons learned using laboratory JET method to measure soil erodibility of compacted soils. *Applied Engineering in Agriculture*, 23(3): 305-312.

Hanson, G. J., Robinson, K. M. and Temple, D. M. (1990). Pressure and Stress Distributions Due to a Submerged Impinging Jet. *Proc. 1990 ASCE National Conference*, *Hydraul. Eng.,* San Diego, California, 30 July – 3 August 1990. ASCE, 525-530.

Hanson, G. J., and Simon, A. (2001). Erodibility of Cohesive Streambeds in the Loess Area of the Midwestern USA. *Hydrol. Process.*, 15(1): 23-38.

Haralampides, K., and Rodriguez, A. (2006). Erosional Properties of the Sediments in the Petitcodica River Estuary at Moncton, New Brunswick. *Can. J. Civ. Eng.,* 33:1209-1216.

Hedges, J. D. (1990). The scour of cohesive soils by an inclined submerged water jet. MSc thesis, Texas A&M University, College Station, Tex.

Hoffmans, G. J. C. M., and Verheij, H. J. (1997). Scour Manual. A. A. Balkema, Rotterdam, The Netherlands.

Hollick, M. (1976). Towards a Routine Assessment of the Critical Tractive Forces of Cohesive Soils. *Trans. ASAE*, 19: 1076-1081.

Houwing, E-J., and van Rijn, L. C. (1998). In Situ Erosion Flume (ISEF): Determination of Bed-Shear Stress and Erosion of a Kaolinite Bed. *J. Sea Res.,* 39(3-4): 243-253

Julien, P. Y. (1998). *Erosion and Sedimentation*. Cambridge University Press, New York, USA.

Karmaker, T., and Dutta, S. (2011). Erodibility of Fine Soil from the Composite River Bank of Brahmaputra in India. *Hydrol. Process.*, 25(1): 104-111.

Khan, I., and Kostaschuk, R. (2011). Erodibility of Cohesive Glacial Till Bed Sediments in Urban Stream Channel Systems. *Can. J. Civ. Eng.,* 38(12): 1363-1372

Knapen, A., Poesen, J., Govers, G., Gyssels, G., and Nachtergaele, J. (2007). Resistance of Soils to Concentrated Flow Erosion: *A Review. Earth-Science Reviews*, 80: 75-109.

Lim, S. S., and Khalili, N. (2009). An Improved Rotating Cylinder Test Design for Laboratory Measurement of Erosion in Clayey Soils. *Geotech. Testing J.*, 32(3): 1-7.

Luthi, M. (2011). *A Modified Hole Erosion Test (HET-P) to Study Erosion Characteristics of Soil.* M.Sc. Thesis, University of British Columbia, Vancouver, British Columbia, Canada.

Marot, D., Regazzoni, P-L., and Wahl, T. (2011). Energy-Based Method for Providing Soil Surface Erodibility Rankings. *J. Geotech. Geoenviro. Eng.,* 137(12): 1290-1293.

Masch, F. D., Epsey , W. H. and Moore, W. L. (1963). Measurements of the Shear Resistance of Cohesive Sediments. *Proc. Of the Federal Interagency Sedimentation Conference Paper No. 23*, Jackson, Mississippi, 28 January – 1 February 1963. USDA, 151-155.

Mazurek, K. A. (2001). *Scour of Clay by Jets*. Ph.D. Thesis, Univ. of Alberta, Edmonton, Alberta, Canada.

Mazurek, K. A. (2010). Erodibility of a Cohesive Soil Using a Submerged Circular Turbulent Impinging Jet Test. *Proc. 2nd Joint Fed. Interagency Conf.,* Las Vegas, Nevada, 27 June – 1 July 2010.

Mazurek, K. A., and Gheisi, A. R. (2009). Assessment of the erodibility of a cohesive soil using a submerged circular turbulent impinging jet. *Proc. 33rd IAHR Congress*, Vancouver, Canada, 9-14 August 2009. IAHR, 1324-1331.

Mazurek, K. A., and Hossain, T. (2007). Scour by Jets in Cohesionless and Cohesive Soil. *Can. J. Civ. Eng.,* 34(6): 744-751.

Mazurek, K.A., Rajaratnam, N. and Sego, D.C. (2001). Scour of a Cohesive Soil by Submerged Circular Turbulent Impinging Jets. *J. of Hydraul. Eng.*, 127(7): 598-606.

Mazurek, K.A., Rajaratnam, N. and Sego, D. C. (2003). Scour of a Cohesive Soil by Submerged Plane Turbulent Wall Jets. *J. of Hydra. Res.*, 41(2): 195-206.

Mercier, F., Golay, F., Bonelli, S., Anselmet, F., Borghi, R., and Philippe, P. (2013). 2D Axisymmetrical Numerical Modelling of the Erosion of a Cohesive Soil by a Submerged Turbulent Impinging Jet. *European J. Mech. - B/Fluids,* 45: 36-50.

Mercier, F., Bonelli, S., Pinettes, P., Golay, F., Anselmet, F., and Philippe, P. (2014). Comparison of Computational Fluid Dynamics Simulations with Experimental Jet Erosion Tests Results. *J. Hydraul. Eng.,* 140(5): 04014006

Mitchener, H., and Torfs, H. (1996). Erosion of Mud/Sand Mixtures. *Coastal Eng.,* 29(1-2): 1-25.

Moore, W. L., and Masch, F. D. (1962). Experiments on the Scour Resistance of Cohesive Sediments. *J. Geophysical Research*, 67(4): 1437-1449.

Mostafa, T. S., Imran, J., Chaudhry, M. H., and Kahn, I. B. (2008). Erosion resistance of cohesive soils. *J. Hydraul. Res.,* 46(6): 777-787.

Partheniades, E. (2009). *Cohesive Sediments in Open Channels: Properties, Transport and Applications*. Elsevier Inc., Oxford, UK.

Rajaratnam, N. (1976). *Turbulent Jets*. Elsevier Scientific Pub. Co., Amsterdam, The Netherlands.

Rajaratnam, N., and Beltaos, S. (1977). Erosion by Impinging Circular Turbulent Jets. *J. Hydraulics Division,* 103(HY10): 1191-1205.

Rajaratnam, N., and Flint-Petersen, L. (1989). Low Reynolds number circular turbulent jets. *Proc. Instn. Civ. Engrs.,* 87(2): 299-305.

Rajaratnam, N., and Mazurek, K. A. (2003) Erosion of Sand by Circular Impinging Water Jets with Small Tailwater. *J. of Hydraul. Eng.*, 129(3): 225-229.

Rajaratnam, N., and Mazurek, K. A. (2005). Impingement of Circular Turbulent Jets on Rough Boundaries. *J. Hydraul. Res.,* 43(6): 688-694.

Roberts, J. D., Jepsen, R. A , and James, S. C. (2003). Measurements of Sediment Erosion and Transport with the Adjustable Shear Stress Erosion and Transport Flume. *J. Hydraul. Eng.,* 129(11): 862-871.

Shan, H. (2010). *Experimental Study on Incipient Motion of Non-Cohesive and Cohesive Sediments*. Ph.D. Thesis, University of Nebraska, Lincoln, Nebraska, USA.

Sharif. A. R. (2003). *Critical Shear Stress and Erosion of Cohesive Soils.* Ph.D. Thesis, State University of New York at Buffalo, Buffalo, New York, USA.

Shugar, D., Kostaschuk, R., Ashmore, P., Desloges, J., and Burge, L. (2007). In Situ Jet-Testing of the Erosional Resistance of Cohesive Streambeds. *Can. J. Civ. Eng.,* 34(9): 1192-1195.

Simon, A., Thomas, R. E. and Klimetz, L. (2010). Comparison and Experiences with Field Techniques to Measure Critical Shear Stress and Erodibility of Cohesive Deposits. *Proc. 2nd Joint Fed. Interagency Conf.,* Las Vegas, Nevada, 27 June – 1 July 2010.

Stein, O. R. (1990). *Mechanics of Headcut Migration in Rills*. PhD thesis, Colorado State University, Fort Collins, Colorado.

Stein, O.R., Julien, P.Y., and Alonso, C.V. (1993). Mechanics of Jet Scour Downstream of a Headcut. *J. Hydraul. Res.*, 31(6): 723-738.

Thoman, R. W., and Niezgoda, S. L. (2008). Determining Erodibility, Critical Shear Stress, and Allowable Discharge Estimates for Cohesive Channels: Case Study in the Powder River Basin of Wyoming. *J. Hydraul. Eng.*, 134(12), 1677-1687.

Topping, J. (1972). *Errors of Observation and their Treatment (4th Ed.)*. Chapman and Hall Ltd., London.

van Ledden, M., van Kesteren, W. G. M., and Winterwerp, J. C. (2004). A Conceptual Framework for the Erosion Behaviour of Sand-Mud Mixtures. *Continental Shelf Res.*, 24(1): 1-11.

Wahl, T. L. (2010). A Comparison of the Hole Erosion Test and Jet Erosion Test. *Proc. 2nd Joint Fed. Interagency Conf.,* Las Vegas, Nevada, 27 June – 1 July 2010.

Walder, J. S. (2016). Dimensionless Erosion Laws for Cohesive Sediments. *J. Hydraul. Eng.,* 142(2): 04015047.

Wan, C. F., and Fell, R. (2002). Investigation of Internal Erosion and Piping of Soils in Embankment Dams by the Slot Erosion Test and the Hole Erosion Test. *UNICIV Rep. R-412*, July 2002, The Univ. of New South Wales, Sydney, Australia.

Weidner, K., Petrie, J., Diplas, P., Nam, S., Gutierrez, M., and Ellenberg, M. (2012). Numerical Simulation of Jet Test and Associated Soil Erosion. *Proc. 6th Inter. Conf. Scour and Erosion,* Paris, 27-31 August 2012. SHF, 609-616.

Westrich, B., and Kobus, H. (1973). Erosion of a Uniform Sand Bed by Continuous and Pulsating Jets. *Proc. 15th IAHR Congress, Vol 1*, Istanbul, Turkey. IAHR, 91-98.

Winterwerp, J. C., and van Kesteren, W. G. M. (2004). *Introduction to the Physics of Cohesive Sediment in the Marine Environment*. Elsevier Inc., Amsterdam, The Neatherlands.

Wynn, T. M. (2004). *The Effects of Vegetation on Stream Bank Erosion*. Ph. D. Thesis, Virginia Polytechnic Institute and State University, Blacksburg, Virginia, USA.

USBR (2006). *Erosion and Sedimentation Manual*. U.S. Department of the Interiorior, Bureau of Reclamation, Denver, Colorado.

Utley, B. C., and Wynn, T. M. (2008). Cohesive Soil Erosion: Theory and Practice. *Proc. World Environ. Water Resources Congress 2008*, Honolulu, Hawaii, 12-16 May 2008. ASCE, 1-10.

Zhu, Y., Lu, J., Liao, H., Wang, J., Fan, B. and Yao, S. (2008). Research on Cohesive Sediment Erosion by Flow: an Overview. *Sci. China. Series E: Tech. and Sci.*, 51(11): 2001-2012.

# APPENDIX A
# TEST DATA

Appendix A contains the experimental data collected for all 31 soil samples. This includes initial setup parameters for the jet test, volumetric flow rates, the centerline and maximum scour depths measured during testing along with observation notes, the centerline scour depth measured at equilibrium state, plots of the scour depth with time (with both arithmetic and logarithmic time axis), photos of the natural samples from before testing (or early in testing) and at the end of jet testing, as well as photos of the manufactured samples from the visual critical flow rate analysis and at the end of jet testing.

Table A-1. Test Data for the South Nation 1 of 2 Sample (Ontario Group)

| | | | | | | | | | |
|---|---|---|---|---|---|---|---|---|---|
| **Sample Name:** | South Nation 1 of 2 | | **Initial Temperature:** | T (˚C) | 6 | | **Volumetric Flow Rate** | | |
| **Batch Number:** | N/A | | **Jet Diameter:** | d (mm) | 8.0 | | Avg Q | 7.49 | Lpm |
| **Tested By:** | Research Assistant | | **Initial Jet Height:** | $H_i$ (mm) | 66 | | 1) | | Lpm |
| **Analysis By:** | Dan Cossette | | **Equilibrium Centerline Depth:** | $\varepsilon_{cl\infty}$ (mm) | 19.79 | | 2) | | Lpm |
| **Date of Testing:** | 2010-02-10 | | **Measured Equilibrium Height:** | $H_{e\ m}$ | 85.79 | | 3) | | Lpm |

| **Magmeter** Q | **Measured Time** $t_m$ | | | **Centerline Scour Depth** $\varepsilon_c$ | **Maximum Scour Depth** $\varepsilon_m$ | **Temp.** T | **Notes** |
|---|---|---|---|---|---|---|---|
| (Lpm) | (Min) | (Hrs) | (s) | (mm) | (mm) | (°C) | |
| 7.2 | 5 | 0:05 | 300 | 1.89 | 2.61 | | Initially, a lot of particle peeled out from top surface. |
| 7.1 | 10 | 0:10 | 600 | 4.00 | 4.40 | | |
| 7.2 | 20 | 0:15 | 1200 | 8.55 | 11.68 | | |
| 7.0 | 30 | 0:20 | 1800 | 10.27 | 14.52 | | |
| 7.0 | 60 | 0:30 | 3600 | 13.69 | 16.10 | | |
| 7.7 | 120 | 0:40 | 7200 | 12.83 | 14.53 | | Vegetative net protected scour hole |
| 7.9 | 240 | 4.00 | 14400 | 13.01 | 16.09 | | |
| 7.9 | 480 | 8.00 | 28800 | 19.23 | 23.27 | | |
| 7.7 | 1080 | 18.00 | 64800 | 19.20 | 23.14 | | Scour almost reaching stability |
| 7.8 | 1324 | 22.07 | 79440 | 19.05 | 21.33 | | |
| 7.5 | 2629 | 43.82 | 157740 | 19.00 | 22.91 | | |
| 7.5 | 3805 | 63.42 | 228300 | 19.79 | 22.75 | | |
| 7.5 | 4075 | 67.92 | 244500 | 19.15 | 23.32 | | |

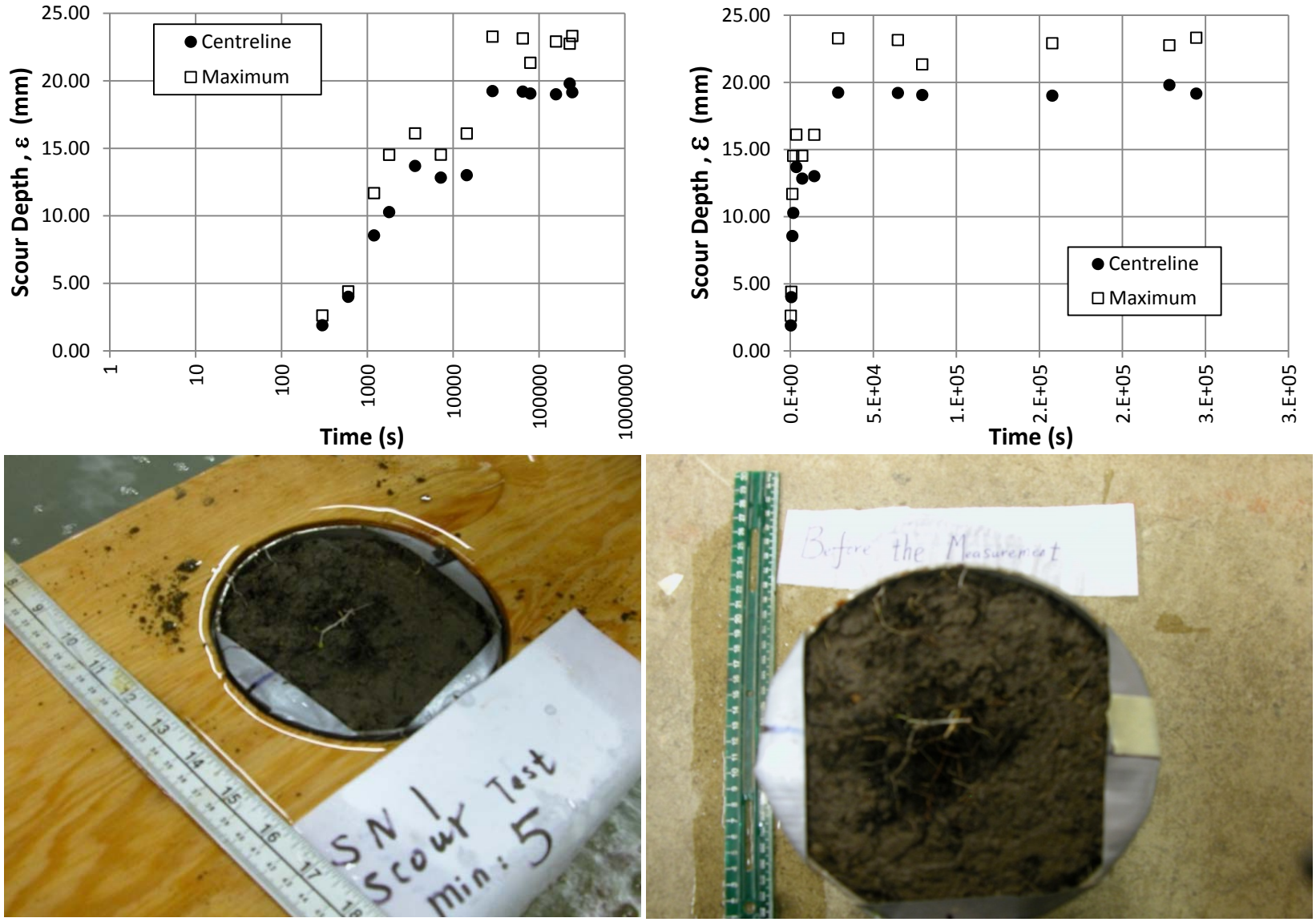


Figure A-1 Observed Time Development of Scour Plots and Test Photos for the South Nation 1 of 2 Sample

Table A-2. Test Data for the South Nation 2 of 2 Sample (Ontario Group)

| | | | | | | | | | |
|---|---|---|---|---|---|---|---|---|---|
| **Sample Name:** | South Nation 2 of 2 | | **Initial Temperature:** | T (˚C) | 6 | | **Volumetric Flow Rate** | | |
| **Batch Number:** | N/A | | **Jet Diameter:** | d (mm) | 8.0 | | Avg Q | 6.28 | Lpm |
| **Tested By:** | Research Assistant | | **Initial Jet Height:** | $H_i$ (mm) | 60 | | 1) | | Lpm |
| **Analysis By:** | Dan Cossette | | **Equilibrium Centerline Depth:** | $\varepsilon_{cl\infty}$ (mm) | 20.36 | | 2) | | Lpm |
| **Date of Testing:** | 2010-02-10 | | **Measured Equilibrium Height:** | $H_{e\ m}$ | 80.36 | | 3) | | Lpm |

| **Magmeter** Q | **Measured Time** $t_m$ | | | **Centerline Scour Depth** $\varepsilon_c$ | **Maximum Scour Depth** $\varepsilon_m$ | **Temp.** T | **Notes** |
|---|---|---|---|---|---|---|---|
| (Lpm) | (Min) | (Hrs) | (s) | (mm) | (mm) | (°C) | |
| 6.0 | 5 | 0:05 | 300 | 5.2 | 17.58 | 22.5 | A lot of block away from the surface, biggest one (5cm); one small rock (1-1.5 cm) erode on the top, Maximum depth around the big rock area. |
| 6.2 | 10 | 0:10 | 600 | 7.77 | 19.53 | 22.5 | Slight large cubic chunks eroded at this time interval |
| 6.5 | 20 | 0:15 | 1200 | 8.11 | 20.44 | 22.0 | |
| 6.2 | 30 | 0:20 | 1800 | 10.05 | 21.98 | 22.0 | |
| 6.1 | 60 | 0:30 | 3600 | 12.4 | 22.47 | 22.0 | |
| 5.8 | 120 | 0:40 | 7200 | 17.16 | 23.42 | 22.5 | Center area large cubic chunks eroded away; erosion noted on the periphery of the sample. |
| 6.5 | 240 | 4.00 | 14400 | 19.32 | 24.18 | 22.5 | |
| 6.1 | 480 | 8.00 | 28800 | 20.14 | 25.3 | 22.0 | |
| 6.5 | 1080 | 18.00 | 64800 | 20.01 | 25.94 | 22.0 | erosion reaching stability |
| 6.4 | 1424 | 23.73 | 85440 | 20.36 | 25.98 | 22.0 | |
| 6.6 | 2500 | 41.67 | 150000 | 20.14 | 25.81 | 22.0 | |
| 6.4 | 2710 | 45.17 | 162600 | 20.14 | 25.88 | 22.0 | |

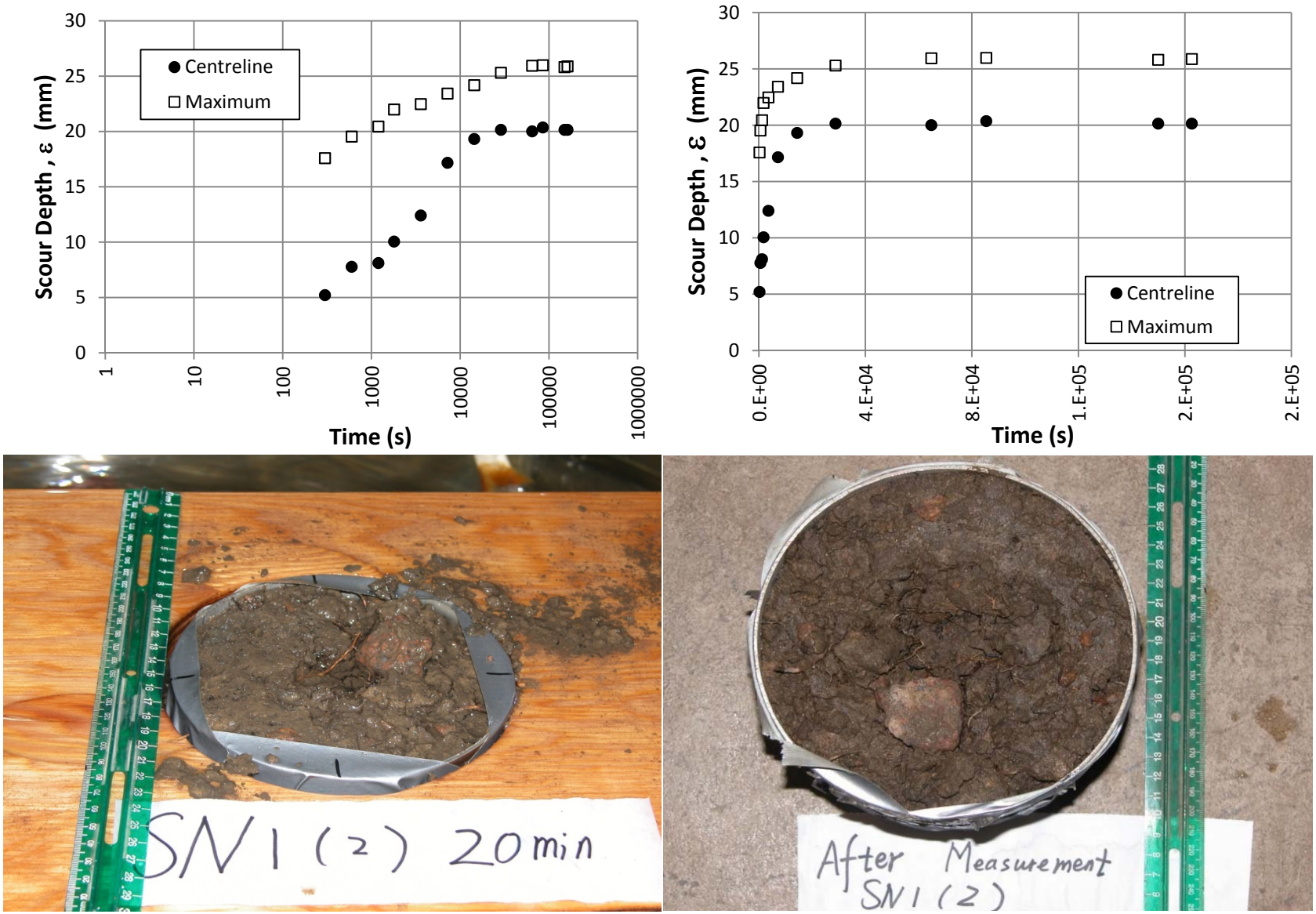


Figure A-2. Observed Time Development of Scour Plots and Test Photos for the South Nation 2 of 2 Sample

Table A-3. Test Data for the Wilton Creek 1 of 2 Sample (Ontario Group)

| | | | | | | | | | |
|---|---|---|---|---|---|---|---|---|---|
| **Sample Name:** | Wilton Creek 1 of 2 | | **Initial Temperature:** | T (˚C) | 6.7 | | **Volumetric Flow Rate** | | |
| **Batch Number:** | N/A | | **Jet Diameter:** | d (mm) | 8.0 | | Avg Q | 5.37 | Lpm |
| **Tested By:** | Research Assistant | | **Initial Jet Height:** | $H_i$ (mm) | 60 | | 1) | 5.39 | Lpm |
| **Analysis By:** | Dan Cossette | | **Equilibrium Centerline Depth:** | $\varepsilon_{cl\infty}$ (mm) | 33.97 | | 2) | 5.35 | Lpm |
| **Date of Testing:** | 2010-03-18 | | **Measured Equilibrium Height:** | $H_{e\ m}$ | 93.97 | | 3) | | Lpm |

| **Magmeter** Q | **Measured Time** $t_m$ | | | **Centerline Scour Depth** $\varepsilon_c$ | **Maximum Scour Depth** $\varepsilon_m$ | **Temp.** T | **Notes** |
|---|---|---|---|---|---|---|---|
| (Lpm) | (Min) | (Hrs) | (s) | (mm) | (mm) | (°C) | |
| 5.4 | 5 | 0:05 | 300 | 14.6 | 25.06 | 8.0 | big flat chunk peeled away, size (2-3 cm); under the sample surface, tiny and slim vegetation net appear (like sprouts). |
| 5.4 | 10 | 0:10 | 600 | 16.71 | 25.69 | | |
| 5.5 | 20 | 0:15 | 1200 | 16.36 | 25.72 | 6.0 | No change |
| 5.3 | 30 | 0:20 | 1800 | 16.36 | 26.52 | 6.0 | |
| 5.6 | 60 | 0:30 | 3600 | 17.33 | 29.51 | 6.0 | |
| 5.4 | 120 | 0:40 | 7200 | 26.9 | 31.31 | 6.0 | |
| 4.7 | 240 | 4.00 | 14400 | 28.34 | 32.25 | 6.5 | |
| 4.9 | 480 | 8.00 | 28800 | 30.04 | 32.56 | 6.5 | |
| 4.7 | 1080 | 18.00 | 64800 | 33.97 | 34.26 | 6.5 | large scour, sample grew in diameter |
| 4.9 | 1440 | 24.00 | 86400 | 33.23 | 34.53 | 7.0 | |
| 5.1 | 2620 | 43.67 | 157200 | 33.54 | 34.91 | 7.0 | |
| 4.9 | 3610 | 60.17 | 216600 | 33.75 | 34.75 | 7.0 | |
| 4.9 | 4730 | 78.83 | 283800 | 33.32 | 34.61 | 7.0 | |
| 4.7 | 5030 | 83.83 | 301800 | 33.49 | 34.6 | 7.0 | |
| 4.9 | 5950 | 99.17 | 357000 | 33.25 | 34.48 | 7.0 | |
| 4.7 | 6150 | 102.50 | 369000 | 33.29 | 34.32 | 7.0 | |

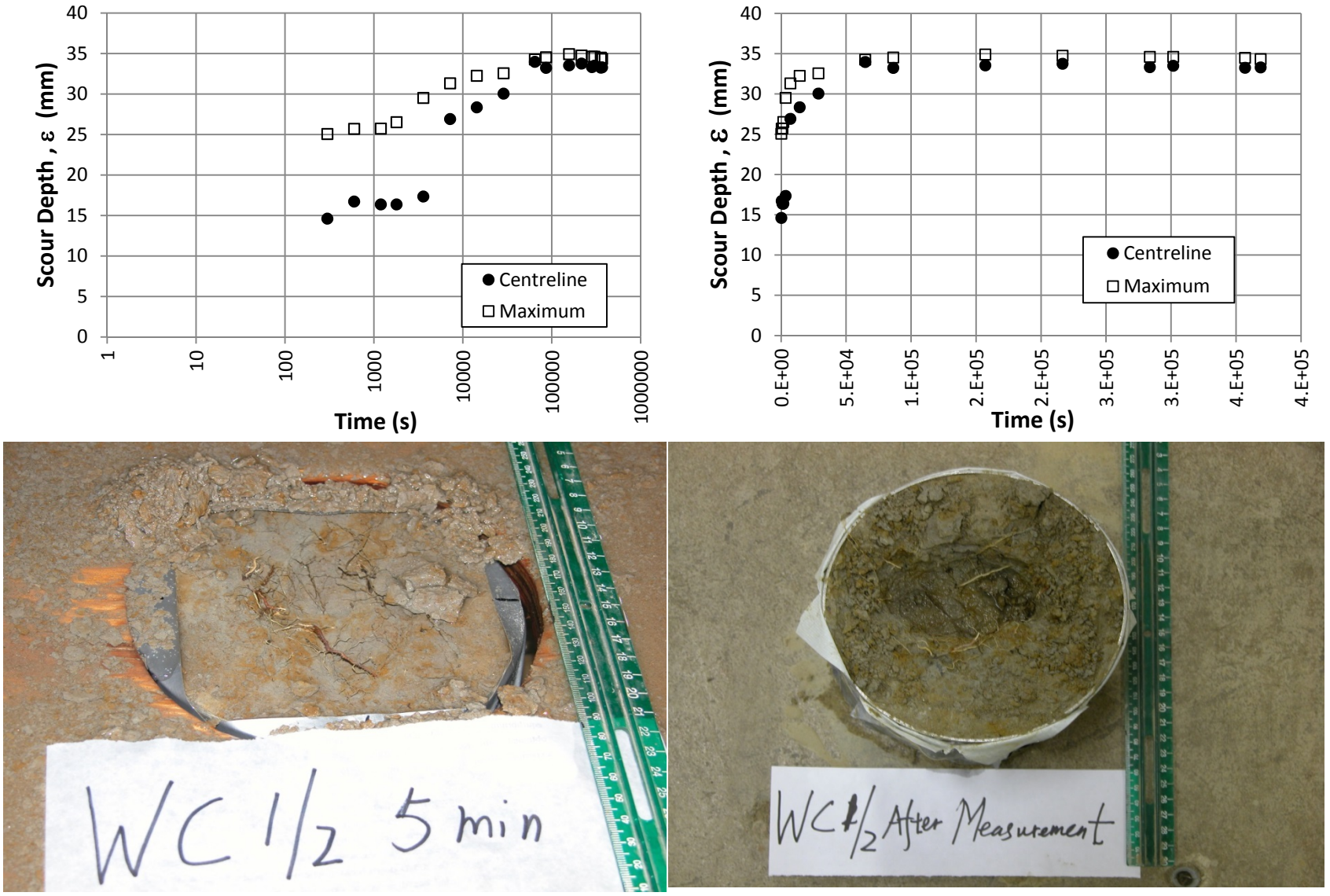


Figure A-3. Observed Time Development of Scour Plots and Test Photos for the Wilton Creek 1 of 2 Sample

Table A-4. Test Data for the Wilton Creek 2 of 2 Sample (Ontario Group)

| | | | | | | | | | |
|---|---|---|---|---|---|---|---|---|---|
| **Sample Name:** | Wilton Creek 2 of 2 | | **Initial Temperature:** | T (˚C) | 6 | | **Volumetric Flow Rate** | | |
| **Batch Number:** | N/A | | **Jet Diameter:** | d (mm) | 8.0 | | Avg Q | 3.81 | Lpm |
| **Tested By:** | Research Assistant | | **Initial Jet Height:** | $H_i$ (mm) | 60 | | 1) | | Lpm |
| **Analysis By:** | Dan Cossette | | **Equilibrium Centerline Depth:** | $\varepsilon_{cl\infty}$ (mm) | 70.74 | | 2) | | Lpm |
| **Date of Testing:** | 2010-02-25 | | **Measured Equilibrium Height:** | $H_{e\ m}$ | 130.74 | | 3) | | Lpm |

| **Magmeter** Q | **Measured Time** $t_m$ | | | **Centerline Scour Depth** $\varepsilon_c$ | **Maximum Scour Depth** $\varepsilon_m$ | **Temp.** T | **Notes** |
|---|---|---|---|---|---|---|---|
| (Lpm) | (Min) | (Hrs) | (s) | (mm) | (mm) | (°C) | |
| 4.0 | 5 | 0:05 | 300 | 15.29 | | | Flat hole with a lot of tiny particle released from sample; no big scour hole happened. |
| 4.0 | 10 | 0:10 | 600 | 25.93 | | | it looks like there is not a lot of cohesion in this sample |
| 4.3 | 20 | 0:15 | 1200 | 32.35 | | | |
| 4.1 | 30 | 0:20 | 1800 | 41.44 | | | |
| 4.2 | 60 | 0:30 | 3600 | 45.63 | | | Sprout roots appear which were under the sample surface |
| 4.0 | 120 | 0:40 | 7200 | 47.16 | | | some particle accumulation on the bottom of hole; meanwhile, there appeared the different layer under the top part. |
| 3.3 | 240 | 4.00 | 14400 | 67.23 | | | flat pieces of sample with the particle size less than 3mm; one cave formed on the edge of the scour hole. |
| 4.1 | 480 | 8.00 | 28800 | 69.03 | | | |
| 3.4 | 1360 | 22.67 | 81600 | 70.74 | | | |
| 3.4 | 1810 | 30.17 | 108600 | 70.22 | | | Scour almost reaching stability |
| 3.3 | 3086 | 51.43 | 185160 | 70.11 | | | No change of scour depth. |
| 3.6 | 4257 | 70.95 | 255420 | 69.32 | | | Max depth located at jet centerline |

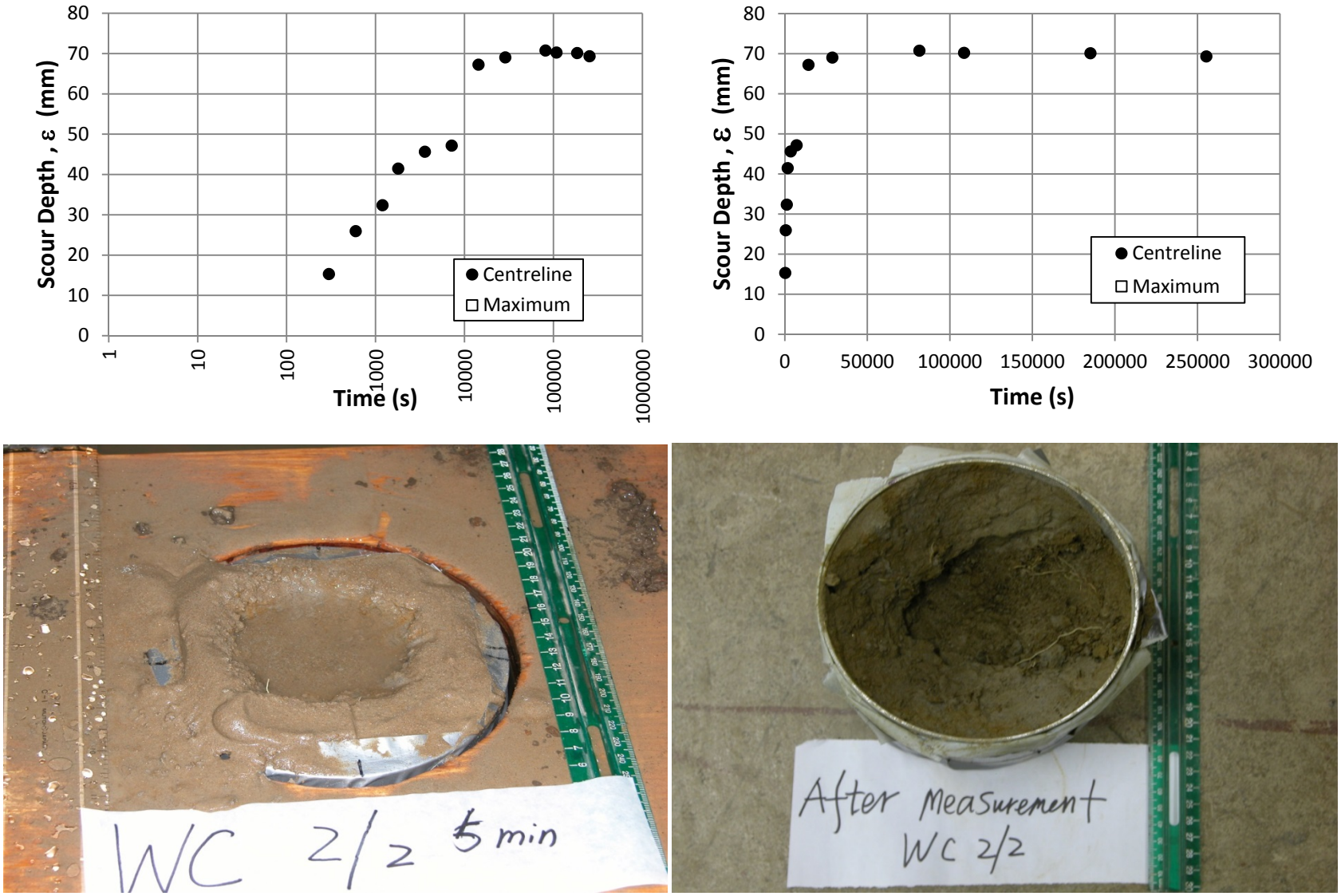


Figure A-4. Observed Time Development of Scour Plots and Test Photos for the Wilton Creek 2 of 2 Sample

Table A-5. Test Data for the Little Cataraqui 1 of 2 Sample (Ontario Group)

| | | | | | | | | | | |
|---|---|---|---|---|---|---|---|---|---|---|
| **Sample Name:** | Little Cataraqui 1 of 2 | | **Initial Temperature:** | T (˚C) | 7.2 | | **Volumetric Flow Rate** | | |
| **Batch Number:** | N/A | | **Jet Diameter:** | d (mm) | 8.0 | | Avg Q | 5.77 | Lpm |
| **Tested By:** | Research Assistant | | **Initial Jet Height:** | $H_i$ (mm) | 60 | | 1) | 5.69 | Lpm |
| **Analysis By:** | Dan Cossette | | **Equilibrium Centerline Depth:** | $\varepsilon_{cl\infty}$ (mm) | 110.73 | | 2) | 5.76 | Lpm |
| **Date of Testing:** | 2010-03-18 | | **Measured Equilibrium Height:** | $H_{e\ m}$ | 170.73 | | 3) | 5.90 | Lpm |
| | | | | | | | 4) | 5.73 | Lpm |

| **Magmeter** Q | **Measured Time** $t_m$ | | | **Centerline Scour Depth** $\varepsilon_c$ | **Maximum Scour Depth** $\varepsilon_m$ | **Temp.** T | **Notes** |
|---|---|---|---|---|---|---|---|
| (Lpm) | (Min) | (Hrs) | (s) | (mm) | (mm) | (°C) | |
| 5.7 | 5 | 0:05 | 300 | 10.75 | | 8.0 | Initially, some particle accumulated on the bottom of scour hole; the particle size maximum 4 mm; most of particle is tiny. |
| 5.1 | 10 | 0:10 | 600 | 13.23 | | 8.0 | |
| 5.2 | 20 | 0:15 | 1200 | 16.6 | | 8.0 | |
| 5.2 | 30 | 0:20 | 1800 | 19.88 | | 8.0 | The scour hole diameter increases with time |
| 5.2 | 60 | 0:30 | 3600 | 23.81 | | 8.0 | |
| 5.1 | 120 | 0:40 | 7200 | 29.28 | | 7.0 | |
| 5.2 | 240 | 4.00 | 14400 | 46.27 | | 7.0 | Bottom of scour hole 75.08mm; loose particle on top of and large mount forming on side. |
| 5.3 | 480 | 8.00 | 28800 | 50.36 | | 7.0 | |
| 5.2 | 1080 | 18.00 | 64800 | 67.03 | | 7.0 | |
| 5.4 | 1415 | 23.58 | 84900 | 70.19 | | 7.0 | not reach stable, still increase the depth of hole |
| 5.5 | 2461 | 41.02 | 147660 | 91.82 | | 7.0 | depth of hole still increase; there are no protection from vegetation net. |
| 5.2 | 2901 | 48.35 | 174060 | 102.5 | | 7.0 | |
| 5.4 | 3876 | 64.60 | 232560 | 102.4 | | 7.0 | |
| 5.2 | 4259 | 70.98 | 255540 | 108 | | 7.0 | |
| 5.3 | 5324 | 88.73 | 319440 | 110.73 | | 7.0 | |
| 5.2 | 5632 | 93.87 | 337920 | 109.89 | | 7.0 | |
| 5.2 | 6752 | 112.53 | 405120 | 109.62 | | 7.0 | |
| 5.4 | 7182 | 119.70 | 430920 | 109.22 | | 7.0 | |
| 5.1 | 8092 | 134.87 | 485520 | 109.17 | | 7.0 | |
| 5.1 | 8461 | 141.02 | 507660 | 109.34 | | 7.0 | |
| 5.2 | 9699 | 161.65 | 581940 | 109.84 | | 7.0 | |

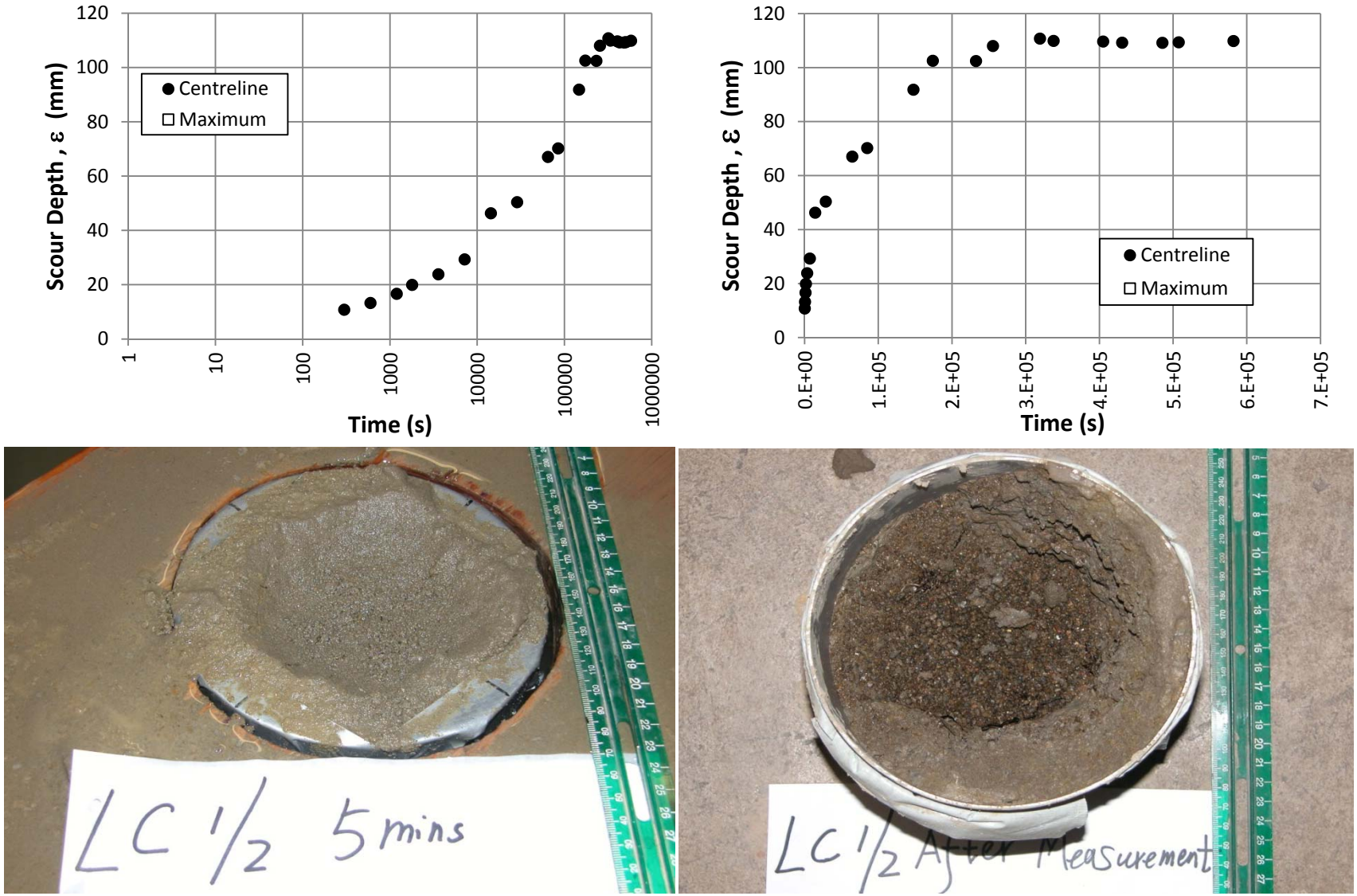


Figure A-5. Observed Time Development of Scour Plots and Test Photos for the Little Cataraqui 1 of 2 Sample

Table A-6. Test Data for the Little Cataraqui 2 of 2 Sample (Ontario Group)

| **Sample Name:** | Little Cataraqui 2 of 2 | | **Initial Temperature:** | T (˚C) | 7.6 | | **Volumetric Flow Rate** | | |
|---|---|---|---|---|---|---|---|---|---|
| **Batch Number:** | N/A | | **Jet Diameter:** | d (mm) | 8.0 | | Avg Q | 3.2 | Lpm |
| **Tested By:** | Research Assistant | | **Initial Jet Height:** | $H_i$ (mm) | 60 | | 1) | | Lpm |
| **Analysis By:** | Dan Cossette | | **Equilibrium Centerline Depth:** | $\varepsilon_{cl\infty}$ (mm) | 42.74 | | 2) | | Lpm |
| **Date of Testing:** | 2010-03-31 | | **Measured Equilibrium Height:** | $H_{e\ m}$ | 102.74 | | 3) | | Lpm |

| **Magmeter** Q | **Measured Time** $t_m$ | | | **Centerline Scour Depth** $\varepsilon_c$ | **Maximum Scour Depth** $\varepsilon_m$ | **Temp.** T | **Notes** |
|---|---|---|---|---|---|---|---|
| (Lpm) | (Min) | (Hrs) | (s) | (mm) | (mm) | (°C) | |
| 3.7 | 5 | 0:05 | 300 | 20.48 | 27.33 | | Initially, some particle accumulated on the bottom of scour hole; the particle size maximum 4 mm; most of particle is tiny. |
| 3.4 | 10 | 0:10 | 600 | 22.79 | 27.93 | 8.0 | |
| 3.4 | 20 | 0:15 | 1200 | 24.45 | 29.41 | 8.0 | |
| 3.5 | 30 | 0:20 | 1800 | 26.52 | 31.06 | 8.0 | The scour hole diameter increases with time |
| 3.6 | 60 | 0:30 | 3600 | 28.88 | 34.55 | 5.0 | |
| 2.8 | 120 | 0:40 | 7200 | 34.44 | 36.56 | 6.0 | |
| 2.8 | 240 | 4.00 | 14400 | 37.94 | | 7.0 | Bottom of scour hole 75.08mm; loose particle on top of and forming large mound on side. |
| 2.8 | 480 | 8.00 | 28800 | 37.52 | | 7.0 | |
| 2.8 | 1080 | 18.00 | 64800 | 37.15 | 39.6 | 8.0 | |
| 2.6 | 1437 | 23.95 | 86220 | 37.36 | 38.52 | 7.0 | not reach stability, still increase the depth of hole |
| 3.2 | 2462 | 41.03 | 147720 | 37.82 | | 8.0 | Depth of hole still increase; there are no protection from vegetation net. |
| 2.8 | 2842 | 47.37 | 170520 | 37.52 | | 8.0 | |
| 3.5 | 3967 | 66.12 | 238020 | 41.49 | | 8.0 | |
| 3.3 | 4381 | 73.02 | 262860 | 39.62 | | 8.0 | |
| 3.4 | 5416 | 90.27 | 324960 | 42.3 | | 9.0 | |
| 3.4 | 5907 | 98.45 | 354420 | 41.5 | | 8.0 | |
| 3.4 | 6724 | 112.07 | 403440 | 42.74 | | 8.0 | |
| 3.1 | 6934 | 115.57 | 416040 | 41.62 | | 8.0 | |

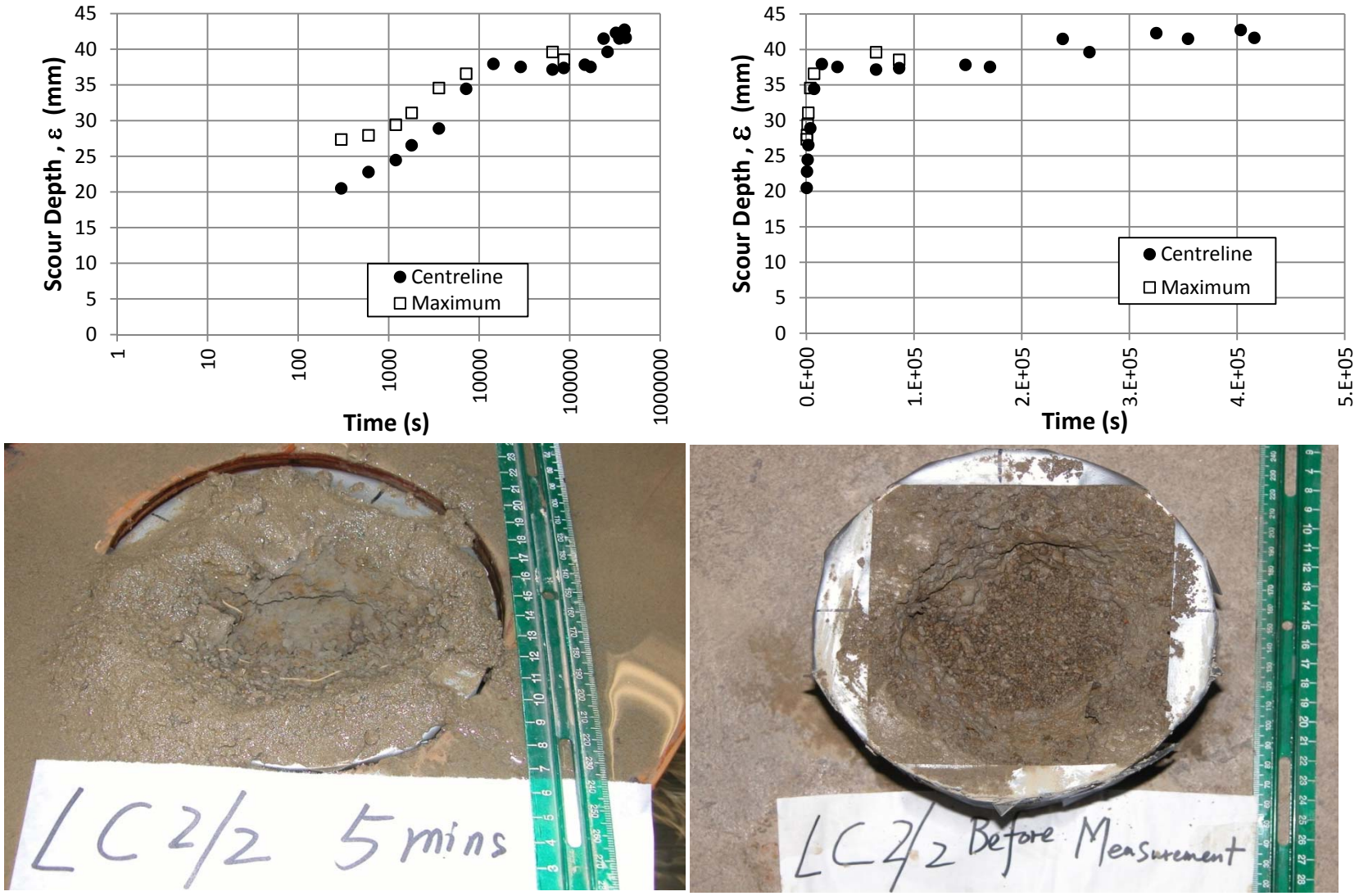


Figure A-6. Observed Time Development of Scour Plots and Test Photos for the Little Cataraqui 2 of 2 Sample

Table A-7. Test Data for the Sawmill Creek 1 of 2 Sample (Ontario Group)

| | | | | | | | | | | |
|---|---|---|---|---|---|---|---|---|---|---|
| **Sample Name:** | Sawmill Creek 1 of 2 | | **Initial Temperature:** | T (˚C) | 6.2 | | **Volumetric Flow Rate** | | |
| **Batch Number:** | N/A | | **Jet Diameter:** | d (mm) | 8.0 | | Avg Q | 17.3 | Lpm |
| **Tested By:** | Research Assistant | | **Initial Jet Height:** | $H_i$ (mm) | 63.49 | | 1) | | Lpm |
| **Analysis By:** | Dan Cossette | | **Equilibrium Centerline Depth:** | $\varepsilon_{cl\infty}$ (mm) | - | | 2) | | Lpm |
| **Date of Testing:** | 2010-04-06 | | **Measured Equilibrium Height:** | $H_{e\ m}$ | - | | 3) | | Lpm |

| **Magmeter** Q | **Measured Time** $t_m$ | | | **Centerline Scour Depth** $\varepsilon_c$ | **Maximum Scour Depth** $\varepsilon_m$ | **Temp.** T | **Notes** |
|---|---|---|---|---|---|---|---|
| (Lpm) | (Min) | (Hrs) | (s) | (mm) | (mm) | (°C) | |
| 16.5 | 5 | 0:05 | 300 | 87.69 | | 6.5 | Big hole formed; small particle accumulated on the top of wood board. Under the surface of the sample, there appear some vegetation. |
| 17.2 | 10 | 0:10 | 600 | 95.16 | | 6.5 | the part of sample filled into the scour hole. |
| 17.2 | 20 | 0:15 | 1200 | 96.25 | | 6.0 | Vegetation net under the surface of sample coming up. |
| 17.3 | 30 | 0:20 | 1800 | 97.41 | | 6.0 | |
| 17.6 | 60 | 0:30 | 3600 | 99.67 | | 6.0 | |
| 17.6 | 120 | 0:40 | 7200 | 101.49 | | 6.0 | no big change happen. |
| 17.6 | 240 | 4.00 | 14400 | 105.4 | | 6.0 | Some block of sample peeled away with maximum size 10 mm. maximum depth begins to deviate from centerline depth |
| 17.0 | 480 | 8.00 | 28800 | 107.28 | | 6.0 | |
| 17.6 | 1080 | 18.00 | 64800 | 120.46 | | 6.5 | sample scoured all the way through |

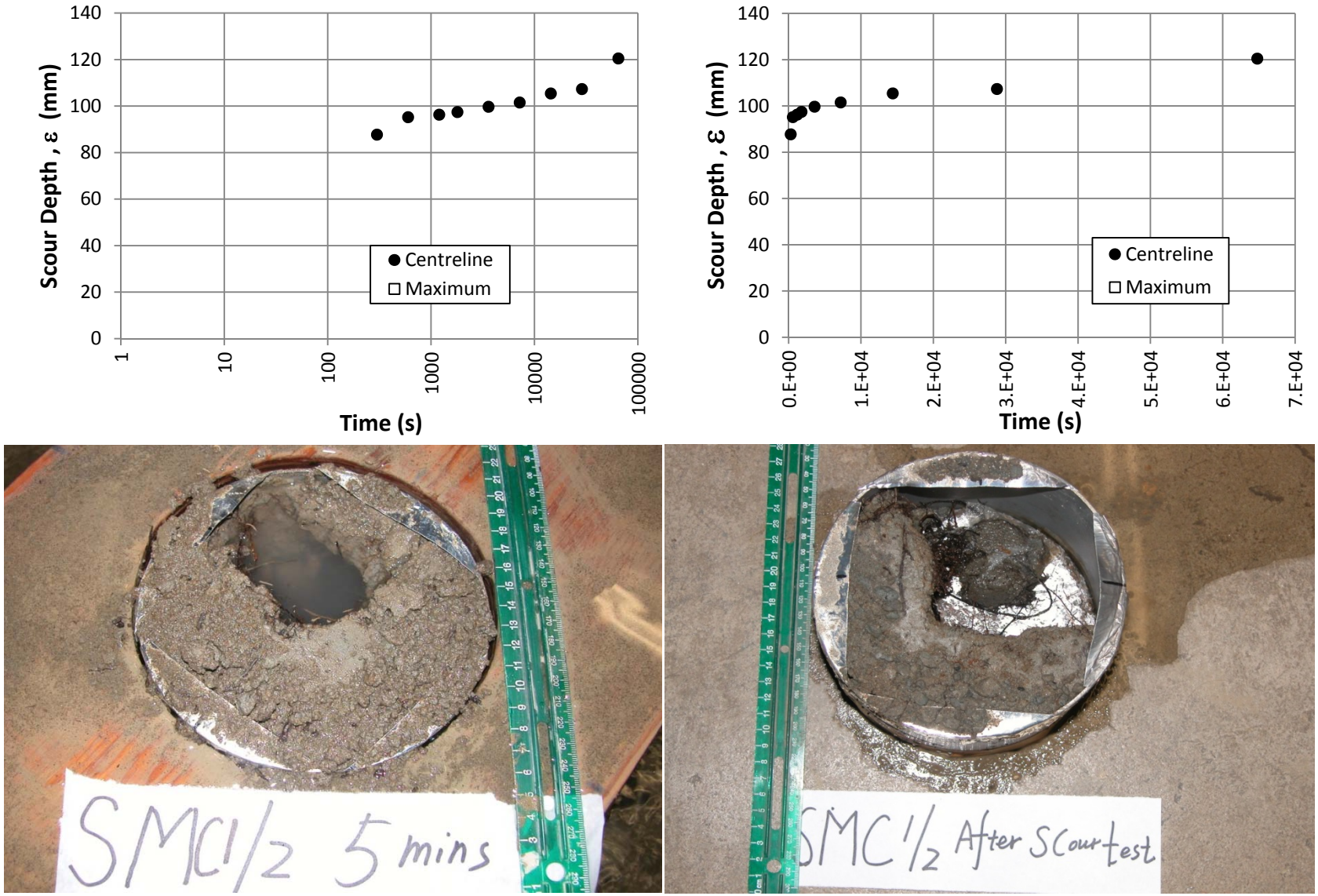


Figure A-7. Observed Time Development of Scour Plots and Test Photos for the Sawmill Creek 1 of 2 Sample

Table A-8. Test Data for the Sawmill Creek 2 of 2 Sample (Ontario Group)

| **Sample Name:** | Sawmill Creek 2 of 2 | | **Initial Temperature:** | T (˚C) | 8.5 | | **Volumetric Flow Rate** | | |
|---|---|---|---|---|---|---|---|---|---|
| **Batch Number:** | N/A | | **Jet Diameter:** | d (mm) | 8.0 | | Avg Q | 7.6 | Lpm |
| **Tested By:** | Research Assistant | | **Initial Jet Height:** | $H_i$ (mm) | 58.96 | | 1) | | Lpm |
| **Analysis By:** | Dan Cossette | | **Equilibrium Centerline Depth:** | $\varepsilon_{cl\infty}$ (mm) | 13.87 | | 2) | | Lpm |
| **Date of Testing:** | 2010-04-09 | | **Measured Equilibrium Height:** | $H_{e\ m}$ | 72.83 | | 3) | | Lpm |

| **Magmeter** Q | **Measured Time** $t_m$ | | | **Centerline Scour Depth** $\varepsilon_c$ | **Maximum Scour Depth** $\varepsilon_m$ | **Temp.** T | **Notes** |
|---|---|---|---|---|---|---|---|
| (Lpm) | (Min) | (Hrs) | (s) | (mm) | (mm) | (°C) | |
| 7.7 | 5 | 0:05 | 300 | 5.14 | | 10.0 | A little of particles peel away with maximum size 2 mm. |
| 7.6 | 10 | 0:10 | 600 | 4.5 | | 10.0 | No big change of scour hole. |
| 7.6 | 20 | 0:20 | 1200 | 4.79 | | 9.0 | Scour hole depth no change, but the perimeter of scour hole increase. |
| 7.6 | 30 | 0:30 | 1800 | 5.65 | | 9.0 | 7-8 flat pieces of sample peel away with maximum size 15 mm. |
| 7.7 | 60 | 1.00 | 3600 | 5.61 | | 9.0 | |
| 7.5 | 120 | 2.00 | 7200 | 5.54 | | 9.0 | No big change |
| 7.8 | 240 | 4.00 | 14400 | 7.78 | | 9.0 | |
| 7.5 | 480 | 8.00 | 28800 | 11.4 | | 9.0 | 60 mm diameter scour hole. |
| 7.5 | 1170 | 19.50 | 70200 | 12.69 | | 9.0 | looks similar to 8 hours |
| 7.7 | 1850 | 30.83 | 111000 | 12.72 | | 9.0 | |
| 7.7 | 2930 | 48.83 | 175800 | 13.47 | | 7.0 | |
| 7.5 | 3530 | 58.83 | 211800 | 13.7 | | 7.0 | |
| 7.7 | 4133 | 68.88 | 247980 | 13.39 | | 7.0 | |
| 7.3 | 4495 | 74.92 | 269700 | 13.53 | | 7.0 | |
| 7.5 | 5525 | 92.08 | 331500 | 13.87 | | 7.0 | end test |

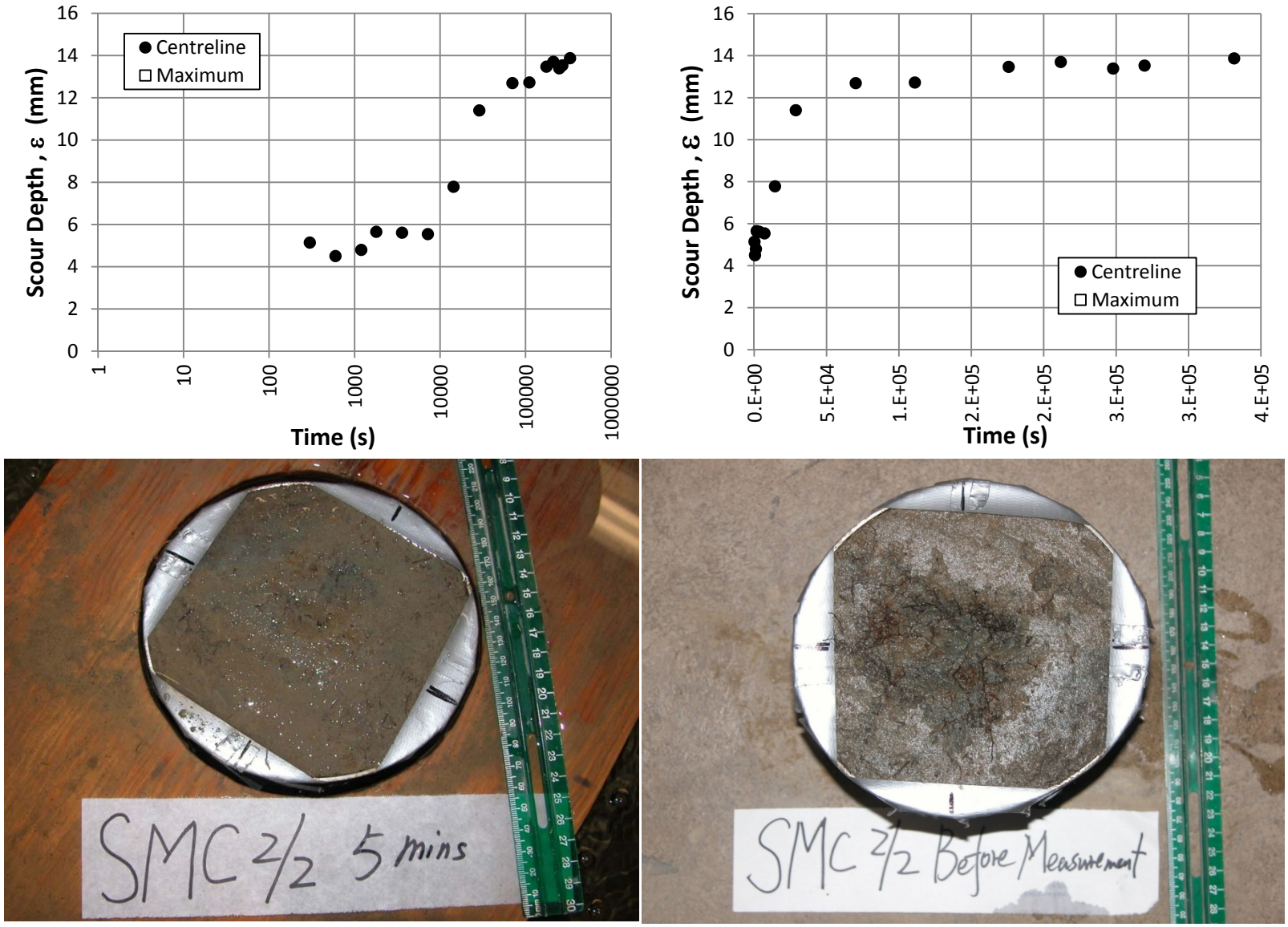


Figure A-8. Observed Time Development of Scour Plots and Test Photos for the Sawmill Creek 2 of 2 Sample

Table A-9. Test Data for the Sawmill Creek 2 of 2 Repeat Sample (Ontario Group)

| | | | | | | | | | |
|---|---|---|---|---|---|---|---|---|---|
| **Sample Name:** | Sawmill Creek 2 of 2 Repeat | | **Initial Temperature:** | T (˚C) | 7.9 | | **Volumetric Flow Rate** | | |
| **Batch Number:** | N/A | | **Jet Diameter:** | d (mm) | 8.0 | | Avg Q | 11.68 | Lpm |
| **Tested By:** | Dan Cossette | | **Initial Jet Height:** | $H_i$ (mm) | 60 | | 1) | | Lpm |
| **Analysis By:** | Dan Cossette | | **Equilibrium Centerline Depth:** | $\varepsilon_{cl\infty}$ (mm) | 65.52 | | 2) | | Lpm |
| **Date of Testing:** | 2010-04-14 | | **Measured Equilibrium Height:** | $H_{e\ m}$ | 125.52 | | 3) | | Lpm |

| **Magmeter** Q | **Measured Time** $t_m$ | | | **Centerline Scour Depth** $\varepsilon_c$ | **Maximum Scour Depth** $\varepsilon_m$ | **Temp.** T | **Notes** |
|---|---|---|---|---|---|---|---|
| (Lpm) | (Min) | (Hrs) | (s) | (mm) | (mm) | (°C) | |
| 10.6 | 5 | 0.08 | 300 | 8.26 | | 10.0 | Some particles peel away with maximum size (5mm) |
| 10.9 | 10 | 0.17 | 600 | 12.69 | | | Big chunk of sample with 30mm size; heavy vegetation has protection effect. |
| 10.7 | 20 | 0.33 | 1200 | 19.75 | | 8.5 | |
| 10.7 | 30 | 0.50 | 1800 | 20.44 | | 7.5 | No change of scour hole |
| 11.1 | 60 | 1.00 | 3600 | 20.41 | | 7.0 | No change of scour hole due to heavy vegetation net. |
| 10.5 | 120 | 2.00 | 7200 | 27.67 | | 7.0 | Big chunk of sample with 2cm size taken away. |
| 11.1 | 240 | 4.00 | 14400 | 30.96 | | 7.0 | maximum depth begins to deviate from centerline depth |
| 11.1 | 480 | 8.00 | 28800 | 42.11 | | 7.0 | |
| 10.9 | 1163 | 19.38 | 69780 | 44.22 | | 7.0 | Big hole formed with a significant amount of sample peeled away. |
| 10.8 | 1511 | 25.18 | 90660 | 43.91 | | 7.0 | |
| 10.8 | 2535 | 42.25 | 152100 | 45.28 | | 7.0 | |
| 11.1 | 3070 | 51.17 | 184200 | 47.47 | | 7.0 | |
| 11.0 | 4070 | 67.83 | 244200 | 48.28 | | 7.0 | |
| 10.8 | 4535 | 75.58 | 272100 | 59.39 | | 7.0 | large scour formed since previous measurement. |
| 10.9 | 5505 | 91.75 | 330300 | 59.98 | | 8.0 | |
| 10.8 | 5970 | 99.50 | 358200 | 60.63 | | 9.0 | |
| 11.0 | 6771 | 112.85 | 406260 | 65.20 | | 9.0 | |
| 11.3 | 7178 | 119.63 | 430680 | 65.52 | | 10.0 | |
| 11.1 | 8234 | 137.23 | 494040 | 65.22 | | 10.0 | End Test |

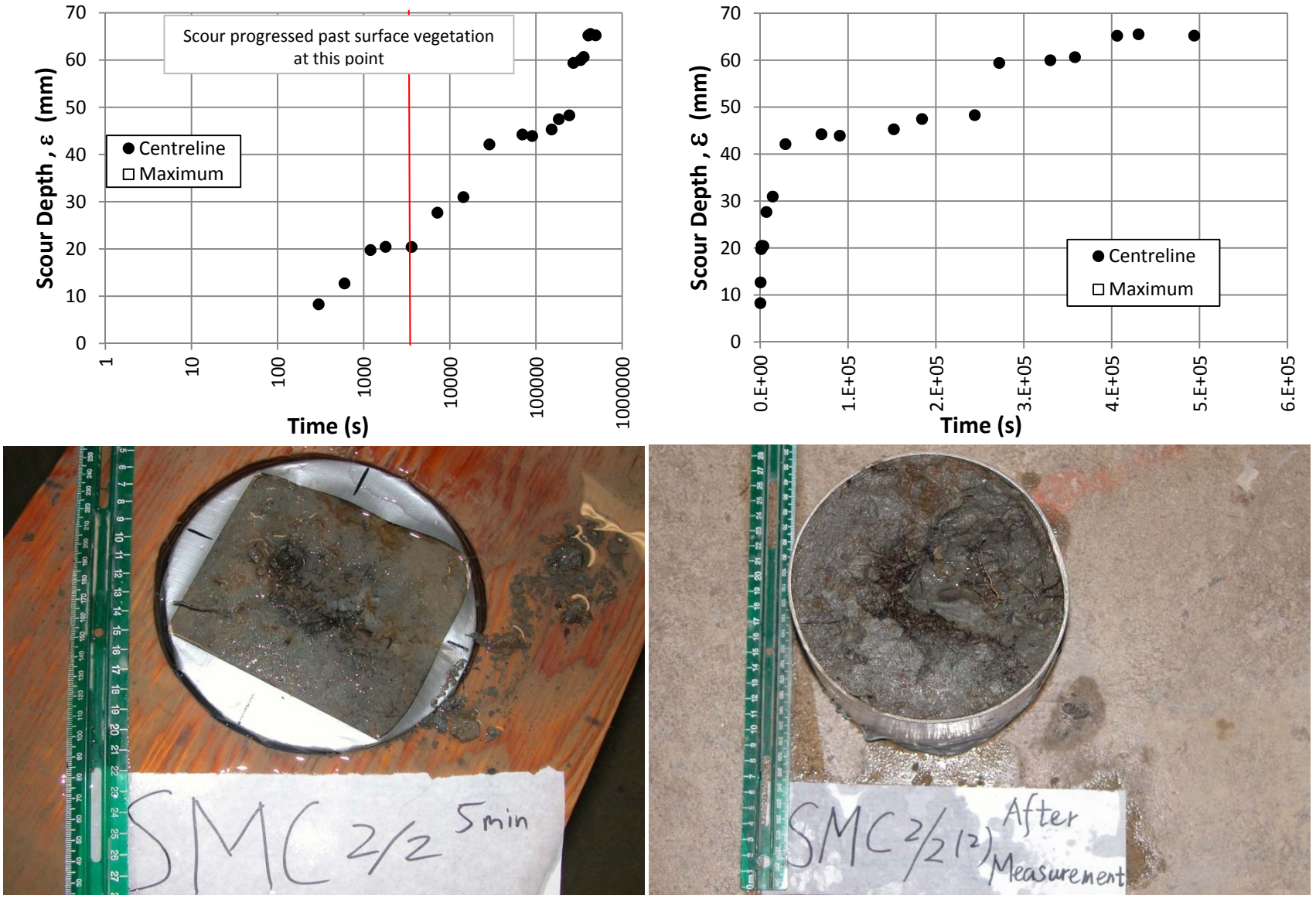


Figure A-9. Observed Time Development of Scour Plots and Test Photos for the Sawmill Creek 2 of 2 Repeat Sample

Table A-10. Test Data for the Bear Brook 1 of 2 Sample (Ontario Group)

| | | | | | | | | | | |
|---|---|---|---|---|---|---|---|---|---|---|
| **Sample Name:** | Bear Brook 1 of 2 | | **Initial Temperature:** | T (˚C) | 12.8 | | **Volumetric Flow Rate** | | |
| **Batch Number:** | N/A | | **Jet Diameter:** | d (mm) | 8.0 | | Avg Q | 4.6 | Lpm |
| **Tested By:** | Dan Cossette | | **Initial Jet Height:** | $H_i$ (mm) | 60 | | 1) | | Lpm |
| **Analysis By:** | Dan Cossette | | **Equilibrium Centerline Depth:** | $\varepsilon_{cl\infty}$ (mm) | 84.96 | | 2) | | Lpm |
| **Date of Testing:** | 2010-04-21 | | **Measured Equilibrium Height:** | $H_{e\ m}$ | 144.96 | | 3) | | Lpm |

| **Magmeter** Q | **Measured Time** $t_m$ | | | **Centerline Scour Depth** $\varepsilon_c$ | **Maximum Scour Depth** $\varepsilon_m$ | **Temp.** T | **Notes** |
|---|---|---|---|---|---|---|---|
| (Lpm) | (Min) | (Hrs) | (s) | (mm) | (mm) | (°C) | |
| 4.8 | 5 | 0.08 | 300 | | 21.72 | 14.0 | Big scour hole formed with some tiny particles (max size 3mm) |
| 4.7 | 10 | 0.17 | 600 | | 24.62 | 14.0 | |
| 4.5 | 20 | 0.33 | 1200 | | 28.19 | 14.0 | Tiny particles (1-3mm) coming out from the scour hole. |
| 4.6 | 30 | 0.50 | 1800 | | 28.9 | 14.0 | |
| 4.7 | 60 | 1.00 | 3600 | | 31.86 | 12.0 | No significant change. |
| 4.9 | 120 | 2.00 | 7200 | | 35.63 | 12.0 | |
| 4.6 | 240 | 4.00 | 14400 | | 50.29 | 12.5 | There is significant change during this time period; the particles accumulated on the top of sample. Maximum depth begins to deviates from centerline depth |
| 4.6 | 480 | 8.00 | 28800 | | 50.57 | 13.0 | |
| 4.8 | 1260 | 21.00 | 75600 | | 51.36 | 12.5 | There are change on the hole perimeter, not the depth of the hole compared with the scour hole at 4 hours. |
| 4.5 | 1590 | 26.50 | 95400 | | 54.95 | 13.0 | |
| 4.7 | 2670 | 44.50 | 160200 | | 54.33 | 13.0 | |
| 4.8 | 3000 | 50.00 | 180000 | | 59.91 | 13.0 | |
| 4.6 | 4260 | 71.00 | 255600 | | 71.17 | 13.0 | Scour has reached the edges of sample container, and deepest point has shifted close to container edge. |
| 4.6 | 4470 | 74.50 | 268200 | | 75.01 | 12.5 | |
| 4.5 | 5640 | 94.00 | 338400 | | 80.13 | 12.5 | Lots of vegetation in scour hole; coarse (1-2mm) particles deposited on and beside sample. |
| 4.6 | 6240 | 104.00 | 374400 | | 84.37 | 13.0 | |
| 4.6 | 6870 | 114.50 | 412200 | | 84.96 | 12.0 | |
| 4.6 | 7211 | 120.18 | 432660 | | 84.45 | 12.0 | |
| 4.3 | 8364 | 139.40 | 501840 | | 84.11 | 12.0 | |
| 4.6 | 8664 | 144.40 | 519840 | | 83.26 | 12.0 | |
| 4.7 | 9898 | 164.97 | 593880 | | 83.81 | 12.0 | |

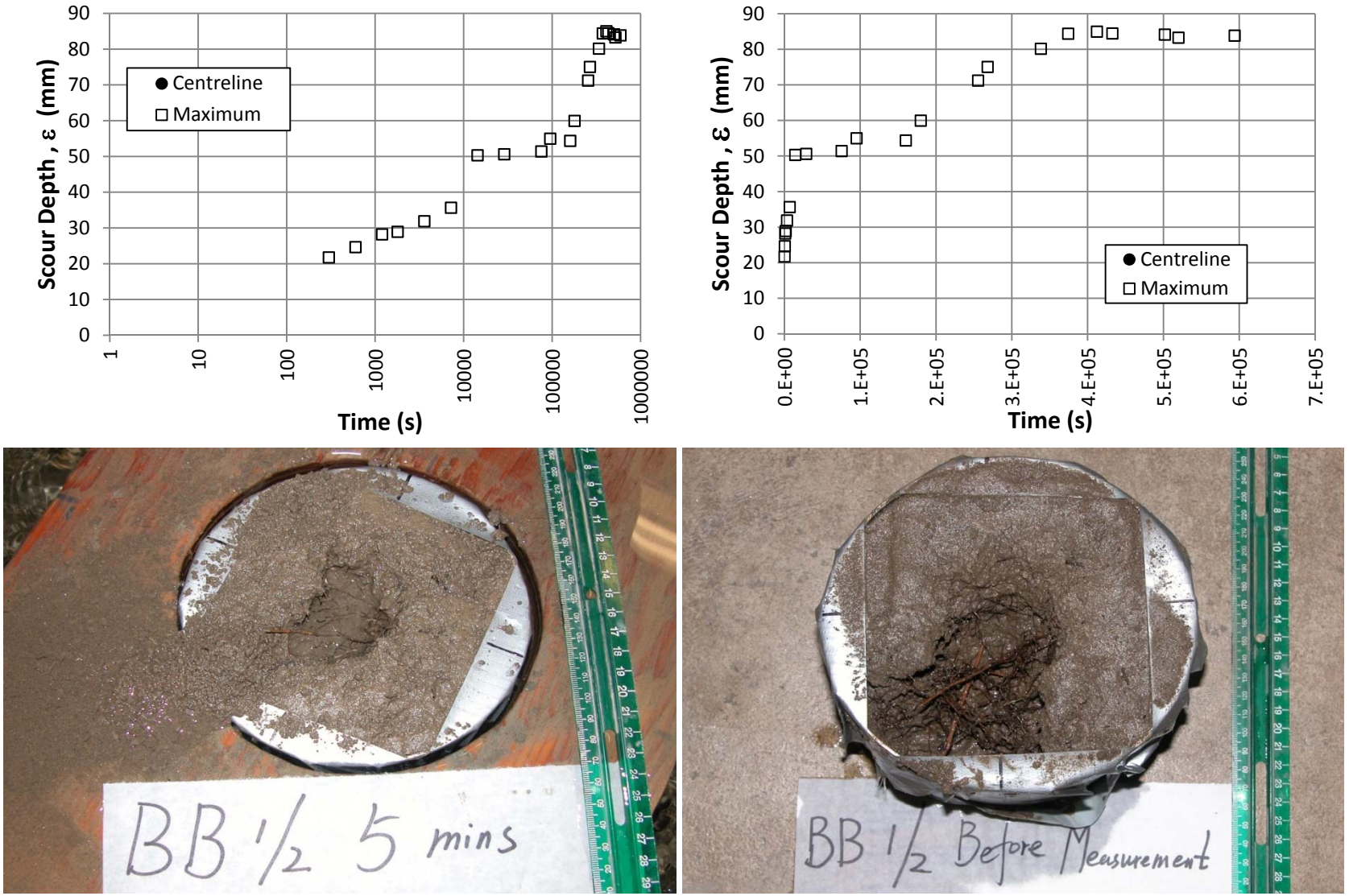


Figure A-10. Observed Time Development of Scour Plots and Test Photos for the Bear Brook 1 of 2 Sample

Table A-11. Test Data for the Bear Brook 2 of 2 Sample (Ontario Group)

| | | | | | | | | | |
|---|---|---|---|---|---|---|---|---|---|
| **Sample Name:** | Bear Brook 2 of 2 | | **Initial Temperature:** | T (˚C) | 12.3 | | **Volumetric Flow Rate** | | |
| **Batch Number:** | N/A | | **Jet Diameter:** | d (mm) | 8.0 | | Avg Q | 4.57 | Lpm |
| **Tested By:** | Dan Cossette | | **Initial Jet Height:** | $H_i$ (mm) | 60 | | 1) | 4.51 | Lpm |
| **Analysis By:** | Dan Cossette | | **Equilibrium Centerline Depth:** | $\varepsilon_{cl\infty}$ (mm) | - | | 2) | 4.54 | Lpm |
| **Date of Testing:** | 2010-05-03 | | **Measured Equilibrium Height:** | $H_{e\ m}$ | - | | 3) | 4.67 | Lpm |

| **Magmeter** Q | **Measured Time** $t_m$ | | | **Centerline Scour Depth** $\varepsilon_c$ | **Maximum Scour Depth** $\varepsilon_m$ | **Temp.** T | **Notes** |
|---|---|---|---|---|---|---|---|
| (Lpm) | (Min) | (Hrs) | (s) | (mm) | (mm) | (°C) | |
| 3.8 | 5 | 0.08 | 300 | 32.12 | | 14.5 | very large root (1.5-2cm) in center of scour hole, very large initial erosion, silty particles 1-5mm |
| 3.5 | 15 | 0.25 | 900 | 36.25 | | 14.0 | |
| 4.0 | 35 | 0.58 | 2100 | 38.14 | | 12.5 | large root seems to be retarding scour, smaller roots starting to expose |
| 4.1 | 60 | 1.00 | 3600 | 37.38 | | 12.0 | |
| 3.7 | 120 | 2.00 | 7200 | 41.67 | | 11.5 | no major change |
| 4.1 | 240 | 4.00 | 14400 | 41.8 | | 12.0 | no major change |
| 3.9 | 480 | 8.00 | 28800 | 45.48 | | 11.5 | |
| 4.3 | 1260 | 21.00 | 75600 | 45.47 | | 11.5 | same depth of scour hole on either side of the root |
| 4.0 | 1601 | 26.68 | 96060 | 45.45 | | 12.0 | scour hole is widening, another root (0.5-1cm) exposed on fringe of scour hole |
| 4.3 | 2650 | 44.17 | 159000 | 43.03 | | 12.0 | not getting any deeper but continuing to grow in diameter |
| 4.3 | 2950 | 49.17 | 177000 | 46.82 | | 12.0 | |
| 4.4 | 3965 | 66.08 | 237900 | 47.56 | | 11. 5 | test terminated before equilibrium state can be confirmed (due to disruptive presence of large root). |

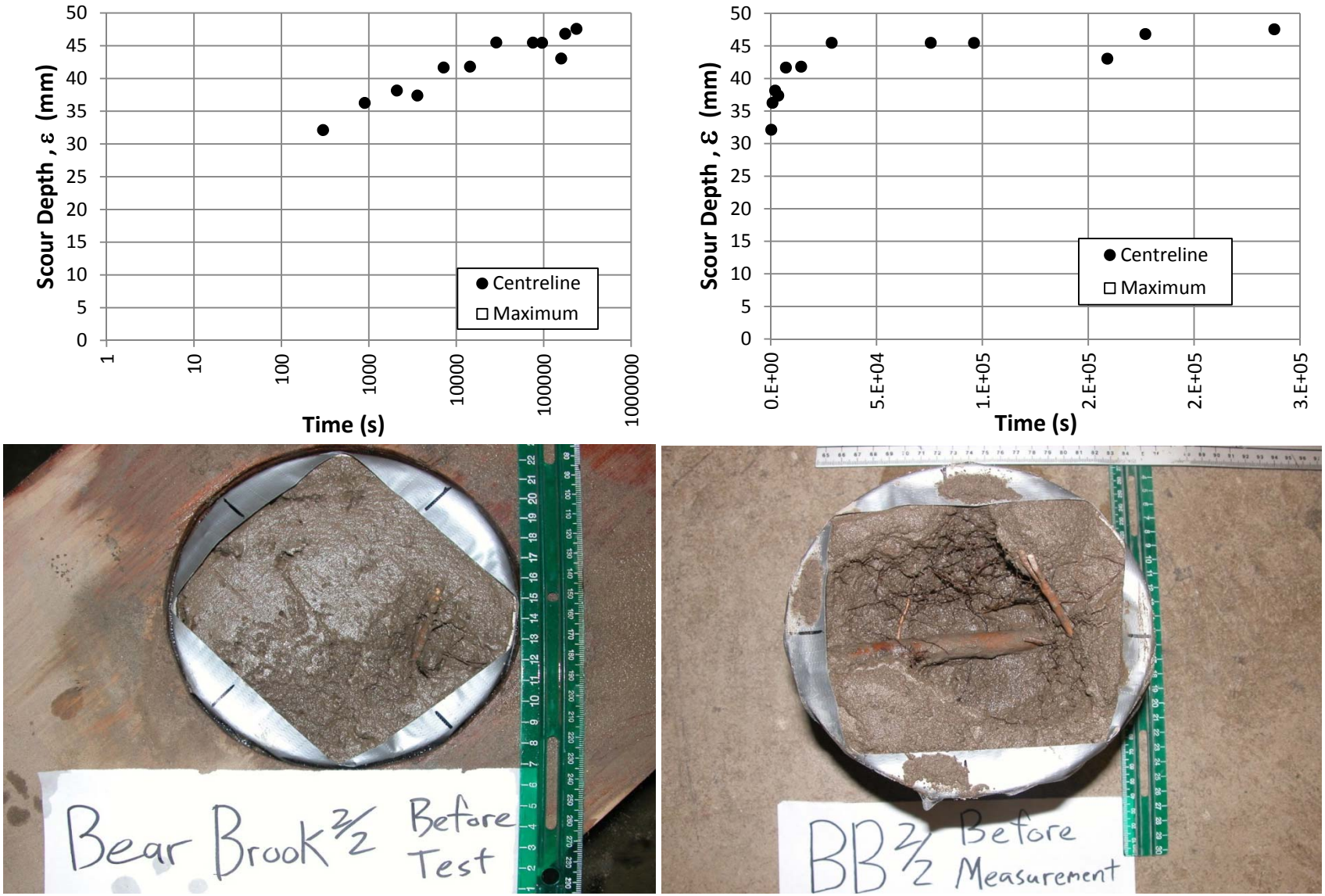


Figure A-11. Observed Time Development of Scour Plots and Test Photos for the Bear Brook 2 of 2 Sample

Table A-12. Test Data for the Bear Brook 2 of 2 Repeat Sample (Ontario Group)

| | | | | | | | | | | |
|---|---|---|---|---|---|---|---|---|---|---|
| **Sample Name:** | Bear Brook 2 of 2 Repeat | | **Initial Temperature:** | T (˚C) | 12.0 | | **Volumetric Flow Rate** | | |
| **Batch Number:** | N/A | | **Jet Diameter:** | d (mm) | 8.0 | | Avg Q | 4.78 | Lpm |
| **Tested By:** | Dan Cossette | | **Initial Jet Height:** | $H_i$ (mm) | 67.13 | | 1) | 4.79 | Lpm |
| **Analysis By:** | Dan Cossette | | **Equilibrium Centerline Depth:** | $\varepsilon_{cl\infty}$ (mm) | 34.79 | | 2) | 4.80 | Lpm |
| **Date of Testing:** | 2010-05-07 | | **Measured Equilibrium Height:** | $H_{e\ m}$ | 101.92 | | 3) | 4.74 | Lpm |

| **Magmeter** Q | **Measured Time** $t_m$ | | | **Centerline Scour Depth** $\varepsilon_c$ | **Maximum Scour Depth** $\varepsilon_m$ | **Temp.** T | **Notes** |
|---|---|---|---|---|---|---|---|
| (Lpm) | (Min) | (Hrs) | (s) | (mm) | (mm) | (°C) | |
| 3.1 | 5 | 0.08 | 300 | 4.12 | | 13.0 | |
| 3.8 | 10 | 0.17 | 600 | 5.18 | | 13.5 | flake erosion of surface, particles up to 5mm |
| 3.8 | 20 | 0.33 | 1200 | 8.81 | | 11.5 | |
| 3.9 | 30 | 0.50 | 1800 | 8.51 | | 11.0 | |
| 4.3 | 60 | 1.00 | 3600 | 10.13 | | 11.0 | |
| 4.1 | 120 | 2.00 | 7200 | 11.26 | | 11.0 | |
| 3.4 | 240 | 4.00 | 14400 | 14.34 | | 11.0 | scour is not really uniform or at center of sample, 2 deeper plunge pools forming not just 1, |
| 3.8 | 480 | 8.00 | 28800 | 12.00 | | 11.5 | |
| 4.0 | 1720 | 28.67 | 103200 | 20.32 | | 11.5 | max depth shifted to center of sample, use to be offset |
| 4.0 | 2995 | 49.92 | 179700 | 31.87 | | 12.0 | exposed vegetation, small roots 1mm thick |
| 4.2 | 3550 | 59.17 | 213000 | 31.99 | | 12.0 | no noticeable change |
| 4.0 | 4125 | 68.75 | 247500 | 32.24 | | 12.0 | |
| 4.1 | 4500 | 75.00 | 270000 | 34.51 | | 12.5 | seem to be getting block erosion under jet |
| 4.1 | 5580 | 93.00 | 334800 | 33.82 | | 12.5 | |
| 4.3 | 6185 | 103.08 | 371100 | 33.67 | | 13.0 | |
| 4.3 | 6945 | 115.75 | 416700 | 34.79 | | 13.0 | deepest hole is almost cubic |

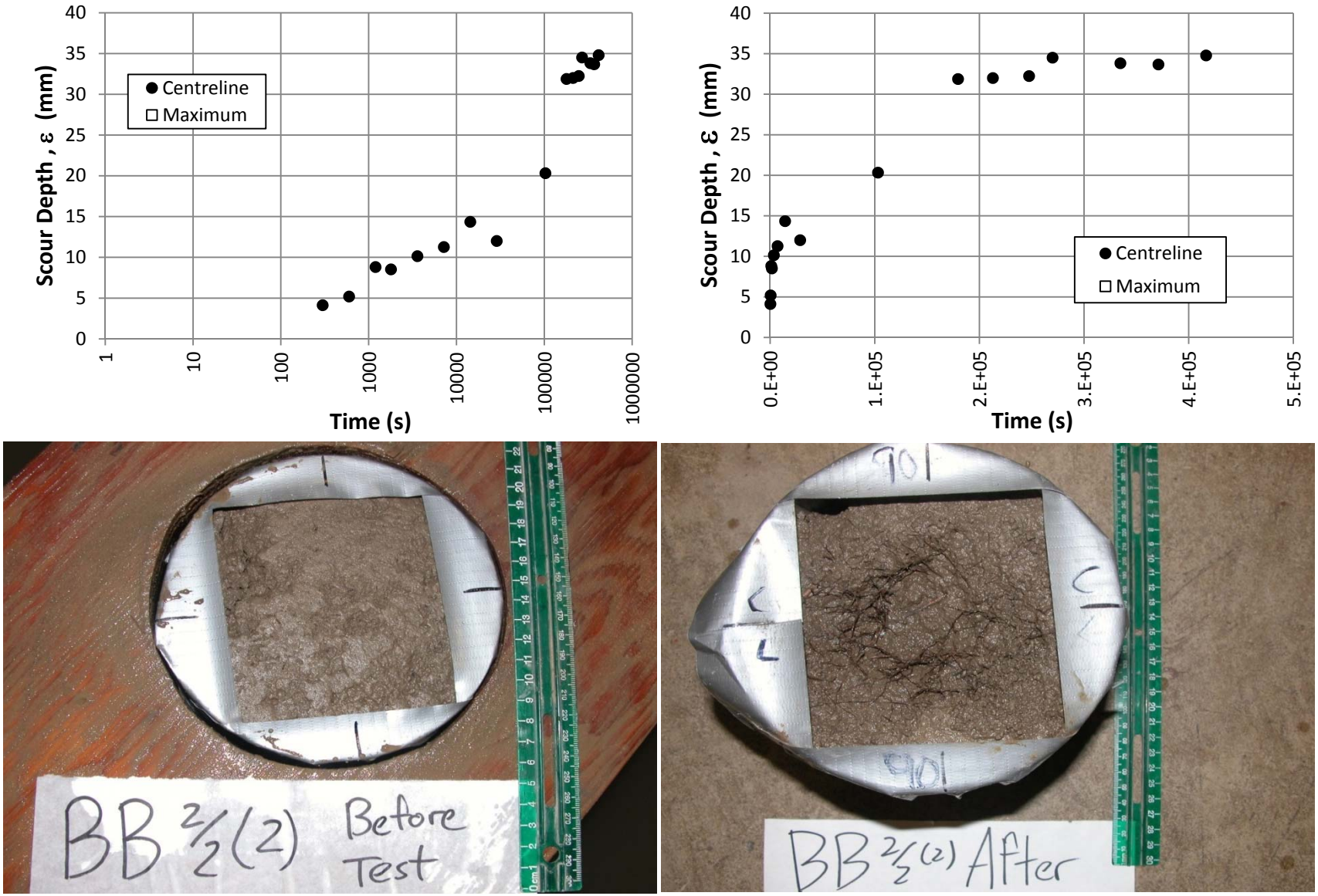


Figure A-12. Observed Time Development of Scour Plots and Test Photos for the Bear Brook 2 of 2 Repeat Sample

Table A-13. Test Data for the Jock River 1 of 2 Sample (Ontario Group)

| | | | | | | | | | | |
|---|---|---|---|---|---|---|---|---|---|---|
| **Sample Name:** | Jock River 1 of 2 | | **Initial Temperature:** | T (˚C) | 17.5 | | **Volumetric Flow Rate** | | |
| **Batch Number:** | N/A | | **Jet Diameter:** | d (mm) | 8.0 | | Avg Q | 6.35 | Lpm |
| **Tested By:** | Dan Cossette | | **Initial Jet Height:** | $H_i$ (mm) | 66.32 | | 1) | 6.32 | Lpm |
| **Analysis By:** | Dan Cossette | | **Equilibrium Centerline Depth:** | $\varepsilon_{cl\infty}$ (mm) | 23.29 | | 2) | 6.37 | Lpm |
| **Date of Testing:** | 2011-06-29 | | **Measured Equilibrium Height:** | $H_{e\ m}$ | 89.61 | | 3) | 6.35 | Lpm |

| **Magmeter** Q | **Measured Time** $t_m$ | | | **Centerline Scour Depth** $\varepsilon_c$ | **Maximum Scour Depth** $\varepsilon_m$ | **Temp.** T | **Notes** |
|---|---|---|---|---|---|---|---|
| (Lpm) | (Min) | (Hrs) | (s) | (mm) | (mm) | (°C) | |
| 5.2 | 5 | 0.08 | 300 | 13.36 | | 18.5 | scour of very large particles (4-9mm), removal in form of clumps of soil, exposed root at edge of sample (2-3mm) |
| 5.5 | 10 | 0.17 | 600 | 14.95 | | 17.5 | large particle (15-20mm) removed , several 2-5mm removed |
| 5.9 | 20 | 0.33 | 1200 | 15.44 | | 17.5 | not much visible change, sample very "spongey" due to heavy vegetation, may be hindering scour |
| 6.1 | 30 | 0.50 | 1800 | 15.63 | | 17.5 | lots of small vegetation particles released (>1mm), no real visible developed scour hole |
| 6.0 | 60 | 1.00 | 3600 | 22.29 | | 17.0 | |
| 6.2 | 120 | 2.00 | 7200 | 22.81 | | 17.5 | no real formation of visible scour hole |
| 5.9 | 240 | 4.00 | 14400 | 22.78 | | 17.0 | |
| 6.1 | 480 | 8.00 | 28800 | 22.86 | | 17.0 | scour hole cleared out so plunge hole is visible |
| 5.9 | 1090 | 18.17 | 65400 | 22.7 | | 17.5 | |
| 6.3 | 1450 | 24.17 | 87000 | 23.29 | | 18.5 | |
| 6.0 | 2536 | 42.27 | 152160 | 22.96 | | 16.5 | |

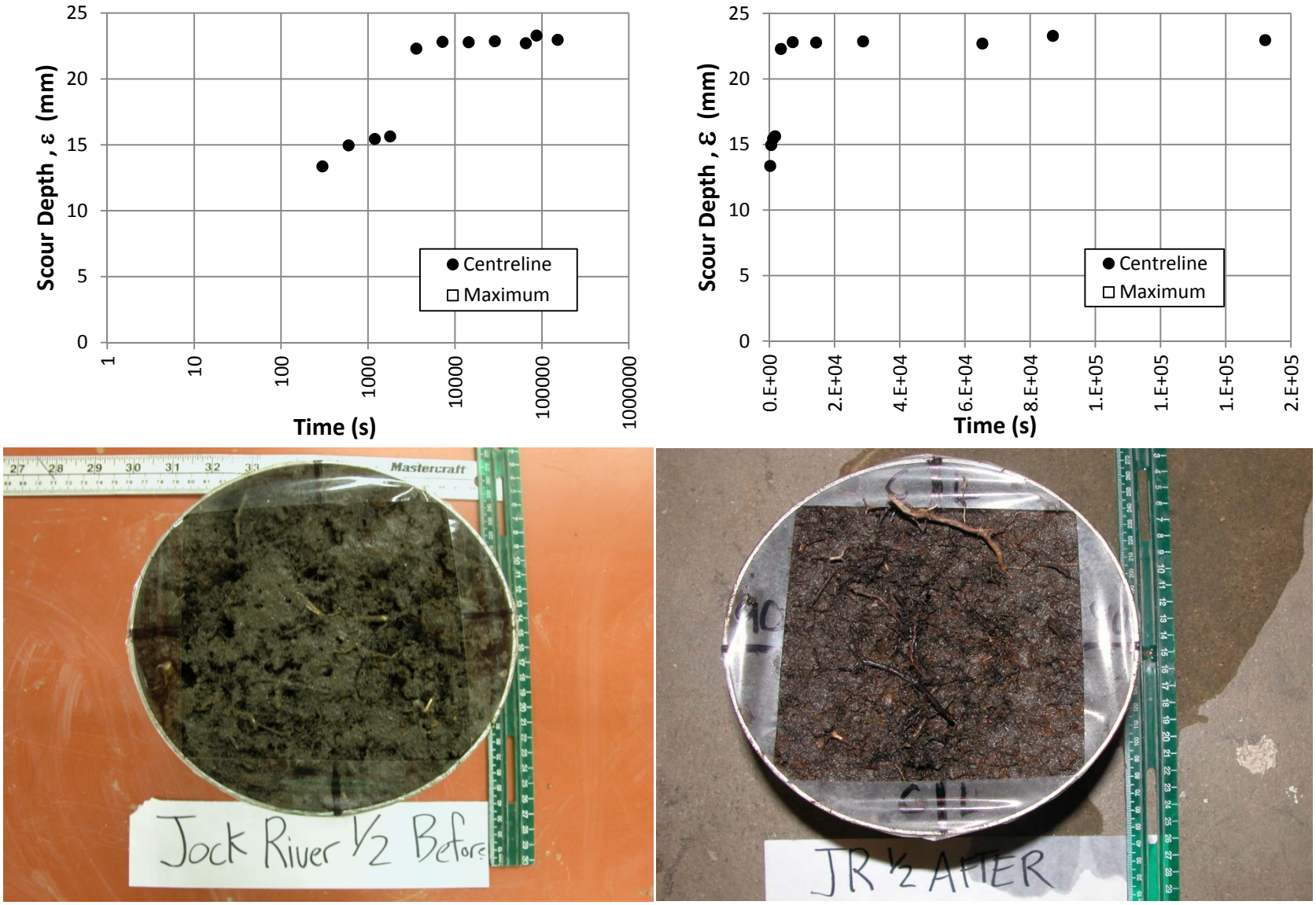


Figure A-13. Observed Time Development of Scour Plots and Test Photos for the Jock River 1 of 2 Sample

Table A-14. Test Data for the Jock River 1 of 2 Repeat Sample (Ontario Group)

| | | | | | | | | | |
|---|---|---|---|---|---|---|---|---|---|
| **Sample Name:** | Jock River 1 of 2 Repeat | | **Initial Temperature:** | T (˚C) | 17.1 | | **Volumetric Flow Rate** | | |
| **Batch Number:** | N/A | | **Jet Diameter:** | d (mm) | 8.0 | | Avg Q | 11.13 | Lpm |
| **Tested By:** | Dan Cossette | | **Initial Jet Height:** | $H_i$ (mm) | 86.93 | | 1) | 11.19 | Lpm |
| **Analysis By:** | Dan Cossette | | **Equilibrium Centerline Depth:** | $\varepsilon_{cl\infty}$ (mm) | 47.6 | | 2) | 11.22 | Lpm |
| **Date of Testing:** | 2010-08-25 | | **Measured Equilibrium Height:** | $H_{e\ m}$ | 134.53 | | 3) | 10.98 | Lpm |

| **Mag -meter** Q | **Measured Time** $t_m$ | | | **Centerline Scour Depth** $\varepsilon_c$ | **Maximum Scour Depth** $\varepsilon_m$ | **Temp.** T | **Notes** |
|---|---|---|---|---|---|---|---|
| (Lpm) | (Min) | (Hrs) | (s) | (mm) | (mm) | (°C) | |
| 9.7 | 5 | 0:05 | 300 | 5.99 | 8.66 | 18.0 | heavy surface vegetation, roots 2-3 mm, eroded clumps on the edge of sample have roots in them |
| 9.8 | 10 | 0:10 | 600 | 7.71 | 10.6 | 17.5 | |
| 9.9 | 15 | 0:15 | 900 | 6.54 | 11.46 | 17.5 | |
| 10.4 | 20 | 0:20 | 1200 | 8.2 | 10.75 | 17.5 | |
| 10.7 | 30 | 0:30 | 1800 | 8.23 | 15.84 | 17.5 | |
| 10.7 | 50 | 0:40 | 3000 | 10.92 | 16.78 | 17.5 | |
| 10.5 | 80 | 1.33 | 4800 | 11.82 | 16.96 | 17.5 | |
| 10.5 | 140 | 2.33 | 8400 | 12.89 | 21.14 | 17.5 | |
| 10.5 | 275 | 4.58 | 16500 | 14.21 | 20.64 | 17.5 | |
| 10.4 | 455 | 7.58 | 27300 | 13.88 | 20.55 | 18.0 | looks like modest growth of scour hole width |
| 10.8 | 891 | 14.85 | 53460 | 17.21 | 21.72 | 18.0 | max is almost center |
| 10.7 | 1796 | 29.93 | 107760 | 18.39 | 22.52 | 18.5 | |
| 10.5 | 2749 | 45.82 | 164940 | 19.68 | 23 | 18.5 | |
| 10.9 | 3199 | 53.32 | 191940 | 20.76 | 23.06 | 19.0 | |
| 10.6 | 4330 | 72.17 | 259800 | 21.91 | 23.84 | 18.5 | |
| 10.5 | 5221 | 87.02 | 313260 | 22.91 | 28.38 | 17.5 | noticeable increase in erosion, scour hole slightly more cleared out, (1) side of sample lifted when putting the jet back in place, possibly got eroded underneath and then the pressure increase from the jet moving into place lifted it out. |
| 10.3 | 6736 | 112.27 | 404160 | 25.42 | 32.5 | 16.5 | |
| 10.5 | 7401 | 123.35 | 444060 | 25.09 | 33.85 | 16.5 | |
| 10.4 | 8093 | 134.88 | 485580 | 24.84 | 33.69 | 16.0 | |
| 10.4 | 8683 | 144.72 | 520980 | 30.11 | 33.97 | 17.0 | |
| 10.2 | 9380 | 156.33 | 562800 | 31.04 | 33.76 | 17.0 | lots of particles dislodged at the start of time interval |

| | | | | | | | |
|---|---|---|---|---|---|---|---|
| 11.1 | 9881 | 164.68 | 592860 | 33.47 | 34.15 | 17.0 | power outage between 33.76-34.15 tested stopped overnight (about 21hrs) pumps and magnetic flow meter left untouched |
| 11.0 | 11661 | 194.35 | 699660 | 35.44 | 38.07 | 17.5 | scour max and center seem to be lining up |
| 10.8 | 12912 | 215.20 | 774720 | 33.39 | 40.13 | 17.5 | max depth very close (about 5mm) to center depth |
| 11.1 | 14071 | 234.52 | 844260 | 41.63 | 41.77 | 17.0 | max and center the same |
| 10.8 | 14939 | 248.98 | 896340 | 42.26 | 42.4 | 17.0 | jet stream is conveyed from the center under the sample surface to the side, seems to be eroding under the surface |
| 10.7 | 16354 | 272.57 | 981240 | 43.18 | 43.32 | 17.0 | |
| 10.6 | 16986 | 283.10 | 1019160 | 44.75 | 44.89 | 17.0 | |
| 10.8 | 18498 | 308.30 | 1109880 | 45 | 45.14 | 16.5 | |
| 10.3 | 19623 | 327.05 | 1177380 | 45.77 | 45.91 | 16.0 | |
| 10.6 | 21161 | 352.68 | 1269660 | 45.11 | 45.25 | 15.5 | |
| 10.8 | 22691 | 378.18 | 1361460 | 46.22 | 47.76 | 15.5 | first reading at 100mm, second and third at 108mm, very narrow scour hole |
| 10.4 | 23850 | 397.50 | 1431000 | 45.65 | 47 | 15.5 | both taken close to same spot in center |
| 10.5 | 25220 | 420.33 | 1513200 | 47.6 | 47.74 | 15.0 | didn't seem to reach equilibrium |

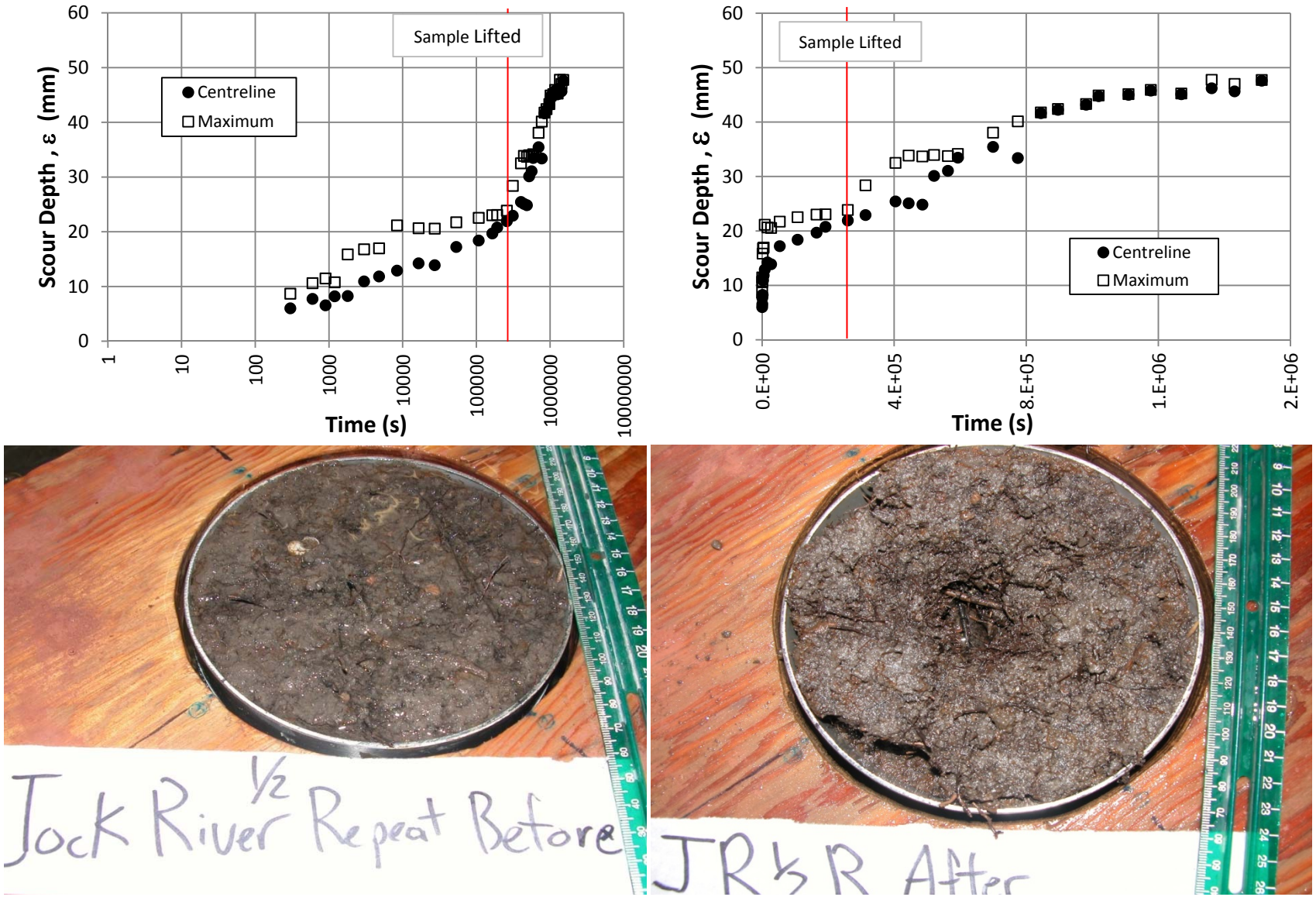


Figure A-14. Observed Time Development of Scour Plots and Test Photos for the Jock River 1 of 2 Repeat Sample

Table A-15. Test Data for the Jock River 2 of 2 Sample (Ontario Group)

| | | | | | | | | | | |
|---|---|---|---|---|---|---|---|---|---|---|
| **Sample Name:** | Jock River 2 of 2 | | **Initial Temperature:** | T (˚C) | 14.9 | | **Volumetric Flow Rate** | | |
| **Batch Number:** | N/A | | **Jet Diameter:** | d (mm) | 8.0 | | Avg Q | 10.09 | Lpm |
| **Tested By:** | Dan Cossette | | **Initial Jet Height:** | $H_i$ (mm) | 84.28 | | 1) | 10.04 | Lpm |
| **Analysis By:** | Dan Cossette | | **Equilibrium Centerline Depth:** | $\varepsilon_{cl\infty}$ (mm) | 32.81 | | 2) | 10.09 | Lpm |
| **Date of Testing:** | 2010-09-17 | | **Measured Equilibrium Height:** | $H_{e\ m}$ | 117.09 | | 3) | 10.15 | Lpm |

| **Mag -meter** Q | **Measured Time** $t_m$ | | | **Centerline Scour Depth** $\varepsilon_c$ | **Maximum Scour Depth** $\varepsilon_m$ | **Temp.** T | **Notes** |
|---|---|---|---|---|---|---|---|
| (Lpm) | (Min) | (Hrs) | (s) | (mm) | (mm) | (°C) | |
| 9.7 | 5 | 0.08 | 300 | 2 | 17.01 | 18.0 | max scour occurred in area already depressed by cutting of surface |
| 9.9 | 10 | 0.17 | 600 | 3.22 | 17.77 | 17.0 | |
| 9.6 | 15 | 0.25 | 900 | 6.06 | 19.05 | 15.5 | |
| 9.6 | 20 | 0.33 | 1200 | 6.32 | 19.33 | 15.0 | |
| 9.3 | 30 | 0.50 | 1800 | 7.33 | 20.33 | 14.5 | |
| 9.6 | 40 | 0.67 | 2400 | 8.01 | 20.64 | 14.0 | |
| 9.5 | 60 | 1.00 | 3600 | 9.03 | 30.77 | 13.5 | max scour occurring along edge of container |
| 9.5 | 90 | 1.50 | 5400 | 10.32 | 32.01 | 13.0 | max depth is right at edge |
| 9.7 | 150 | 2.50 | 9000 | 11.59 | 31.08 | 13.5 | |
| 9.3 | 270 | 4.50 | 16200 | 12.16 | 32.69 | 13.5 | |
| 9.6 | 515 | 8.58 | 30900 | 12.55 | 32.97 | 13.5 | very fine roots exposed in center(<1mm) and larger root exposed on peripheral (2-3mm) |
| 9.2 | 1333 | 22.22 | 79980 | 12.73 | 33.2 | 13.5 | |
| 9.5 | 1855 | 30.92 | 111300 | 13.55 | 33.57 | 14.0 | |
| 9.6 | 2593 | 43.22 | 155580 | 14.39 | 33.82 | 14.5 | |
| 9.5 | 3368 | 56.13 | 202080 | 14.74 | 34.06 | 14.5 | substantial vegetation net (small/fine roots) in center of sample |
| 9.7 | 4000 | 66.67 | 240000 | 15.61 | 34.38 | 14.0 | max depth at edge of container *also jet was left to the side for about 8 hours overnight |
| 9.6 | 5054 | 84.23 | 303240 | 16.16 | 33.78 | 14.0 | |
| 9.6 | 6779 | 112.98 | 406740 | 17.18 | 34.59 | 15.0 | |
| 9.8 | 7690 | 128.17 | 461400 | 18.12 | 34.89 | 15.0 | |
| 9.6 | 8545 | 142.42 | 512700 | 18.92 | 35.61 | 15.0 | |
| 9.6 | 9232 | 153.87 | 553920 | 19.85 | 35.76 | 15.0 | very fine vegetation net at center, very clumpy soil (2-4mm) |
| 9.8 | 10057 | 167.62 | 603420 | 21.37 | 35.95 | 15.5 | |

| | | | | | | | |
|---|---|---|---|---|---|---|---|
| 9.9 | 10714 | 178.57 | 642840 | 22.63 | 35.79 | 16. 0 | first center reading was lower than pervious. I took a few more and depth seemed to increase from 81.40-83.04 mm with readings. The way in which measurements are being taken may be effecting the scour depth for this sample |
| 9.9 | 12007 | 200.12 | 720420 | 24.6 | 35.9 | 15.5 | |
| 9.6 | 13288 | 221.47 | 797280 | 24.84 | 36.28 | 16.0 | |
| 9.6 | 13490 | 224.83 | 809400 | 26.42 | 36.08 | 15.5 | |
| 9.5 | 16295 | 271.58 | 977700 | 27.42 | 36.3 | 15.5 | |
| 9.5 | 17905 | 298.42 | 1074300 | 27.5 | 36.39 | 15.0 | |
| 9.6 | 19330 | 322.17 | 1159800 | 27.89 | 36.48 | 15.0 | |
| 9.6 | 20615 | 343.58 | 1236900 | 29.83 | 36.44 | 15.5 | |
| 9.8 | 22245 | 370.75 | 1334700 | 32.11 | 36.97 | 15.5 | |
| 9.6 | 23434 | 390.57 | 1406040 | 32.81 | 36.01 | 15.0 | |

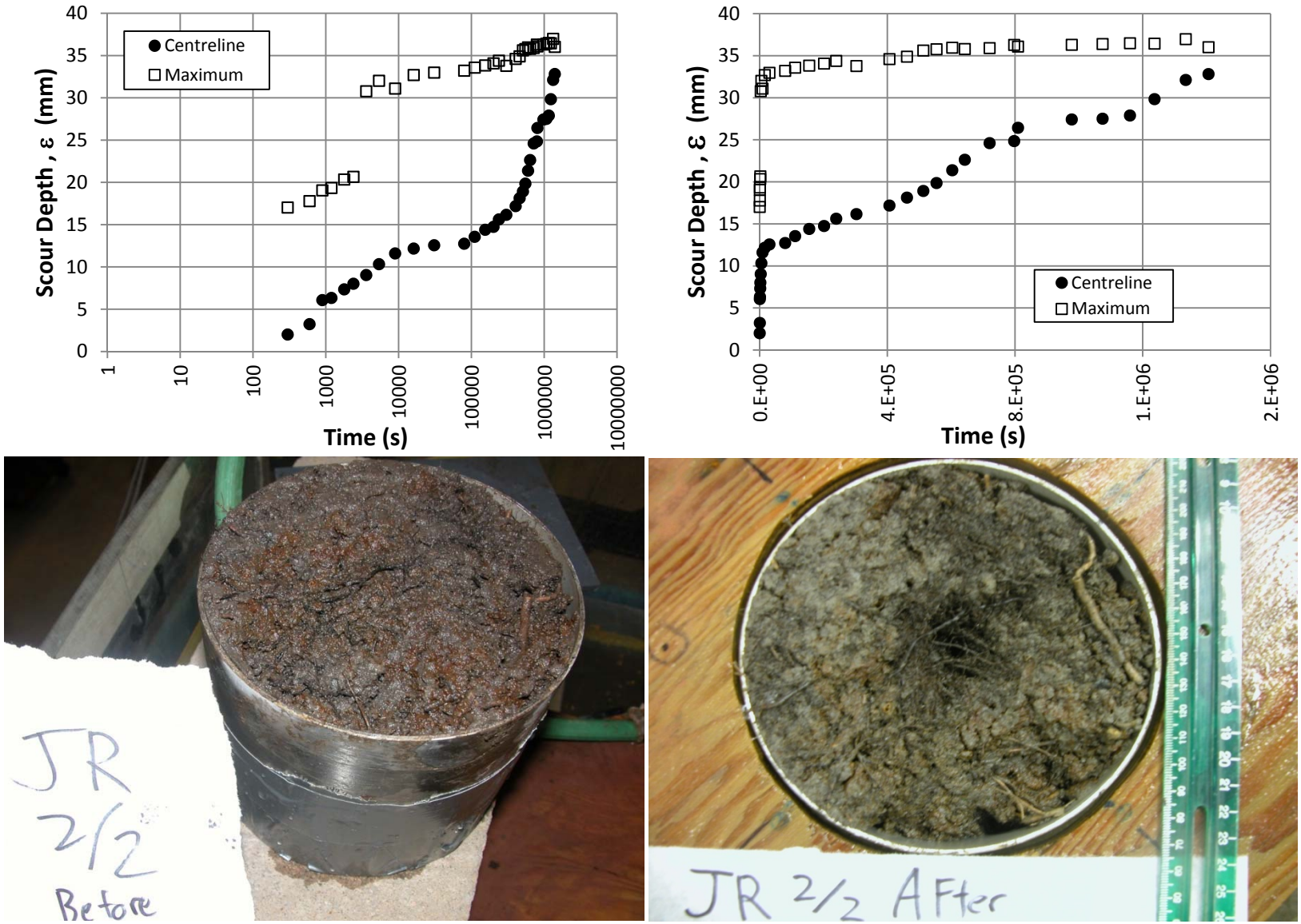


Figure A-15. Observed Time Development of Scour Plots and Test Photos for the Jock River 2 of 2 Sample

Table A-16. Test Data for the Raisin River 1 of 2 Sample (Ontario Group)

| | | | | | | | | | |
|---|---|---|---|---|---|---|---|---|---|
| **Sample Name:** | Raisin River 1 of 2 | | **Initial Temperature:** | T (˚C) | 22.4 | | **Volumetric Flow Rate** | | |
| **Batch Number:** | N/A | | **Jet Diameter:** | d (mm) | 8.0 | | Avg Q | 17.74 | Lpm |
| **Tested By:** | Dan Cossette | | **Initial Jet Height:** | $H_i$ (mm) | 91.26 | | 1) | 18.07 | Lpm |
| **Analysis By:** | Dan Cossette | | **Equilibrium Centerline Depth:** | $\varepsilon_{cl\infty}$ (mm) | 70.84 | | 2) | 17.66 | Lpm |
| **Date of Testing:** | 2011-02-11 | | **Measured Equilibrium Height:** | $H_{e\ m}$ | 162.1 | | 3) | 17.49 | Lpm |

| **Mag -meter** Q | **Measured Time** $t_m$ | | | **Centerline Scour Depth** $\varepsilon_c$ | **Maximum Scour Depth** $\varepsilon_m$ | **Temp.** T | **Notes** |
|---|---|---|---|---|---|---|---|
| (Lpm) | (Min) | (Hrs) | (s) | (mm) | (mm) | (°C) | |
| 14.9 | 5 | 0.08 | 300 | 4.29 | 7.63 | 22.0 | lots of particle erosion, pock marked surface |
| 16.4 | 10 | 0.17 | 600 | 5.56 | 11.56 | 23.0 | clumps 2-5mm removed |
| 16.4 | 15 | 0.25 | 900 | 5.67 | 13.83 | 22.5 | |
| 16.7 | 20 | 0.33 | 1200 | 5.81 | 14.5 | 23.0 | |
| 17.1 | 30 | 0.50 | 1800 | 8.78 | 14.74 | 24.0 | |
| 16.5 | 40 | 0.67 | 2400 | 15.42 | 17.19 | 23.0 | |
| 16.9 | 60 | 1.00 | 3600 | 15.99 | 17.47 | 22.5 | |
| 17.0 | 90 | 1.50 | 5400 | 18.64 | 18.64 | 22.5 | |
| 16.7 | 150 | 2.50 | 9000 | 19.89 | 22.66 | 22.0 | |
| 16.6 | 270 | 4.50 | 16200 | 28.76 | 29.37 | 22.0 | large volume of material eroded in the 1-2 quadrant |
| 16.7 | 510 | 8.50 | 30600 | 30.69 | 34.24 | 23.5 | more erosion from same side |
| 16.3 | 1127 | 18.78 | 67620 | 37.23 | 39.99 | 22.0 | |
| 16.2 | 1783 | 29.72 | 106980 | 37.9 | 41.31 | 22.0 | |
| 16.1 | 2459 | 40.98 | 147540 | 38.33 | 41.47 | 22.0 | |
| 15.8 | 2907 | 48.45 | 174420 | 38.14 | 41.97 | 22.0 | |
| 15.5 | 4319 | 71.98 | 259140 | 38.73 | 46.54 | 22.0 | When re-centering the jet a large chunk of material was removed, when sample soaks perhaps it weakens the soil structure and sudden changes cause erosion |
| 15.8 | 5516 | 91.93 | 330960 | 38.5 | 49.15 | 22.0 | Scour occurring under the surface, would be undermined (mass erosion) if not for vegetation |
| 15.5 | 6909 | 115.15 | 414540 | 38.6 | 45 | 22.0 | |
| 15.6 | 8224 | 137.07 | 493440 | 38.39 | 49.59 | 22.0 | |
| 15.8 | 9679 | 161.32 | 580740 | 37.54 | 49.63 | 22.0 | |
| 16.2 | 11082 | 184.70 | 664920 | 37.83 | 49.19 | 22.0 | |
| 16.1 | 12342 | 205.70 | 740520 | 38.42 | 50.58 | 22.0 | some small particles removed when jet was re-centered |

| | | | | | | | |
|---|---|---|---|---|---|---|---|
| 16.5 | 13912 | 231.87 | 834720 | 37.93 | 49.19 | 22.0 | |
| 16.9 | 16596 | 276.60 | 995760 | 39.65 | 51.31 | 22.0 | noticeable erosion still |
| 17.0 | 17957 | 299.28 | 1077420 | 56.66 | 56.66 | 22.0 | large chunk removed from center |
| 17.0 | 19076 | 317.93 | 1144560 | 61.64 | 61.64 | 22.0 | |
| 16.4 | 20638 | 343.97 | 1238280 | 68.74 | 68.74 | 22.5 | |
| 16.8 | 22041 | 367.35 | 1322460 | 69.42 | 69.42 | 22.5 | |
| 16.4 | 23421 | 390.35 | 1405260 | 69.85 | 69.85 | 22.5 | |
| 16.7 | 24820 | 413.67 | 1489200 | 70.84 | 70.84 | 22.5 | |
| 16.4 | 26339 | 438.98 | 1580340 | 69.91 | 69.91 | 22.5 | |
| 16.5 | 27949 | 465.82 | 1676940 | 70.35 | 70.35 | 22.5 | |
| 16.7 | 30139 | 502.32 | 1808340 | 70.34 | 70.34 | 22.5 | |
| 16.2 | 32779 | 546.32 | 1966740 | 70.64 | 70.64 | 22.5 | |
| 16.0 | 37289 | 621.48 | 2237340 | 69.75 | 69.75 | 22.5 | When profiling the sample there was a mass of soil at the surface that was only attached via roots and was obscuring part of the scour hole. This mass was removed before profiling the sample surface (this can be seen in the sample photographs) |

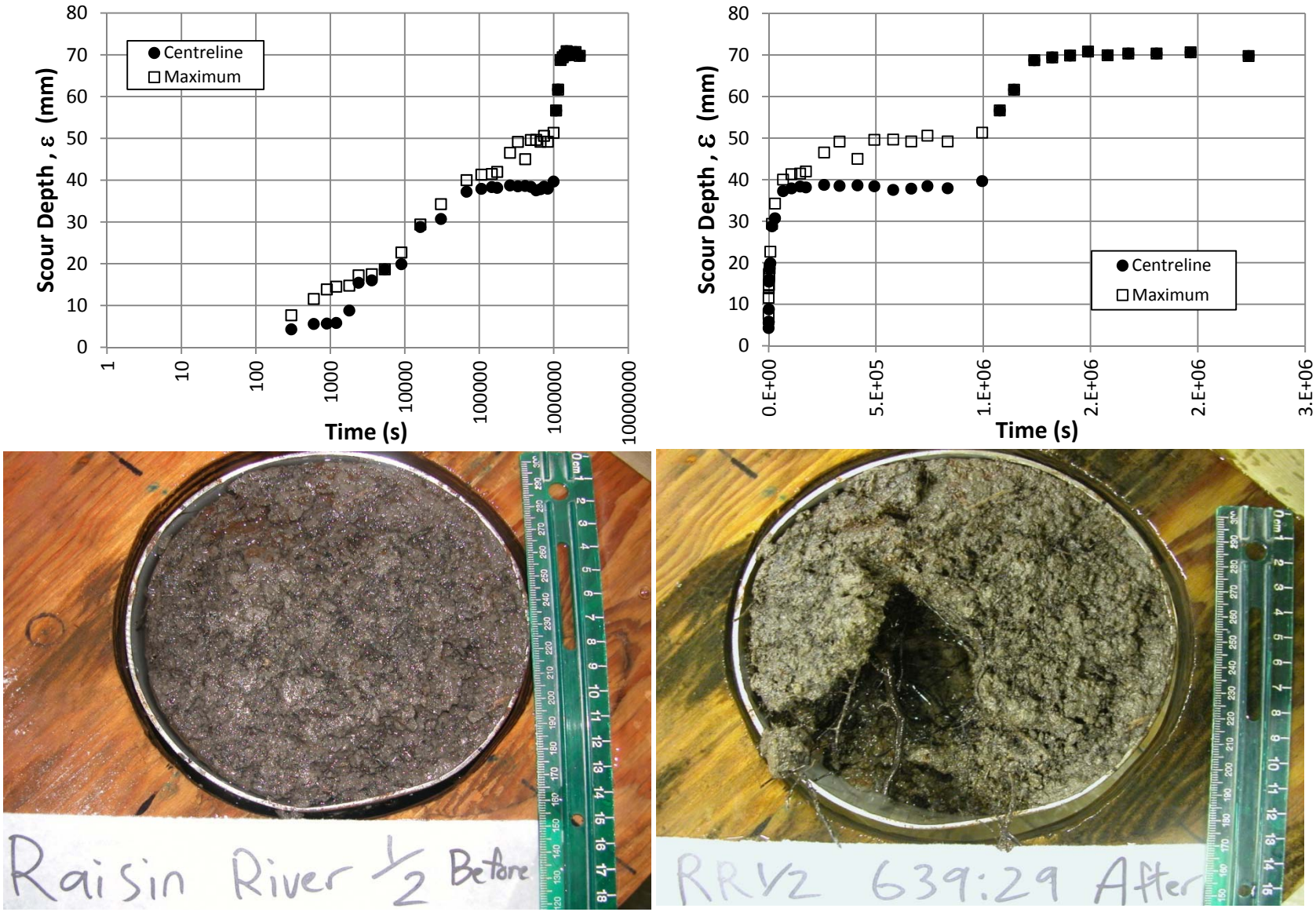


Figure A-16. Observed Time Development of Scour Plots and Test Photos for the Raisin River 1 of 2 Sample

Table A-17. Test Data for the Raisin River 2 of 2 Sample (Ontario Group)

| | | | | | | | | | |
|---|---|---|---|---|---|---|---|---|---|
| **Sample Name:** | Raisin River 2 of 2 | | **Initial Temperature:** | T (˚C) | 20.3 | | **Volumetric Flow Rate** | | |
| **Batch Number:** | N/A | | **Jet Diameter:** | d (mm) | 8.0 | | Avg Q | 14.12 | Lpm |
| **Tested By:** | Dan Cossette | | **Initial Jet Height:** | $H_i$ (mm) | 98.29 | | 1) | 13.83 | Lpm |
| **Analysis By:** | Dan Cossette | | **Equilibrium Centerline Depth:** | $\varepsilon_{cl\infty}$ (mm) | 38.51 | | 2) | 14.31 | Lpm |
| **Date of Testing:** | 2011-04-05 | | **Measured Equilibrium Height:** | $H_{e\ m}$ | 136.8 | | 3) | 14.21 | Lpm |

| **Mag -meter** Q | **Measured Time** $t_m$ | | | **Centerline Scour Depth** $\varepsilon_c$ | **Maximum Scour Depth** $\varepsilon_m$ | **Temp.** T | **Notes** |
|---|---|---|---|---|---|---|---|
| (Lpm) | (Min) | (Hrs) | (s) | (mm) | (mm) | (°C) | |
| 12.7 | 5 | 0.08 | 300 | 2.8 | 18.67 | 21.5 | Many clay particles torn off in chunks from 1mm to 20mm, many flat/plate-like |
| 12.5 | 10 | 0.17 | 600 | 6.18 | 20.97 | 21.5 | |
| 13.8 | 15 | 0.25 | 900 | 14.73 | 26.19 | 19.5 | |
| 13.5 | 20 | 0.33 | 1200 | 23.16 | 27.85 | 18.0 | |
| 13.5 | 30 | 0.50 | 1800 | 23.55 | 29.45 | 19.5 | |
| 13.5 | 40 | 0.67 | 2400 | 28.39 | 29.21 | 20.5 | |
| 13.7 | 60 | 1.00 | 3600 | 32.84 | 33.66 | 19.5 | Centerline reading taken in what appears to be a worm hole, just wide enough for wooden dowel |
| 13.8 | 90 | 1.50 | 5400 | 34.89 | 35.71 | 20.0 | |
| 13.9 | 150 | 2.50 | 9000 | 34.26 | 35.08 | 20.0 | scour hole was widening |
| 13.5 | 305 | 5.08 | 18300 | 35.42 | 36.24 | 18.0 | Material removed |
| 13.4 | 560 | 9.33 | 33600 | 35.46 | 36.28 | 18.5 | side widening out, still being scoured |
| 13.3 | 1251 | 20.85 | 75060 | 36.16 | 37.75 | 19.0 | widening |
| 13.0 | 2691 | 44.85 | 161460 | 38.38 | 39.2 | 20.0 | |
| 13.1 | 4191 | 69.85 | 251460 | 37.92 | 39.72 | 20.5 | lots of edge material removed |
| 13.1 | 5941 | 99.02 | 356460 | 38.51 | 39.33 | 21.5 | |
| 12.9 | 8451 | 140.85 | 507060 | 37.1 | 37.92 | 24.0 | |
| 12.9 | 10231 | 170.52 | 613860 | 37.33 | 38.25 | 22.0 | |
| 13.2 | 14176 | 236.27 | 850560 | 37.28 | 38.16 | 22.5 | significant widening over this last interval. Two live shoots of grass/macrophytes on the sample surface. Wooden support platform is slimy, perhaps indicates presence of Extracellular Polymer Substance (EPS) |

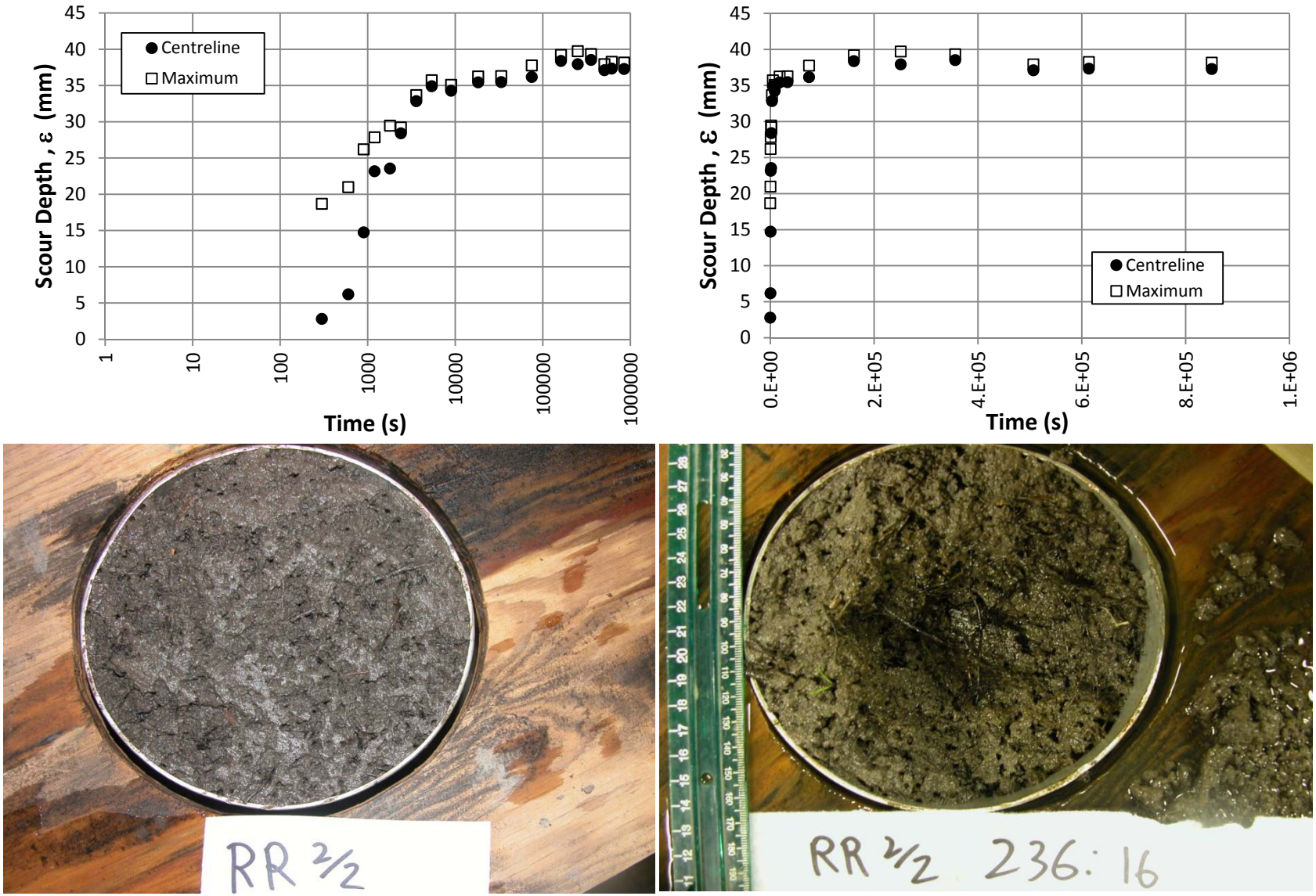


Figure A-17. Observed Time Development of Scour Plots and Test Photos for the Raisin River 2 of 2 Sample

Table A-18. Test Data for the M-390 1 of 2 Sample (Manufactured Clay Group)

| | | | | | | | | | |
|---|---|---|---|---|---|---|---|---|---|
| **Sample Name:** | M-390 1 of 2 | | **Initial Temperature:** | T (˚C) | 19.6 | | **Volumetric Flow Rate** | | |
| **Batch Number:** | 5731721 | | **Jet Diameter:** | d (mm) | 8.0 | | Avg Q | 44.5 | Lpm |
| **Tested By:** | Dan Cossette | | **Initial Jet Height:** | $H_i$ (mm) | 80.56 | | 1) | | Lpm |
| **Analysis By:** | Dan Cossette | | **Equilibrium Centerline Depth:** | $\varepsilon_{cl\infty}$ (mm) | - | | 2) | | Lpm |
| **Date of Testing:** | 2010-08-09 | | **Measured Equilibrium Height:** | $H_{e\ m}$ | - | | 3) | | Lpm |

| **Magmeter** Q | **Measured Time** $t_m$ | | | **Centerline Scour Depth** $\varepsilon_c$ | **Maximum Scour Depth** $\varepsilon_m$ | **Temp.** T | **Notes** |
|---|---|---|---|---|---|---|---|
| (Lpm) | (Min) | (Hrs) | (s) | (mm) | (mm) | (°C) | |
| 41.6 | 5 | 0:05 | 300 | 14.34 | 16.38 | 21.5 | surface of water tank very irregular, can see the jet bubbling up |
| 41.6 | 10 | 0:10 | 600 | 24.15 | 45.48 | 21.5 | large chunks lost, 4 - 7 cm, massive erosion |
| 41.6 | 15 | 0:15 | 900 | 25.98 | 46.27 | 21.5 | soil surface directly under jet is sloped not horizontal. 8 mm nozzle blew out of the jet plenum, had to pause test and reattach nozzel using silicon. Flow rate seems a little bit higher than initially |
| 41.8 | 20 | 0:20 | 1200 | 27.2 | 47.71 | 21.0 | water for first 3 runs was murky, hard to see what was happening. Now can see large flat clay clumps flaking off (3 - 20 mm) |
| 41.7 | 30 | 0:30 | 1800 | 30.08 | 48.32 | 20.5 | problems with timer so the time associated with this reading is likely +/- 2 min |
| 41.4 | 40 | 0:40 | 2400 | 33.71 | 48.54 | 20.5 | |
| 41.8 | 50 | 0.83 | 3000 | 35.05 | 49.77 | 17.5 | |
| 41.6 | 70 | 1.17 | 4200 | 36.08 | 50.26 | 17.5 | |
| 41.7 | 100 | 1.67 | 6000 | 38.82 | 49.92 | 17.5 | |
| 41.6 | 160 | 2.67 | 9600 | 41.03 | 50.17 | 17.0 | seems to be eroding more along the centerline. Max depth probably influenced by explosion of sample at 10 min |
| | | | | | | | nozzle blew out of jet again, not sure when this happened so decided not to take a depth reading and terminate test |

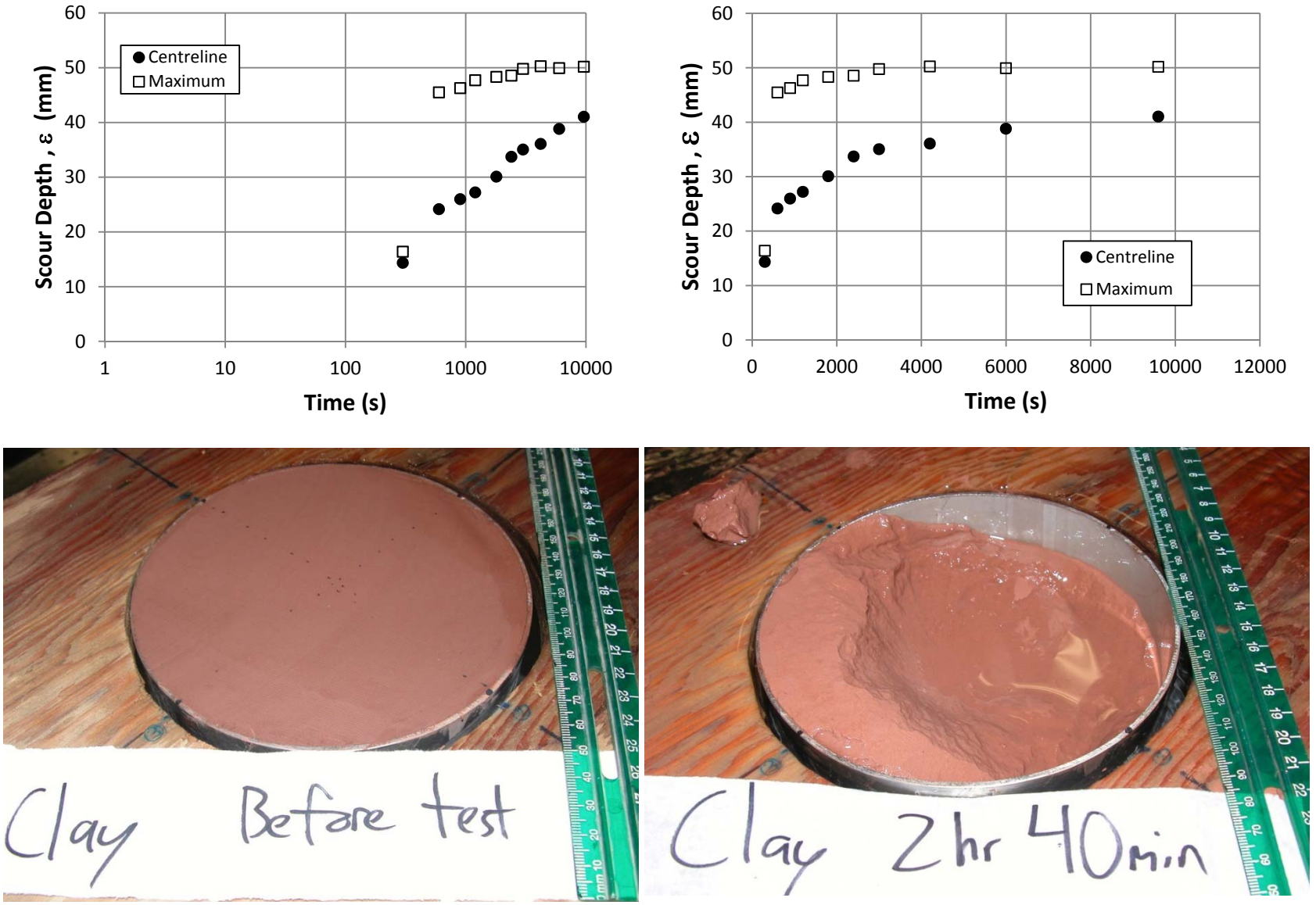


Figure A-18. Observed Time Development of Scour Plots and Test Photos for the M-390 1 of 2 Sample

Table A-19. Test Data for the M-390 2 of 2 Sample (Manufactured Clay Group)

| | | | | | | | | | |
|---|---|---|---|---|---|---|---|---|---|
| **Sample Name:** | M-390 2 of 2 | | **Initial Temperature:** | T (˚C) | 22.8 | | **Volumetric Flow Rate** | | |
| **Batch Number:** | 5731721 | | **Jet Diameter:** | d (mm) | 8.0 | | Avg Q | 37.7 | Lpm |
| **Tested By:** | Dan Cossette | | **Initial Jet Height:** | $H_i$ (mm) | 101.28 | | 1) | 37.56 | Lpm |
| **Analysis By:** | Dan Cossette | | **Equilibrium Centerline Depth:** | $\varepsilon_{cl\infty}$ (mm) | 41.41 | | 2) | 37.91 | Lpm |
| **Date of Testing:** | 2011-06-29 | | **Measured Equilibrium Height:** | $H_{e\ m}$ | 142.69 | | 3) | 37.56 | Lpm |

| **Mag -meter** Q | **Measured Time** $t_m$ | | | **Centerline Scour Depth** $\varepsilon_c$ | **Maximum Scour Depth** $\varepsilon_m$ | **Temp.** T | **Notes** |
|---|---|---|---|---|---|---|---|
| (Lpm) | (Min) | (Hrs) | (s) | (mm) | (mm) | (°C) | |
| 34.5 | 5 | 0:05 | 300 | 9.71 | 14.71 | 23.0 | |
| 33.9 | 10 | 0:10 | 600 | 13.15 | 17.56 | 24.0 | |
| 33.9 | 15 | 0:15 | 900 | 16.68 | 24.82 | 23.0 | large flat pieces being ripped from surface 1 - 5 cm similar to |
| 33.8 | 20 | 0:20 | 1200 | 19.11 | 24.75 | 23.0 | |
| 33.9 | 30 | 0:30 | 1800 | 21.73 | 27.81 | 23.0 | |
| 33.9 | 40 | 0:40 | 2400 | 22.69 | 28.28 | 23.0 | |
| 33.9 | 60 | 1.00 | 3600 | 24.89 | 29.32 | 23.5 | |
| 33.7 | 90 | 1.50 | 5400 | 27.21 | 29.61 | 23.0 | scour hole becoming more symmetrical |
| 33.8 | 150 | 2.50 | 9000 | 28.92 | 30.67 | 22.5 | max depth moving towards centerline |
| 33.6 | 270 | 4.50 | 16200 | 29.77 | 31.20 | 22.5 | |
| 33.8 | 570 | 9.50 | 34200 | 33.27 | 34.06 | 22.5 | |
| 33.0 | 2025 | 33.75 | 121500 | 36.97 | 38.74 | 22.5 | noticeable erosion, clay material on platform around sample |
| 32.2 | 3610 | 60.17 | 216600 | 39.32 | 40.45 | 22.5 | scour hole widened, lots of material removed |
| 32.1 | 6075 | 101.25 | 364500 | 40.57 | 41.45 | 22.5 | |
| 31.9 | 7785 | 129.75 | 467100 | 40.98 | 41.84 | 22.5 | noticeable erosion, material beside scour hole |
| 32.0 | 10530 | 175.50 | 631800 | 41.41 | 42.31 | 22.5 | one 3 to 5 cm chunk of clay removed |
| 32.1 | 14160 | 236.00 | 849600 | 41.38 | 42.50 | 22.5 | lowered water in tank without moving jet, caught it just as it was |

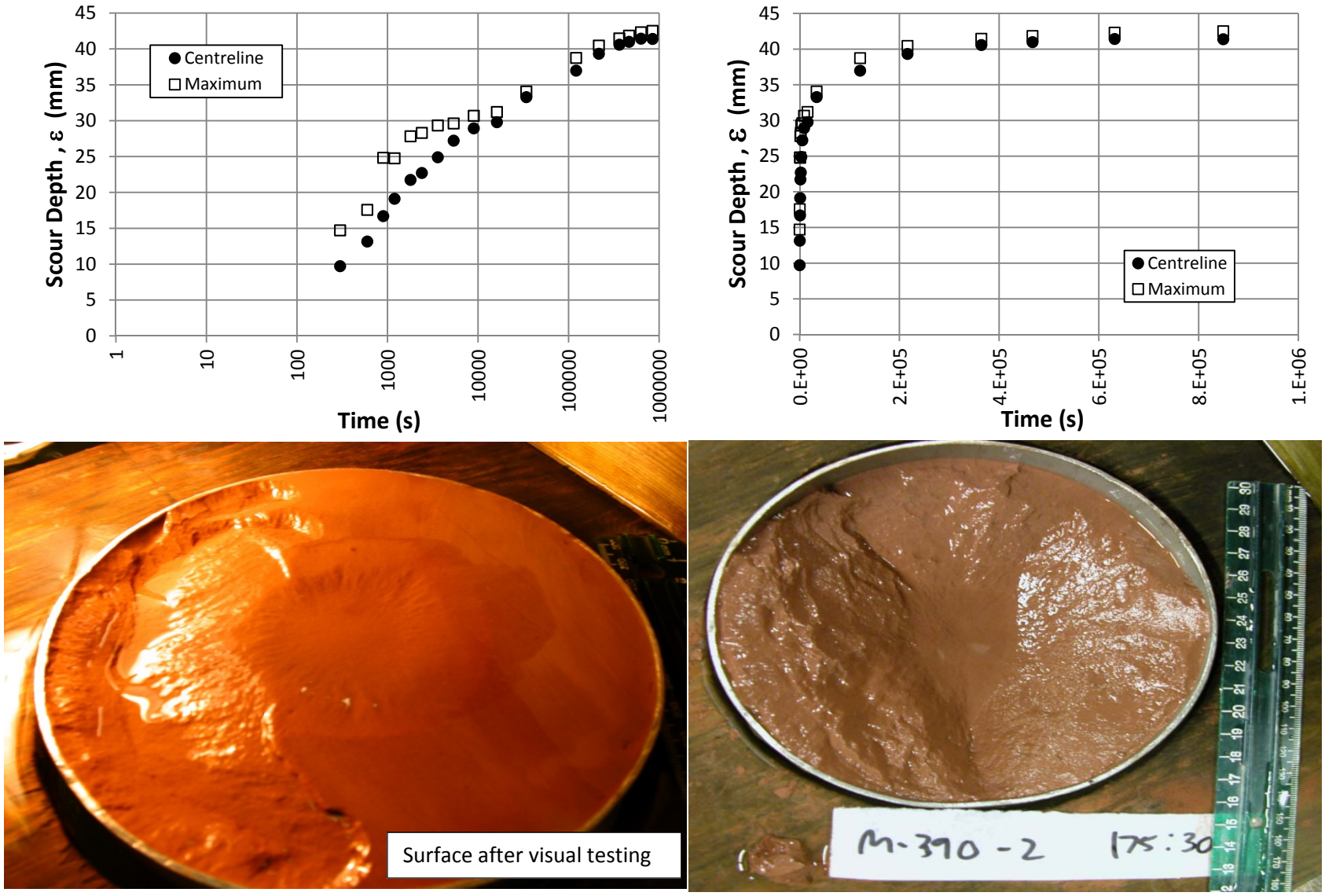


Figure A-19. Observed Time Development of Scour Plots and Test Photos for the M-390 2 of 2 Sample

Table A-20. Test Data for the P-300 1 of 3 Sample (Manufactured Clay Group)

| | | | | | | | | | |
|---|---|---|---|---|---|---|---|---|---|
| **Sample Name:** | P-300 1 of 3 | | **Initial Temperature:** | T (˚C) | 21.8 | | **Volumetric Flow Rate** | | |
| **Batch Number:** | 5612830 | | **Jet Diameter:** | d (mm) | 8.0 | | Avg Q | 32.4 | Lpm |
| **Tested By:** | Dan Cossette | | **Initial Jet Height:** | $H_i$ (mm) | 78.75 | | 1) | 31.8 | Lpm |
| **Analysis By:** | Dan Cossette | | **Equilibrium Centerline Depth:** | $\varepsilon_{cl\infty}$ (mm) | 32.00 | | 2) | 32.5 | Lpm |
| **Date of Testing:** | 2011-01-09 | | **Measured Equilibrium Height:** | $H_{e\ m}$ | 110.75 | | 3) | 32.9 | Lpm |

| **Mag -meter** Q | **Measured Time** $t_m$ | | | **Centerline Scour Depth** $\varepsilon_c$ | **Maximum Scour Depth** $\varepsilon_m$ | **Temp.** T | **Notes** |
|---|---|---|---|---|---|---|---|
| (Lpm) | (Min) | (Hrs) | (s) | (mm) | (mm) | (°C) | |
| 31.3 | 5 | 0:05 | 300 | 2.33 | 9.02 | 22.5 | uneven initial scour, stepped erosion, looks like layers |
| 31.4 | 10 | 0:10 | 600 | 3.11 | 9.79 | 22.0 | lots of initial erosion at start of time (flakes b=2cm) |
| 30.9 | 15 | 0:15 | 900 | 5.27 | 15 | 22.0 | the center isn't scouring in the same way, smooth center about 3cm diameter surrounded by rough shear zone |
| 31.1 | 20 | 0:20 | 1200 | 5.86 | 15.19 | 22.5 | |
| 31.1 | 30 | 0:30 | 1800 | 10.07 | 18.8 | 22.0 | |
| 31.2 | 40 | 0:40 | 2400 | 11.01 | 19.01 | 22.0 | |
| 31.4 | 60 | 1.00 | 3600 | 13.43 | 26.55 | 23.0 | the 2 smaller individual scour holes joined to make one larger scour hole just off center |
| 31.2 | 90 | 1.50 | 5400 | 17.49 | 29.52 | 21.5 | |
| 30.9 | 150 | 2.50 | 9000 | 19.8 | 30.61 | 21.5 | |
| 31.2 | 270 | 4.50 | 16200 | 22.53 | 29.91 | 21.5 | hit edge of cylinder |
| 31.1 | 390 | 6.50 | 23400 | 23.24 | 30.67 | 21.5 | |
| 31.0 | 982 | 16.37 | 58920 | 26.47 | 30.44 | 21.5 | no observable soil loss when positioning the jet back into place |
| 30.9 | 1616 | 26.93 | 96960 | 27.32 | 31.15 | 21.5 | |
| 31.0 | 2413 | 40.22 | 144780 | 29.67 | 32.96 | 21.5 | |
| 30.9 | 3123 | 52.05 | 187380 | 30.14 | 33.75 | 21.5 | |
| 30.7 | 3786 | 63.10 | 227160 | 30.06 | 33.89 | 21.5 | |
| 30.5 | 4517 | 75.28 | 271020 | 31.12 | 33.47 | 21.5 | slight yellowish discoloration |
| 30.6 | 5237 | 87.28 | 314220 | 30.87 | 34.35 | 21.5 | |
| 29.9 | 6665 | 111.08 | 399900 | 32.00 | 34.62 | 21.5 | test ended, sample disrupted due to unsubmerged jet impinging on surface |

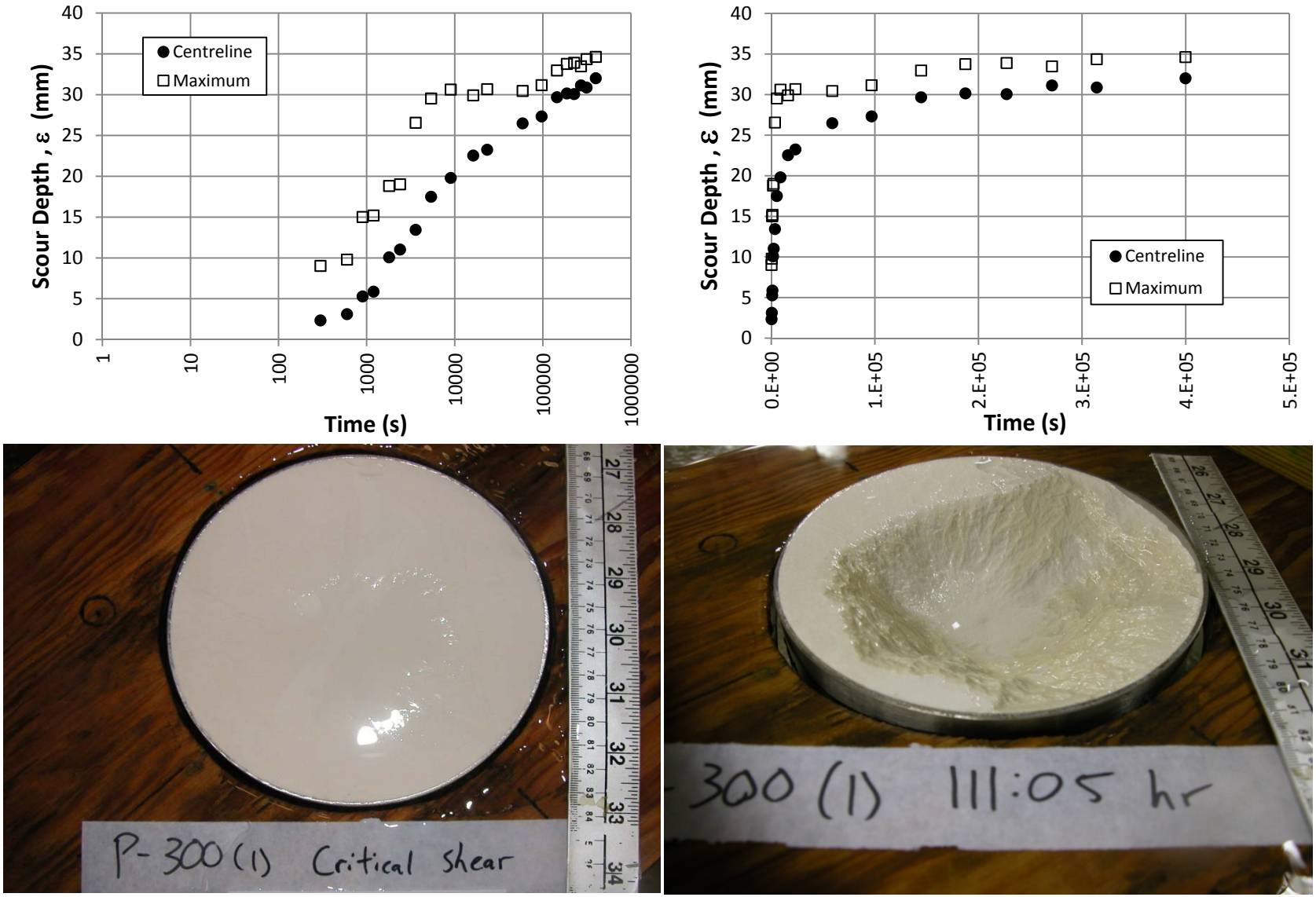


Figure A-20. Observed Time Development of Scour Plots and Test Photos for the P-300 1 of 3 Sample

Table A-21. Test Data for the P-300 2 of 3 Sample (Manufactured Clay Group)

| | | | | | | | | | |
|---|---|---|---|---|---|---|---|---|---|
| **Sample Name:** | P-300 2 of 3 | | **Initial Temperature:** | T (˚C) | 23.5 | | **Volumetric Flow Rate** | | |
| **Batch Number:** | 5612830 | | **Jet Diameter:** | d (mm) | 8.0 | | Avg Q | 31.74 | Lpm |
| **Tested By:** | Dan Cossette | | **Initial Jet Height:** | $H_i$ (mm) | 110.13 | | 1) | 31.78 | Lpm |
| **Analysis By:** | Dan Cossette | | **Equilibrium Centerline Depth:** | $\varepsilon_{cl\infty}$ (mm) | 36.79 | | 2) | 31.48 | Lpm |
| **Date of Testing:** | 2011-11-21 | | **Measured Equilibrium Height:** | $H_{e\ m}$ | 146.92 | | 3) | 31.96 | Lpm |

| **Mag -meter** Q | **Measured Time** $t_m$ | | | **Centerline Scour Depth** $\varepsilon_c$ | **Maximum Scour Depth** $\varepsilon_m$ | **Temp.** T | **Notes** |
|---|---|---|---|---|---|---|---|
| (Lpm) | (Min) | (Hrs) | (s) | (mm) | (mm) | (°C) | |
| 28.8 | 5 | 0:05 | 300 | 3.64 | 19.82 | 24.0 | |
| 27.5 | 10 | 0:10 | 600 | 4.23 | 19.98 | 24.0 | |
| 29.1 | 15 | 0:15 | 900 | 5.69 | 24.53 | 24.0 | |
| 28.5 | 20 | 0:20 | 1200 | 6.8 | 24.7 | 24.0 | |
| 29.0 | 30 | 0:30 | 1800 | 8.23 | 25.11 | 24.0 | |
| 28.9 | 40 | 0:40 | 2400 | 8.81 | 25.17 | 24.0 | |
| 28.8 | 60 | 1.00 | 3600 | 9.92 | 25.66 | 24.0 | |
| 28.9 | 90 | 1.50 | 5400 | 11.67 | 26.16 | 24.0 | test paused 7pm Dec 2 |
| 29.0 | 150 | 2.50 | 9000 | 32.19 | 39.93 | 23.0 | large volume of clay removed, chunks 2 - 10 cm, were flat. Scour hole 'rounded out' and is more concave |
| 28.9 | 270 | 4.50 | 16200 | 33.35 | 40.32 | 23.0 | no noticeable large amount of erosion |
| 29.1 | 525 | 8.75 | 31500 | 34.63 | 43.29 | 23.0 | increase in maximum depth locally but not really on whole sample |
| 28.8 | 2885 | 48.08 | 173100 | 36.63 | 45.04 | 23.0 | max depth doesn't seem to change location (same spot) |
| 28.8 | 7230 | 120.50 | 433800 | 36.79 | 44.54 | 23.0 | |
| 28.7 | 11985 | 199.75 | 719100 | 36.64 | 45.06 | 23.0 | no visual change in scour hole |
| 28.8 | 14465 | 241.08 | 867900 | 36.69 | 45.34 | 22.5 | |

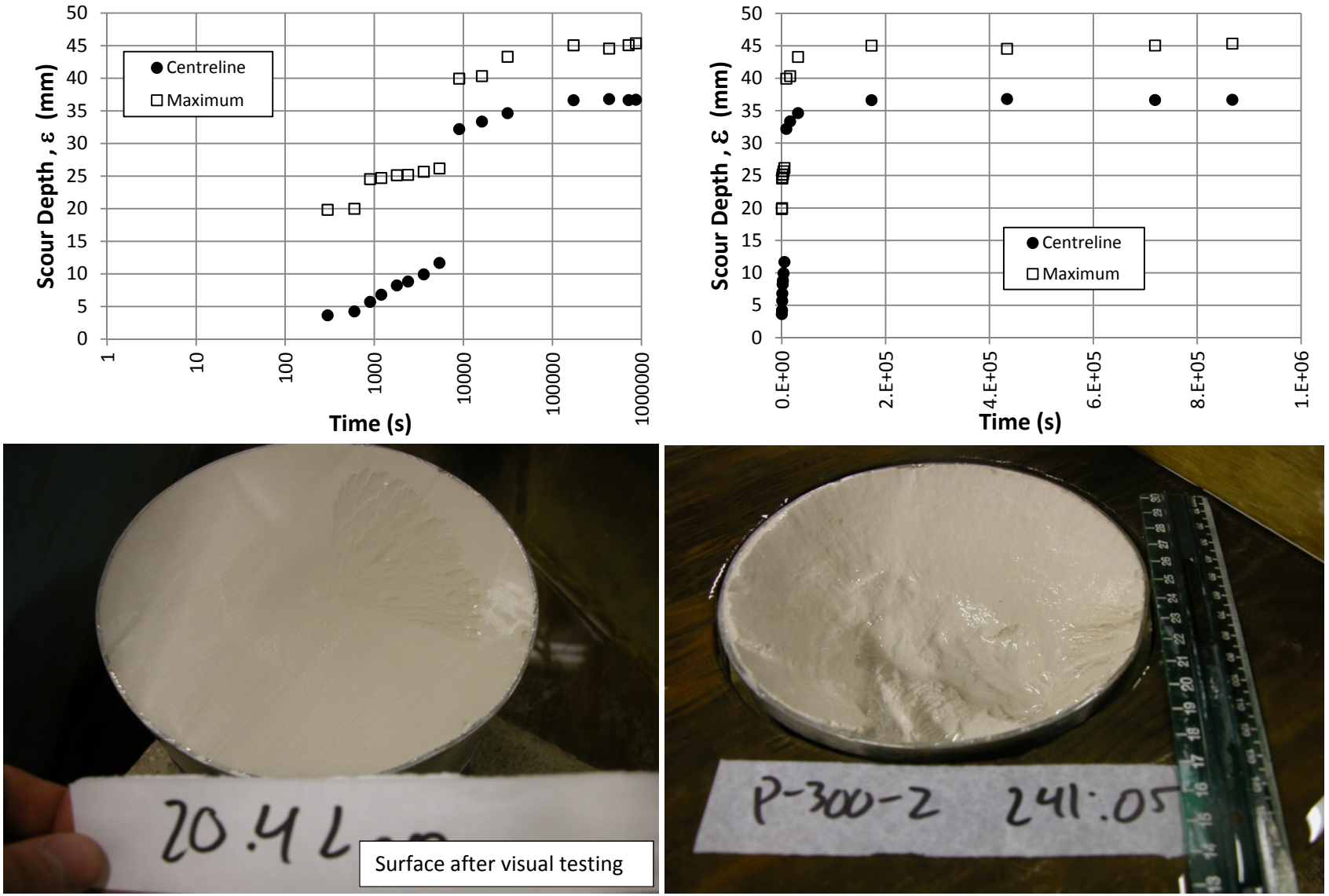


Figure A-21. Observed Time Development of Scour Plots and Test Photos for the P-300 2 of 3 Sample

Table A-22. Test Data for the P-300 3 of 3 Sample (Manufactured Clay Group)

| | | | | | | | | | |
|---|---|---|---|---|---|---|---|---|---|
| **Sample Name:** | P-300 3 of 3 | | **Initial Temperature:** | T (˚C) | 23.0 | | **Volumetric Flow Rate** | | |
| **Batch Number:** | 56742580 | | **Jet Diameter:** | d (mm) | 8.0 | | Avg Q | 43.00 | Lpm |
| **Tested By:** | Dan Cossette | | **Initial Jet Height:** | $H_i$ (mm) | 123.32 | | 1) | 43.16 | Lpm |
| **Analysis By:** | Dan Cossette | | **Equilibrium Centerline Depth:** | $\varepsilon_{cl\infty}$ (mm) | 26.02 | | 2) | 43.23 | Lpm |
| **Date of Testing:** | 2012-03-01 | | **Measured Equilibrium Height:** | $H_{e\ m}$ | 149.34 | | 3) | 42.60 | Lpm |

| **Mag -meter** Q | **Measured Time** $t_m$ | | | **Centerline Scour Depth** $\varepsilon_c$ | **Maximum Scour Depth** $\varepsilon_m$ | **Temp.** T | **Notes** |
|---|---|---|---|---|---|---|---|
| (Lpm) | (Min) | (Hrs) | (s) | (mm) | (mm) | (°C) | |
| 36.8 | 5 | 0:05 | 300 | 2.42 | 2.42 | 24.5 | |
| 37.5 | 10 | 0:10 | 600 | 4.08 | 4.81 | 24.0 | erosion around container edge is encroaching on the centerline |
| 37.5 | 15 | 0:15 | 900 | 6.07 | 7.06 | 23.0 | |
| 37.1 | 20 | 0:20 | 1200 | 8.57 | 14.69 | 23.0 | |
| 36.7 | 30 | 0:30 | 1800 | 11.03 | 26.22 | 23.0 | max depth moving closer to centerline |
| 36.8 | 40 | 0:40 | 2400 | 15.82 | 26.34 | 23.0 | |
| 36.5 | 60 | 1.00 | 3600 | 17.92 | 26.97 | 23.0 | |
| 36.7 | 90 | 1.50 | 5400 | 19.28 | 28.6 | 23.0 | let test wait for 12 hours |
| 36.8 | 150 | 2.50 | 9000 | 22.46 | 29.92 | 23.0 | lots of erosion after recentering jet over sample, large piece about 8 mm long removed |
| 36.4 | 270 | 4.50 | 16200 | 23.21 | 34.84 | 23.0 | |
| 36.5 | 510 | 8.50 | 30600 | 23.66 | 37.81 | 22.5 | obvious scour still taking place |
| 36.5 | 1883 | 31.38 | 112980 | 24.88 | 38.13 | 22.5 | |
| 35.9 | 4268 | 71.13 | 256080 | 24.96 | 40.14 | 23.0 | very clear water in tank very small clay clumps on the table |
| 36.2 | 6728 | 112.13 | 403680 | 25.18 | 39.9 | 22.5 | lots of material removed around container edge |
| 36.2 | 11213 | 186.88 | 672780 | 25.78 | 39.78 | 22.5 | no material around sample on table |
| 36.0 | 15053 | 250.88 | 903180 | 26.02 | 39.88 | 22.5 | |

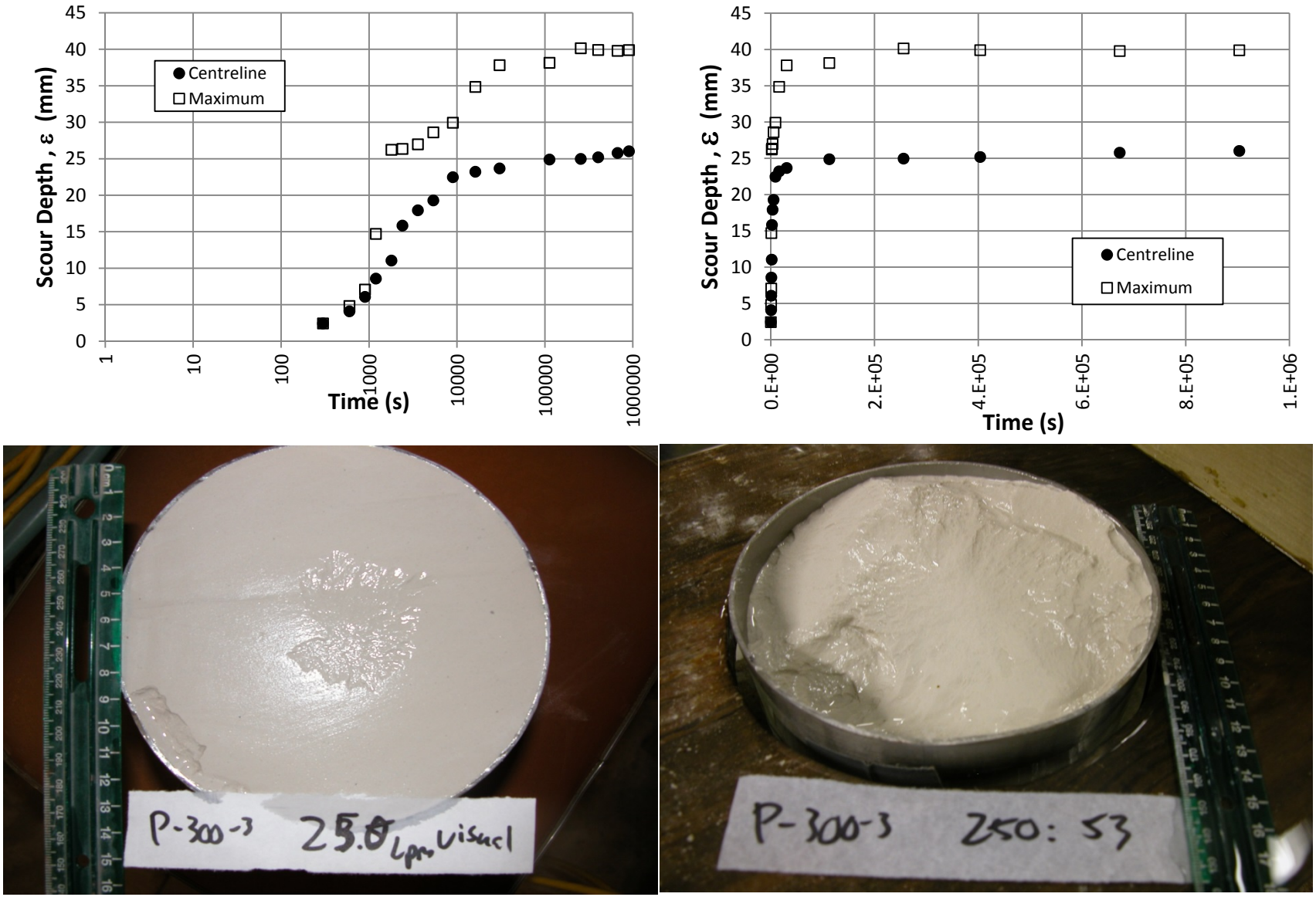


Figure A-22. Observed Time Development of Scour Plots and Test Photos for the P-300 3 of 3 Sample

Table A-23. Test Data for the M-332 1 of 1 Sample (Manufactured Clay Group)

| | | | | | | | | | | |
|---|---|---|---|---|---|---|---|---|---|---|
| **Sample Name:** | M-332 1 of 1 | | **Initial Temperature:** | T (˚C) | 17.9 | | **Volumetric Flow Rate** | | |
| **Batch Number:** | 556520109 | | **Jet Diameter:** | d (mm) | 8.0 | | Avg Q | 42.00 | Lpm |
| **Tested By:** | Dan Cossette | | **Initial Jet Height:** | $H_i$ (mm) | 97.98 | | 1) | 41.2 | Lpm |
| **Analysis By:** | Dan Cossette | | **Equilibrium Centerline Depth:** | $\varepsilon_{cl\infty}$ (mm) | 34.16 | | 2) | 42.2 | Lpm |
| **Date of Testing:** | 2011-05-25 | | **Measured Equilibrium Height:** | $H_{e\ m}$ | 132.14 | | 3) | 42.6 | Lpm |

| **Mag -meter** Q | **Measured Time** $t_m$ | | | **Centerline Scour Depth** $\varepsilon_c$ | **Maximum Scour Depth** $\varepsilon_m$ | **Temp.** T | **Notes** |
|---|---|---|---|---|---|---|---|
| (Lpm) | (Min) | (Hrs) | (s) | (mm) | (mm) | (°C) | |
| | 5 | 0:05 | 300 | 2.79 | 2.79 | 15.0 | seems like flake erosion at start of test |
| | 10 | 0:10 | 600 | 4.77 | 4.77 | 16.5 | not able to detect the clay particles that are being removed |
| | 15 | 0:15 | 900 | 5.74 | 5.74 | 16.0 | very little progression of scour hole, hard to tell if removal is due to shear or if pressure from jet is causing an indentation |
| | 20 | 0:20 | 1200 | 6.88 | 6.88 | 15.5 | |
| | 30 | 0:30 | 1800 | 8.5 | 8.5 | 15.5 | |
| | 40 | 0:40 | 2400 | 9.77 | 9.77 | 15.5 | |
| | 60 | 1.00 | 3600 | 10.3 | 10.3 | 15.0 | |
| | 90 | 1.50 | 5400 | 10.49 | 10.49 | 14.5 | |
| | 150 | 2.50 | 9000 | 11.55 | 11.55 | 15.0 | |
| | 270 | 4.50 | 16200 | 13.72 | 13.72 | 15.5 | |
| | 510 | 8.50 | 30600 | 16.06 | 16.06 | 16.0 | |
| | 1165 | 19.42 | 69900 | 18.77 | 18.77 | 17.5 | |
| | 1945 | 32.42 | 116700 | 21.75 | 21.75 | 18.5 | clay removal around container edge |
| | 2442 | 40.70 | 146520 | 20.3 | 23.4 | 19.0 | |
| | 5412 | 90.20 | 324720 | 25.13 | 25.13 | 22.5 | significant widening and mass erosion, 5 flat clumps removed average of 0.5 - 2 cm |
| | 6895 | 114.92 | 413700 | 27.19 | 27.19 | 21.5 | widening, more mass erosion similar to the last time step |
| | 8642 | 144.03 | 518520 | 27.46 | 28.14 | 18.5 | |
| | 10070 | 167.83 | 604200 | 29.34 | 29.75 | 19.0 | |
| | 12973 | 216.22 | 778380 | 30.36 | 30.89 | 18.0 | |
| | 15853 | 264.22 | 951180 | 31.4 | 32.49 | 18.5 | flat chunks about 2 cm largest diameter removed |
| | 21543 | 359.05 | 1292580 | 31.31 | 33.31 | 19.5 | |
| | 25318 | 421.97 | 1519080 | 30.93 | 33.44 | 20.5 | |
| | 35578 | 592.97 | 2134680 | 33.7 | 34.37 | 23.0 | |
| | 40038 | 667.30 | 2402280 | 34.1 | 36.12 | 21.5 | |

| | | | | | | | |
|---|---|---|---|---|---|---|---|
| | 45558 | 759.30 | 2733480 | 34.16 | 34.25 | 22.0 | |

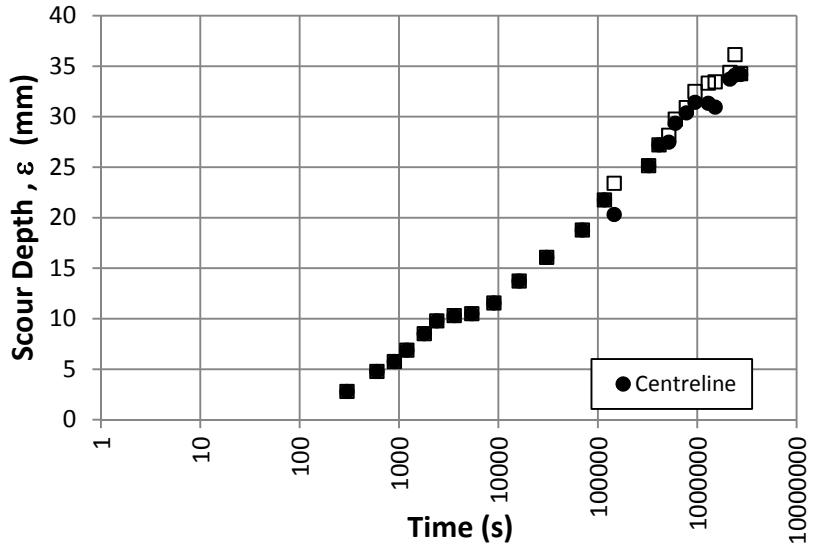


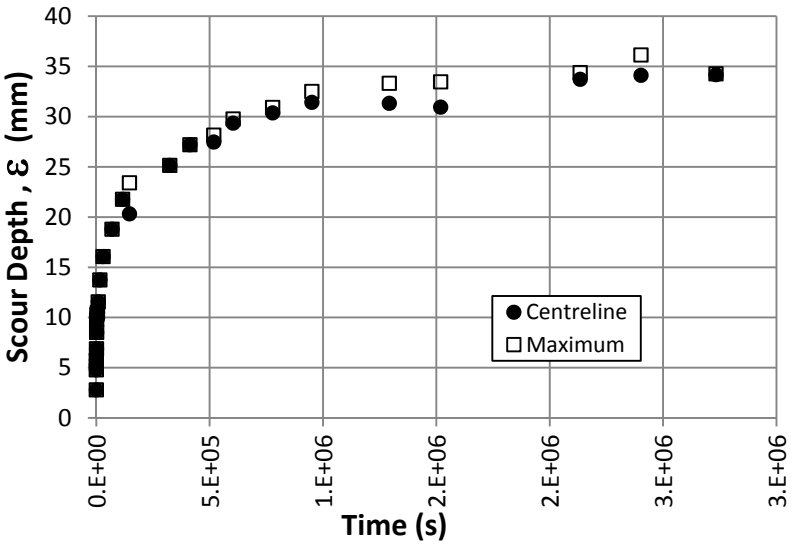




Figure A-23. Observed Time Development of Scour Plots and Test Photos for the M-332 1 of 1 Sample

Table A-24. Test Data for the M-370 1 of 2 Sample (Manufactured Clay Group)

| | | | | | | | | | |
|---|---|---|---|---|---|---|---|---|---|
| **Sample Name:** | M-370 1 of 2 | | **Initial Temperature:** | T (˚C) | 22.2 | | **Volumetric Flow Rate** | | |
| **Batch Number:** | 57441631 | | **Jet Diameter:** | d (mm) | 8.0 | | Avg Q | 35.18 | Lpm |
| **Tested By:** | Dan Cossette | | **Initial Jet Height:** | $H_i$ (mm) | 98.08 | | 1) | 35.21 | Lpm |
| **Analysis By:** | Dan Cossette | | **Equilibrium Centerline Depth:** | $\varepsilon_{cl\infty}$ (mm) | 39.26 | | 2) | 35.46 | Lpm |
| **Date of Testing:** | 2011-06-29 | | **Measured Equilibrium Height:** | $H_{e\ m}$ | 137.34 | | 3) | 34.87 | Lpm |

| **Mag -meter** Q | **Measured Time** $t_m$ | | | **Centerline Scour Depth** $\varepsilon_c$ | **Maximum Scour Depth** $\varepsilon_m$ | **Temp.** T | **Notes** |
|---|---|---|---|---|---|---|---|
| (Lpm) | (Min) | (Hrs) | (s) | (mm) | (mm) | (°C) | |
| 35.7 | 5 | 0:05 | 300 | 3.72 | 24.43 | 22.5 | max depth at edge of sample container |
| 35.5 | 10 | 0:10 | 600 | 6.33 | 30.85 | 22.5 | |
| 35.8 | 15 | 0:15 | 900 | 9.42 | 32.84 | 22.0 | |
| 35.7 | 20 | 0:20 | 1200 | 11.11 | 37.1 | 22.0 | |
| 35.7 | 30 | 0:30 | 1800 | 15.21 | 39.74 | 22.0 | |
| 35.4 | 40 | 0:40 | 2400 | 18.52 | 40.35 | 22.5 | |
| 35.4 | 60 | 1.00 | 3600 | 20.39 | 42.41 | 22.5 | |
| 35.7 | 90 | 1.50 | 5400 | 24.59 | 44.05 | 22.0 | |
| 35.4 | 150 | 2.50 | 9000 | 26.82 | 45.9 | 22.0 | |
| 35.4 | 270 | 4.50 | 16200 | 30.21 | 48.45 | 22.0 | |
| 35.3 | 1206 | 20.10 | 72360 | 34.96 | 47.72 | 22.0 | |
| 34.5 | 4366 | 72.77 | 261960 | 36.78 | 47.68 | 22.0 | lots of material removed from edge of scour hole |
| 33.7 | 6451 | 107.52 | 387060 | 39.07 | 48.76 | 22.5 | between 4366 and 6451 min pump stopped running due to bad connection at the plug. It was about 20hrs before this was noticed, not sure exactly when it stopped. Took depth reading at 72:48+20:00 hrs cl=104.70 approx. assumed pump stopped at 10hrs in order to determine the next time interval and kept running. maybe don't use this reading or beyond for hanson's analysis. also no clay left on platform at 6451 min |
| 33.8 | 9315 | 155.25 | 558900 | 38.99 | 48.91 | 22.5 | doesn't look like any clay has been removed |
| 33.6 | 14670 | 244.50 | 880200 | 39.26 | 48.26 | 22.5 | |

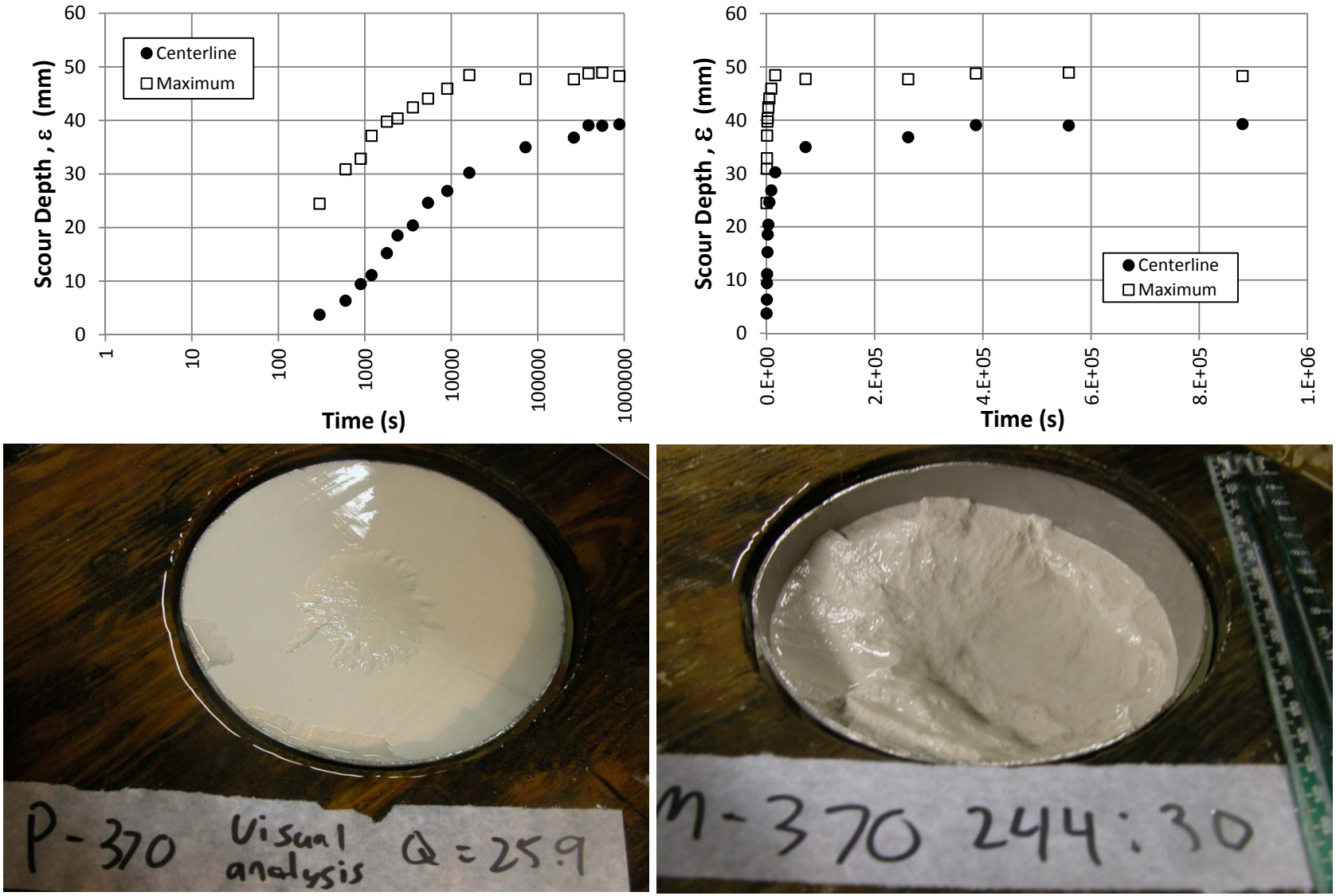


Figure A-24. Observed Time Development of Scour Plots and Test Photos for the M-370 1 of 2 Sample

Table A-25. Test Data for the M-370 2 of 2 Sample (Manufactured Clay Group)

| | | | | | | | | | |
|---|---|---|---|---|---|---|---|---|---|
| **Sample Name:** | M-370 2 of 2 | | **Initial Temperature:** | T (˚C) | 22.8 | | **Volumetric Flow Rate** | | |
| **Batch Number:** | 57441631 | | **Jet Diameter:** | d (mm) | 8.0 | | Avg Q | 31.34 | Lpm |
| **Tested By:** | Dan Cossette | | **Initial Jet Height:** | $H_i$ (mm) | 89.8 | | 1) | 31.49 | Lpm |
| **Analysis By:** | Dan Cossette | | **Equilibrium Centerline Depth:** | $\varepsilon_{cl\infty}$ (mm) | 43.73 | | 2) | 31.61 | Lpm |
| **Date of Testing:** | 2012-02-08 | | **Measured Equilibrium Height:** | $H_{e\ m}$ | 133.53 | | 3) | 30.93 | Lpm |

| **Mag -meter** Q | **Measured Time** $t_m$ | | | **Centerline Scour Depth** $\varepsilon_c$ | **Maximum Scour Depth** $\varepsilon_m$ | **Temp.** T | **Notes** |
|---|---|---|---|---|---|---|---|
| (Lpm) | (Min) | (Hrs) | (s) | (mm) | (mm) | (°C) | max depth occurs at container edge where sample is being torn off. Centerline scour is shallower |
| 30.8 | 5 | 0:05 | 300 | 6.17 | 11.79 | 22.5 | |
| 31.5 | 10 | 0:10 | 600 | 7.11 | 18.68 | 23.0 | |
| 29.7 | 15 | 0:15 | 900 | 8.16 | 19.35 | 23.0 | scour from container edge starting to merge with centerline |
| 30.4 | 20 | 0:20 | 1200 | 11.11 | 26.65 | 23.5 | |
| 29.8 | 30 | 0:30 | 1800 | 13.55 | 28.78 | 23.0 | |
| 29.7 | 40 | 0:40 | 2400 | 16.29 | 29.18 | 24.0 | |
| 30.1 | 60 | 1.00 | 3600 | 18.53 | 29.27 | 23.0 | |
| 29.9 | 90 | 1.50 | 5400 | 21.97 | 31.76 | 23.0 | max depth moving towards centerline |
| 30.0 | 150 | 2.50 | 9000 | 25.66 | 33.41 | 22.5 | |
| 30.1 | 270 | 4.50 | 16200 | 26.53 | 34.66 | 22.5 | |
| 29.9 | 510 | 8.50 | 30600 | 34.86 | 38.53 | 22.5 | |
| 29.7 | 1162 | 19.37 | 69720 | 36.24 | 39.86 | 22.5 | |
| 29.8 | 2122 | 35.37 | 127320 | 36.89 | 40.65 | 22.5 | |
| 29.8 | 4532 | 75.53 | 271920 | 39.43 | 42.72 | 22.5 | large block removed |
| 29.6 | 6015 | 100.25 | 360900 | 40.8 | 43.85 | 22.5 | |
| 29.4 | 7497 | 124.95 | 449820 | 43.22 | 43.86 | 22.5 | |
| 29.4 | 10657 | 177.62 | 639420 | 43.73 | 44.85 | 23.0 | |
| 29.1 | 16437 | 273.95 | 986220 | 43.68 | 44.55 | 22.5 | max depth occurs at container edge where sample is being torn off. Centerline scour is shallower |

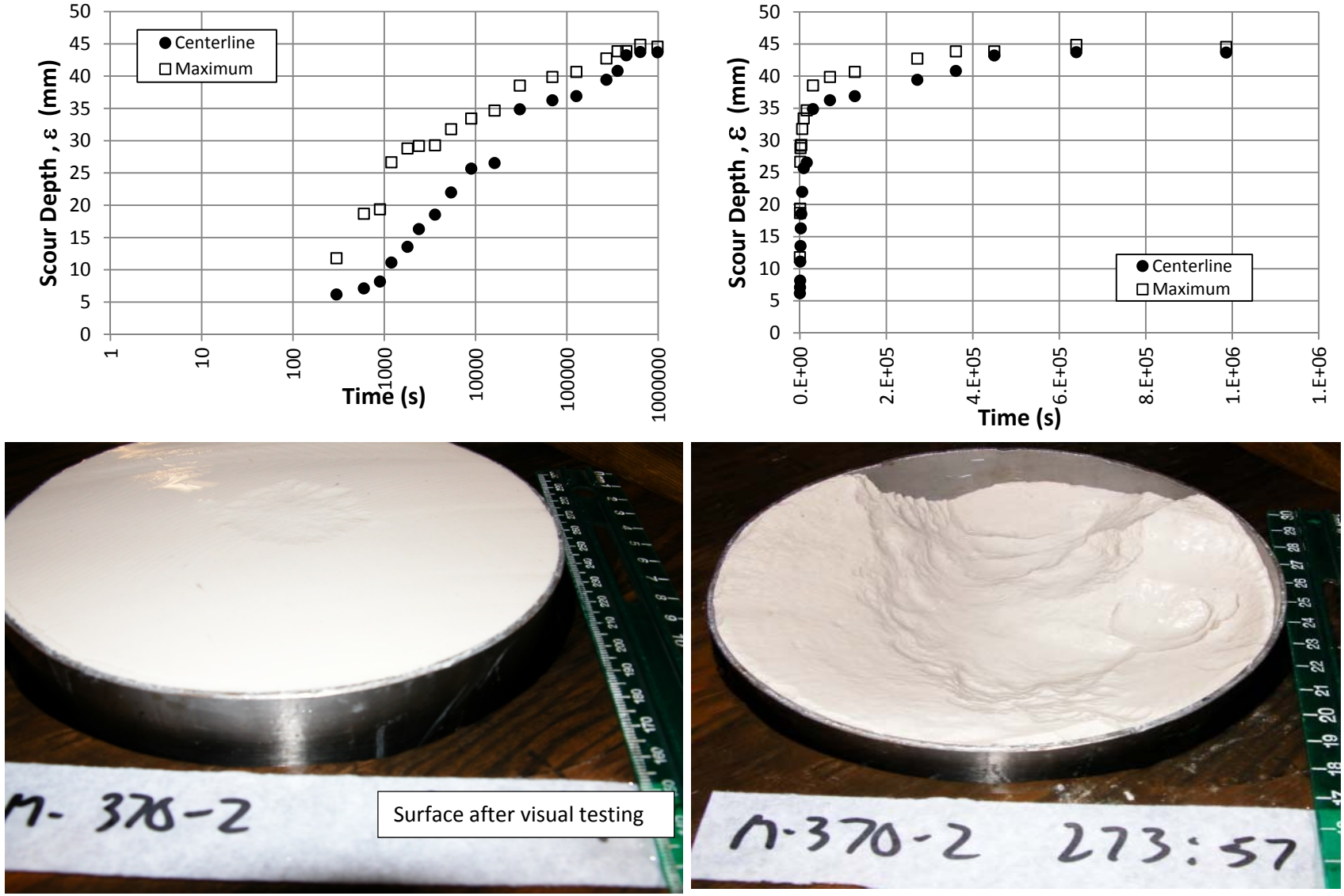


Figure A-25. Observed Time Development of Scour Plots and Test Photos for the M-370 2 of 2 Sample

Table A-26. Test Data for the Buff Stone 1 of 2 Sample (Manufactured Clay Group)

| | | | | | | | | | |
|---|---|---|---|---|---|---|---|---|---|
| **Sample Name:** | Buff Stone 1 of 2 | | **Initial Temperature:** | T (˚C) | | | **Volumetric Flow Rate** | | |
| **Batch Number:** | 56077911 | | **Jet Diameter:** | d (mm) | 8.0 | | Avg Q | 34.8 | Lpm |
| **Tested By:** | Dan Cossette | | **Initial Jet Height:** | $H_i$ (mm) | 88.06 | | 1) | 34.9 | Lpm |
| **Analysis By:** | Dan Cossette | | **Equilibrium Centerline Depth:** | $\varepsilon_{cl\infty}$ (mm) | 49.71 | | 2) | 34.7 | Lpm |
| **Date of Testing:** | 2011-07-14 | | **Measured Equilibrium Height:** | $H_{e\ m}$ | 137.77 | | | | |

| **Mag -meter** Q | **Measured Time** $t_m$ | | | **Centerline Scour Depth** $\varepsilon_c$ | **Maximum Scour Depth** $\varepsilon_m$ | **Temp.** T | **Notes** |
|---|---|---|---|---|---|---|---|
| (Lpm) | (Min) | (Hrs) | (s) | (mm) | (mm) | (°C) | |
| 33.0 | 5 | 0:05 | 300 | 4.46 | 4.46 | 26.0 | Flat chunks removed from container edge |
| 33.9 | 10 | 0:10 | 600 | 6.78 | 6.78 | 24.5 | |
| 32.6 | 15 | 0:15 | 900 | 9.34 | 9.34 | 24.0 | |
| 32.8 | 20 | 0:20 | 1200 | 11.26 | 11.84 | 24.5 | Max depth taken in trench that has been eroded radially similar to flake erosion process |
| 32.4 | 30 | 0:30 | 1800 | 14.08 | 17.57 | 24.0 | |
| 32.8 | 40 | 0:40 | 2400 | 15.91 | 25.74 | 24.0 | |
| 32.5 | 60 | 1.00 | 3600 | 19.21 | 29.91 | 23.0 | |
| 32.4 | 90 | 1.50 | 5400 | 23.12 | 30.74 | 22.5 | |
| 32.6 | 150 | 2.50 | 9000 | 26.25 | 34.93 | 22.5 | |
| 33.0 | 270 | 4.50 | 16200 | 30.52 | 35.06 | 22.5 | |
| 32.8 | 510 | 8.50 | 30600 | 32.02 | 34.72 | 22.5 | |
| 32.5 | 1110 | 18.50 | 66600 | 35.67 | 36.86 | 22.5 | |
| 32.6 | 2560 | 42.67 | 153600 | 37.83 | 38.91 | 22.5 | |
| 32.4 | 3935 | 65.58 | 236100 | 40.71 | 41.19 | 23.0 | |
| 32.7 | 5815 | 96.92 | 348900 | 41.37 | 42.50 | 23.0 | |
| 33.0 | 9700 | 161.67 | 582000 | 44.01 | 44.47 | 23.0 | |
| 32.6 | 15500 | 258.33 | 930000 | 46.34 | 46.34 | 23.0 | |
| 32.6 | 21640 | 360.67 | 1298400 | 48.38 | 49.06 | 23.5 | |
| 32.4 | 35940 | 599.00 | 2156400 | 49.18 | 49.38 | 23.5 | |
| 32.4 | 40230 | 670.50 | 2413800 | 49.71 | 49.71 | 23.5 | |

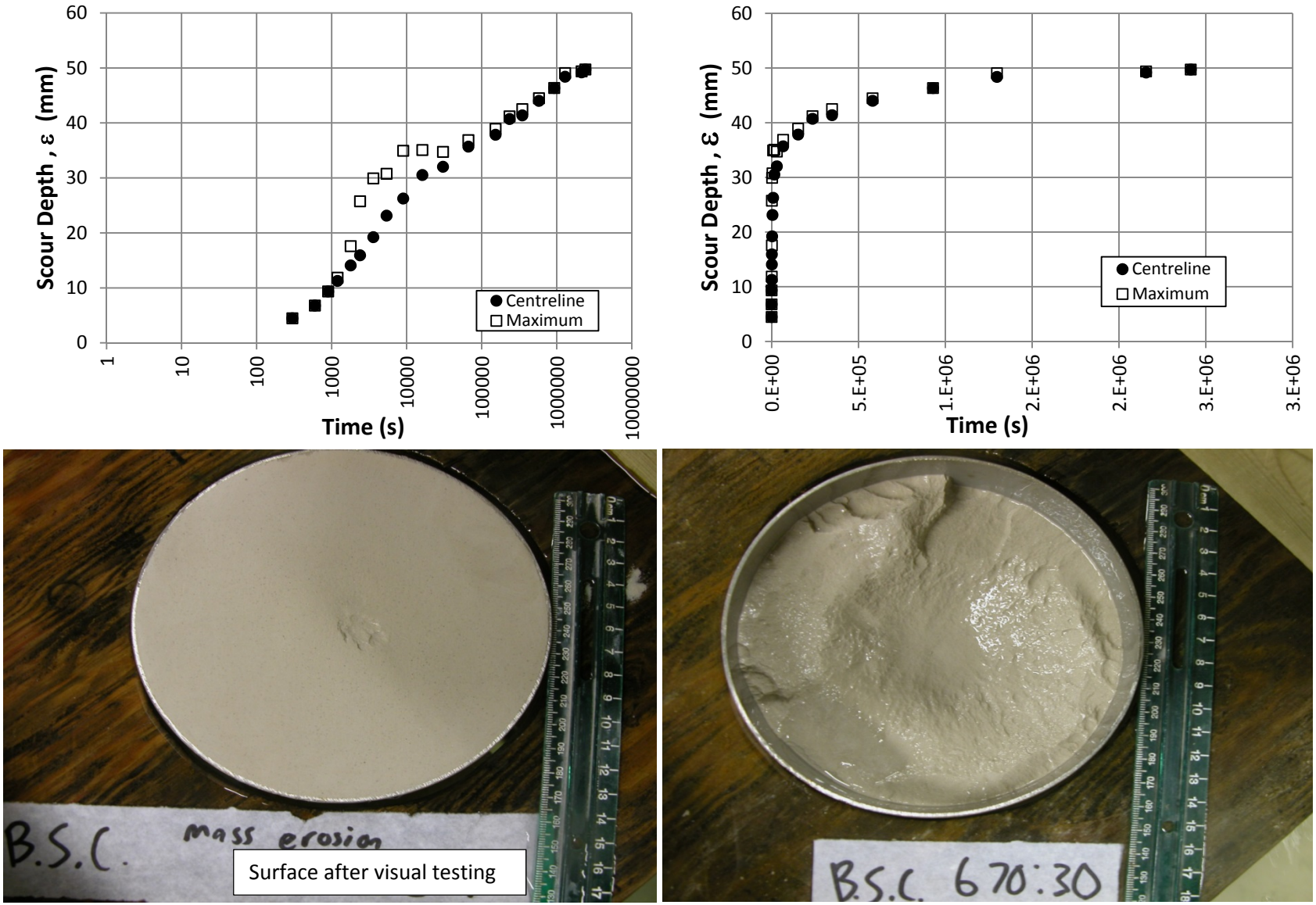


Figure A-26. Observed Time Development of Scour Plots and Test Photos for the Buff Stone 1 of 2 Sample

Table A-27. Test Data for the Buff Stone 2 of 2 Sample (Manufactured Clay Group)

| | | | | | | | | | |
|---|---|---|---|---|---|---|---|---|---|
| **Sample Name:** | Buff Stone 2 of 2 | | **Initial Temperature:** | T (˚C) | | | **Volumetric Flow Rate** | | |
| **Batch Number:** | 57472831 | | **Jet Diameter:** | d (mm) | 8.0 | | Avg Q | 26.48 | Lpm |
| **Tested By:** | Dan Cossette | | **Initial Jet Height:** | $H_i$ (mm) | 93.37 | | 1) | 26.52 | Lpm |
| **Analysis By:** | Dan Cossette | | **Equilibrium Centerline Depth:** | $\varepsilon_{cl\infty}$ (mm) | 34.49 | | 2) | 26.44 | Lpm |
| **Date of Testing:** | 2011-09-28 | | **Measured Equilibrium Height:** | $H_{e\ m}$ | 127.86 | | 3) | 26.48 | Lpm |

| **Mag -meter** Q | **Measured Time** $t_m$ | | | **Centerline Scour Depth** $\varepsilon_c$ | **Maximum Scour Depth** $\varepsilon_m$ | **Temp.** T | **Notes** |
|---|---|---|---|---|---|---|---|
| (Lpm) | (Min) | (Hrs) | (s) | (mm) | (mm) | (°C) | |
| 23.4 | 5 | 0:05 | 300 | 4.57 | 20.00 | 24.5 | There was a surface crack on sample which was exploited and lots of chunks removed around it. Cloud of particles at beginning of test |
| 23.7 | 10 | 0:10 | 600 | 6.83 | 20.81 | 25.0 | |
| 23.7 | 15 | 0:15 | 900 | 9.58 | 21.69 | 25.0 | still flake erosion from surface |
| 23.6 | 20 | 0:20 | 1200 | 11.59 | 22.19 | 25.5 | |
| 23.7 | 30 | 0:30 | 1800 | 12.69 | 23.19 | 25.0 | |
| 23.6 | 40 | 0:40 | 2400 | 14.8 | 26.89 | 29.5 | |
| 23.8 | 60 | 1.00 | 3600 | 17.08 | 27.23 | 24.0 | |
| 23.8 | 90 | 1.50 | 5400 | 17.41 | 27.47 | 24.0 | |
| 24.0 | 150 | 2.50 | 9000 | 21.42 | 28.00 | 23.5 | rounding out of scour hole, shifting towards center |
| 23.8 | 270 | 4.50 | 16200 | 23.38 | 28.84 | 23.5 | |
| 23.8 | 510 | 8.50 | 30600 | 26.36 | 29.50 | 23.5 | scour hole becoming more symmetrical, max depth moving towards centerline, bowl shaped hole |
| 24.3 | 1236 | 20.60 | 74160 | 29.72 | 30.38 | 23.0 | |
| 24.1 | 1958 | 32.63 | 117480 | 31.27 | 31.58 | 23.5 | scour hole looks almost completely centered |
| 24.3 | 3034 | 50.57 | 182040 | 32.59 | 32.59 | 23.5 | flake erosion covering almost all of sample surface, scoured to edge of container |
| 24.1 | 5909 | 98.48 | 354540 | 33.7 | 33.70 | 23.0 | |
| 24.4 | 9333 | 155.55 | 559980 | 34.2 | 34.20 | 23.5 | |
| 24.2 | 12340 | 205.67 | 740400 | 34.47 | 34.54 | 23.5 | |
| 24.0 | 19040 | 317.33 | 1142400 | 34.49 | 34.49 | 23.5 | no noticeable growth of scour hole (depth wise or laterally) no clay material on support table |
| | | | | | | | |
| | | | | | | | |

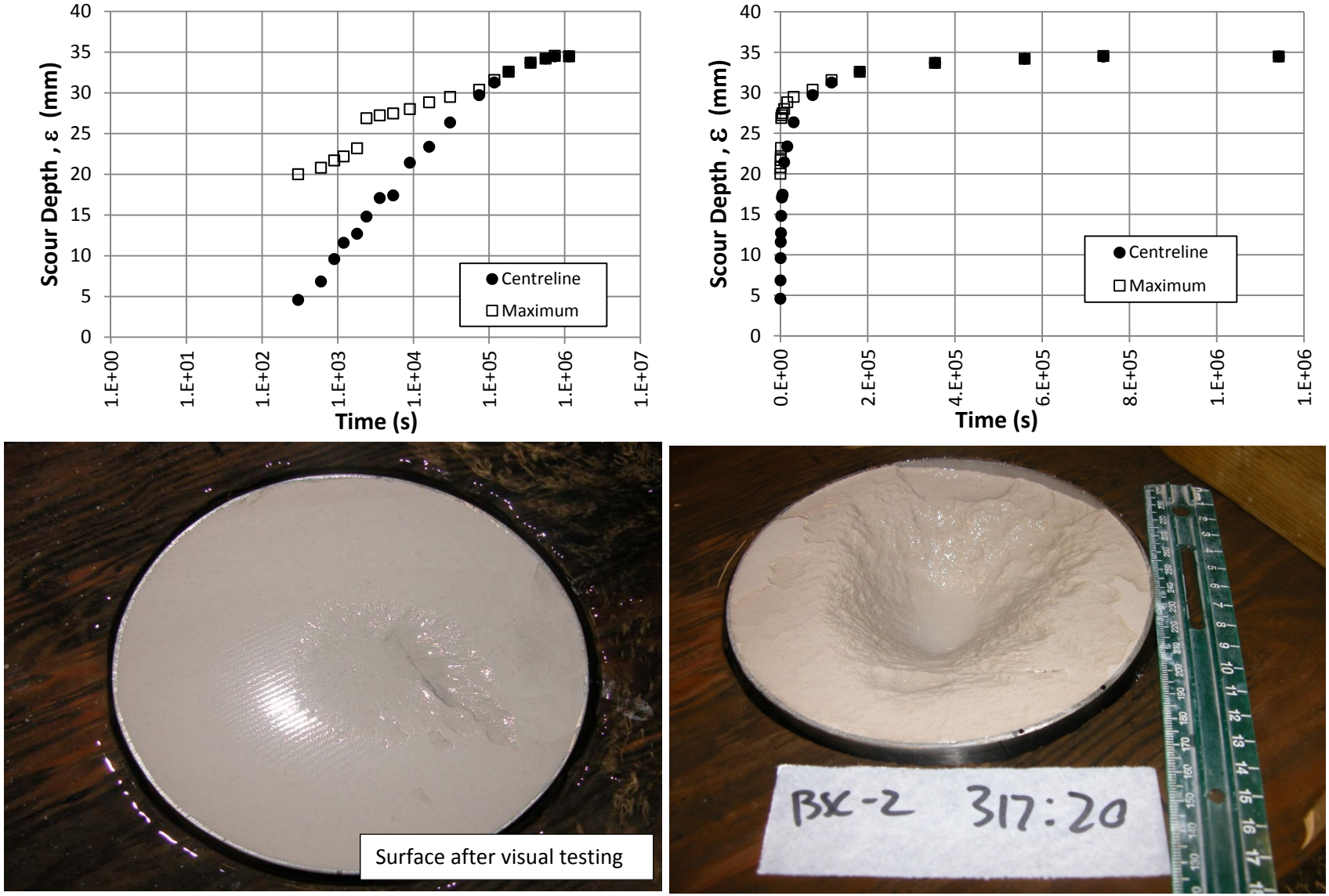


Figure A-27. Observed Time Development of Scour Plots and Test Photos for the Buff Stone 2 of 2 Sample

Table A-28. Test Data for the East College Park 1 of 2 Sample (Saskatoon Group)

| | | | | | | | | | |
|---|---|---|---|---|---|---|---|---|---|
| **Sample Name:** | East College Park 1 of 2 | | **Initial Temperature:** | T (˚C) | 22.7 | | **Volumetric Flow Rate** | | |
| **Batch Number:** | N/A | | **Jet Diameter:** | d (mm) | 8.0 | | Avg Q | 14.01 | Lpm |
| **Tested By:** | Dan Cossette | | **Initial Jet Height:** | $H_i$ (mm) | 108.97 | | 1) | 13.92 | Lpm |
| **Analysis By:** | Dan Cossette | | **Equilibrium Centerline Depth:** | $\varepsilon_{cl\infty}$ (mm) | - | | 2) | 14.04 | Lpm |
| **Date of Testing:** | 2011-10-27 | | **Measured Equilibrium Height:** | $H_{e\ m}$ | - | | 3) | 14.07 | Lpm |

| **Magmeter** Q | **Measured Time** $t_m$ | | | **Centerline Scour Depth** $\varepsilon_c$ | **Maximum Scour Depth** $\varepsilon_m$ | **Temp.** T | **Notes** |
|---|---|---|---|---|---|---|---|
| (Lpm) | (Min) | (Hrs) | (s) | (mm) | (mm) | (°C) | |
| 13.8 | 5 | 0:05 | 300 | 22.23 | 35.8 | 22.0 | Continuous erosion, cloud of particles removed |
| 14.3 | 10 | 0:10 | 600 | 24.38 | 39.17 | 23.0 | lots of roots present (3mm thick) |
| 14.0 | 15 | 0:15 | 900 | 37.87 | 60.53 | 24.0 | hole off centered |
| 13.8 | 20 | 0:20 | 1200 | 39.5 | 65.84 | 25.0 | |
| 13.7 | 30 | 0:30 | 1800 | 48.95 | 67.75 | 22.0 | |
| 13.7 | 40 | 0:40 | 2400 | 51.07 | 74.01 | 23.5 | large burst of particles (1-5mm) upon reentering the jet |
| 13.2 | 60 | 1.00 | 3600 | 52.94 | 75.81 | 22.0 | |
| 13.2 | 90 | 1.50 | 5400 | 53.31 | 75.92 | 22.5 | |
| 13.2 | 150 | 2.50 | 9000 | 78.55 | 124.51 | 22.5 | scoured to edge of container, soil clinging to container edge and overhanging |
| 13.5 | 270 | 4.50 | 16200 | 86.82 | 133.71 | 22.0 | |
| 13.3 | 510 | 8.50 | 30600 | 89.09 | 165.81 | 21.5 | cloud of particle upon re-centering (1-3mm) |
| | | | | | | | Test End-sample completely scoured out, no clay left just fill material. |

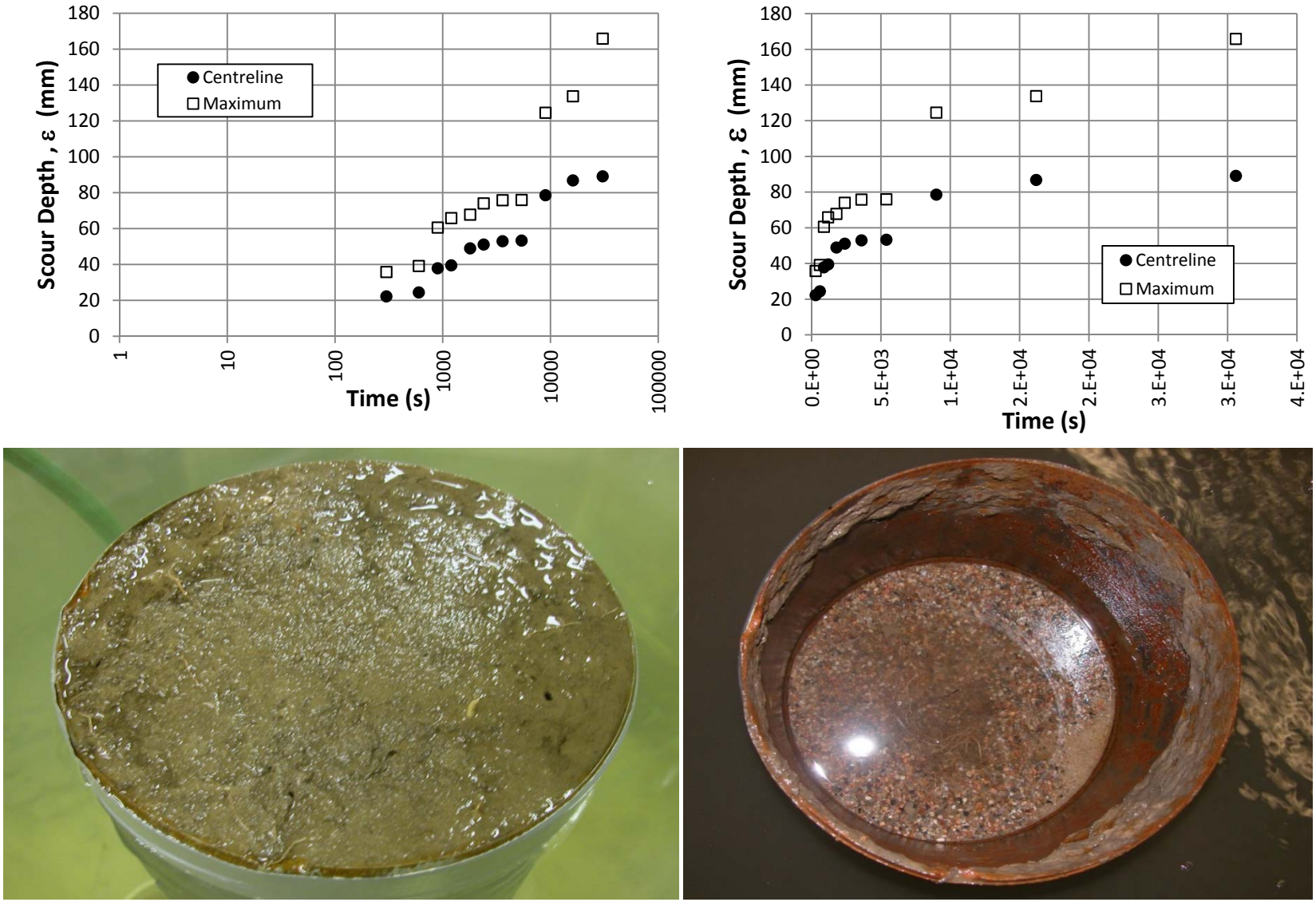


Figure A-28. Observed Time Development of Scour Plots and Test Photos for the East College Park 1 of 2 Sample

Table A-29. Test Data for the East College Park 2 of 2 Sample (Saskatoon Group)

| | | | | | | | | | |
|---|---|---|---|---|---|---|---|---|---|
| **Sample Name:** | East College Park 2 of 2 | | **Initial Temperature:** | T (˚C) | 25.1 | | **Volumetric Flow Rate** | | |
| **Batch Number:** | N/A | | **Jet Diameter:** | d (mm) | 8.0 | | Avg Q | 6.20 | Lpm |
| **Tested By:** | Dan Cossette | | **Initial Jet Height:** | $H_i$ (mm) | 92.04 | | 1) | 6.20 | Lpm |
| **Analysis By:** | Dan Cossette | | **Equilibrium Centerline Depth:** | $\varepsilon_{cl\infty}$ (mm) | 40.58 | | 2) | 6.20 | Lpm |
| **Date of Testing:** | 2012-01-09 | | **Measured Equilibrium Height:** | $H_{e\ m}$ | 132.62 | | 3) | 6.21 | Lpm |

| **Magmeter** Q | **Measured Time** $t_m$ | | | **Centerline Scour Depth** $\varepsilon_c$ | **Maximum Scour Depth** $\varepsilon_m$ | **Temp.** T | **Notes** |
|---|---|---|---|---|---|---|---|
| (Lpm) | (Min) | (Hrs) | (s) | (mm) | (mm) | (°C) | |
| 5.6 | 5 | 0.08 | 300 | 17.72 | 29.17 | 24.5 | rapid removal of smaller particles (1-2mm) (cloud) |
| 5.8 | 10 | 0.17 | 600 | 18.4 | 31.84 | 26.5 | several 1-2mm roots exposed. A couple tube like structures visible similar to worm holes but smaller |
| 6.1 | 15 | 0.25 | 900 | 18.68 | 31.98 | 26.0 | There are some small roots under the centerline that are coming off of the larger roots. |
| 6.0 | 20 | 0.33 | 1200 | 22.49 | 32.4 | 26.5 | scour hole has flatter bottom (not concave) soil may be slightly fractured. |
| 5.8 | 30 | 0.50 | 1800 | 24.93 | 34.88 | 26.5 | |
| 5.7 | 40 | 0.67 | 2400 | 27.39 | 37.13 | 26.0 | |
| 5.6 | 60 | 1.00 | 3600 | 27.66 | 37.39 | 26.0 | |
| 5.9 | 90 | 1.50 | 5400 | 28.4 | 37.41 | 25.5 | |
| 5.8 | 150 | 2.50 | 9000 | 33.19 | 44.49 | 26.0 | max depth taken in small local pocket/hole. Bit of an anomaly, not representative of hydraulic shear but sample nonuniformity. |
| 6.0 | 270 | 4.50 | 16200 | 36.66 | 44.85 | 25.0 | 2 areas with similar max depth (noticeable scour/erosion) |
| 5.1 | 1145 | 19.08 | 68700 | 39.12 | 48.02 | 23.5 | max depth changed position to opposite side of centerline |
| 5.2 | 2540 | 42.33 | 152400 | 39.46 | 50.15 | 23.5 | |
| 5.2 | 3975 | 66.25 | 238500 | 39.89 | 50.98 | 23.5 | |
| 5.2 | 5375 | 89.58 | 322500 | 39.56 | 51.15 | 23.5 | no real noticeable erosion |
| 5.1 | 9625 | 160.42 | 577500 | 40.58 | 51.38 | 23.5 | |

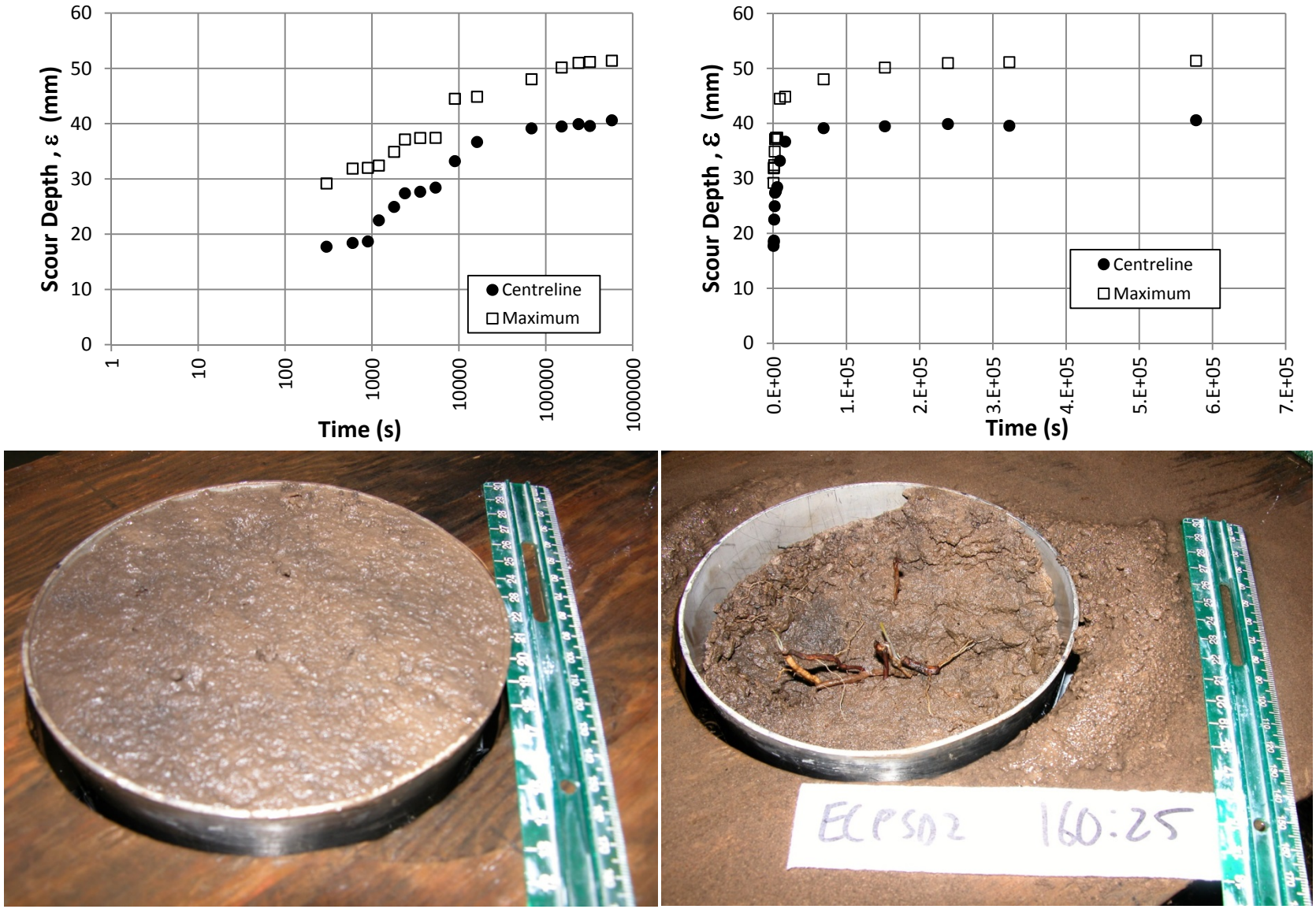


Figure A-29. Observed Time Development of Scour Plots and Test Photos for the East College Park 2 of 2 Sample

Table A-30. Test Data for the Lake Wood 1 of 2 Sample (Saskatoon Group)

| | | | | | | | | | | |
|---|---|---|---|---|---|---|---|---|---|---|
| **Sample Name:** | Lake Wood 1 of 2 | | **Initial Temperature:** | T (˚C) | 24.7 | | **Volumetric Flow Rate** | | |
| **Batch Number:** | N/A | | **Jet Diameter:** | d (mm) | 8.0 | | Avg Q | 11.68 | Lpm |
| **Tested By:** | Dan Cossette | | **Initial Jet Height:** | $H_i$ (mm) | 100.46 | | 1) | 11.74 | Lpm |
| **Analysis By:** | Dan Cossette | | **Equilibrium Centerline Depth:** | $\varepsilon_{cl\infty}$ (mm) | 22.93 | | 2) | 11.63 | Lpm |
| **Date of Testing:** | 2011-11-15 | | **Measured Equilibrium Height:** | $H_{e\ m}$ | 123.39 | | 3) | | Lpm |

| **Magmeter** Q | **Measured Time** $t_m$ | | | **Centerline Scour Depth** $\varepsilon_c$ | **Maximum Scour Depth** $\varepsilon_m$ | **Temp.** T | **Notes** |
|---|---|---|---|---|---|---|---|
| (Lpm) | (Min) | (Hrs) | (s) | (mm) | (mm) | (°C) | |
| 8.2 | 5 | 0.08 | 300 | 20.26 | 22.43 | 26.0 | surface is very blockish/fractured. Clay removed as flat and wide particles. Large buildup of these particles around edge of container. Some sparse/thin (1 to 2mm) vegetation/roots |
| 8.2 | 10 | 0.17 | 600 | 22.02 | 24.65 | 26.5 | cloud of particles when jet is reentered. Not as intense as other samples |
| 8.2 | 15 | 0.25 | 900 | 22.35 | 24.84 | 26.5 | bottom of scour hole not concave but irregular and block like. Soil isn't eroding in as small particles but rather seems to be failing at fractures in the sample. Soil is very dense. |
| 8.2 | 20 | 0.33 | 1200 | 22.44 | 25.42 | 24.0 | |
| 8.2 | 30 | 0.50 | 1800 | 22.49 | 25.85 | 25.0 | |
| 8.2 | 40 | 0.67 | 2400 | 22.55 | 25.31 | 26.0 | max depth not approaching centerline. Soil surface doesn't seem to be eroding but rather weaknesses b/w chunks are being exploited (pressure fluctuations) and flat plate like particles are being removed. |
| 8.2 | 60 | 1.00 | 3600 | 22.45 | 26.07 | 25.5 | Wide and shallow scour hole. |
| 8.2 | 90 | 1.50 | 5400 | 22.71 | 27.64 | 25.0 | hole is quickly draining after emptying tank indicating that fissures may run throughout sample. |
| 8.2 | 150 | 2.50 | 9000 | 22.74 | 27.72 | 25.0 | |
| 8.2 | 270 | 4.50 | 16200 | 22.54 | 25.75 | 24.0 | |
| 8.2 | 510 | 8.50 | 30600 | 22.42 | 30.06 | 23.0 | |
| 8.2 | 1098 | 18.30 | 65880 | 22.93 | 30.34 | 23.0 | loose clay particles near center of jet are rounded from tumbling around in the jet. Some of the surface cracks have deepened/widened. |
| 8.2 | 2943 | 49.05 | 176580 | 22.44 | 29.34 | 23.0 | |
| 8.2 | 8448 | 140.80 | 506880 | 22.43 | 30.71 | 23.5 | |

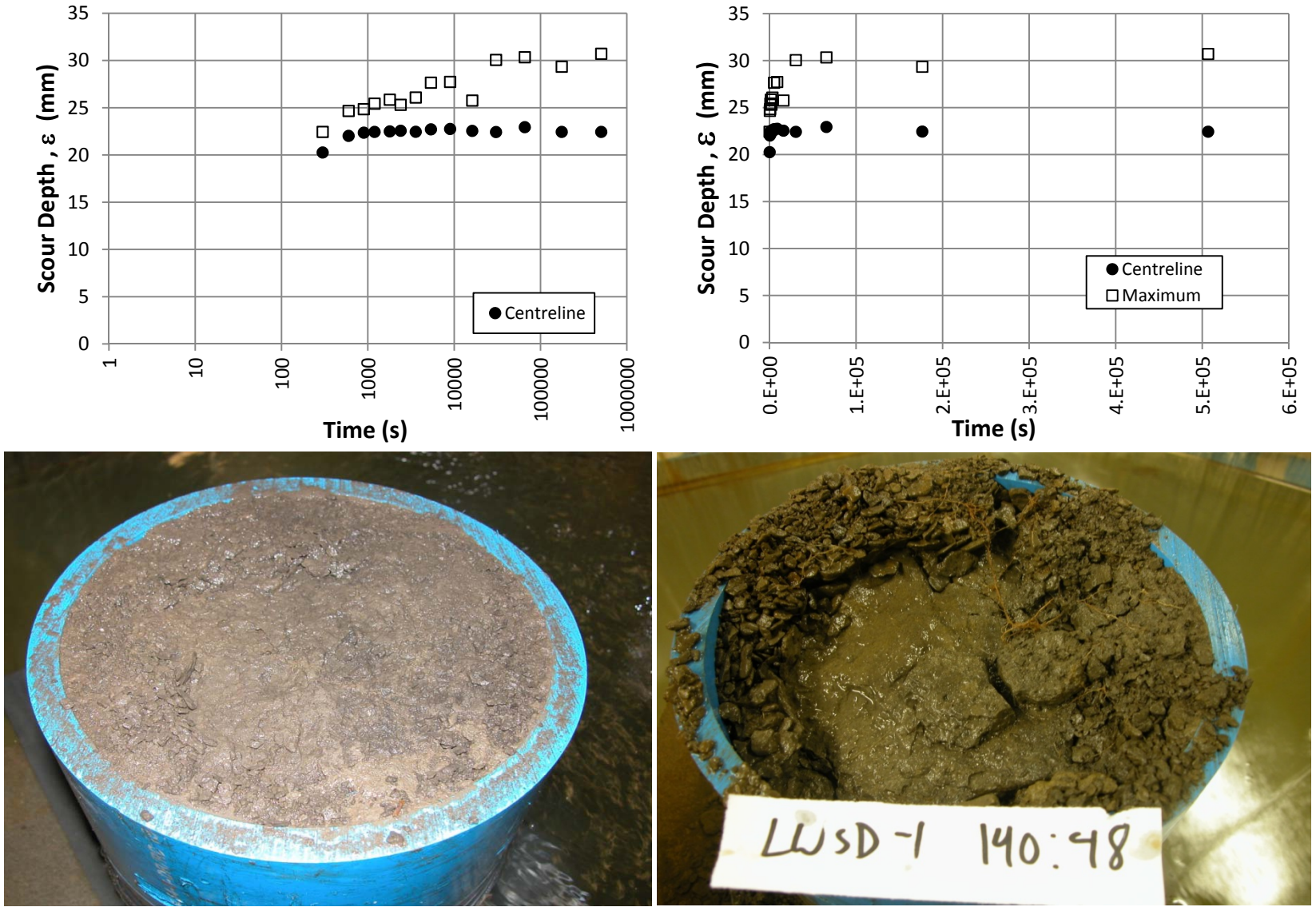


Figure A-30. Observed Time Development of Scour Plots and Test Photos for the Lake Wood 1 of 2 Sample

Table A-31. Test Data for the Lake Wood 2 of 2 Sample (Saskatoon Group)

| | | | | | | | | | | |
|---|---|---|---|---|---|---|---|---|---|---|
| **Sample Name:** | Lake Wood 2 of 2 | | **Initial Temperature:** | T (˚C) | 24.9 | | **Volumetric Flow Rate** | | |
| **Batch Number:** | N/A | | **Jet Diameter:** | d (mm) | 8.0 | | Avg Q | 7.93 | Lpm |
| **Tested By:** | Dan Cossette | | **Initial Jet Height:** | $H_i$ (mm) | 103.99 | | 1) | 7.90 | Lpm |
| **Analysis By:** | Dan Cossette | | **Equilibrium Centerline Depth:** | $\varepsilon_{cl\infty}$ (mm) | - | | 2) | 7.92 | Lpm |
| **Date of Testing:** | 2012-01-24 | | **Measured Equilibrium Height:** | $H_{e\ m}$ | - | | 3) | 7.97 | Lpm |

| **Magmeter** Q | **Measured Time** $t_m$ | | | **Centerline Scour Depth** $\varepsilon_c$ | **Maximum Scour Depth** $\varepsilon_m$ | **Temp.** T | **Notes** |
|---|---|---|---|---|---|---|---|
| (Lpm) | (Min) | (Hrs) | (s) | (mm) | (mm) | (°C) | looks like non cohesive scour hole |
| 6.8 | 5 | 0.08 | 300 | 18.12 | 18.12 | 25.0 | hole back fills making it difficult to get depth readings. Dowel |
| 7.4 | 10 | 0.17 | 600 | 20.68 | 20.68 | 25.0 | |
| 7.5 | 15 | 0.25 | 900 | 24.47 | 24.47 | 24.5 | |
| 7.9 | 20 | 0.33 | 1200 | 26.18 | 26.18 | 25.0 | |
| 7.6 | 30 | 0.50 | 1800 | 26.88 | 26.88 | 25.5 | |
| 7.5 | 40 | 0.67 | 2400 | 40.55 | 40.55 | 25.5 | |
| 7.6 | 60 | 1.00 | 3600 | 50.25 | 50.25 | 26.0 | |
| 7.1 | 90 | 1.50 | 5400 | 52.05 | 52.05 | 25.5 | |
| 7.2 | 150 | 2.50 | 9000 | 64.25 | 64.25 | 24.5 | |
| 7.2 | 320 | 5.33 | 19200 | 110.04 | 110.04 | 24.0 | |
| 7.1 | 560 | 9.33 | 33600 | 111.7 | 111.7 | 23.5 | |
| | | | | | | | TEST ENDED-SAMPLE SCOURED THROUGH |

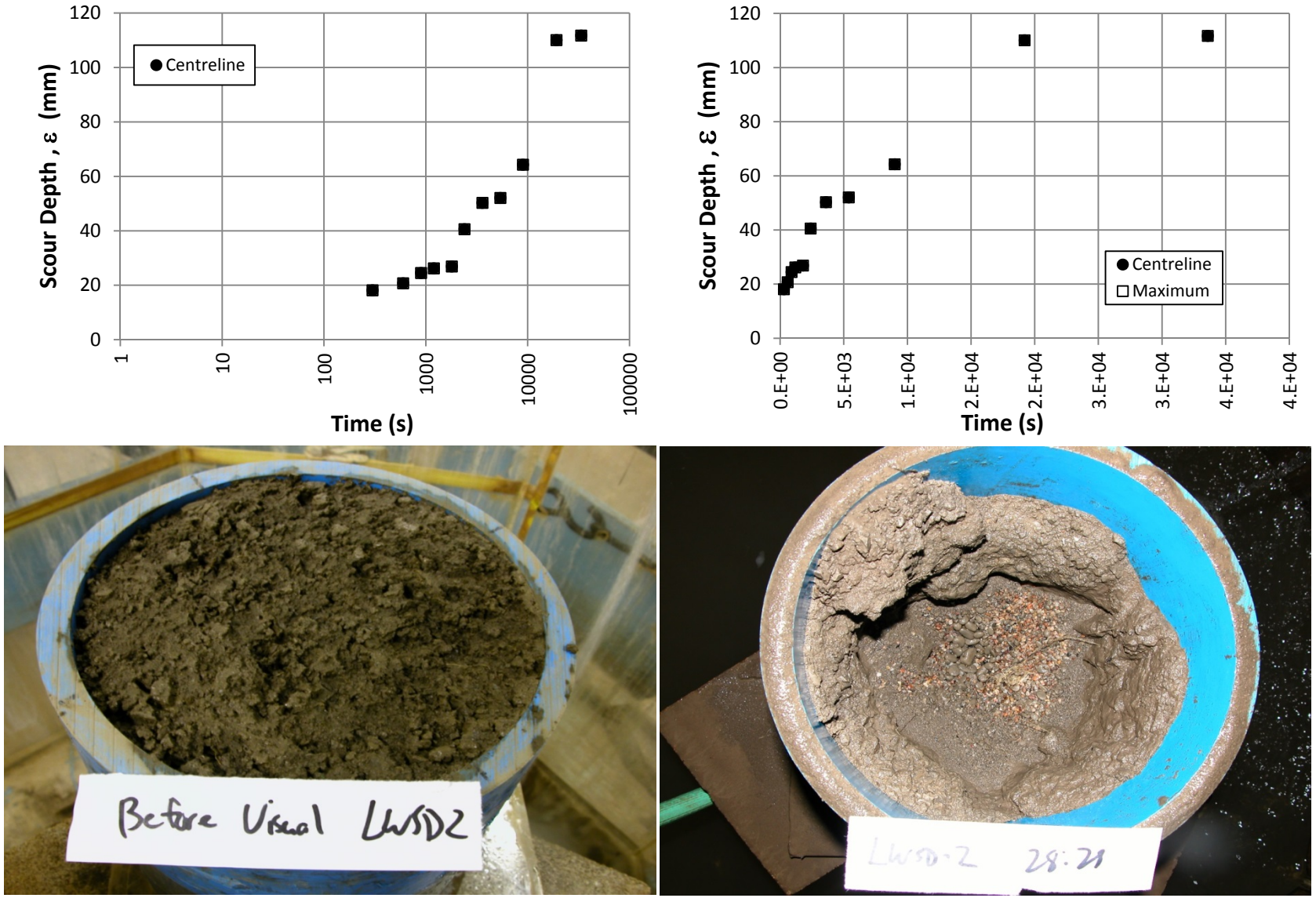


Figure A-31. Observed Time Development of Scour Plots and Test Photos for the Lake Wood 2 of 2 Sample

# APPENDIX B
# EXAMPLE ANALYSIS SPREAD SHEETS FOR MANUFACTURED SAMPLE M390(2)

Appendix B contains all of the analysis spread sheets for sample M390(2) to serve as an example for all 31 tests that were conducted. This includes input parameters and results for all critical shear stress methods ( $\tau_{c\_V}$, $\tau_{c\_Ec}$, $\tau_{c\_B1}$, $\tau_{c\_B2}$, $\tau_{c\_B3}$, $\tau_{c\_T1}$, $\tau_{c\_T2}$, $\tau_{c\_T3}$ ), input parameters and results for all erodibility coefficient methods ($k_{H1}$, $k_{H2}$, $k_{H3}$, $k_{H3\_E}$, $k_{T1}$, $k_{T2}$, $k_{T3}$ ), and all input parameters and results for the excess shear stress exponent analysis ($n_{T1}$, $n_{T2}$, $n_{T3}$ ). In the analysis spread sheet blue cells are static or calculated values, white cells are input cells, orange and red cells are target cells for the solver function to minimize, cells with red and orange boarders are associated with the same color target cell and are solved iteratively using the solver function, and last of all green cells are final analysis results.

**Equilibrium Method**

| | | | |
|---|---|---|---|
| Equ. Scour depth under center | | 41.41 | mm |
| Max Scour depth at equilibrium | | 42.50 | mm |
| Jet diameter | $d_e$ (mm) | 8.000 | |
| Flow Area at Nozzle | A ($m^2$) | 5.027E-05 | |
| Initial Jet Height | $H_i$ (mm) | 101.28 | |
| Equilibrium Jet Height | Hem (mm) | 142.69 | |
| Relative Imping. Height | $H_e/d$ | 17.84 | |
| Flow Rate | Q ($m^3/s$) | 0.0006279 | |
| Jet Velocity | $U_e$ (m/s) | 12.49 | |
| Test Temperature | T (°C) | 22.80 | |
| Fluid Density | ρ (kg/m3) | 997.75 | |
| Kinematic Viscosity | μ (m2/s) | 9.461E-07 | |
| Jet Reynolds Number | $R_e$ | 105635 | |
| Diffusion Coefficient | $C_D$ | 6.3 | |
| Friction Coefficient | $C_f$ | 0.00416 | |
| Combined Coefficient | $C_D^2C_f$ | 0.165 | |
| **Critical Shear Stress** | **$\tau_{c\_Ec}$ (Pa)** | **80.81** | |

Figure B-1. Sample M390(2) Analysis Spreadsheet Printout for the Equilibrium Method

## Visual Method

**Sample Name and ID:** M-390-2

**Analysis By:** Dan Cossette

| | No Mass Erosion | Selected | Definite Mass Erosion |
|---|---|---|---|
| **$\tau_{c\_v}$ (Pa)** | 87.00 | **99.26** | 111.38 |

**Test conditions for which no mass erosion was observed**

| | | |
|---|---|---|
| Jet diameter | d (mm) | 8.0 |
| Flow Area at Nozzle | A ($m^2$) | 5.027E-05 |
| Jet Height | $H_j$ (mm) | 93.55 |
| Relative Imping. Height | $H_j/d$ | 11.69 |
| Flow Rate | Q ($m^3/s$) | 4.27E-04 |
| Jet Velocity | $U_e$ (m/s) | 8.50 |
| Test Temperature | T (°C) | 23 |
| Fluid Density | ρ ($kg/m^3$) | 997.6 |
| Kinematic Viscosity | μ ($m^2/s$) | 9.35E-07 |
| Jet Reynolds Number | $R_e$ | 72699 |
| Diffusion Coefficient | $C_D$ | 6.3 |
| Friction Coefficient | $C_f$ | 0.00416 |
| Combined Coefficient | $C_D^2C_f$ | 0.165 |
| **Critical Shear Stress** | **$\tau_c$ (Pa)** | **87.00** |

Flow Meter (not verified)

| **Flow Rate From Visual Test:** | | |
|---|---|---|
| Flow Meter | 22.0 | Lpm |
| | 3.67E-04 | $m^3/s$ |
| verified multiplier | 1.165 | |
| adjusted flow rate | 4.27E-04 | $m^3/s$ |

| Volume (L) | Time (Min) | Q (Lpm) |
|---|---|---|
| | | |
| | | |
| | | |
| | Average=> | |
| Adjusted flow | 25.63 | Lpm |

Notes:

starting to see slight surface effects, not mass erosion

**Test conditions for which mass erosion was observed by operator**

| | | |
|---|---|---|
| Jet diameter | d (mm) | 8.0 |
| Flow Area at Nozzle | A ($m^2$) | 5.027E-05 |
| Jet Height | $H_j$ (mm) | 93.55 |
| Relative Imping. Height | $H_j/d$ | 11.69 |
| Flow Rate | Q ($m^3/s$) | 4.56E-04 |
| Jet Velocity | $U_e$ (m/s) | 9.08 |
| Test Temperature | T (°C) | 23 |
| Fluid Density | ρ ($kg/m^3$) | 997.6 |
| Kinematic Viscosity | μ ($m^2/s$) | 9.35E-07 |
| Jet Reynolds Number | $R_e$ | 77654 |
| Diffusion Coefficient | $C_D$ | 6.3 |
| Friction Coefficient | $C_f$ | 0.00416 |
| Combined Coefficient | $C_D^2C_f$ | 0.165 |
| **Critical Shear Stress** | **$\tau_c$ (Pa)** | **99.26** |

| **Flow Rate From Visual Test:** | | |
|---|---|---|
| Critical flow rate | 27.377 | Lpm |
| | 4.56E-04 | $m^3/s$ |

| Volume (L) | Time (Min) | Q (Lpm) |
|---|---|---|
| 98.00 | 3.595 | 27.26 |
| 98.10 | 3.575 | 27.44 |
| 98.02 | 3.573 | 27.43 |
| | Average=> | 27.38 |
| Flow Meter | 23.3 | Lpm |

Notes:

Large half of sample removed, doesn't appear to be mass erosion caused by shear stresses but rather an imperfection in the sample that was exploited by fluctuating pressures.

**Test conditions for which mass erosion was confirmed**

| | | |
|---|---|---|
| Jet diameter | d (mm) | 8.0 |
| Flow Area at Nozzle | A ($m^2$) | 5.027E-05 |
| Jet Height | $H_j$ (mm) | 93.55 |
| Relative Imping. Height | $H_j/d$ | 11.69 |
| Flow Rate | Q ($m^3/s$) | 4.83E-04 |
| Jet Velocity | $U_e$ (m/s) | 9.62 |
| Test Temperature | T (°C) | 23 |
| Fluid Density | ρ ($kg/m^3$) | 997.6 |
| Kinematic Viscosity | μ ($m^2/s$) | 9.35E-07 |
| Jet Reynolds Number | $R_e$ | 82258 |
| Diffusion Coefficient | $C_D$ | 6.3 |
| Friction Coefficient | $C_f$ | 0.00416 |
| Combined Coefficient | $C_D^2C_f$ | 0.165 |
| **Critical Shear Stress** | **$\tau_c$ (Pa)** | **111.38** |

Volumetrically verified flow rate

| **Flow Rate From Visual Test:** | | |
|---|---|---|
| Volumetric Q | 29.0 | Lpm |
| | 4.83E-04 | $m^3/s$ |

| Volume (L) | Time (Min) | Q (Lpm) |
|---|---|---|
| 107.8 | 3.698 | 29.15 |
| 98.05 | 3.394 | 28.89 |
| 98.00 | 3.384 | 28.96 |
| | Average=> | 29.0 |
| Flow Meter | 24.9 | Lpm |

Notes:

Definite mass erosion observed from under the jet centreline

Figure B-2. Sample M390(2) Analysis Spreadsheet Printout for the Visual Method

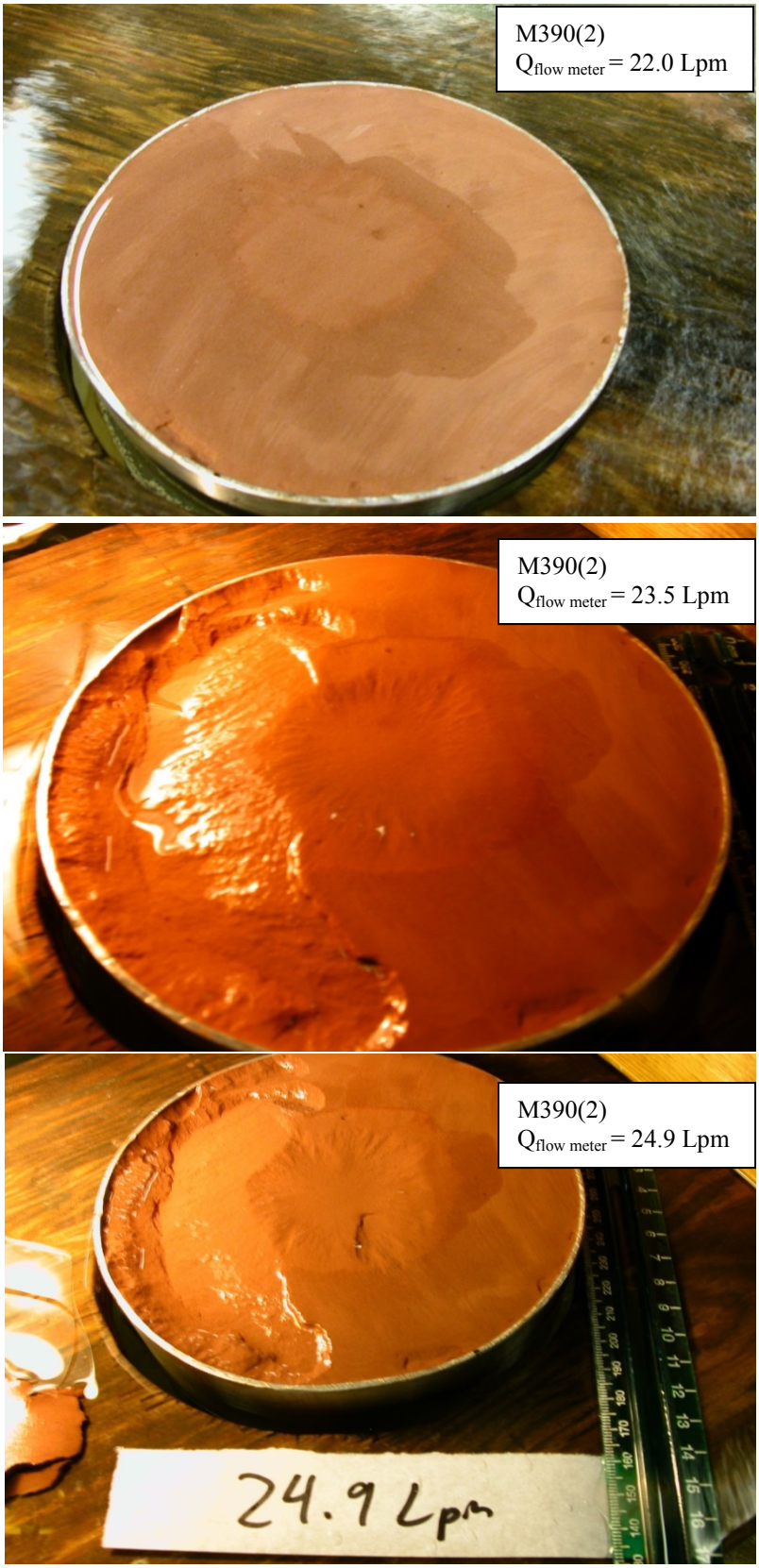


Figure B-3. M390(2) Sample Photos for the Visual Critical Shear Stress Testing

**Hanson and Cook's (2004) Method 1** Analysis uses scour data up to and including 120 min of testing

**Sample Name and ID:** M-390-2

**Analysis By:** Dan Cossette

| | | |
|---|---|---|
| Jet diameter | d (mm) | 8 |
| Jet Height | $H_i$ (mm) | 101.28 |
| Flow Rate | Q ($m^3$/s) | 0.0006279 |
| Jet Velocity | $U_o$ (m/s) | 12.49 |
| Test Temperature | T (°C) | 22.8 |
| Kinematic Viscosity | μ ($m^2$/s) | 9.46E-07 |
| Jet Reynolds Number | $R_e$ | 105635 |
| Diffusion Coefficient | $C_D$ | 6.3 |
| Friction Coefficient | $C_f$ | 0.00416 |
| Combined Coefficient | $C_D^2C_f$ | 0.165 |
| **Maximum Shear Stress** | **$\tau_{cm}$ (Pa)** | **160.41** |

| Hanson 1 Results | | |
|---|---|---|
| fo | 1.519 | |
| $He_{B1}$ (mm) | 264.4 | Equ. [2-8] |
| **$\tau_{c\_B1}$ (Pa)** | **23.5** | Equ. [2-5] |
| $H_i^*=H_i/H_{eB}$ | 0.3830 | Equ [2-18] |
| **$k_{H1}$ ($cm^3$/N-s)** | **0.0897** | |
| Tr (s) | 125255 | Equ [2-16] |

| | | |
|---|---|---|
| Hp (mm) | 50.4 | Equ. 3 Hanson & Cook (1997) |
| $Hp^*=Hp/He_B$ | 0.1906 | |
| Tp* | 0.0072 | Equ. 15 Hanson & Cook (1997) |
| Ti* | 0.0254 | Equ. 17 Hanson & Cook (1997) |
| ti (s) | 3181 | |

| Measured Time, $t_m$ | | | Centerline Scour Depth, | H=e+Hi | H*=H/He | x | f | $A^2$ | Data $T_m^*$ | Equ 20 H & C (1997) $T_m^*$ | MARE | t = tm + ti | Data T* | Equ 18 H & C (1997) T* | MARE |
|---|---|---|---|---|---|---|---|---|---|---|---|---|---|---|---|
| (Min) | (Hrs) | (s) | (mm) | (mm) | | | | | | | | (s) | | | |
| 5 | 0:05 | 300 | 9.71 | 111.0 | 0.4197 | 5.671 | -4.528 | 4.418 | 2.40E-03 | 7.06E-03 | 1.9481 | 3481 | 0.02779 | 0.03246 | 0.1679 |
| 10 | 0:10 | 600 | 13.15 | 114.4 | 0.4327 | 5.972 | -4.816 | 4.477 | 4.79E-03 | 9.95E-03 | 1.0770 | 3781 | 0.03018 | 0.03534 | 0.1709 |
| 15 | 0:15 | 900 | 16.68 | 118.0 | 0.4461 | 6.148 | -4.979 | 4.434 | 7.19E-03 | 1.31E-02 | 0.8292 | 4081 | 0.03258 | 0.03854 | 0.1829 |
| 20 | 0:20 | 1200 | 19.11 | 120.4 | 0.4553 | 6.273 | -5.095 | 4.404 | 9.58E-03 | 1.55E-02 | 0.6164 | 4381 | 0.03498 | 0.04088 | 0.1688 |
| 30 | 0:30 | 1800 | 21.73 | 123.0 | 0.4652 | 6.449 | -5.262 | 4.398 | 1.44E-02 | 1.81E-02 | 0.2629 | 4981 | 0.03977 | 0.04354 | 0.0950 |
| 40 | 0:40 | 2400 | 22.69 | 124.0 | 0.4688 | 6.574 | -5.384 | 4.434 | 1.92E-02 | 1.92E-02 | 0.0000 | 5581 | 0.04456 | 0.04456 | 0.0000 |
| 60 | 1.00 | 3600 | 24.89 | 126.2 | 0.4771 | 6.750 | -5.552 | 4.442 | 2.87E-02 | 2.16E-02 | 0.2499 | 6781 | 0.05414 | 0.04695 | 0.1327 |
| 90 | 1.50 | 5400 | 27.21 | 128.5 | 0.4859 | 6.926 | -5.720 | 4.440 | 4.31E-02 | 2.42E-02 | 0.4385 | 8581 | 0.06851 | 0.04960 | 0.2760 |
| | | | | | | | $f_o$ | 1.519 | | SUM | 0.6778 | | | SUM | 0.1493 |
| | | | | | | | Average value | **4.431** | | | | | | | |
| | | | | | | | Stdev | 0.025 | | | | | | | |

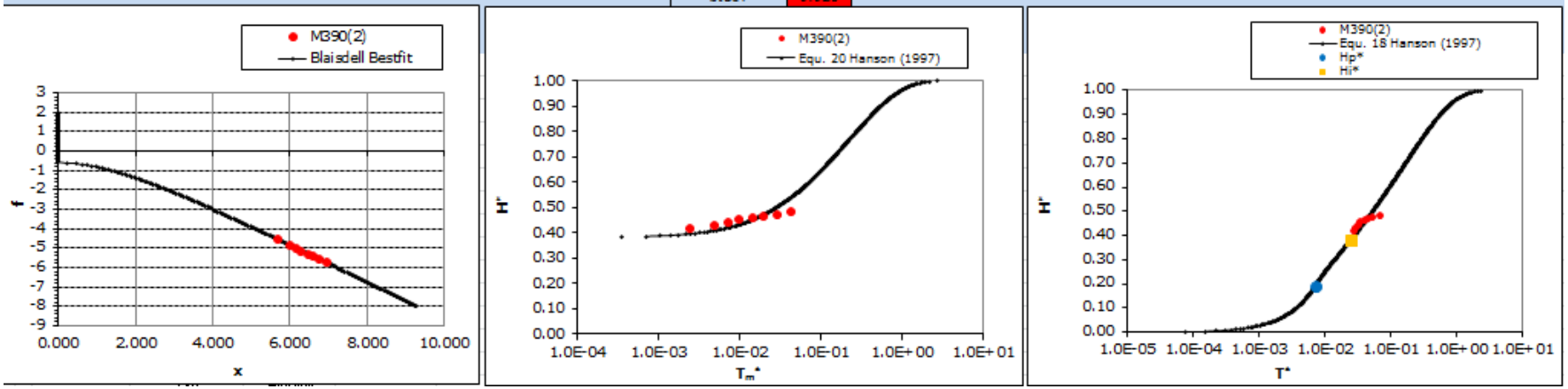


Figure B-4. Sample M390(2) Analysis Spreadsheet Printout for Hanson and Cook's (2004) Method using the First 120 Minutes of Test Data

**Hanson and Cook's (2004) Method 2** Analysis uses scour data up to and including first 10 readings

**Sample Name and ID:** M-390-2

**Analysis By:** Dan Cossette

| | | |
|---|---|---|
| Jet diameter | d (mm) | 8 |
| Jet Height | $H_i$ (mm) | 101.28 |
| Flow Rate | Q ($m^3/s$) | 0.0006279 |
| Jet Velocity | $U_o$ (m/s) | 12.49 |
| Test Temperature | T (°C) | 22.8 |
| Kinematic Viscosity | $\mu$ ($m^2/s$) | 9.46E-07 |
| Jet Reynolds Number | $R_e$ | 105635 |
| Diffusion Coefficient | $C_D$ | 6.3 |
| Friction Coefficient | $C_f$ | 0.00416 |
| Combined Coefficient | $C_D^2C_f$ | 0.165 |
| **Maximum Shear Stress** | **$\tau_{cm}$ (Pa)** | **160.41** |

| Hanson 2 Results | | |
|---|---|---|
| fo | 1.480 | |
| $He_{B2}$ (mm) | 241.9 | Equ. [2-8] |
| **$\tau_{c\_B2}$ (Pa)** | **28.1** | Equ. [2-5] |
| $H_i^*=H_i/H_{cB}$ | 0.4187 | Equ [2-18] |
| **$k_{H2}$ ($cm^3$/N-s)** | **0.0705** | |
| Tr (s) | 121908 | Equ [2-16] |

| | | |
|---|---|---|
| Hp (mm) | 50.4 | Equ. 3 Hanson & Cook (1997) |
| $Hp^*=Hp/He_B$ | 0.2084 | |
| Tp* | 0.0095 | Equ. 15 Hanson & Cook (1997) |
| Ti* | 0.0338 | Equ. 17 Hanson & Cook (1997) |
| ti (s) | 4119 | |

| Measured Time, $t_m$ | | | Centerline Scour Depth, | H=e+Hi | H*=H/He | x | f | $A^2$ | Equ 20 Data $T_m^*$ | Equ 20 H & C (1997) $T_m^*$ | Equ 20 MARE | t = tm + ti | Equ 18 Data T* | Equ 18 & C (1997) T* | Equ 18 MARE |
|---|---|---|---|---|---|---|---|---|---|---|---|---|---|---|---|
| (Min) | (Hrs) | (s) | (mm) | (mm) | | | | | | | | (s) | | | |
| 5 | 0:05 | 300 | 9.71 | 111.0 | 0.4589 | 5.671 | -4.528 | 3.951 | 2.46E-03 | 9.59E-03 | 2.8971 | 4419 | 0.03625 | 0.04338 | 0.1967 |
| 10 | 0:10 | 600 | 13.15 | 114.4 | 0.4731 | 5.972 | -4.816 | 3.988 | 4.92E-03 | 1.35E-02 | 1.7503 | 4719 | 0.03871 | 0.04732 | 0.2226 |
| 15 | 0:15 | 900 | 16.68 | 118.0 | 0.4877 | 6.148 | -4.979 | 3.932 | 7.38E-03 | 1.79E-02 | 1.4268 | 5019 | 0.04117 | 0.05170 | 0.2559 |
| 20 | 0:20 | 1200 | 19.11 | 120.4 | 0.4978 | 6.273 | -5.095 | 3.893 | 9.84E-03 | 2.11E-02 | 1.1474 | 5319 | 0.04363 | 0.05492 | 0.2589 |
| 30 | 0:30 | 1800 | 21.73 | 123.0 | 0.5086 | 6.449 | -5.262 | 3.873 | 1.48E-02 | 2.48E-02 | 0.6803 | 5919 | 0.04855 | 0.05860 | 0.2069 |
| 40 | 0:40 | 2400 | 22.69 | 124.0 | 0.5126 | 6.574 | -5.384 | 3.900 | 1.97E-02 | 2.62E-02 | 0.3313 | 6519 | 0.05347 | 0.06000 | 0.1220 |
| 60 | 1.00 | 3600 | 24.89 | 126.2 | 0.5217 | 6.750 | -5.552 | 3.895 | 2.95E-02 | 2.95E-02 | 0.0000 | 7719 | 0.06332 | 0.06332 | 0.0000 |
| 90 | 1.50 | 5400 | 27.21 | 128.5 | 0.5312 | 6.926 | -5.720 | 3.881 | 4.43E-02 | 3.32E-02 | 0.2503 | 9519 | 0.07808 | 0.06699 | 0.1420 |
| 150 | 2.50 | 9000 | 28.92 | 130.2 | 0.5383 | 7.148 | -5.936 | 3.917 | 7.38E-02 | 3.60E-02 | 0.5118 | 13119 | 0.10761 | 0.06983 | 0.3511 |
| 270 | 4.50 | 16200 | 29.77 | 131.1 | 0.5418 | 7.403 | -6.189 | 4.011 | 1.33E-01 | 3.75E-02 | 0.7179 | 20319 | 0.16667 | 0.07127 | 0.5724 |
| | | | | | | | $f_o$ | 1.480 | | SUM | 0.9713 | | | SUM | 0.2328 |
| | | | | | | | Average value | **3.924** | | | | | | | |
| | | | | | | | Stdev | 0.046 | | | | | | | |

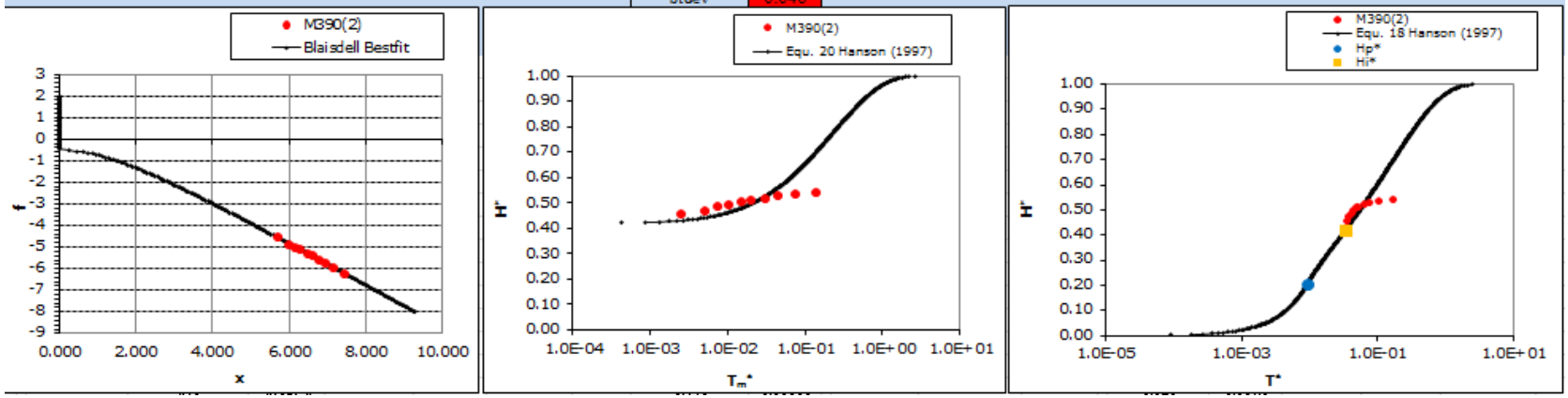


Figure B-5. Sample M390(2) Analysis Spreadsheet Printout for Hanson and Cook's (2004) Method using the First 10 Test Data Measurements

**Hanson and Cook's (2004) Method 3** Analysis uses all scour data

| | | |
|---|---|---|
| **Sample Name and ID:** | | M-390-2 |
| **Analysis By:** | | Dan Cossette |
| Jet diameter | d (mm) | 8 |
| Jet Height | $H_i$ (mm) | 101.28 |
| Flow Rate | Q ($m^3/s$) | 0.0006279 |
| Jet Velocity | $U_o$ (m/s) | 12.49 |
| Kinematic Viscosity | $\mu$ ($m^2/s$) | 9.46E-07 |
| Jet Reynolds Number | $R_e$ | 105635 |
| Diffusion Coefficient | $C_D$ | 6.3 |
| Friction Coefficient | $C_f$ | 0.00416 |
| Combined Coefficient | $C_D^2 C_f$ | 0.165 |
| **Maximum Shear Stress** | $\tau_{max}$ (Pa) | **160.41** |

| | | |
|---|---|---|
| fo | 1.437 | |
| $He_{B3}$ (mm) | 218.6 | Equ. [2-8] |
| $\tau_{c\ B3}$ (Pa) | **34.4** | Equ. [2-5] |
| $H_i^* = H_i/H_{eB}$ | 0.4633 | Equ [2-18] |
| $k_{B3}$ ($cm^3/N-s$) | **0.0755** | |
| Tr (s) | 84041 | Equ [2-16] |

| | | |
|---|---|---|
| Hp (mm) | 50.4 | Equ. 3 H&C (1997) |
| $Hp^* = Hp/He_B$ | 0.2306 | |
| $Tp^*$ | 0.0129 | Equ. 15 H&C (1997) |
| $Ti^*$ | 0.0469 | Equ. 17 H&C (1997) |
| ti (s) | 3945 | |

| Measured Time, $t_m$ | | | Centerline Scour Depth, | H=e+Hi | $H^*=H/He$ | x | f | $A^2$ | $T_m^*$ Data | $T_m^*$ Equ 20 H&C (1997) | MARE | t = tm + ti | $T^*$ Data | $T^*$ Equ 18 H&C (1997) | MARE |
|---|---|---|---|---|---|---|---|---|---|---|---|---|---|---|---|
| (Min) | (Hrs) | (s) | (mm) | (mm) | | | | | | | | (s) | | | |
| 5 | 0:05 | 300 | 9.71 | 111.0 | 0.5077 | 5.671 | -4.528 | 3.425 | 3.57E-03 | 1.37E-02 | 2.8463 | 4245 | 0.05051 | 0.06067 | 0.2012 |
| 10 | 0:10 | 600 | 13.15 | 114.4 | 0.5235 | 5.972 | -4.816 | 3.436 | 7.14E-03 | 1.94E-02 | 1.7216 | 4545 | 0.05408 | 0.06637 | 0.2273 |
| 15 | 0:15 | 900 | 16.68 | 118.0 | 0.5396 | 6.148 | -4.979 | 3.366 | 1.07E-02 | 2.58E-02 | 1.4084 | 4845 | 0.05765 | 0.07273 | 0.2617 |
| 20 | 0:20 | 1200 | 19.11 | 120.4 | 0.5507 | 6.273 | -5.095 | 3.317 | 1.43E-02 | 3.05E-02 | 1.1356 | 5145 | 0.06121 | 0.07743 | 0.2649 |
| 30 | 0:30 | 1800 | 21.73 | 123.0 | 0.5627 | 6.449 | -5.262 | 3.283 | 2.14E-02 | 3.59E-02 | 0.6752 | 5745 | 0.06835 | 0.08282 | 0.2116 |
| 40 | 0:40 | 2400 | 22.69 | 124.0 | 0.5671 | 6.574 | -5.384 | 3.299 | 2.86E-02 | 3.79E-02 | 0.3285 | 6345 | 0.07549 | 0.08487 | 0.1242 |
| 60 | 1.00 | 3600 | 24.89 | 126.2 | 0.5772 | 6.750 | -5.552 | 3.279 | 4.28E-02 | 4.28E-02 | 0.0000 | 7545 | 0.08977 | 0.08977 | 0.0000 |
| 90 | 1.50 | 5400 | 27.21 | 128.5 | 0.5878 | 6.926 | -5.720 | 3.250 | 6.43E-02 | 4.83E-02 | 0.2485 | 9345 | 0.11119 | 0.09522 | 0.1436 |
| 150 | 2.50 | 9000 | 28.92 | 130.2 | 0.5956 | 7.148 | -5.936 | 3.268 | 1.07E-01 | 5.25E-02 | 0.5097 | 12945 | 0.15403 | 0.09944 | 0.3544 |
| 270 | 4.50 | 16200 | 29.77 | 131.1 | 0.5995 | 7.403 | -6.189 | 3.339 | 1.93E-01 | 5.47E-02 | 0.7164 | 20145 | 0.23970 | 0.10160 | 0.5761 |
| 570 | 9.50 | 34200 | 33.27 | 134.6 | 0.6155 | 7.728 | -6.502 | 3.302 | 4.07E-01 | 6.40E-02 | 0.8427 | 38145 | 0.45388 | 0.11097 | 0.7555 |
| 2025 | 33.75 | 121500 | 36.97 | 138.3 | 0.6325 | 8.278 | -7.041 | 3.334 | 1.45E+00 | 7.48E-02 | 0.9482 | 125445 | 1.49267 | 0.12176 | 0.9184 |
| 3610 | 60.17 | 216600 | 39.32 | 140.6 | 0.6432 | 8.529 | -7.284 | 3.306 | 2.58E+00 | 8.22E-02 | 0.9681 | 220545 | 2.62426 | 0.12914 | 0.9508 |
| 6075 | 101.25 | 364500 | 40.57 | 141.9 | 0.6489 | 8.755 | -7.507 | 3.324 | 4.34E+00 | 8.63E-02 | 0.9801 | 368445 | 4.38412 | 0.13324 | 0.9696 |
| 7785 | 129.75 | 467100 | 40.98 | 142.3 | 0.6508 | 8.863 | -7.613 | 3.342 | 5.56E+00 | 8.77E-02 | 0.9842 | 471045 | 5.60496 | 0.13461 | 0.9760 |
| 10530 | 175.50 | 631800 | 41.41 | 142.7 | 0.6528 | 8.994 | -7.743 | 3.367 | 7.52E+00 | 8.91E-02 | 0.9881 | 635745 | 7.56473 | 0.13606 | 0.9820 |
| | | | | | | | $f_o$ | 1.437 | | SUM | 0.9584 | | | SUM | 0.5238 |
| | | | | | | | Average value | **3.332** | | | | | | | |
| | | | | | | | Stdev | 0.055 | | | | | | | |

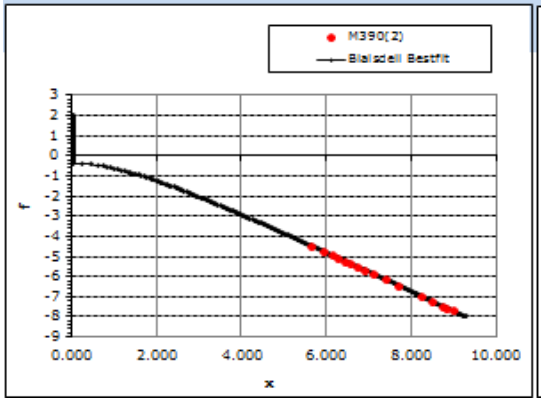


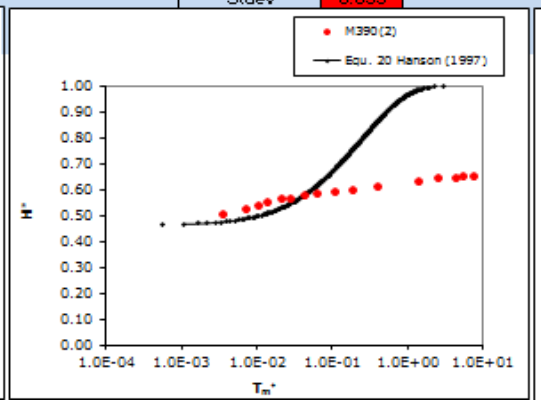


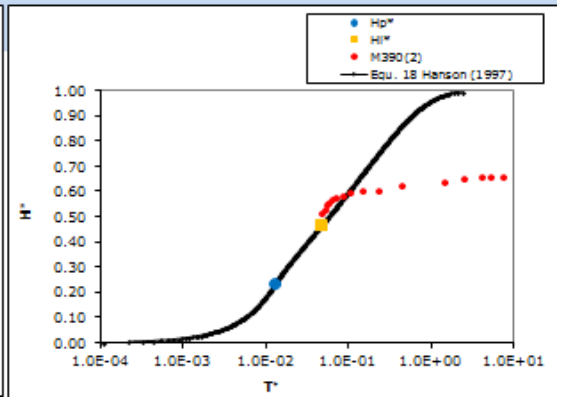


Figure B-6. Sample M390(2) Analysis Spreadsheet Printout for Hanson and Cook's (2004) Method using All Test Data

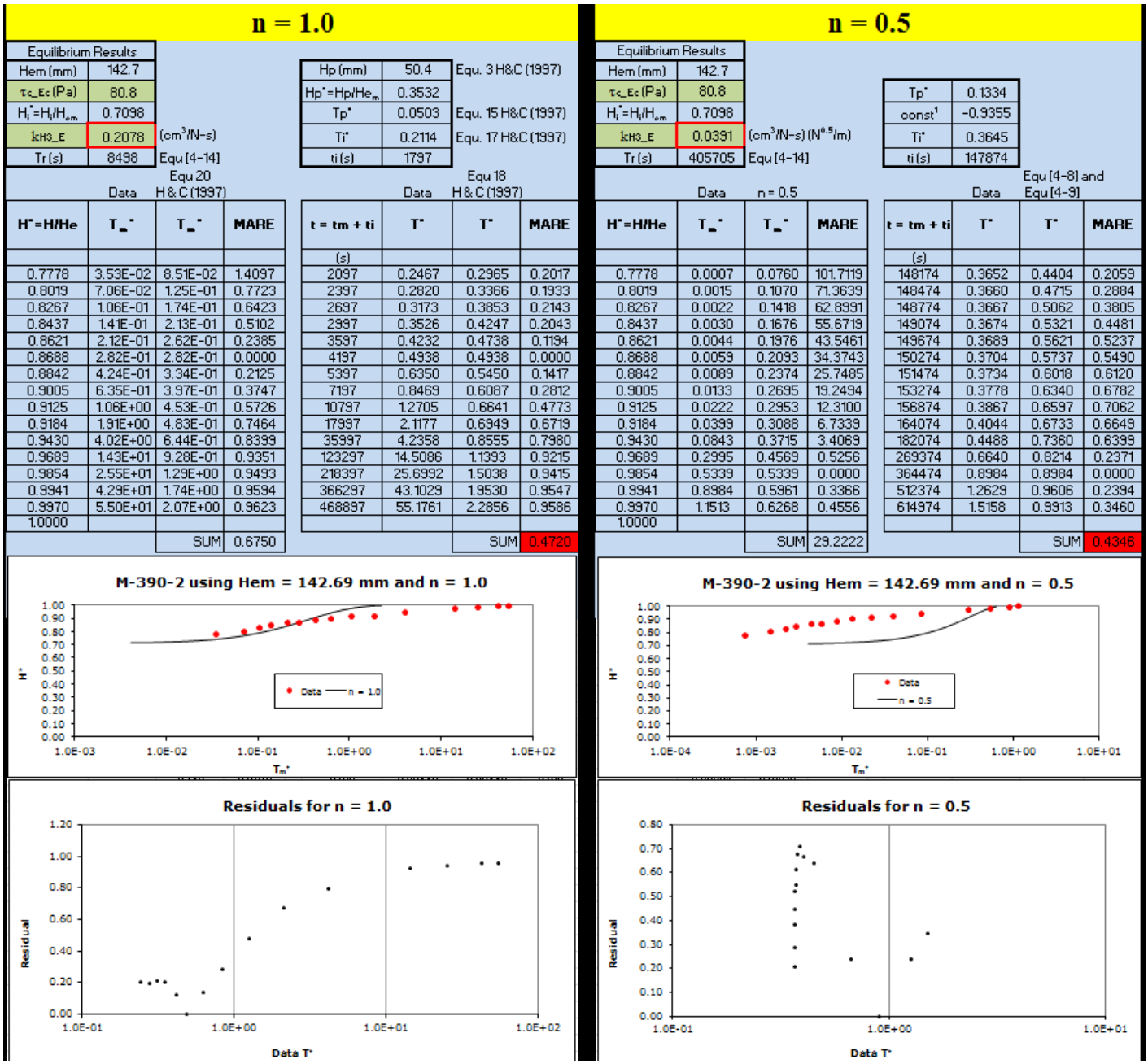


Figure B-7. Sample M390(2) Analysis Spreadsheet Printout for Hanson and Cook's (2004) Non-Linear Method (n = 1.0 and 0.5)

## n = 1.5

| Equilibrium Results | |
|---|---|
| Hem (mm) | 142.7 |
| $\tau_{c\_Ec}$ (Pa) | 80.8 |
| $H_i^* = H_i/H_{em}$ | 0.7098 |
| $k_{H3\_E}$ | 0.0320 |
| Tr (s) | 6143 |

$(cm^3/N\text{-}s)\,(m/N^{0.5})$

Equ [4-14]

| | |
|---|---|
| $Tp^*$ | 0.0190 |
| const[1] | 2.004 |
| $Ti^*$ | 0.1386 |
| ti (s) | 851 |

| | Data | n = 1.5 | | | Data | Equ [4-10] and Equ [4-11] | |
|---|---|---|---|---|---|---|---|
| $H^* = H/He$ | $T_{-}^*$ | $T_{-}^*$ | MARE | t = tm + ti | $T^*$ | $T^*$ | MARE |
| | | | | (s) | | | |
| 0.7778 | 0.0488 | 0.0956 | 0.9578 | 1151 | 0.1874 | 0.2342 | 0.2495 |
| 0.8019 | 0.0977 | 0.1473 | 0.5080 | 1451 | 0.2363 | 0.2859 | 0.2100 |
| 0.8267 | 0.1465 | 0.2159 | 0.4736 | 1751 | 0.2851 | 0.3545 | 0.2433 |
| 0.8437 | 0.1953 | 0.2757 | 0.4112 | 2051 | 0.3340 | 0.4143 | 0.2406 |
| 0.8621 | 0.2930 | 0.3560 | 0.2149 | 2651 | 0.4316 | 0.4946 | 0.1459 |
| 0.8688 | 0.3907 | 0.3907 | 0.0000 | 3251 | 0.5293 | 0.5293 | 0.0000 |
| 0.8842 | 0.5860 | 0.4841 | 0.1740 | 4451 | 0.7247 | 0.6227 | 0.1407 |
| 0.9005 | 0.8791 | 0.6103 | 0.3058 | 6251 | 1.0177 | 0.7489 | 0.2641 |
| 0.9125 | 1.4651 | 0.7292 | 0.5023 | 9851 | 1.6037 | 0.8678 | 0.4589 |
| 0.9184 | 2.6372 | 0.7994 | 0.6969 | 17051 | 2.7758 | 0.9380 | 0.6621 |
| 0.9430 | 5.5675 | 1.2126 | 0.7822 | 35051 | 5.7061 | 1.3512 | 0.7632 |
| 0.9689 | 19.7792 | 2.1636 | 0.8906 | 122351 | 19.9178 | 2.3022 | 0.8844 |
| 0.9854 | 35.2607 | 3.9106 | 0.8891 | 217451 | 35.3993 | 4.0492 | 0.8856 |
| 0.9941 | 59.3375 | 7.2139 | 0.8784 | 365351 | 59.4761 | 7.3525 | 0.8764 |
| 0.9970 | 76.0399 | 10.8442 | 0.8574 | 467951 | 76.1785 | 10.9828 | 0.8558 |
| 1.0000 | | | | | | | |
| | | SUM | 0.5695 | | | SUM | 0.4587 |

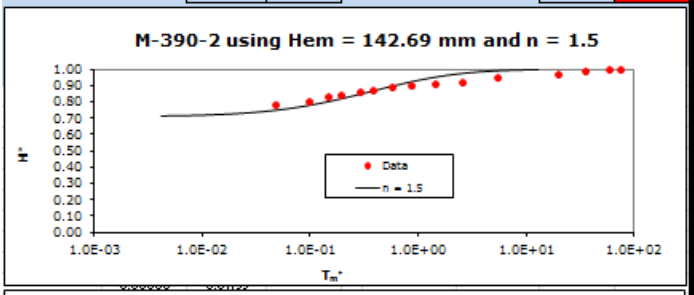


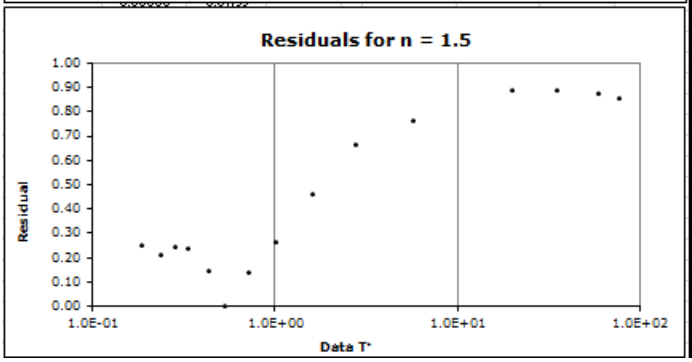


## n = 2.0

| Equilibrium Results | |
|---|---|
| Hem (mm) | 142.7 |
| $\tau_{c\_Ec}$ (Pa) | 80.8 |
| $H_i^* = H_i/H_{em}$ | 0.7098 |
| $k_{H3\_E}$ | 0.0050 |
| Tr (s) | 4336 |

$(cm^3/N\text{-}s)\,(m^2/N)$

Equ [4-14]

| | |
|---|---|
| $Tp^*$ | 0.0072 |
| const[1] | 0.0013 |
| $Ti^*$ | 0.1007 |
| ti (s) | 437 |

| | Data | n = 2.0 | | | Data | Equ [4-12] and Equ [4-13] | |
|---|---|---|---|---|---|---|---|
| $H^* = H/He$ | $T_{-}^*$ | $T_{-}^*$ | MARE | t = tm + ti | $T^*$ | $T^*$ | MARE |
| | | | | (s) | | | |
| 0.7778 | 0.0692 | 0.5672 | 7.1986 | 737 | 0.1699 | 0.2086 | 0.2275 |
| 0.8019 | 0.1384 | 0.8264 | 4.9728 | 1037 | 0.2391 | 0.2753 | 0.1514 |
| 0.8267 | 0.2075 | 1.1435 | 4.5098 | 1337 | 0.3083 | 0.3718 | 0.2060 |
| 0.8437 | 0.2767 | 1.4035 | 4.0719 | 1637 | 0.3775 | 0.4627 | 0.2259 |
| 0.8621 | 0.4151 | 1.7374 | 3.1855 | 2237 | 0.5158 | 0.5942 | 0.1520 |
| 0.8688 | 0.5534 | 1.8777 | 2.3928 | 2837 | 0.6542 | 0.6542 | 0.0000 |
| 0.8842 | 0.8302 | 2.2479 | 1.7078 | 4037 | 0.9309 | 0.8245 | 0.1143 |
| 0.9005 | 1.2453 | 2.7381 | 1.1988 | 5837 | 1.3460 | 1.0748 | 0.2015 |
| 0.9125 | 2.0754 | 3.1958 | 0.5398 | 9437 | 2.1762 | 1.3306 | 0.3886 |
| 0.9184 | 3.7358 | 3.4659 | 0.0722 | 16637 | 3.8365 | 1.4903 | 0.6115 |
| 0.9430 | 7.8866 | 5.0876 | 0.3549 | 34637 | 7.9874 | 2.5564 | 0.6799 |
| 0.9689 | 28.0183 | 9.2317 | 0.6705 | 121937 | 28.1190 | 5.7715 | 0.7947 |
| 0.9854 | 49.9487 | 18.8544 | 0.6225 | 217037 | 50.0494 | 14.2515 | 0.7153 |
| 0.9941 | 84.0550 | 44.9498 | 0.4652 | 364937 | 84.1557 | 38.9729 | 0.5369 |
| 0.9970 | 107.7149 | 85.9482 | 0.2021 | 467537 | 107.8156 | 78.9647 | 0.2676 |
| 1.0000 | | | | | | | |
| | | SUM | 2.1444 | | | SUM | 0.3515 |

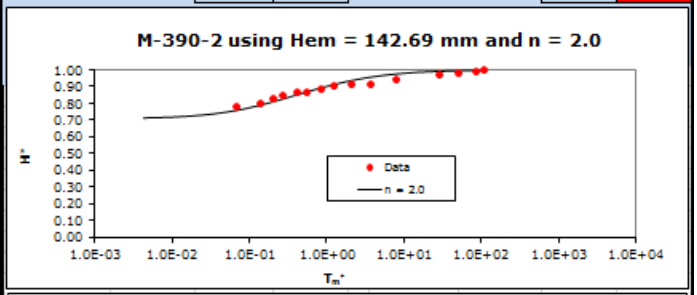


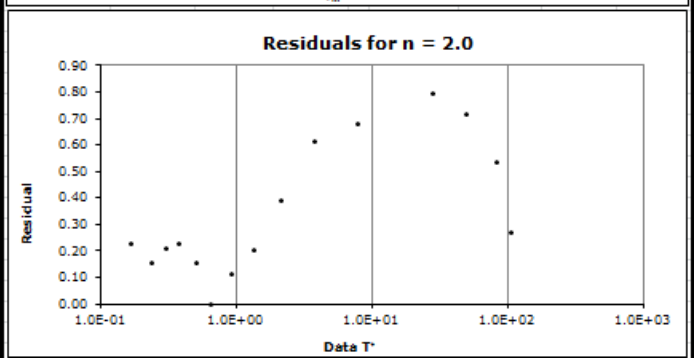


Figure B-8. Sample M390(2) Analysis Spreadsheet Printout for Hanson and Cook's (2004) Non-Linear Method (n = 1.5 and 2.0)

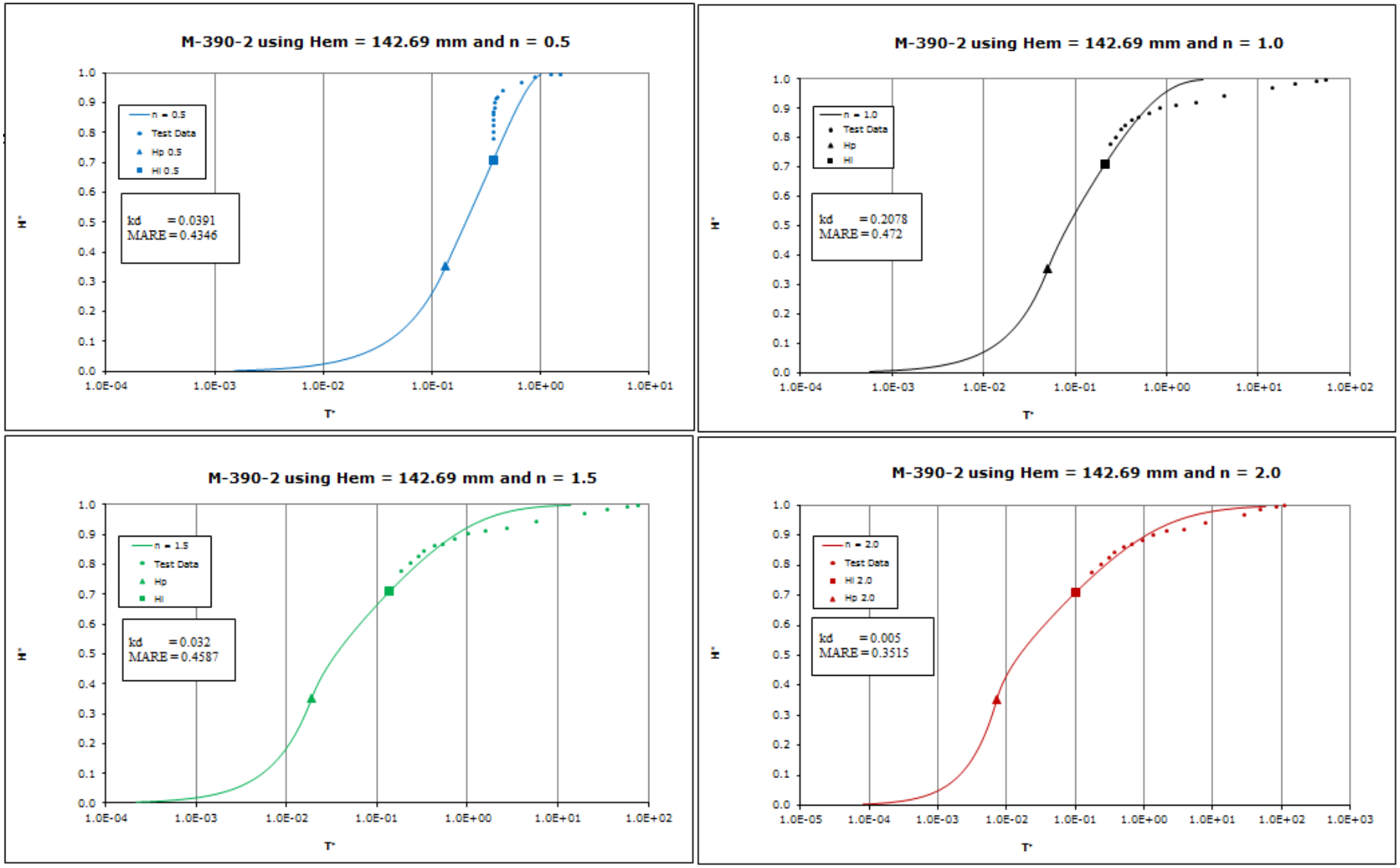


Figure B-9. Sample M390(2) Time Development of Scour Plots for Hanson and Cook's (2004) Non-Linear Analysis Method

**Hanson and Cook's (2004) Method 1** Analysis uses scour data up to and including 120 min of testing

**Sample Name and ID:** M-390-2

**Analysis By:** Dan Cossette

| | | |
|---|---|---|
| Jet diameter | d (mm) | 8 |
| Jet Height | $H_i$ (mm) | 101.28 |
| Flow Rate | Q ($m^3$/s) | 0.0006279 |
| Jet Velocity | $U_o$ (m/s) | 12.49 |
| Test Temperature | T (°C) | 22.8 |
| Kinematic Viscosity | μ ($m^2$/s) | 9.46E-07 |
| Jet Reynolds Number | $R_e$ | 105635 |
| Diffusion Coefficient | $C_D$ | 6.3 |
| Friction Coefficient | $C_f$ | 0.00416 |
| Combined Coefficient | $C_D^2C_f$ | 0.165 |
| **Maximum Shear Stress** | **$\tau_{cm}$ (Pa)** | **160.41** |

| Hanson 1 Results | | |
|---|---|---|
| fo | 1.519 | |
| $He_{B1}$ (mm) | 264.4 | Equ. [2-8] |
| **$\tau_{c\_B1}$ (Pa)** | **23.5** | Equ. [2-5] |
| $H_i^*=H_i/H_{eB}$ | 0.3830 | Equ [2-18] |
| **$k_{H1}$ ($cm^3$/N-s)** | **0.0897** | |
| Tr (s) | 125255 | Equ [2-16] |

| | | |
|---|---|---|
| Hp (mm) | 50.4 | Equ. 3 Hanson & Cook (1997) |
| $Hp^*=Hp/He_B$ | 0.1906 | |
| Tp* | 0.0072 | Equ. 15 Hanson & Cook (1997) |
| Ti* | 0.0254 | Equ. 17 Hanson & Cook (1997) |
| ti (s) | 3181 | |

| Measured Time, $t_m$ | | | Centerline Scour Depth, | H=e+Hi | H*=H/He | x | f | $A^2$ | Data $T_m^*$ | Equ 20 H & C (1997) $T_m^*$ | MARE | t = tm + ti | Data T* | Equ 18 H & C (1997) T* | MARE |
|---|---|---|---|---|---|---|---|---|---|---|---|---|---|---|---|
| (Min) | (Hrs) | (s) | (mm) | (mm) | | | | | | | | (s) | | | |
| 5 | 0:05 | 300 | 9.71 | 111.0 | 0.4197 | 5.671 | -4.528 | 4.418 | 2.40E-03 | 7.06E-03 | 1.9481 | 3481 | 0.02779 | 0.03246 | 0.1679 |
| 10 | 0:10 | 600 | 13.15 | 114.4 | 0.4327 | 5.972 | -4.816 | 4.477 | 4.79E-03 | 9.95E-03 | 1.0770 | 3781 | 0.03018 | 0.03534 | 0.1709 |
| 15 | 0:15 | 900 | 16.68 | 118.0 | 0.4461 | 6.148 | -4.979 | 4.434 | 7.19E-03 | 1.31E-02 | 0.8292 | 4081 | 0.03258 | 0.03854 | 0.1829 |
| 20 | 0:20 | 1200 | 19.11 | 120.4 | 0.4553 | 6.273 | -5.095 | 4.404 | 9.58E-03 | 1.55E-02 | 0.6164 | 4381 | 0.03498 | 0.04088 | 0.1688 |
| 30 | 0:30 | 1800 | 21.73 | 123.0 | 0.4652 | 6.449 | -5.262 | 4.398 | 1.44E-02 | 1.81E-02 | 0.2629 | 4981 | 0.03977 | 0.04354 | 0.0950 |
| 40 | 0:40 | 2400 | 22.69 | 124.0 | 0.4688 | 6.574 | -5.384 | 4.434 | 1.92E-02 | 1.92E-02 | 0.0000 | 5581 | 0.04456 | 0.04456 | 0.0000 |
| 60 | 1.00 | 3600 | 24.89 | 126.2 | 0.4771 | 6.750 | -5.552 | 4.442 | 2.87E-02 | 2.16E-02 | 0.2499 | 6781 | 0.05414 | 0.04695 | 0.1327 |
| 90 | 1.50 | 5400 | 27.21 | 128.5 | 0.4859 | 6.926 | -5.720 | 4.440 | 4.31E-02 | 2.42E-02 | 0.4385 | 8581 | 0.06851 | 0.04960 | 0.2760 |
| | | | | | | | $f_o$ | 1.519 | | SUM | 0.6778 | | | SUM | 0.1493 |
| | | | | | | | Average value | **4.431** | | | | | | | |
| | | | | | | | Stdev | 0.025 | | | | | | | |

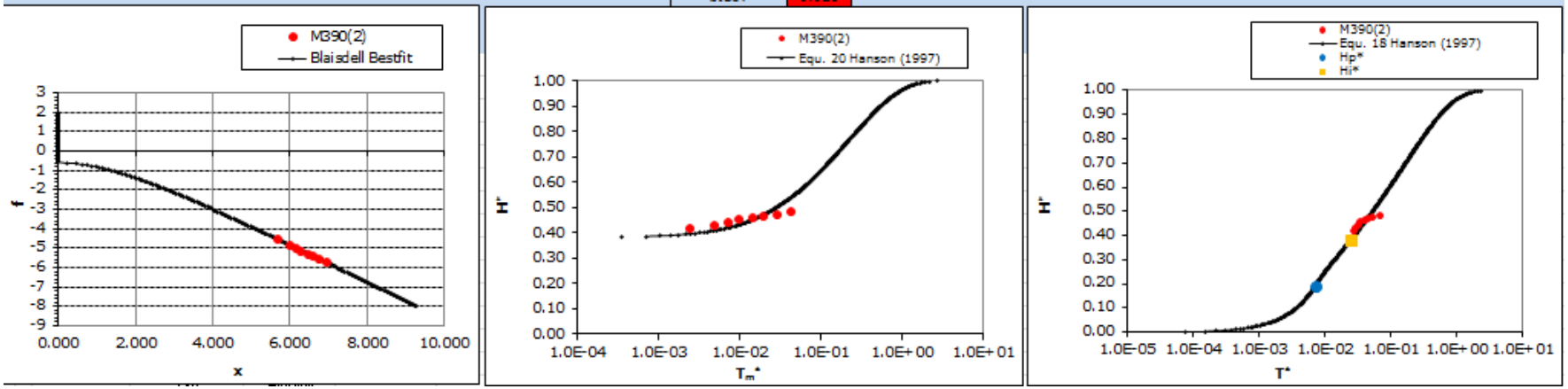


Figure B-4. Sample M390(2) Analysis Spreadsheet Printout for Hanson and Cook's (2004) Method using the First 120 Minutes of Test Data

**Hanson and Cook's (2004) Method 2** Analysis uses scour data up to and including first 10 readings

**Sample Name and ID:** M-390-2

**Analysis By:** Dan Cossette

| | | |
|---|---|---|
| Jet diameter | d (mm) | 8 |
| Jet Height | $H_i$ (mm) | 101.28 |
| Flow Rate | Q ($m^3/s$) | 0.0006279 |
| Jet Velocity | $U_o$ (m/s) | 12.49 |
| Test Temperature | T (°C) | 22.8 |
| Kinematic Viscosity | $\mu$ ($m^2/s$) | 9.46E-07 |
| Jet Reynolds Number | $R_e$ | 105635 |
| Diffusion Coefficient | $C_D$ | 6.3 |
| Friction Coefficient | $C_f$ | 0.00416 |
| Combined Coefficient | $C_D^2C_f$ | 0.165 |
| **Maximum Shear Stress** | **$\tau_{cm}$ (Pa)** | **160.41** |

| Hanson 2 Results | | |
|---|---|---|
| fo | 1.480 | |
| $He_{B2}$ (mm) | 241.9 | Equ. [2-8] |
| **$\tau_{c\_B2}$ (Pa)** | **28.1** | Equ. [2-5] |
| $H_i^*=H_i/H_{cB}$ | 0.4187 | Equ [2-18] |
| **$k_{H2}$ ($cm^3$/N-s)** | **0.0705** | |
| Tr (s) | 121908 | Equ [2-16] |

| | | |
|---|---|---|
| Hp (mm) | 50.4 | Equ. 3 Hanson & Cook (1997) |
| $Hp^*=Hp/He_B$ | 0.2084 | |
| Tp* | 0.0095 | Equ. 15 Hanson & Cook (1997) |
| Ti* | 0.0338 | Equ. 17 Hanson & Cook (1997) |
| ti (s) | 4119 | |

| Measured Time, $t_m$ | | | Centerline Scour Depth, | H=e+Hi | H*=H/He | x | f | $A^2$ | Equ 20 Data $T_m^*$ | Equ 20 H & C (1997) $T_m^*$ | Equ 20 MARE | t = tm + ti | Equ 18 Data T* | Equ 18 & C (1997) T* | Equ 18 MARE |
|---|---|---|---|---|---|---|---|---|---|---|---|---|---|---|---|
| (Min) | (Hrs) | (s) | (mm) | (mm) | | | | | | | | (s) | | | |
| 5 | 0:05 | 300 | 9.71 | 111.0 | 0.4589 | 5.671 | -4.528 | 3.951 | 2.46E-03 | 9.59E-03 | 2.8971 | 4419 | 0.03625 | 0.04338 | 0.1967 |
| 10 | 0:10 | 600 | 13.15 | 114.4 | 0.4731 | 5.972 | -4.816 | 3.988 | 4.92E-03 | 1.35E-02 | 1.7503 | 4719 | 0.03871 | 0.04732 | 0.2226 |
| 15 | 0:15 | 900 | 16.68 | 118.0 | 0.4877 | 6.148 | -4.979 | 3.932 | 7.38E-03 | 1.79E-02 | 1.4268 | 5019 | 0.04117 | 0.05170 | 0.2559 |
| 20 | 0:20 | 1200 | 19.11 | 120.4 | 0.4978 | 6.273 | -5.095 | 3.893 | 9.84E-03 | 2.11E-02 | 1.1474 | 5319 | 0.04363 | 0.05492 | 0.2589 |
| 30 | 0:30 | 1800 | 21.73 | 123.0 | 0.5086 | 6.449 | -5.262 | 3.873 | 1.48E-02 | 2.48E-02 | 0.6803 | 5919 | 0.04855 | 0.05860 | 0.2069 |
| 40 | 0:40 | 2400 | 22.69 | 124.0 | 0.5126 | 6.574 | -5.384 | 3.900 | 1.97E-02 | 2.62E-02 | 0.3313 | 6519 | 0.05347 | 0.06000 | 0.1220 |
| 60 | 1.00 | 3600 | 24.89 | 126.2 | 0.5217 | 6.750 | -5.552 | 3.895 | 2.95E-02 | 2.95E-02 | 0.0000 | 7719 | 0.06332 | 0.06332 | 0.0000 |
| 90 | 1.50 | 5400 | 27.21 | 128.5 | 0.5312 | 6.926 | -5.720 | 3.881 | 4.43E-02 | 3.32E-02 | 0.2503 | 9519 | 0.07808 | 0.06699 | 0.1420 |
| 150 | 2.50 | 9000 | 28.92 | 130.2 | 0.5383 | 7.148 | -5.936 | 3.917 | 7.38E-02 | 3.60E-02 | 0.5118 | 13119 | 0.10761 | 0.06983 | 0.3511 |
| 270 | 4.50 | 16200 | 29.77 | 131.1 | 0.5418 | 7.403 | -6.189 | 4.011 | 1.33E-01 | 3.75E-02 | 0.7179 | 20319 | 0.16667 | 0.07127 | 0.5724 |
| | | | | | | | $f_o$ | 1.480 | | SUM | 0.9713 | | | SUM | 0.2328 |
| | | | | | | | Average value | **3.924** | | | | | | | |
| | | | | | | | Stdev | 0.046 | | | | | | | |

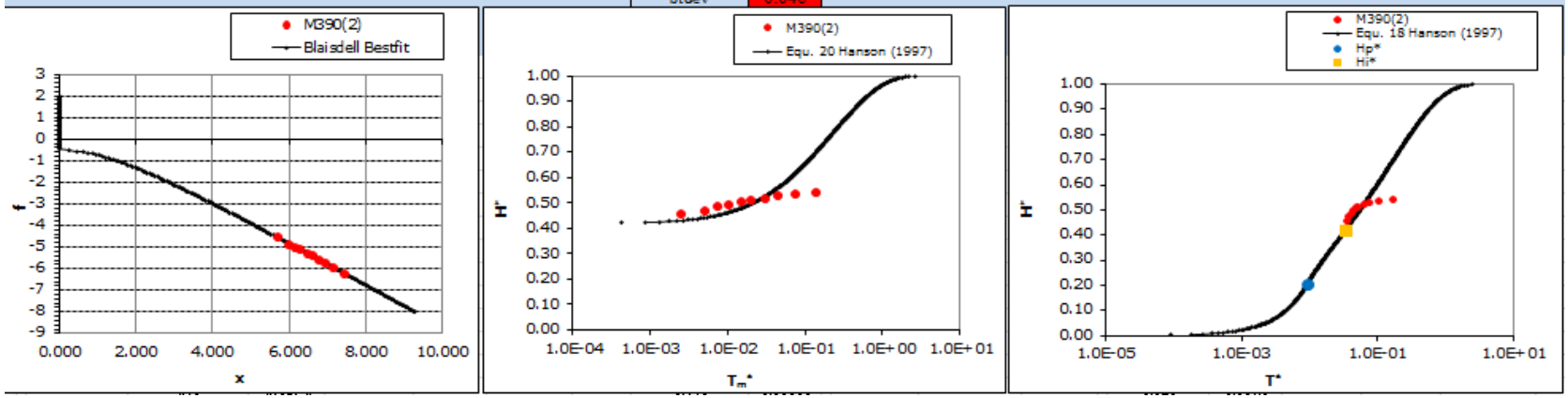


Figure B-5. Sample M390(2) Analysis Spreadsheet Printout for Hanson and Cook's (2004) Method using the First 10 Test Data Measurements

**Hanson and Cook's (2004) Method 3** Analysis uses all scour data

| | | |
|---|---|---|
| **Sample Name and ID:** | | M-390-2 |
| **Analysis By:** | | Dan Cossette |
| Jet diameter | d (mm) | 8 |
| Jet Height | $H_i$ (mm) | 101.28 |
| Flow Rate | Q ($m^3/s$) | 0.0006279 |
| Jet Velocity | $U_o$ (m/s) | 12.49 |
| Kinematic Viscosity | $\mu$ ($m^2/s$) | 9.46E-07 |
| Jet Reynolds Number | $R_e$ | 105635 |
| Diffusion Coefficient | $C_D$ | 6.3 |
| Friction Coefficient | $C_f$ | 0.00416 |
| Combined Coefficient | $C_D^2 C_f$ | 0.165 |
| **Maximum Shear Stress** | $\tau_{max}$ (Pa) | **160.41** |

| | | |
|---|---|---|
| fo | 1.437 | |
| $He_{B3}$ (mm) | 218.6 | Equ. [2-8] |
| $\tau_{c\ B3}$ (Pa) | **34.4** | Equ. [2-5] |
| $H_i^* = H_i/H_{eB}$ | 0.4633 | Equ [2-18] |
| $k_{B3}$ ($cm^3/N-s$) | **0.0755** | |
| Tr (s) | 84041 | Equ [2-16] |

| | | |
|---|---|---|
| Hp (mm) | 50.4 | Equ. 3 H&C (1997) |
| $Hp^* = Hp/He_B$ | 0.2306 | |
| $Tp^*$ | 0.0129 | Equ. 15 H&C (1997) |
| $Ti^*$ | 0.0469 | Equ. 17 H&C (1997) |
| ti (s) | 3945 | |

| Measured Time, $t_m$ | | | Centerline Scour Depth, | H=e+Hi | $H^*=H/He$ | x | f | $A^2$ | $T_m^*$ Data | $T_m^*$ Equ 20 H&C (1997) | MARE | t = tm + ti | $T^*$ Data | $T^*$ Equ 18 H&C (1997) | MARE |
|---|---|---|---|---|---|---|---|---|---|---|---|---|---|---|---|
| (Min) | (Hrs) | (s) | (mm) | (mm) | | | | | | | | (s) | | | |
| 5 | 0:05 | 300 | 9.71 | 111.0 | 0.5077 | 5.671 | -4.528 | 3.425 | 3.57E-03 | 1.37E-02 | 2.8463 | 4245 | 0.05051 | 0.06067 | 0.2012 |
| 10 | 0:10 | 600 | 13.15 | 114.4 | 0.5235 | 5.972 | -4.816 | 3.436 | 7.14E-03 | 1.94E-02 | 1.7216 | 4545 | 0.05408 | 0.06637 | 0.2273 |
| 15 | 0:15 | 900 | 16.68 | 118.0 | 0.5396 | 6.148 | -4.979 | 3.366 | 1.07E-02 | 2.58E-02 | 1.4084 | 4845 | 0.05765 | 0.07273 | 0.2617 |
| 20 | 0:20 | 1200 | 19.11 | 120.4 | 0.5507 | 6.273 | -5.095 | 3.317 | 1.43E-02 | 3.05E-02 | 1.1356 | 5145 | 0.06121 | 0.07743 | 0.2649 |
| 30 | 0:30 | 1800 | 21.73 | 123.0 | 0.5627 | 6.449 | -5.262 | 3.283 | 2.14E-02 | 3.59E-02 | 0.6752 | 5745 | 0.06835 | 0.08282 | 0.2116 |
| 40 | 0:40 | 2400 | 22.69 | 124.0 | 0.5671 | 6.574 | -5.384 | 3.299 | 2.86E-02 | 3.79E-02 | 0.3285 | 6345 | 0.07549 | 0.08487 | 0.1242 |
| 60 | 1.00 | 3600 | 24.89 | 126.2 | 0.5772 | 6.750 | -5.552 | 3.279 | 4.28E-02 | 4.28E-02 | 0.0000 | 7545 | 0.08977 | 0.08977 | 0.0000 |
| 90 | 1.50 | 5400 | 27.21 | 128.5 | 0.5878 | 6.926 | -5.720 | 3.250 | 6.43E-02 | 4.83E-02 | 0.2485 | 9345 | 0.11119 | 0.09522 | 0.1436 |
| 150 | 2.50 | 9000 | 28.92 | 130.2 | 0.5956 | 7.148 | -5.936 | 3.268 | 1.07E-01 | 5.25E-02 | 0.5097 | 12945 | 0.15403 | 0.09944 | 0.3544 |
| 270 | 4.50 | 16200 | 29.77 | 131.1 | 0.5995 | 7.403 | -6.189 | 3.339 | 1.93E-01 | 5.47E-02 | 0.7164 | 20145 | 0.23970 | 0.10160 | 0.5761 |
| 570 | 9.50 | 34200 | 33.27 | 134.6 | 0.6155 | 7.728 | -6.502 | 3.302 | 4.07E-01 | 6.40E-02 | 0.8427 | 38145 | 0.45388 | 0.11097 | 0.7555 |
| 2025 | 33.75 | 121500 | 36.97 | 138.3 | 0.6325 | 8.278 | -7.041 | 3.334 | 1.45E+00 | 7.48E-02 | 0.9482 | 125445 | 1.49267 | 0.12176 | 0.9184 |
| 3610 | 60.17 | 216600 | 39.32 | 140.6 | 0.6432 | 8.529 | -7.284 | 3.306 | 2.58E+00 | 8.22E-02 | 0.9681 | 220545 | 2.62426 | 0.12914 | 0.9508 |
| 6075 | 101.25 | 364500 | 40.57 | 141.9 | 0.6489 | 8.755 | -7.507 | 3.324 | 4.34E+00 | 8.63E-02 | 0.9801 | 368445 | 4.38412 | 0.13324 | 0.9696 |
| 7785 | 129.75 | 467100 | 40.98 | 142.3 | 0.6508 | 8.863 | -7.613 | 3.342 | 5.56E+00 | 8.77E-02 | 0.9842 | 471045 | 5.60496 | 0.13461 | 0.9760 |
| 10530 | 175.50 | 631800 | 41.41 | 142.7 | 0.6528 | 8.994 | -7.743 | 3.367 | 7.52E+00 | 8.91E-02 | 0.9881 | 635745 | 7.56473 | 0.13606 | 0.9820 |
| | | | | | | | $f_o$ | 1.437 | | SUM | 0.9584 | | | SUM | 0.5238 |
| | | | | | | | Average value | **3.332** | | | | | | | |
| | | | | | | | Stdev | 0.055 | | | | | | | |

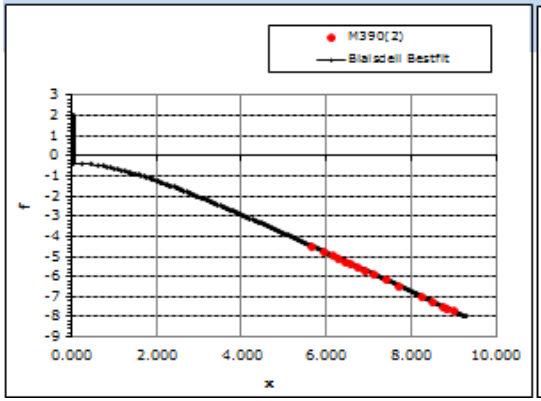


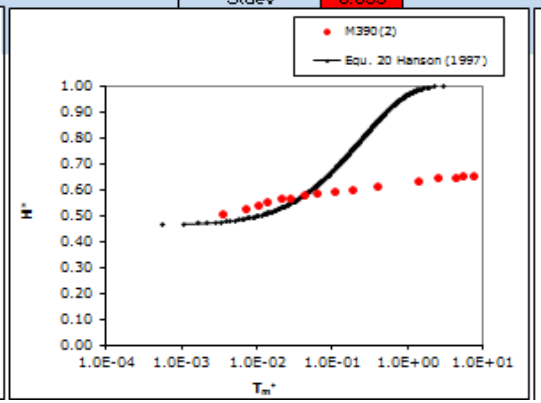


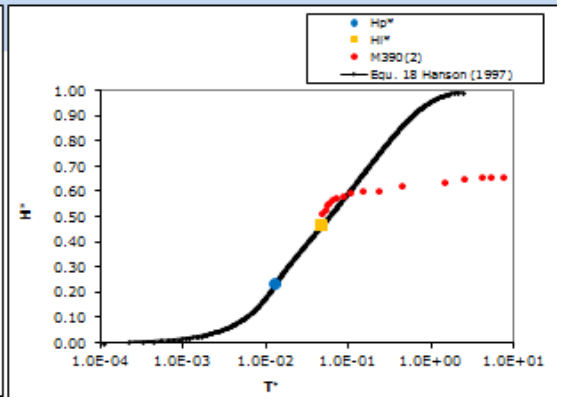


Figure B-6. Sample M390(2) Analysis Spreadsheet Printout for Hanson and Cook's (2004) Method using All Test Data

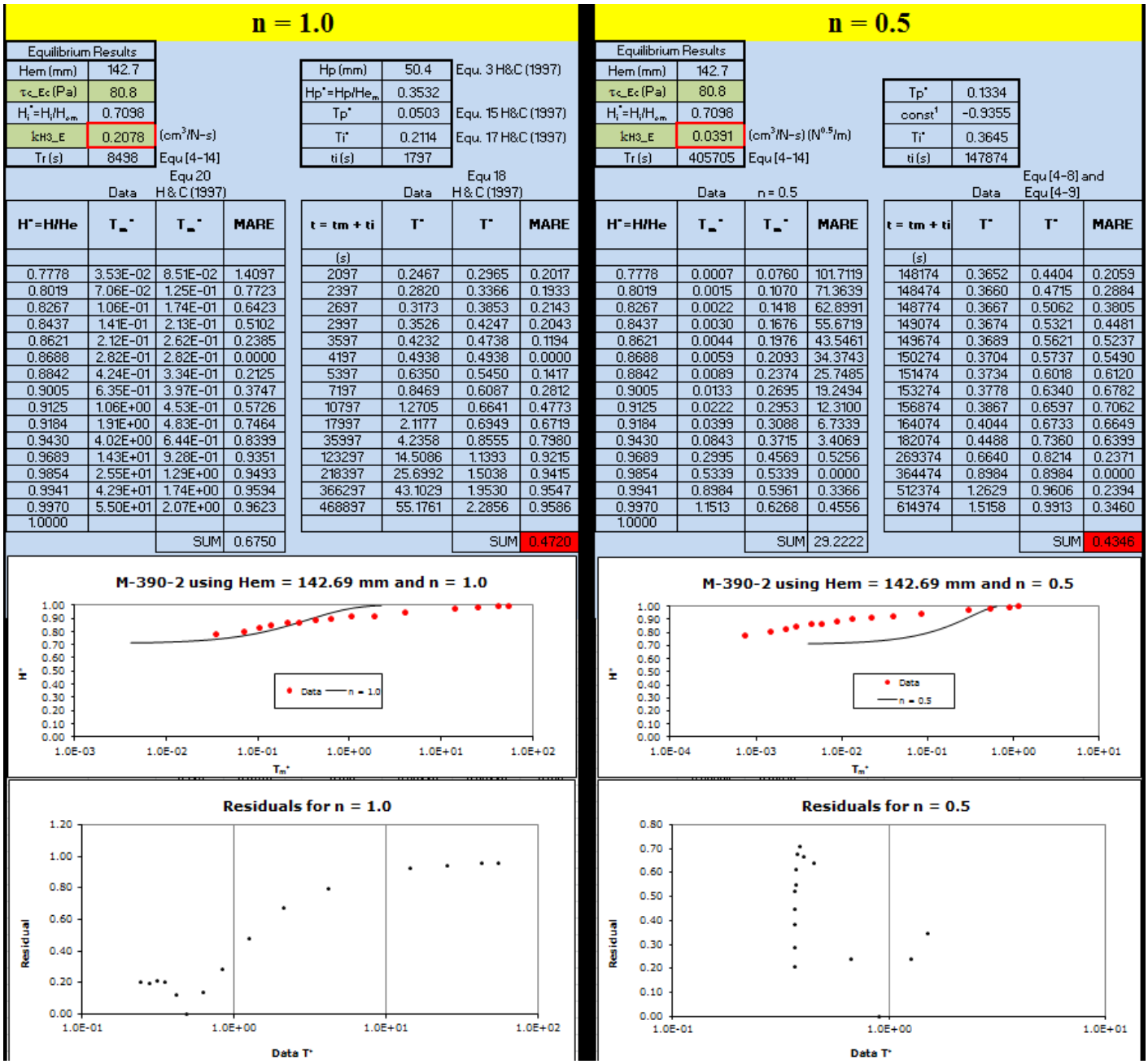


Figure B-7. Sample M390(2) Analysis Spreadsheet Printout for Hanson and Cook's (2004) Non-Linear Method (n = 1.0 and 0.5)

## n = 1.5

| Equilibrium Results | |
|---|---|
| Hem (mm) | 142.7 |
| $\tau_{c\_Ec}$ (Pa) | 80.8 |
| $H_i^* = H_i/H_{em}$ | 0.7098 |
| $k_{H3\_E}$ | 0.0320 |
| Tr (s) | 6143 |

$(cm^3/N\text{-}s)\,(m/N^{0.5})$

Equ [4-14]

| | |
|---|---|
| $Tp^*$ | 0.0190 |
| const[1] | 2.004 |
| $Ti^*$ | 0.1386 |
| ti (s) | 851 |

| | Data | n = 1.5 | | | Data | Equ [4-10] and Equ [4-11] | |
|---|---|---|---|---|---|---|---|
| $H^* = H/He$ | $T_{-}^*$ | $T_{-}^*$ | MARE | t = tm + ti | $T^*$ | $T^*$ | MARE |
| | | | | (s) | | | |
| 0.7778 | 0.0488 | 0.0956 | 0.9578 | 1151 | 0.1874 | 0.2342 | 0.2495 |
| 0.8019 | 0.0977 | 0.1473 | 0.5080 | 1451 | 0.2363 | 0.2859 | 0.2100 |
| 0.8267 | 0.1465 | 0.2159 | 0.4736 | 1751 | 0.2851 | 0.3545 | 0.2433 |
| 0.8437 | 0.1953 | 0.2757 | 0.4112 | 2051 | 0.3340 | 0.4143 | 0.2406 |
| 0.8621 | 0.2930 | 0.3560 | 0.2149 | 2651 | 0.4316 | 0.4946 | 0.1459 |
| 0.8688 | 0.3907 | 0.3907 | 0.0000 | 3251 | 0.5293 | 0.5293 | 0.0000 |
| 0.8842 | 0.5860 | 0.4841 | 0.1740 | 4451 | 0.7247 | 0.6227 | 0.1407 |
| 0.9005 | 0.8791 | 0.6103 | 0.3058 | 6251 | 1.0177 | 0.7489 | 0.2641 |
| 0.9125 | 1.4651 | 0.7292 | 0.5023 | 9851 | 1.6037 | 0.8678 | 0.4589 |
| 0.9184 | 2.6372 | 0.7994 | 0.6969 | 17051 | 2.7758 | 0.9380 | 0.6621 |
| 0.9430 | 5.5675 | 1.2126 | 0.7822 | 35051 | 5.7061 | 1.3512 | 0.7632 |
| 0.9689 | 19.7792 | 2.1636 | 0.8906 | 122351 | 19.9178 | 2.3022 | 0.8844 |
| 0.9854 | 35.2607 | 3.9106 | 0.8891 | 217451 | 35.3993 | 4.0492 | 0.8856 |
| 0.9941 | 59.3375 | 7.2139 | 0.8784 | 365351 | 59.4761 | 7.3525 | 0.8764 |
| 0.9970 | 76.0399 | 10.8442 | 0.8574 | 467951 | 76.1785 | 10.9828 | 0.8558 |
| 1.0000 | | | | | | | |
| | | SUM | 0.5695 | | | SUM | 0.4587 |

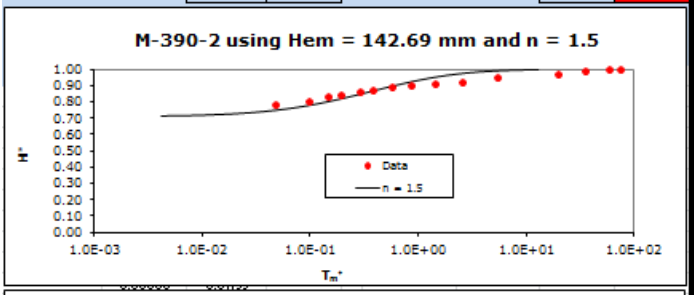


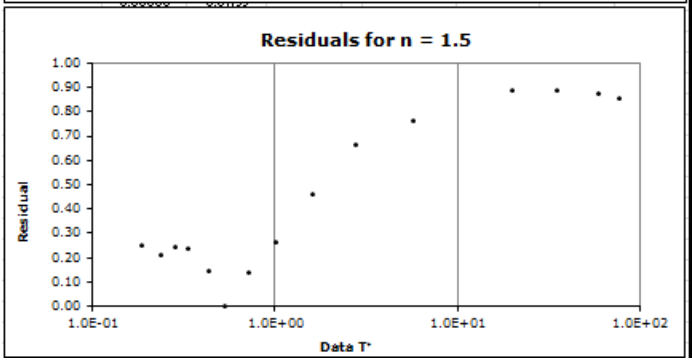


## n = 2.0

| Equilibrium Results | |
|---|---|
| Hem (mm) | 142.7 |
| $\tau_{c\_Ec}$ (Pa) | 80.8 |
| $H_i^* = H_i/H_{em}$ | 0.7098 |
| $k_{H3\_E}$ | 0.0050 |
| Tr (s) | 4336 |

$(cm^3/N\text{-}s)\,(m^2/N)$

Equ [4-14]

| | |
|---|---|
| $Tp^*$ | 0.0072 |
| const[1] | 0.0013 |
| $Ti^*$ | 0.1007 |
| ti (s) | 437 |

| | Data | n = 2.0 | | | Data | Equ [4-12] and Equ [4-13] | |
|---|---|---|---|---|---|---|---|
| $H^* = H/He$ | $T_{-}^*$ | $T_{-}^*$ | MARE | t = tm + ti | $T^*$ | $T^*$ | MARE |
| | | | | (s) | | | |
| 0.7778 | 0.0692 | 0.5672 | 7.1986 | 737 | 0.1699 | 0.2086 | 0.2275 |
| 0.8019 | 0.1384 | 0.8264 | 4.9728 | 1037 | 0.2391 | 0.2753 | 0.1514 |
| 0.8267 | 0.2075 | 1.1435 | 4.5098 | 1337 | 0.3083 | 0.3718 | 0.2060 |
| 0.8437 | 0.2767 | 1.4035 | 4.0719 | 1637 | 0.3775 | 0.4627 | 0.2259 |
| 0.8621 | 0.4151 | 1.7374 | 3.1855 | 2237 | 0.5158 | 0.5942 | 0.1520 |
| 0.8688 | 0.5534 | 1.8777 | 2.3928 | 2837 | 0.6542 | 0.6542 | 0.0000 |
| 0.8842 | 0.8302 | 2.2479 | 1.7078 | 4037 | 0.9309 | 0.8245 | 0.1143 |
| 0.9005 | 1.2453 | 2.7381 | 1.1988 | 5837 | 1.3460 | 1.0748 | 0.2015 |
| 0.9125 | 2.0754 | 3.1958 | 0.5398 | 9437 | 2.1762 | 1.3306 | 0.3886 |
| 0.9184 | 3.7358 | 3.4659 | 0.0722 | 16637 | 3.8365 | 1.4903 | 0.6115 |
| 0.9430 | 7.8866 | 5.0876 | 0.3549 | 34637 | 7.9874 | 2.5564 | 0.6799 |
| 0.9689 | 28.0183 | 9.2317 | 0.6705 | 121937 | 28.1190 | 5.7715 | 0.7947 |
| 0.9854 | 49.9487 | 18.8544 | 0.6225 | 217037 | 50.0494 | 14.2515 | 0.7153 |
| 0.9941 | 84.0550 | 44.9498 | 0.4652 | 364937 | 84.1557 | 38.9729 | 0.5369 |
| 0.9970 | 107.7149 | 85.9482 | 0.2021 | 467537 | 107.8156 | 78.9647 | 0.2676 |
| 1.0000 | | | | | | | |
| | | SUM | 2.1444 | | | SUM | 0.3515 |

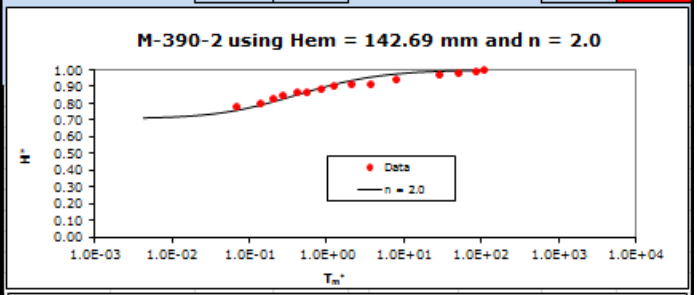


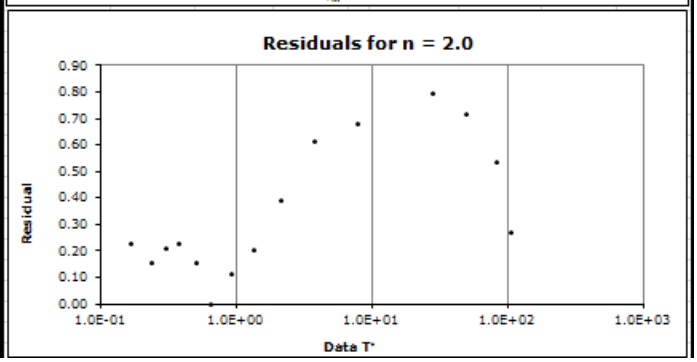


Figure B-8. Sample M390(2) Analysis Spreadsheet Printout for Hanson and Cook's (2004) Non-Linear Method (n = 1.5 and 2.0)

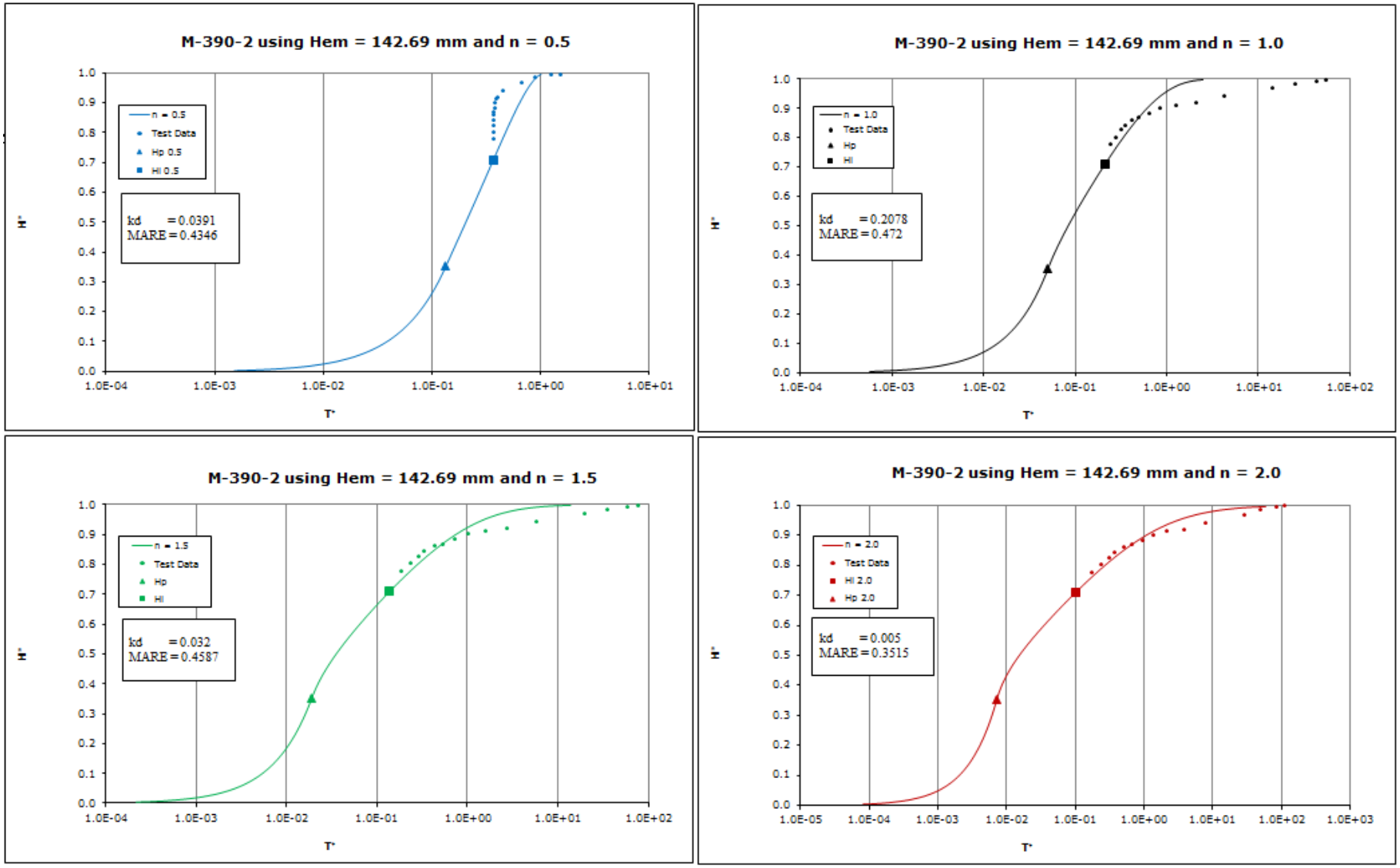


Figure B-9. Sample M390(2) Time Development of Scour Plots for Hanson and Cook's (2004) Non-Linear Analysis Method

## Thomas' Method

**Sample Name and ID:** M-390-2

**Analysis By:** Dan Cossette

| | | |
|---|---|---|
| Jet diameter | d (mm) | 8.000 |
| Flow Area at Nozzle | A ($m^2$) | 5.03E-05 |
| Jet Height | $H_i$ (mm) | 101.28 |
| | $H_i/d$ | 12.66 |
| Flow Rate | Q ($m^3/s$) | 0.0006279 |
| Jet Velocity | $U_o$ (m/s) | 12.49 |
| Test Temperature | T (°C) | 22.8 |
| Fluid Density | ρ ($kg/m^3$) | 997.7 |
| Kinematic Viscosity | μ ($m^2/s$) | 9.46E-07 |
| Jet Reynolds Number | $R_e$ | 105635 |
| Diffusion Coefficient | $C_D$ | 6.3 |
| Friction Coefficient | $C_f$ | 0.00416 |
| Combined Coefficient | $C_D^2 C_f$ | 0.165 |
| **Maximum Shear Stress** | **τom (Pa)** | 160.41 |

LINEST

y = mx + b

–or–

y = m1x1 + m2x2 + ... + b

LOGEST

y = b*m^x

or

y = (b*(m1^x1)*(m2^x2)*_)

| | A | B | C | D | E | F |
|---|---|---|---|---|---|---|
| 1 | $m_n$ | $m_{n-1}$ | . . . | $m_2$ | $m_1$ | b |
| 2 | $se_n$ | $se_{n-1}$ | . . . | $se_2$ | $se_1$ | $se_b$ |
| 3 | $r^2$ | $se_y$ | | | | |
| 4 | F | $d_f$ | | | | |
| 5 | $ss_{reg}$ | $ss_{resid}$ | | | | |

**Erodibility Parameters**

| Thomas 1 | | | Thomas 2 | | | Thomas 3 | | |
|---|---|---|---|---|---|---|---|---|
| τc_T1 (Pa) | 101.4 | calculated from 'b' | τc_T2 (Pa) | 96.3 | calculated from 'b' | τc_T3 (Pa) | 80.8 | calculated from 'b' |
| kT1 | 0.130 | | kT2 | 0.034 | | kT3 | 0.002 | |
| nT1 | 1.44 | | nT2 | 1.75 | | nT3 | 2.35 | |

Erosion Rate vs Tavg

Linear Function Parameters: m = slope, b = intercept

| | Thomas 1 m | Thomas 1 b | Thomas 1 $R^2$ | Thomas 2 m | Thomas 2 b | Thomas 2 $R^2$ | Thomas 3 m | Thomas 3 b | Thomas 3 $R^2$ |
|---|---|---|---|---|---|---|---|---|---|
| Linear | 6.68E-04 | -0.0694 | 0.9213 | 6.01E-04 | -0.0608 | 0.9049 | 0.0004 | -0.0360 | 0.7693 |

Erosion Rate vs Excess Shear Stress

Power Function Parameters: m = coefficient, n = exponent

| | Thomas 1 m | Thomas 1 n | Thomas 1 RSS | Thomas 1 $R^2$ | Thomas 2 m | Thomas 2 n | Thomas 2 RSS | Thomas 2 $R^2$ | Thomas 3 m | Thomas 3 n | Thomas 3 RSS | Thomas 3 $R^2$ |
|---|---|---|---|---|---|---|---|---|---|---|---|---|
| Initial | 1.00E-01 | 1.00 | | | 1.00E-01 | 1.00 | | | 1.00E-01 | 1.00 | | |
| Final | 1.30E-04 | 1.4391 | 0.0056 | 0.9613 | 3.38E-05 | 1.7453 | 0.0051 | 0.9709 | 1.56E-06 | 2.3486 | 0.0058 | 0.9754 |

For a linear excess shear stress function (n = 1.0) the erodibility coefficient kT1 = 0.668 $cm^3/N\text{-}s$

| Measured Time, $t_m$ | | | Centerline Scour Depth, $e_c$ | H=e+Hi | All Data Points | | | | | Thomas 1 | | | | | Thomas 2 | | | | | Thomas 3 | | | | |
|---|---|---|---|---|---|---|---|---|---|---|---|---|---|---|---|---|---|---|---|---|---|---|---|---|
| | | | | | Erosion rate | τ | $\tau_{avg}$ (linear) | $\tau_{avg}$ (nonlin) | t-tc | Erosion rate | τ | τavg (nonlin) | t-tc | Erosion rate (model) | Erosion rate | τ | τavg (nonlin) | t-tc | Erosion rate (model) | Erosion rate | τ | τavg (nonlin) | t-tc | Erosion rate (model) |
| (Min) | (Hrs) | (s) | (mm) | (mm) | (mm/s) | (Pa) | (Pa) | (Pa) | (Pa) | (mm/s) | (Pa) | (Pa) | (Pa) | (mm/s) | (mm/s) | (Pa) | (Pa) | (Pa) | (mm/s) | (mm/s) | (Pa) | (Pa) | (Pa) | (mm/s) |
| 0 | 0 | 0 | 0 | 101.3 | - | 160.4 | - | - | 79.6 | - | 160.4 | - | 59.0 | | - | 160.4 | - | 64.1 | | - | 160.4 | - | 79.6 | |
| 5 | 0:05 | 300 | 9.71 | 111.0 | 3.24E-02 | 133.6 | 147.0 | 146.4 | 65.6 | 3.24E-02 | 133.6 | 146.4 | 45.0 | 3.11E-02 | 3.24E-02 | 133.6 | 146.4 | 50.1 | 3.13E-02 | 3.24E-02 | 133.6 | 146.4 | 65.6 | 2.88E-02 |
| 10 | 0:10 | 600 | 13.15 | 114.4 | 1.15E-02 | 125.7 | 129.6 | 129.6 | 48.7 | 1.15E-02 | 125.7 | 129.6 | 28.2 | 1.59E-02 | 1.15E-02 | 125.7 | 129.6 | 33.3 | 1.53E-02 | 1.15E-02 | 125.7 | 129.6 | 48.7 | 1.44E-02 |
| 15 | 0:15 | 900 | 16.68 | 118.0 | 1.18E-02 | 118.3 | 122.0 | 121.9 | 41.1 | 1.18E-02 | 118.3 | 121.9 | 20.5 | 1.00E-02 | 1.18E-02 | 118.3 | 121.9 | 25.6 | 9.70E-03 | 1.18E-02 | 118.3 | 121.9 | 41.1 | 9.62E-03 |
| 20 | 0:20 | 1200 | 19.11 | 120.4 | 8.10E-03 | 113.5 | 115.9 | 115.9 | 35.1 | 8.10E-03 | 113.5 | 115.9 | 14.5 | 6.08E-03 | 8.10E-03 | 113.5 | 115.9 | 19.6 | 6.07E-03 | 8.10E-03 | 113.5 | 115.9 | 35.1 | 6.62E-03 |
| 30 | 0:30 | 1800 | 21.73 | 123.0 | 4.37E-03 | 108.7 | 111.1 | 111.1 | 30.3 | 4.37E-03 | 108.7 | 111.1 | 9.7 | 3.43E-03 | 4.37E-03 | 108.7 | 111.1 | 14.8 | 3.73E-03 | 4.37E-03 | 108.7 | 111.1 | 30.3 | 4.70E-03 |
| 40 | 0:40 | 2400 | 22.69 | 124.0 | 1.60E-03 | 107.1 | 107.9 | 107.9 | 27.1 | 1.60E-03 | 107.1 | 107.9 | 6.5 | 1.92E-03 | 1.60E-03 | 107.1 | 107.9 | 11.6 | 2.44E-03 | 1.60E-03 | 107.1 | 107.9 | 27.1 | 3.62E-03 |
| 60 | 1.0 | 3600 | 24.89 | 126.2 | 1.83E-03 | 103.4 | 105.2 | 105.2 | 24.4 | 1.83E-03 | 103.4 | 105.2 | 3.8 | 8.87E-04 | 1.83E-03 | 103.4 | 105.2 | 8.9 | 1.53E-03 | 1.83E-03 | 103.4 | 105.2 | 24.4 | 2.82E-03 |
| 90 | 1.5 | 5400 | 27.21 | 128.5 | 1.29E-03 | 99.7 | 101.5 | 101.5 | 20.7 | 1.29E-03 | 99.7 | 101.5 | 0.1 | 4.53E-06 | 1.29E-03 | 99.7 | 101.5 | 5.2 | 6.00E-04 | 1.29E-03 | 99.7 | 101.5 | 20.7 | 1.92E-03 |
| 150 | 2.5 | 9000 | 28.92 | 130.2 | 4.75E-04 | 97.1 | 98.4 | 98.4 | 17.5 | | | | | | 4.75E-04 | 97.1 | 98.4 | 2.1 | 1.19E-04 | 4.75E-04 | 97.1 | 98.4 | 17.5 | 1.30E-03 |
| 270 | 4.5 | 16200 | 29.77 | 131.1 | 1.18E-04 | 95.8 | 96.4 | 96.4 | 15.6 | | | | | | 1.18E-04 | 95.8 | 96.4 | 0.1 | 1.01E-06 | 1.18E-04 | 95.8 | 96.4 | 15.6 | 9.92E-04 |
| 570 | 9.5 | 34200 | 33.27 | 134.6 | 1.94E-04 | 90.9 | 93.3 | 93.3 | 12.5 | | | | | | | | | | | 1.94E-04 | 90.9 | 93.3 | 12.5 | 5.88E-04 |
| 2025 | 33.8 | 121500 | 36.97 | 138.3 | 4.24E-05 | 86.1 | 88.5 | 88.5 | 7.6 | | | | | | | | | | | 4.24E-05 | 86.1 | 88.5 | 7.6 | 1.85E-04 |
| 3610 | 60.2 | 216600 | 39.32 | 140.6 | 2.47E-05 | 83.2 | 84.7 | 84.7 | 3.8 | | | | | | | | | | | 2.47E-05 | 83.2 | 84.7 | 3.8 | 3.67E-05 |
| 6075 | 101.3 | 364500 | 40.57 | 141.9 | 8.45E-06 | 81.8 | 82.5 | 82.5 | 1.7 | | | | | | | | | | | 8.45E-06 | 81.8 | 82.5 | 1.7 | 5.33E-06 |
| 7785 | 129.8 | 467100 | 40.98 | 142.3 | 4.00E-06 | 81.3 | 81.5 | 81.5 | 0.7 | | | | | | | | | | | 4.00E-06 | 81.3 | 81.5 | 0.7 | 7.32E-07 |
| 10530 | 175.5 | 631800 | 41.41 | 142.7 | 2.61E-06 | 80.8 | 81.1 | 81.1 | 0.2 | | | | | | | | | | | 2.61E-06 | 80.8 | 81.1 | 0.2 | 5.70E-08 |
| 14160 | 236.0 | 849600 | 41.38 | 142.7 | -1.38E-07 | 80.8 | 80.8 | 80.8 | 0.0 | | | | | | | | | | | | | | | |

Figure B-10. Sample M390(2) Analysis Spreadsheet Printout for Thomas' Method

## Thomas' Method

**Sample Name and ID:** M-390-2

**Analysis By:** Dan Cossette

| | | |
|---|---|---|
| Jet diameter | d (mm) | 8.000 |
| Flow Area at Nozzle | A ($m^2$) | 5.03E-05 |
| Jet Height | $H_i$ (mm) | 101.28 |
| | $H_i/d$ | 12.66 |
| Flow Rate | Q ($m^3/s$) | 0.0006279 |
| Jet Velocity | $U_o$ (m/s) | 12.49 |
| Test Temperature | T (°C) | 22.8 |
| Fluid Density | ρ ($kg/m^3$) | 997.7 |
| Kinematic Viscosity | μ ($m^2/s$) | 9.46E-07 |
| Jet Reynolds Number | $R_e$ | 105635 |
| Diffusion Coefficient | $C_D$ | 6.3 |
| Friction Coefficient | $C_f$ | 0.00416 |
| Combined Coefficient | $C_D^2 C_f$ | 0.165 |
| **Maximum Shear Stress** | **τom (Pa)** | 160.41 |

LINEST

y = mx + b

–or–

y = m1x1 + m2x2 + ... + b

LOGEST

y = b*m^x

or

y = (b*(m1^x1)*(m2^x2)*_)

| | A | B | C | D | E | F |
|---|---|---|---|---|---|---|
| 1 | $m_n$ | $m_{n-1}$ | . . . | $m_2$ | $m_1$ | b |
| 2 | $se_n$ | $se_{n-1}$ | . . . | $se_2$ | $se_1$ | $se_b$ |
| 3 | $r^2$ | $se_y$ | | | | |
| 4 | F | $d_f$ | | | | |
| 5 | $ss_{reg}$ | $ss_{resid}$ | | | | |

**Erodibility Parameters**

| Thomas 1 | | | Thomas 2 | | | Thomas 3 | | |
|---|---|---|---|---|---|---|---|---|
| τc_T1 (Pa) | 101.4 | calculated from 'b' | τc_T2 (Pa) | 96.3 | calculated from 'b' | τc_T3 (Pa) | 80.8 | calculated from 'b' |
| kT1 | 0.130 | | kT2 | 0.034 | | kT3 | 0.002 | |
| nT1 | 1.44 | | nT2 | 1.75 | | nT3 | 2.35 | |

Erosion Rate vs Tavg

Linear Function Parameters: m = slope, b = intercept

| | Thomas 1 m | Thomas 1 b | Thomas 1 $R^2$ | Thomas 2 m | Thomas 2 b | Thomas 2 $R^2$ | Thomas 3 m | Thomas 3 b | Thomas 3 $R^2$ |
|---|---|---|---|---|---|---|---|---|---|
| Linear | 6.68E-04 | -0.0694 | 0.9213 | 6.01E-04 | -0.0608 | 0.9049 | 0.0004 | -0.0360 | 0.7693 |

Erosion Rate vs Excess Shear Stress

Power Function Parameters: m = coefficient, n = exponent

| | Thomas 1 m | Thomas 1 n | Thomas 1 RSS | Thomas 1 $R^2$ | Thomas 2 m | Thomas 2 n | Thomas 2 RSS | Thomas 2 $R^2$ | Thomas 3 m | Thomas 3 n | Thomas 3 RSS | Thomas 3 $R^2$ |
|---|---|---|---|---|---|---|---|---|---|---|---|---|
| Initial | 1.00E-01 | 1.00 | | | 1.00E-01 | 1.00 | | | 1.00E-01 | 1.00 | | |
| Final | 1.30E-04 | 1.4391 | 0.0056 | 0.9613 | 3.38E-05 | 1.7453 | 0.0051 | 0.9709 | 1.56E-06 | 2.3486 | 0.0058 | 0.9754 |

For a linear excess shear stress function (n = 1.0) the erodibility coefficient kT1 = 0.668 $cm^3/N\text{-}s$

| Measured Time, $t_m$ | | | Centerline Scour Depth, $e_c$ | H=e+Hi | All Data Points | | | | | Thomas 1 | | | | | Thomas 2 | | | | | Thomas 3 | | | | |
|---|---|---|---|---|---|---|---|---|---|---|---|---|---|---|---|---|---|---|---|---|---|---|---|---|
| | | | | | Erosion rate | τ | $\tau_{avg}$ (linear) | $\tau_{avg}$ (nonlin) | t-tc | Erosion rate | τ | τavg (nonlin) | t-tc | Erosion rate (model) | Erosion rate | τ | τavg (nonlin) | t-tc | Erosion rate (model) | Erosion rate | τ | τavg (nonlin) | t-tc | Erosion rate (model) |
| (Min) | (Hrs) | (s) | (mm) | (mm) | (mm/s) | (Pa) | (Pa) | (Pa) | (Pa) | (mm/s) | (Pa) | (Pa) | (Pa) | (mm/s) | (mm/s) | (Pa) | (Pa) | (Pa) | (mm/s) | (mm/s) | (Pa) | (Pa) | (Pa) | (mm/s) |
| 0 | 0 | 0 | 0 | 101.3 | - | 160.4 | - | - | 79.6 | - | 160.4 | - | 59.0 | | - | 160.4 | - | 64.1 | | - | 160.4 | - | 79.6 | |
| 5 | 0:05 | 300 | 9.71 | 111.0 | 3.24E-02 | 133.6 | 147.0 | 146.4 | 65.6 | 3.24E-02 | 133.6 | 146.4 | 45.0 | 3.11E-02 | 3.24E-02 | 133.6 | 146.4 | 50.1 | 3.13E-02 | 3.24E-02 | 133.6 | 146.4 | 65.6 | 2.88E-02 |
| 10 | 0:10 | 600 | 13.15 | 114.4 | 1.15E-02 | 125.7 | 129.6 | 129.6 | 48.7 | 1.15E-02 | 125.7 | 129.6 | 28.2 | 1.59E-02 | 1.15E-02 | 125.7 | 129.6 | 33.3 | 1.53E-02 | 1.15E-02 | 125.7 | 129.6 | 48.7 | 1.44E-02 |
| 15 | 0:15 | 900 | 16.68 | 118.0 | 1.18E-02 | 118.3 | 122.0 | 121.9 | 41.1 | 1.18E-02 | 118.3 | 121.9 | 20.5 | 1.00E-02 | 1.18E-02 | 118.3 | 121.9 | 25.6 | 9.70E-03 | 1.18E-02 | 118.3 | 121.9 | 41.1 | 9.62E-03 |
| 20 | 0:20 | 1200 | 19.11 | 120.4 | 8.10E-03 | 113.5 | 115.9 | 115.9 | 35.1 | 8.10E-03 | 113.5 | 115.9 | 14.5 | 6.08E-03 | 8.10E-03 | 113.5 | 115.9 | 19.6 | 6.07E-03 | 8.10E-03 | 113.5 | 115.9 | 35.1 | 6.62E-03 |
| 30 | 0:30 | 1800 | 21.73 | 123.0 | 4.37E-03 | 108.7 | 111.1 | 111.1 | 30.3 | 4.37E-03 | 108.7 | 111.1 | 9.7 | 3.43E-03 | 4.37E-03 | 108.7 | 111.1 | 14.8 | 3.73E-03 | 4.37E-03 | 108.7 | 111.1 | 30.3 | 4.70E-03 |
| 40 | 0:40 | 2400 | 22.69 | 124.0 | 1.60E-03 | 107.1 | 107.9 | 107.9 | 27.1 | 1.60E-03 | 107.1 | 107.9 | 6.5 | 1.92E-03 | 1.60E-03 | 107.1 | 107.9 | 11.6 | 2.44E-03 | 1.60E-03 | 107.1 | 107.9 | 27.1 | 3.62E-03 |
| 60 | 1.0 | 3600 | 24.89 | 126.2 | 1.83E-03 | 103.4 | 105.2 | 105.2 | 24.4 | 1.83E-03 | 103.4 | 105.2 | 3.8 | 8.87E-04 | 1.83E-03 | 103.4 | 105.2 | 8.9 | 1.53E-03 | 1.83E-03 | 103.4 | 105.2 | 24.4 | 2.82E-03 |
| 90 | 1.5 | 5400 | 27.21 | 128.5 | 1.29E-03 | 99.7 | 101.5 | 101.5 | 20.7 | 1.29E-03 | 99.7 | 101.5 | 0.1 | 4.53E-06 | 1.29E-03 | 99.7 | 101.5 | 5.2 | 6.00E-04 | 1.29E-03 | 99.7 | 101.5 | 20.7 | 1.92E-03 |
| 150 | 2.5 | 9000 | 28.92 | 130.2 | 4.75E-04 | 97.1 | 98.4 | 98.4 | 17.5 | | | | | | 4.75E-04 | 97.1 | 98.4 | 2.1 | 1.19E-04 | 4.75E-04 | 97.1 | 98.4 | 17.5 | 1.30E-03 |
| 270 | 4.5 | 16200 | 29.77 | 131.1 | 1.18E-04 | 95.8 | 96.4 | 96.4 | 15.6 | | | | | | 1.18E-04 | 95.8 | 96.4 | 0.1 | 1.01E-06 | 1.18E-04 | 95.8 | 96.4 | 15.6 | 9.92E-04 |
| 570 | 9.5 | 34200 | 33.27 | 134.6 | 1.94E-04 | 90.9 | 93.3 | 93.3 | 12.5 | | | | | | | | | | | 1.94E-04 | 90.9 | 93.3 | 12.5 | 5.88E-04 |
| 2025 | 33.8 | 121500 | 36.97 | 138.3 | 4.24E-05 | 86.1 | 88.5 | 88.5 | 7.6 | | | | | | | | | | | 4.24E-05 | 86.1 | 88.5 | 7.6 | 1.85E-04 |
| 3610 | 60.2 | 216600 | 39.32 | 140.6 | 2.47E-05 | 83.2 | 84.7 | 84.7 | 3.8 | | | | | | | | | | | 2.47E-05 | 83.2 | 84.7 | 3.8 | 3.67E-05 |
| 6075 | 101.3 | 364500 | 40.57 | 141.9 | 8.45E-06 | 81.8 | 82.5 | 82.5 | 1.7 | | | | | | | | | | | 8.45E-06 | 81.8 | 82.5 | 1.7 | 5.33E-06 |
| 7785 | 129.8 | 467100 | 40.98 | 142.3 | 4.00E-06 | 81.3 | 81.5 | 81.5 | 0.7 | | | | | | | | | | | 4.00E-06 | 81.3 | 81.5 | 0.7 | 7.32E-07 |
| 10530 | 175.5 | 631800 | 41.41 | 142.7 | 2.61E-06 | 80.8 | 81.1 | 81.1 | 0.2 | | | | | | | | | | | 2.61E-06 | 80.8 | 81.1 | 0.2 | 5.70E-08 |
| 14160 | 236.0 | 849600 | 41.38 | 142.7 | -1.38E-07 | 80.8 | 80.8 | 80.8 | 0.0 | | | | | | | | | | | | | | | |

Figure B-10. Sample M390(2) Analysis Spreadsheet Printout for Thomas' Method

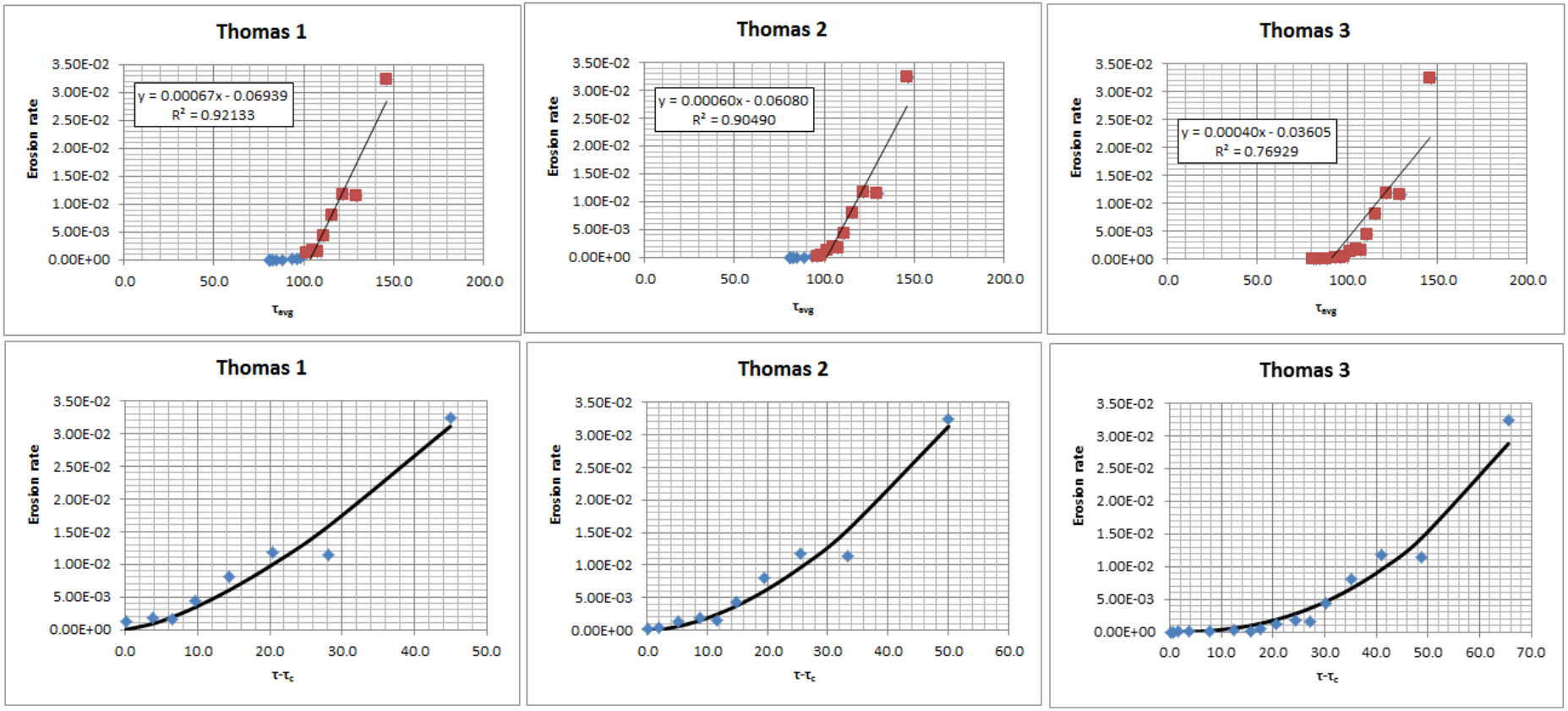


Figure B-11. Sample M390(2) Analysis Plots for Thomas' Method